Some contributions to the analysis of the Half-Space Matching Method for scattering problems and extension to 3D elastic plates

Yohanes Tjandrawidjaja

THÈSE DE DOCTORAT
DE L'UNIVERSITÉ PARIS-SACLAY

préparée à

L'ENSTA Paris

Laboratoire d'accueil : Unité de Mathématiques Appliquées, ENSTA-CNRS-INRIA

ÉCOLE DOCTORALE N°574

École Doctorale de Mathématiques Hadamard (EDMH)

Spécialité de doctorat : Mathématiques appliquées

par

Yohanes TJANDRAWIDJAJA

Some contributions to the analysis of the Half-Space Matching Method for scattering problems and extension to 3D elastic plates

Thèse présentée et soutenue à Palaiseau, le 17 décembre 2019

Composition du jury :

M. Didier CLOUTEAU	Président	CentraleSupélec
M. Raphaël ASSIER	Rapporteur	University of Manchester
M. Lothar NANNEN	Rapporteur	TU Wien
Mme Hélène BARUCQ	Examinatrice	MAGIQUE 3D INRIA
M. Xavier CLAEYS	Examinateur	Laboratoire Jacques Louis-Lions
Mme Anne-Sophie BONNET-BEN DHIA	Directrice de thèse	ENSTA Paris
Mme Sonia FLISS	Co-directrice de thèse	ENSTA Paris
M. Vahan BARONIAN	Co-directeur de thèse	CEA-LIST
M. Antoine TONNOIR	Invité	INSA Rouen

Remerciements

Cette thèse marque la fin d'une aventure que je n'avais jamais imaginé pouvoir réaliser. Et si j'arrivais jusqu'au bout, c'est grâce aux nombreuses personnes qui m'ont soutenu tout au long de ce merveilleux parcours.

Tout d'abord, c'est grâce à ma directrice Anne-Sophie Bonnet-Ben Dhia et mes encadrants Sonia Fliss et Vahan Baronian que j'ai pu commencer ma carrière scientifique. Je les remercie profondément pour leur partage de connaissances ainsi que pour leur soutien et leurs encouragements, chacun à sa façon. Un grand merci également à Antoine Tonnoir, un grand frère de ce monde de la recherche, pour son aide, nos petites discussions et son soutien jusqu'au bout en étant invité dans mon jury.

Je remercie également mes rapporteurs : Raphaël Assier et Lothar Nannen, pour leur temps consacré et leur commentaires tres constructifs. J'adresse aussi mes remerciements à mes examinateurs : Didier Clouteau, Xavier Claeys et Hélène Barucq, pour avoir accepté d'être membres de mon jury, malgré la grève et la difficulté pendant le jour de soutenance. Merci aussi à Simon Chandler-Wilde qui s'intéresse à ce que j'ai fait depuis la première rencontre et qui m'a beaucoup aidé lors de ma recherche de postdoc.

Ensuite, je tiens à remercier tous les membres de POEMS, permanents ou non, pour ces 3 ans ++. Je remercie en particulier Stéphanie Chaillat, pour la discussion et la collaboration sur l'optimisation de mon code. Merci aussi à Nicolas Kielbasiewicz et Eric Lunéville que j'ai beaucoup sollicités avec mes questions sur XLiFE++, qui sont parfois très basiques. Merci aux stagiaires, doctorants et postdoctorants de POEMS avec qui j'ai pu partagé le bureau : Emile, Hajer, Damien M.-M., Hélèna, Khawla et recemment Meryem, et aussi les amis de couloir : Antoine, Sandrine, Clément, Maryna, Arnaud, Laure, Félix, Dmitry, Jean-François, Damien C. et Mahran.

Merci aussi à mes amis indonésiens avec qui j'ai beaucoup partagé la vie dans ce pays lointain qu'on appelle la deuxième maison.

Finalement, merci a ma famille ; mon papa, qui me fait toujours confiance, même quand je n'en ai pas en moi, ma maman pour son soutien infini par appels téléphonique chaque semaine, et ma sœur avec qui je tchatte sans fin.

Cette thèse n'est pas seulement une fin mais un début de mon nouveau départ.

Contents

Introduction

The general motivation of this thesis is the Non-Destructive Testing (NDT) by ultrasonic waves. NDT is a non-intrusive technique used to detect potential defects in a piece, for example a hole, a crack, or a corrosion area. The principle is simple: a transmitter produces ultrasonic waves that propagate inside the piece and interact with the defect (if there is any), and a sensor monitors the scattered waves. From this information, one tries to detect, and if possible localize and describe the defects. Such a technique is used in many industries, for example in nuclear engineering, aeronautics, or oil and gas industries.

Such NDT techniques can be developed and optimized by using numerical simulations, before being used in real life situations. At this aim, different numerical tools have been implemented in the CIVA platform of CEA LIST. In order to simulate the whole process, one has to treat the different aspects: emission/reception of waves, propagation, and interaction with the defects. The propagation can be efficiently modeled by analytical approaches (rays in volume pieces, modes in waveguides like bars or plates) but the interaction with the defect needs more versatile techniques, like Finite Elements Method (FEM) that can handle any kind of defect. The collaboration between POEMS and CEA LIST is devoted to this last aspect. Two theses (the one of V. Baronian [9] and the one of L. Taupin [67]) were devoted to the interaction of modes with a localized defect in an infinite waveguide (with one infinite direction). Similar methods coupling FEM and modal decomposition have been developed by several authors for isotropic [33, 47, 48] and anisotropic [10] elastic waveguides.

The objective of this thesis is to model the scattering by localized defects in an elastic plate, with a finite thickness. To focus only on the interaction with the localized defects and not on the border, we assume that the plate is infinite in the two other directions. There are two main difficulties in this problem: a theoretical one concerning the definition of the physical solution, and a practical one concerning the numerical computation of the solution since the problem is posed in an unbounded domain.

To obtain a physical solution, we usually define it as the only solution of a well-posed problem. Scattering problems are in general not well-posed in the L^2 framework due to the slow decay of the solution at infinity, while in the L^2_{loc} framework there exist infinitely many solutions. Therefore, one has to select the "outgoing" solution to obtain the well-posedness.

Concerning the computation of the solution, numerous methods have been developed to tackle similar difficulties in the simpler acoustic case. The usual approach is to implement a coupling between the Finite Element Method (FEM) for a bounded region where the defects are located and another method to treat the exterior domain. However, these methods cannot be extended easily to treat the problem at hand. Let us take a closer look to these methods.

1. The Perfectly Matched Layers (PML) method.

   This method was firstly introduced by Bérenger [15] for transient Maxwell equations, and has been studied extensively for other equations and also for time-harmonic problems [18, 62]. The idea of the method is to englobe the domain of interest (typically where the

defects or the support of the source term are located) by layers that absorb the waves that are scattered to the exterior of this domain of interest. These waves are absorbed and not reflected back, thus mimicking the behavior of the waves at infinity. The absorbing layers are modeled by a complex dilation in the direction of the propagation so that the *outgoing* waves are attenuated.

Unfortunately, it is known that cartesian PMLs fail in some complex configurations. This is due to the fact that phase and group velocities do not have the same direction, and PMLs only consider the phase velocity, which is not the relevant quantity. In anisotropic infinite media, it has been proved in [14] that cartesian PMLs may be unstable in the time domain. In the frequency domain, PMLs may create spurious effects. It is also well-known that PMLs are unstable in the time domain for the 2D problem even in an isotropic elastic layer. The reason is the presence of the so-called backward propagating Lamb modes, which have phase and group velocity with opposite directions [18, 63]. This time, the counterpart in the frequency domain is that PMLs will converge, but to a wrong solution. In the problem we are interested in, which is the case of an anisotropic elastic plate, both difficulties mentioned above are expected to occur.

One can also mention the connection of the PML method and the ones based on pole conditions to select outgoing waves [46, 60], like the Hardy space infinite element method [40, 41, 45]. This method has been applied successfully to isotropic elastic waveguides with one infinite direction and also to isotropic elastic plates [42], even in presence of backward propagating modes. But up to our knowledge, it does not allow to treat the case of anisotropic elastic plates that we want to consider here.

2. Boundary Integral Equation (BIE) method.

This method is also a popular choice, used when the exterior of the domain of interest is homogeneous. The integral method exploits the fact that the solution of the exterior domain can be expressed as an integral representation involving some potential functions living on the boundary of the domain and the Green's function [8, 17, 22, 51]. Thus, instead of considering the infinite space, it is enough to find these potentials and apply the integral formula. With this integral formula, the formulation is exact in the exterior domain and thus some numerical dispersion can be avoided.

However, the BIE method requires the knowledge of the Green's function of the medium. In isotropic media, the Green's function can be obtained easily and we have an explicit formula for it. Moreover, it only depends on the distance between two points. In an elastic plate, computing the Green's tensor becomes more expensive, one of the reason is because it cannot be expressed in a closed form. In the isotropic plate, the Green's tensor depends on the respective position of the two points in the thickness. In a general anisotropic plate, it also depends on the position of the two points in the horizontal plane [71]. The computation of the Green's tensor becomes as expensive as solving the problem itself.

The list above is far from being exhaustive, and there exist a lot of different approaches (OSRC, FMM, ...) [3, 13, 30, 34, 39, 43] to treat the case of homogeneous isotropic infinite media that we do not investigate here, since they seem not appropriate to the problem we have in mind.

In view of these difficulties, the CEA LIST and POEMS (CNRS - INRIA - ENSTA) have decided to develop a new approach. This was started during the thesis of A. Tonnoir [68]. The idea was to adapt to the case of elastic plates a method firstly introduced in the 2D periodic case by S. Fliss and P. Joly [31, 32]. This led finally to the so-called Half-Space Matching (HSM) Method which was applied by A. Tonnoir to 2D acoustic and elastic homogeneous media, and

then by J. Ott [57] to 2D junctions of open waveguides. A theoretical analysis of the continuous formulation has been given by A.-S. Bonnet-Ben Dhia, S. Fliss, and A. Tonnoir [19] in the dissipative case (that is for a complex frequency).

The idea of this method is to decompose the exterior domain in several overlapping half-spaces. For each half-space, we use the analytic expression of the solution in terms of the trace on the border of the half-space. The analytic expression of the solution is obtained by applying the appropriate transform, for example the Fourier transform for a homogeneous domain. By imposing that the half-space representations have to match where they coexist, we obtain some compatibility relations imposed on the traces via Fourier integral formula. Finally, we have a system of equations involving several unknowns: a volume unknown in a bounded domain around the defect and the traces on the infinite lines bordering the half-spaces.

My contribution to this study is the extension of the method to the elastic 3D plate. This extension is not immediate; there are several difficulties that rise up which were not encountered in the previous cases. We address these difficulties one at a time in each chapter of the thesis. The thesis plan is as follows.

0. **Principles of the HSM Method**

   This chapter is a short summary of the method described in the thesis of A. Tonnoir [68] as a reminder on the principles of the method. The method is presented to solve the simple model problem of a Helmholtz equation with a localized obstacle.

1. **Numerical analysis of the HSM Method**

   We continue with the numerical analysis of the HSM Method for a problem set in the exterior to a polygon with a Robin boundary condition for a complex frequency. We first show that the continuous formulation is of Fredholm type. The difficulty comes from the cross-points between the infinite lines, which are responsible for the non-compactness of the integral operator. Precise estimates are derived using the Mellin transform which allow to prove the well-posedness of the formulation. To prove the convergence of the discretization, the difficulty is that the previous approach, used in for the continuous problem, does not work anymore for the discrete one, because of the Fourier integral truncation. The idea is then to apply the Mellin calculus to a decomposition of the traces in symmetric and antisymmetric parts, with respect to the cross-points. Indeed, this decomposition is stable with respect to the Fourier truncation. At the end of the chapter, we derive error estimates with respect to the different discretization parameters.

2. **Scattering problem in 2D plane**

   While the previous chapter was devoted to the dissipative problem (with a complex frequency), we consider here the scattering problem by localized obstacles with a real frequency. We show several possible HSM formulations to treat this problem based on the choice of the unknowns which can be written on the total field or the scattered field. These formulations are derived formally since there is no theory for real frequency. We show that although the theory is only established for a complex frequency, the simulations work well for real frequencies up to a finer discretization in the Fourier variable.

3. **Elasticity problem in 3D plates**

   This chapter is devoted to the main objective of the thesis, which is the extension of the HSM method to 3D elastic plates. First we introduce a decomposition of the infinite plate into a bounded region which contains the defects and four semi-infinite half-plates. The principle of the method is again to derive semi-analytical representations of the elastic field

in the half-plates and then to impose the compatibility between different representations in the overlapping zones where they coexist. A difficult part of the work consists in deriving these semi-analytical representations. A natural idea is to apply first a Fourier transform in the infinite direction. Then, for each value of the Fourier variable ξ, the elastic field can be represented as a modal expansion, involving specific modes that we call the "Lamb ξ modes". The properties of these modes are carefully studied, and a bi-othogonality relation is derived. This bi-orthogonality relation is then used to compute the modal amplitudes in the modal expansion. A main difference compared to the scalar case is that, due to the form of the bi-orthogonality relation, these modal amplitudes are functions of both the traces of the displacement and of the normal stress on the boundary of the half-plate. That is why we have to introduce a multi-unknown HSM formulation with 3 different types of unknowns: the volume unknown in the bounded region, the displacement traces, and the normal stress traces on the infinite strips, that are the boundaries of the half-plates. The theoretical difficulties induced by the presence of the two Cauchy traces (displacement and normal stress) are not studied here, but they are described and partially analyzed in a simpler scalar case in chapter 4.The challenge here is to implement and solve a problem which is much larger than the 2D acoustic case considered in chapters 1 and 2 because it is at the same time 3D, vectorial and with twice as many trace unknowns. Finally, some numerical results are presented in the isotropic case.

4. **Multi-unknown Half-Space Matching method**

The formulation developed in Chapter 3 raises several theoretical difficulties, one of them is that two types of traces are used to obtain the half-plate representations. To focus on this difficulty, we study and justify our formulation with two types of traces, but for a simpler acoustic model problem. The main difficulty comes from the fact that the unknowns are in Sobolev spaces $H^{1/2}$ and $H^{-1/2}$, while the formulation is naturally given piecewisely, thus "cutting" the traces. We show that a particular choice of test functions, different from the unknowns, allows to derive a correct mathematical formulation of the compatibility equations. We show the equivalence of the multi-unknowns problem with the original problem by using the analytic continuation of the representation in a Riemann-surface-like domain. However, we did not succeed to prove the well-posedness, which is still an open question. At the end we also show that the multi-unknown formulation can be rewritten using the Green's function in which no Fourier transform is used. Thus, instead of looking for a representation in half-spaces, we can consider subdomains whose boundaries are not necessarily straight lines.

5. **Complex-scaled Half-Space Matching method for the non-dissipative case**

This is a part of a collaborative work with Christophe Hazard from POEMS and Simon Chandler-Wilde and Karl-Mikael Perfekt from University of Reading. So far, the theoretical analysis for the HSM method was only developed for the dissipative case. For the non-dissipative case, an analysis similar to that of the dissipative case cannot be conducted because the traces are not in L^2. However, the numerical results show that this method works well for the non-dissipative case. To overcome this difficulty, the solution that we have explored is to design a slightly different formulation of the HSM method that, contrary to the classical one, can be theoretically validated in the non-dissipative case. The idea of the method is to apply a complex scaling on the traces (similar to the PML method), so that the new unknowns decay exponentially and the L^2 framework is recovered. This comes with a price: the half-space representations are replaced by representations which are valid only in a subregion of the half-space, depending on the complex scaling parameter (the bigger the parameter is, the faster the trace decays but the smaller the

subregion is). We show that Fredholm alternative also holds for this problem through an analysis similar to the one done in Chapter 1.

Throughout this thesis, I have obtained all the numerical results by implementing the methods in XLiFE++, a C++ Finite Element library developed by POEMS and IRMAR [50].

Chapter 1 is also published as a chapter in the following book:

A.-S. Bonnet-BenDhia, S. Fliss, and Y. Tjandrawidjaja. Numerical analysis of the Half-Space Matching method with Robin traces on a convex polygonal scatterer. *Radon Series on Computational and Applied Mathematics* 24, De Gruyter, May, 2019.

Résumé détaillé de la thèse

La motivation générale de cette thèse est le contrôle non destructif (CND) par ondes ultrasonores. Le CND est une technique non intrusive utilisée pour détecter les défauts potentiels dans une pièce, par exemple un trou, une fissure ou une zone de corrosion. Le principe est simple : un émetteur produit des ondes ultrasonores qui se propagent à l'intérieur de la pièce et interagissent avec le défaut (le cas échéant), et un capteur mesure les ondes diffractées. A partir de ces informations, on essaie de détecter, et si possible localiser et décrire les défauts. Une telle technique est utilisée dans de nombreuses industries, par exemple dans les industries du génie nucléaire, de l'aéronautique ou du pétrole et du gaz.

Ces techniques CND peuvent être développées et optimisées à l'aide de simulations numériques, avant d'être utilisées dans des situations réelles. Dans ce but, différents outils numériques ont été mis en œuvre dans la plateforme CIVA du CEA LIST. Afin de simuler l'ensemble du processus, il faut traiter les différents aspects : émission/réception des ondes, propagation et interaction avec les défauts. La propagation peut être efficacement modélisée par des approches analytiques (méthodes de rayons dans des pièces volumiques, modes dans les guides d'ondes comme les barres ou les plaques) mais l'interaction avec le défaut nécessite des techniques plus polyvalentes, comme la méthode des éléments finis (MEF) qui peut gérer tout type de défaut. La collaboration entre POEMS et le CEA LIST est consacrée à ce dernier aspect. Deux thèses (celle de V. Baronian [9] et celle de L. Taupin [67]) ont été consacrées à l'interaction des modes avec un défaut localisé dans un guide d'onde infini (avec une direction infinie). Des méthodes similaires couplant la MEF et la décomposition modale ont été développées par plusieurs auteurs pour les guides d'ondes élastiques isotropes [33, 47, 48] et anisotropes [10].

L'objectif de cette thèse est de modéliser la diffraction par des défauts localisés dans une plaque élastique, d'épaisseur finie. Pour se concentrer uniquement sur l'interaction avec les défauts localisés et non avec la frontière, nous supposons que la plaque est infinie dans les deux autres directions. Il y a deux difficultés principales dans ce problème : une de nature théorique concernant la définition de la solution physique, et une de nature pratique concernant le calcul numérique de la solution car le problème se pose dans un domaine infini.

Pour obtenir une solution physique, nous la définissons généralement comme la seule solution d'un problème bien posé. Les problèmes de diffraction ne sont généralement pas bien posés dans le cadre L^2 en raison de la décroissance lente de la solution à l'infini, tandis que dans le cadre L_{loc}^2, il existe une infinité de solutions. Par conséquent, il faut sélectionner la solution "sortante" pour obtenir le caractère bien posé.

Concernant le calcul de la solution, de nombreuses méthodes ont été développées pour faire face à des difficultés similaires dans le cas plus simple des ondes acoustiques. L'approche habituelle consiste à implémenter un couplage entre la MEF dans un domaine borné contenant les défauts et une autre méthode pour traiter le domaine extérieur. Cependant, ces méthodes ne peuvent pas être étendues facilement pour traiter le problème en question. Examinons de plus près ces méthodes.

1. La méthode des couches parfaitement adaptées (PML pour Perfectly Matched Layers en anglais).

   Cette méthode a été introduite par Bérenger [15] pour les équations de Maxwell transitoires, et a été étudiée de manière approfondie pour d'autres équations et également pour les problèmes harmoniques temporels [18, 62]. L'idée de la méthode est d'englober le domaine d'intérêt (typiquement la zone qui contient les défauts et le support du terme source) par des couches qui absorbent les ondes qui sont diffractées à l'extérieur de ce domaine d'intérêt. Ces ondes sont absorbées et non réfléchies, imitant ainsi le comportement des ondes à l'infini. Les couches absorbantes sont modélisées par une dilatation complexe dans le sens de la propagation de sorte que les ondes *sortantes* sont atténuées.

   Malheureusement, il est connu que les PML cartésiennes échouent dans certaines configurations complexes. Cela est dû au fait que la vitesse de phase et la vitesse de groupe n'ont pas la même direction, et les PML ne prennent en compte que la vitesse de phase, qui n'est pas la quantité pertinente. Dans les milieux infinis anisotropes, il a été prouvé dans [14] que les PML cartésiennes peuvent être instables dans le domaine temporel. Dans le domaine fréquentiel, les PML peuvent créer des effets parasites. Il est également bien connu que les PML sont instables dans le domaine temporel pour le problème 2D même dans une couche élastique isotrope. La raison en est la présence des modes de Lamb inverses, qui ont des vitesses de phase et de groupe de directions opposées [18, 63]. Cette fois, la contrepartie dans le domaine fréquentiel est que les PML convergeront, mais vers une mauvaise solution. Dans le problème qui nous intéresse, qui est le cas d'une plaque élastique anisotrope, on s'attend à ce que les deux difficultés mentionnées ci-dessus se produisent.

   On peut également mentionner le lien entre la méthode PML et celles utilisant la "pole condition" pour sélectionner les ondes sortantes [46, 60], comme la méthode des "Hardy space infinite elements" [40, 41, 45]. Cette méthode a été appliquée avec succès aux guides d'ondes élastiques isotropes à une direction infinie et également aux plaques élastiques isotropes [42], même en présence de modes inverses. Mais à notre connaissance, cela ne permet pas de traiter le cas des plaques élastiques anisotropes que nous voulons considérer ici.

2. La methode des équation intégrales (BIE pour Boundary Integral Equation en anglais). Cette méthode, également très répandue, est utilisée lorsque l'extérieur du domaine d'intérêt est homogène. La méthode intégrale exploite le fait que la solution du domaine extérieur peut être exprimée comme une représentation intégrale impliquant certaines fonctions potentielles vivant sur la frontière du domaine et la fonction de Green [8, 17, 22, 51]. Ainsi, au lieu de considérer l'espace infini, il suffit de trouver ces potentiels et d'appliquer la formule intégrale. Avec cette formule intégrale, la formulation est exacte dans le domaine extérieur et ainsi une certaine dispersion numérique peut être évitée.

   Cependant, la méthode BIE nécessite la connaissance de la fonction de Green du milieu. Dans les milieux isotropes, la fonction de Green peut être obtenue facilement et elle a une formule explicite. De plus, elle ne dépend que de la distance entre deux points. Dans une plaque élastique, le calcul du tenseur de Green devient plus cher, notamment parce qu'il ne peut pas être exprimé sous une forme explicite. Dans la plaque isotrope, le tenseur de Green dépend de la position respective des deux points dans l'épaisseur. Dans une plaque anisotrope générale, il dépend aussi de la position des deux points dans le plan horizontal [71]. Le calcul du tenseur de Green devient aussi coûteux que la résolution du problème lui-même.

La liste ci-dessus est loin d'être exhaustive, et il existe de nombreuses approches différentes

(OSRC, FMM, ...) [3, 13, 30, 34, 39, 43] pour traiter le cas des milieux infinis isotropes homogènes que nous n'étudions pas ici, car ils ne semblent pas appropriés au problème que nous voulons résoudre.

Face à ces difficultés, le CEA LIST et POEMS (CNRS - INRIA - ENSTA) ont décidé de développer une nouvelle approche. Cela a commencé lors de la thèse d'A. Tonnoir [68]. L'idée était d'adapter au cas des plaques élastiques une méthode d'abord introduite dans le cas périodique 2D par S. Fliss et P. Joly [31, 32]. Cela a finalement conduit à la méthode dite Half-Space Matching (HSM) qui a été appliquée par A. Tonnoir aux milieux homogènes acoustiques et élastiques 2D, puis par J. Ott [57] aux jonctions 2D de guides d'ondes ouverts. Une analyse théorique de la formulation continue a été développée par A.-S. Bonnet-Ben Dhia, S. Fliss et A. Tonnoir [19] dans le cas dissipatif (c'est-à-dire pour une fréquence complexe).

L'idée de cette méthode est de décomposer le domaine extérieur en plusieurs demi-espaces qui se recouvrent. Pour chaque demi-espace, nous utilisons l'expression analytique de la solution en fonction de la trace à la frontière du demi-espace. L'expression analytique de la solution est obtenue en appliquant la bonne transformation, par exemple la transformée de Fourier pour un domaine homogène. En imposant que les représentations de demi-espace doivent coïncider là où elles coexistent, nous obtenons des relations de compatibilité imposées aux traces via une formule intégrale de Fourier. Nous obtenons finalement un système d'équations impliquant plusieurs inconnues : une inconnue volumique dans un domaine borné autour du défaut et les traces sur les lignes infinies correspondant aux bords des demi-espaces.

Ma contribution à cette étude est l'extension de la méthode à la plaque élastique 3D. Cette extension n'est pas immédiate ; plusieurs difficultés qui n'ont pas été rencontrées dans les cas précédents apparaissent. Nous abordons ces difficultés une par une dans chaque chapitre de la thèse. Le plan de la thèse est le suivant.

0. **Principes de la méthode HSM**

   Ce chapitre est un bref résumé de la méthode décrite dans la thèse d'A. Tonnoir [68]. La méthode est présentée pour résoudre le problème modèle simple de l'équation de Helmholtz avec un obstacle localisé.

1. **Analyse numérique de la HSM Method**

   Nous poursuivons l'analyse numérique de la méthode HSM pour un problème posé à l'extérieur d'un polygone avec une condition aux limites de type Robin et pour une fréquence complexe. Nous montrons d'abord que la formulation continue est de type Fredholm. La difficulté vient des points de croisement entre les lignes infinies, qui sont responsables de la non-compacité de l'opérateur intégral. Des estimations précises sont dérivées à l'aide de la transformée de Mellin qui permettent de prouver le caractère bien-posé de la formulation. Pour montrer la convergence de la discrétisation, la difficulté est que l'approche précédente, utilisée pour le problème continu, ne fonctionne plus pour le problème discret, à cause de la troncature de l'intégrale de Fourier. L'idée est alors d'appliquer le calcul de Mellin à une décomposition des traces en parties symétriques et antisymétriques, par rapport aux points de croisement. En effet, cette décomposition est stable par rapport à la troncature de Fourier. À la fin du chapitre, nous dérivons des estimations d'erreur par rapport aux différents paramètres de discrétisation.

2. **Problème de diffration dans le plan 2D**

   Alors que le chapitre précédent était consacré au problème dissipatif (avec une fréquence complexe), nous considérons ici le problème de diffraction par des obstacles localisés avec une fréquence réelle. Nous montrons plusieurs formulations HSM possibles pour traiter ce

problème en fonction du choix des inconnues qui peuvent être écrites sur le champ total ou le champ diffracté. Ces formulations sont dérivées formellement car il n'y a pas de cadre théorique pour la fréquence réelle. Nous montrons que, bien que la théorie ne soit établie que pour une fréquence complexe, les simulations fonctionnent bien pour des fréquences réelles à condition d'utiliser une discrétisation suffisamment fine des intégrales de Fourier.

3. **Problème d'élasticité dans les plaques 3D**

Ce chapitre est consacré à l'objectif principal de la thèse, qui est l'extension de la méthode HSM aux plaques élastiques 3D. Nous introduisons d'abord une décomposition de la plaque infinie en une région bornée qui contient les défauts et quatre demi-plaques semi-infinies. Le principe de la méthode est à nouveau de dériver des représentations semi-analytiques du champ élastique dans les demi-plaques puis d'imposer la compatibilité entre différentes représentations dans les zones de recouvrement où elles coexistent. Une partie difficile du travail consiste à dériver ces représentations semi-analytiques. Une idée naturelle est d'appliquer d'abord une transformée de Fourier dans la direction infinie. Ensuite, pour chaque valeur de la variable de Fourier ξ, le champ élastique peut être représenté à l'aide d'une décomposition modale, impliquant des modes spécifiques que nous appelons les "modes Lamb ξ". Les propriétés de ces modes sont soigneusement étudiées et une relation de bi-othogonalité est démontrée. Cette relation de bi-orthogonalité est ensuite utilisée pour calculer les amplitudes modales dans la série modale. Une différence majeure par rapport au cas scalaire est que, du fait de la forme de la relation de bi-orthogonalité, ces amplitudes modales sont des fonctions à la fois des traces du déplacement et de la contrainte normale à la frontière de la demi-plaque. C'est pourquoi nous devons introduire une formulation HSM multi-inconnue avec 3 types d'inconnues différents : l'inconnue volumique dans le domaine borné, les traces de déplacement et les traces de contraintes normales sur les bandes infinies, qui sont les bords des demi-plaques. Les difficultés théoriques induites par la présence des deux traces de Cauchy (déplacement et contrainte normale) ne sont pas étudiées ici, mais elles sont décrites et partiellement analysées dans un cas scalaire plus simple au chapitre 4. Le défi ici est de mettre en œuvre et de résoudre un problème qui est de beaucoup plus grande taille que dans le cas acoustique 2D considéré dans les chapitres 1 et 2 car il est à la fois 3D, vectoriel et avec deux fois plus d'inconnues de traces. Enfin, quelques résultats numériques sont présentés dans le cas isotrope.

4. **Méthode HSM multi-inconnues**

La formulation développée au chapitre 3 pose plusieurs difficultés théoriques, l'une d'elles est que deux types de traces sont utilisés pour obtenir les représentations de demi-plaque. Pour nous concentrer sur cette difficulté, nous étudions et justifions notre formulation avec deux types de traces, mais pour un problème modèle acoustique plus simple. La difficulté principale vient du fait que les inconnues se trouvent dans les espaces de Sobolev $H^{1/2}$ et $H^{-1/2}$, alors que la formulation est naturellement donnée par morceaux, "coupant" ainsi les traces. Nous montrons qu'un choix particulier de fonctions de test, différent des inconnues, permet d'écrire une formulation mathématique correcte des équations de compatibilité. Nous montrons l'équivalence du problème multi-inconnues avec le problème de départ en utilisant le prolongement analytique de la représentation dans un domaine de type surface de Riemann. Cependant, nous n'avons pas réussi à prouver le caractère bien-posé, qui reste une question ouverte. À la fin, nous montrons également que la formulation multi-inconnue peut être réécrite en utilisant la fonction de Green et en n'utilisant plus de transformée de Fourier. Ainsi, au lieu de chercher une représentation de demi-espace, on peut considérer des sous-domaines dont les frontières ne sont pas nécessairement des lignes droites.

5. **HSM Method avec une dilatation complexe pour le cas non dissipatif**

Cette partie s'inscrit dans le cadre d'une collaboration avec Christophe Hazard de POEMS et Simon Chandler-Wilde et Karl-Mikael Perfekt de l'Université de Reading. Jusqu'à présent, l'analyse théorique de la méthode HSM n'a été développée que pour le cas dissipatif. Pour le cas non dissipatif, une analyse similaire à celle du cas dissipatif ne peut être effectuée car les traces ne sont pas dans L^2. Cependant, les résultats numériques montrent que cette méthode fonctionne bien pour le cas non dissipatif. Pour surmonter cette difficulté, la solution que nous avons explorée est de concevoir une formulation légèrement différente de la méthode HSM qui, contrairement à la méthode classique, peut être théoriquement validée dans le cas non dissipatif. L'idée de la méthode est d'appliquer une dilatation complexe sur les traces (similaire à la méthode PML), de sorte que les nouvelles inconnues soient exponentiellement décroissantes et que le cadre L^2 soit récupéré. Cela a un prix : les représentations du demi-espace sont remplacées par des représentations qui ne sont valables que dans un sous-domaine du demi-espace, en fonction du paramètre de la dilatation complexe (plus le paramètre est grand, plus la trace décroît rapidement mais plus le sous-domaine est petit). Nous montrons que l'alternative de Fredholm est également valable pour ce problème grâce à une analyse similaire à celle effectuée dans le chapitre 1.

Tout au long de cette thèse, j'ai obtenu tous les résultats numériques en implémentant les méthodes dans XLiFE ++, une bibliothèque d'éléments finis C ++ développée par POEMS et IRMAR [50].

Le chapitre 1 est également publié en tant que chapitre dans le livre suivant :

A.-S. Bonnet-BenDhia, S. Fliss, and Y. Tjandrawidjaja. Numerical analysis of the Half-Space Matching method with Robin traces on a convex polygonal scatterer. *Radon Series on Computational and Applied Mathematics* 24, De Gruyter, May, 2019.

Chapter 0

The Principle of the Half-Space Matching Method

Summary

In this chapter, we briefly recall the main features of the Half-Space Matching Method which has been developed in [68].

0.1 Introduction

We consider a time-harmonic wave equation (also known as the Helmholtz equation) in an infinite 2D domain with localized obstacles $\mathcal{O}$:

$$\left| \begin{aligned} -\Delta p(\mathbf{x}) - \omega^2 p(\mathbf{x}) &= f(\mathbf{x}) && \text{in } \Omega := \mathbb{R}^2 \backslash \mathcal{O}, \\ \nabla p \cdot n &= 0 && \text{on } \partial\Omega, \end{aligned} \right. \tag{0.1}$$

where ω is called the frequency and f is a compactly supported source term. To simplify the problem, we will consider the *dissipative* case, modeled by a complex frequency ω:

$$\text{Re}(\omega) > 0, \text{Im}(\omega) = \varepsilon > 0.$$

Thanks to the dissipation, the problem is coercive in $H^1(\mathbb{R}^2 \backslash \mathcal{O})$. The case of a real frequency will be discussed in Chapter 2 and 5.

0.2   The Half-Space Matching method

The idea of the method is to use a Finite Element representation in a bounded domain where the support of the source term and the defects are located. To treat the exterior of this bounded domain, we cover it with 4 overlapping half-planes and represent the solution in each half-plane from the trace on the boundary. Coupling these different representations, we have a system of equations where the unknowns are the volume unknown on the bounded domain and the traces of the solution on the boundaries of the half-planes.

0.2.1   Some notations

For the rest of the chapter, we use some notations described here. Let us note

$$\begin{aligned}
\Omega_a &= (-a, a)^2 \backslash \mathcal{O} \text{ and } \Omega_a^c = \mathbb{R}^2 \backslash (-a, a)^2, \\
\Omega_b &= (-b, b)^2 \backslash \mathcal{O} \text{ and } \Omega_b^c = \mathbb{R}^2 \backslash (-b, b)^2,
\end{aligned} \tag{0.2}$$

where a and b are strictly positive real numbers with $a < b$, $\ell := b - a > 0$, $\mathcal{O} \subset (-a, a)^2$, and $\operatorname{supp}(f) \subset (-a, a)^2$. We call the domain Ω_b the *interior domain* and Ω_a^c the *exterior domain*.
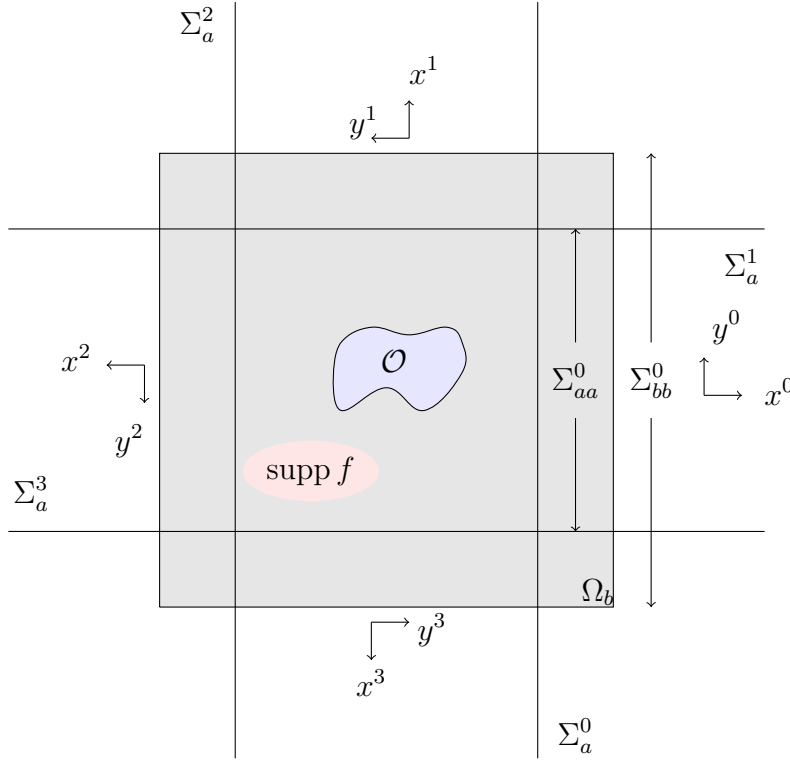
Figure 1: Geometry of the problem.

We define a local coordinates system for each $j \in \{0, 1, 2, 3\}$:

$$\begin{bmatrix} x^j \\ y^j \end{bmatrix} = \begin{bmatrix} \cos \theta^j & \sin \theta^j \\ -\sin \theta^j & \cos \theta^j \end{bmatrix} \begin{bmatrix} x \\ y \end{bmatrix}, \text{ where } \theta^j = \frac{j\pi}{2}.$$

Using the local coodinate systems, we define the half-planes as

$$\Omega_a^j = \{x^j \geq a\} \times \{y^j \in \mathbb{R}\},$$

and the lines that border the half-planes and the segments

$$\Sigma_a^j = \{x^j = a\} \times \{y^j \in \mathbb{R}\},$$
$$\Sigma_{aa}^j = \{x^j = a\} \times \{y^j \in [-a, a]\}.$$

Finally, the boundary of Ω_b is decomposed into 4 segments

$$\Sigma_{bb}^j = \{x^j = b\} \times \{y^j \in [-b, b]\},$$

and the union of these segments are denoted as

$$\Sigma_{aa} = \bigcup_{j=0}^{3} \Sigma_{aa}^j$$

$$\Sigma_{bb} = \bigcup_{j=0}^{3} \Sigma_{bb}^j.$$

Remark 0.2.1. *Here we define a domain decomposition with overlap between the interior domain Ω_b and the half-planes Ω_a^j. If we take $a = b$, there is no overlap between Ω_b and Ω_a^c. The formulation with overlap has several advantages from a theoretical point of view, although numerically both formulations work well and give the same results qualitatively. For more details, see [68].*

0.2.2 The half-space representation

In this section, we derive the half-plane representation, meaning that we want to have an explicit formula of the solution of the half-plane in terms of its trace on the boundary. More explicitly, given $\psi \in H^{\frac{1}{2}}(\Sigma_a^j)$, we want to find $P^j(\psi) \in H^1(\Omega_a^j)$ that satisfies

$$\left| \begin{array}{l} \Delta P^j + \omega^2 P^j = 0 \text{ in } \Omega_a^j \\ \qquad P^j = \psi \text{ on } \Sigma_a^j. \end{array} \right. \tag{0.3}$$

We define the Fourier transform in y^j as

$$\hat{\psi}(\xi) = \frac{1}{\sqrt{2\pi}} \int_{\mathbb{R}} \psi(y^j) e^{-\imath \xi y^j} \mathrm{d}y^j. \tag{0.4}$$

Taking the Fourier transform of (0.3), we obtain an ordinary differential equation in x^j

$$\left| \begin{array}{l} \dfrac{\mathrm{d}^2 \hat{P}^j}{(\mathrm{d}x^j)^2} + (\omega^2 - \xi^2)\hat{P}^j = 0, \quad x^j > a, \\ \qquad\qquad \hat{P}^j = \hat{\psi}, \quad x^j = a. \end{array} \right. \tag{0.5}$$

The general solution of this equation is

$$\hat{P}^j(x, \xi) = A(\xi) e^{\imath \sqrt{\omega^2 - \xi^2}(x^j - a)} + B(\xi) e^{-\imath \sqrt{\omega^2 - \xi^2}(x^j - a)},$$

where we take the convention $\mathrm{Im} \sqrt{z} \geq 0$ for all $z \in \mathbb{C}$. Since we are looking for an $H^1(\Omega_a^j)$, B has to be 0. Thus, the unique solution is

$$\hat{P}^j(x^j, \xi) = \hat{\psi}(\xi) e^{\imath \sqrt{\omega^2 - \xi^2}(x^j - a)}.$$

Taking the inverse Fourier transform, we obtain

$$P^j(\psi)(x^j, y^j) = \frac{1}{\sqrt{2\pi}} \int_{\mathbb{R}} \hat{\psi}(\xi) e^{\imath \sqrt{\omega^2 - \xi^2}(x^j - a)} e^{\imath \xi y^j} \mathrm{d}\xi. \tag{0.6}$$

In addition, we also define the trace of p in Σ_a^j:

$$\varphi^j := p|_{\Sigma_a^j} \quad \forall j \in \{0, 1, 2, 3\}. \tag{0.7}$$

0.2.3   The half-space matching formulation

We define the restrictions of the unknown p in several subdomains:

- in the bounded subdomain Ω_b, we define the restriction $p^b = p|_{\Omega_b}$ which satisfies

$$\left| \begin{aligned} -\Delta p^b - \omega^2 p^b &= f \text{ in } \Omega_b, \\ \nabla p^b \cdot n &= 0 \text{ on } \partial\mathcal{O}. \end{aligned} \right. \tag{0.8}$$

- in the 4 half-planes, we define the restriction $p^j = p|_{\Omega_a^j}$ which satisfies

$$\left| -\Delta p^j - \omega^2 p^j = 0 \text{ in } \Omega_a^j, j \in \{0, 1, 2, 3\}. \right. \tag{0.9}$$

By definition of the restrictions in 2 different half-planes Ω_a^j and $\Omega_a^{j\pm1}$, these two restrictions have to coincide in the quarter plane where they coexist:

$$p^j = p^{j\pm1} \text{ in } \Omega_a^j \cap \Omega_a^{j\pm1}. \tag{0.10}$$

To ensure this, we impose a compatibility condition on the boundary of this quarter plane:

$$p^j = p^{j\pm1} \text{ on } \partial\left(\Omega_a^j \cap \Omega_a^{j\pm1}\right). \tag{0.11}$$
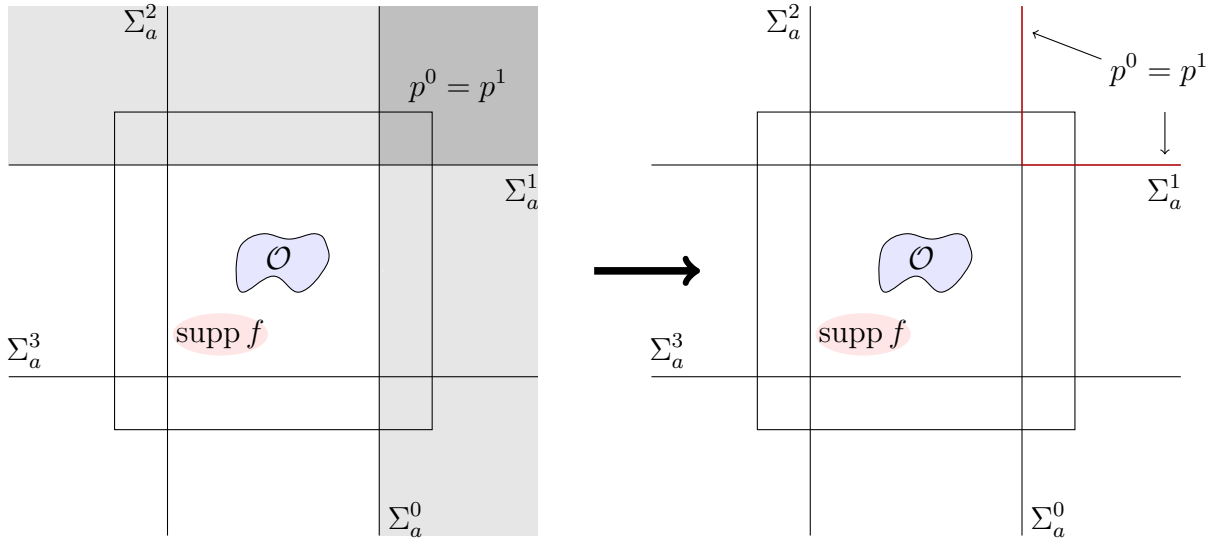
Figure 2: Zone where representations for Ω_a^0 and Ω_a^1 coincide.

To be able to write the compatibility condition (0.11) in terms of the traces, we define the following operator.

Definition 0.2.2. *The operator $D^{j,j\pm1}$ is the continuous operator from $H^{1/2}(\Sigma_a^j)$ to $H^{1/2}(\Sigma_a^{j\pm1} \cap \Omega_a^j)$ defined by*

$$D^{j,j\pm1}\psi = P^j(\psi)\Big|_{\Sigma_a^{j\pm1}\cap\Omega_a^j} \quad on \ \Sigma_a^{j\pm1} \cap \Omega_a^j. \tag{0.12}$$

The operator $D^{j,j\pm1}$ has the following explicit expression:

$$D^{j,j\pm1}\psi(x^j, \pm a) = \frac{1}{\sqrt{2\pi}} \int_{\mathbb{R}} \hat{\psi}(\xi) e^{i\sqrt{\omega^2 - \xi^2}(x^j - a)} e^{\pm i\xi a} d\xi. \tag{0.13}$$

With this operator, the compatibility relation (0.11) can be written in terms of the traces φ^j:

$$\varphi^j = D^{j\pm1,j}\varphi^{j\pm1} \text{ on } \Sigma_a^j \cap \Omega_a^{j\pm1} \text{ for } j \in \mathbb{Z}/4\mathbb{Z}. \tag{0.14}$$

In $\Omega_b \cap \Omega_a^j$, we also need to ensure the compatibility

$$p^b = p^j \text{ in } \Omega_b \cap \Omega_a^j. \tag{0.15}$$

There are several possible compatibility relations that can be imposed on the boundary of this zone. We choose for example:

$$p^b = p^j \qquad\qquad \text{on } \Sigma_{aa}^j, \tag{0.16}$$
$$\nabla p^b \cdot n = \nabla p^j \cdot n \qquad\qquad \text{on } \Sigma_{bb}^j, \forall j \in \{0,1,2,3\}. \tag{0.17}$$
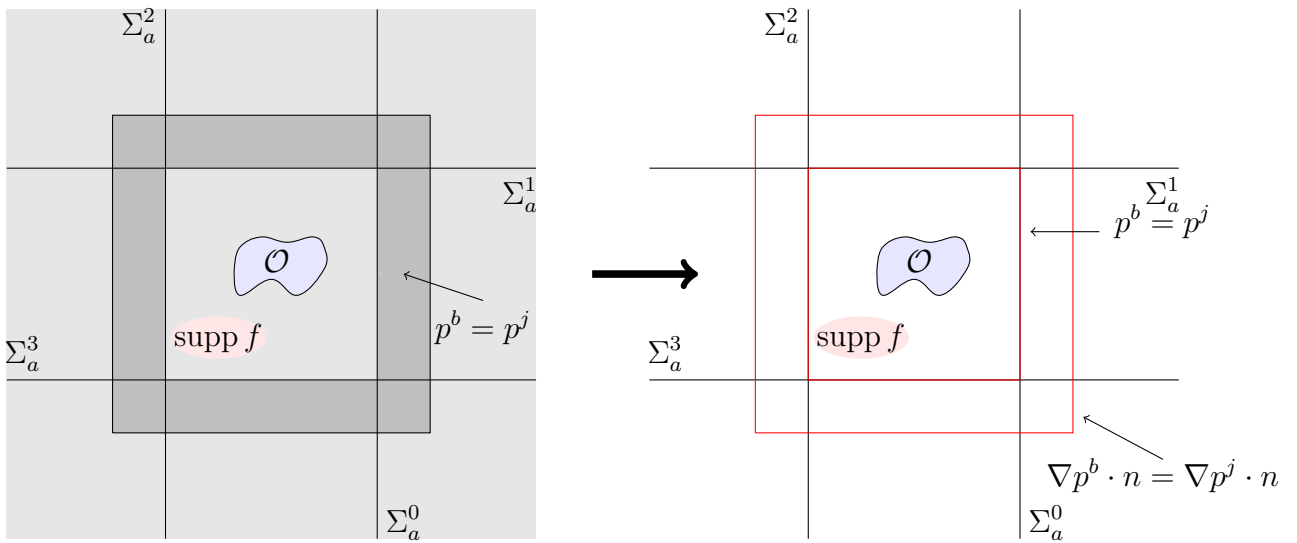
Figure 3: Zone where representations for Ω_b and Ω_a^j coincide.

The compatibility condition (0.16) can be expressed in terms of the traces as

$$p^b = \varphi^j \text{ on } \Sigma_{aa}^j. \tag{0.18}$$

The compatibility condition (0.17) can also be written in terms of the traces φ^j using the following operator.

Definition 0.2.3. *The operator Λ^j is the continuous operator from $H^{1/2}(\Sigma_a^j)$ to $H^{-1/2}(\Sigma_{bb}^j)$ defined by*

$$\Lambda^j \psi = \nabla P^j(\psi) \cdot n\Big|_{\Sigma_{bb}^j} \text{ on } \Sigma_{bb}^j. \tag{0.19}$$

This operator Λ^j has the following explicit expression

$$\Lambda^j \psi(b, y^j) = \frac{1}{\sqrt{2\pi}} \int_{\mathbb{R}} \hat{\psi}(\xi) \imath \sqrt{\omega^2 - \xi^2} e^{\imath \sqrt{\omega^2 - \xi^2}\ell} e^{\imath \xi y^j} \mathrm{d}\xi, \tag{0.20}$$

where $\ell = b - a$. We can write the compatibility condition (0.17) as

$$\nabla p^b \cdot n = \Lambda^j \varphi^j \text{ on } \Sigma_{bb}^j. \tag{0.21}$$

Remark 0.2.4. *In the case without overlap $\ell = b - a = 0$, the segments Σ_{aa}^j coincide with Σ_{bb}^j. Thus, the two conditions are imposed on the same segments. Furthermore, the definition of the operator Λ^j becomes more intricate. In this case, the operator Λ^j is a priori defined from $H^{1/2}(\Sigma_a^j)$ to $H^{-1/2}(\Sigma_a^j)$ but its restriction in Σ_{aa}^j is not in $H^{-1/2}(\Sigma_{aa}^j) := (\tilde{H}^{1/2}(\Sigma_{aa}^j))'$, where $\tilde{H}^{1/2}(\Sigma_{aa}^j)$ consists of functions in $H^{1/2}(\Sigma_{aa}^j)$ which, when extended by 0, are in $H^{1/2}(\Sigma_{aa})$. For more details, see [68].*

Finally, gathering equations (0.8, 0.14, 0.18, 0.21), we have a system of equations

Find p^b in $H^1(\Omega)$ and $(\varphi^j)_{j \in \{0,1,2,3\}}$ in $H^{\frac{1}{2}}(\Sigma_a^j)$ such that

$$
\left|
\begin{array}{ll}
-\Delta p^b - \omega^2 p^b = f & \text{in } \Omega_b \\
\nabla p^b \cdot n = 0 & \text{on } \partial\mathcal{O} \\
\nabla p^b \cdot n = \Lambda^j \varphi^j & \text{on } \Sigma_{bb}^j \\
p^b = \varphi^j & \text{on } \Sigma_{aa}^j \\
\varphi^j = D^{j\pm1,j}\varphi^{j\pm1} & \text{on } \Sigma_a^j \cap \Omega^{j\pm1}.
\end{array}
\right.
\tag{0.22}
$$

Formulation (0.22) can be shown to be equivalent to the original problem (0.1). Moreover, in [19], this problem is shown to be well-posed (Fredholm type or coercive + compact).

0.3   Discretization

To discretize the system of equation (0.22) by Finite Element method, we need to write the variational formulation, and writing one with φ^j in $H^{1/2}(\Sigma_a^j)$ would be intricate. Instead, we consider looking for solution φ^j in $L^2(\Sigma_a^j)$. We define the following space

$$
V := \left\{ (q, \psi^0, \psi^1, \psi^2, \psi^3),\ q \in H^1(\Omega_b), \forall j \in \{0,1,2,3\}\ \psi^j \in L^2(\Sigma_a^j), q = \psi^j \text{ on } \Sigma_{aa}^j \right\}. \tag{0.23}
$$

Remark that the operators Λ^j and $D^{j,j\pm1}$ are well-defined and continuous from $L^2(\Sigma_a^j)$ in $L^2(\Sigma_{bb}^j)$ and $L^2(\Sigma_a^j)$ in $L^2(\Sigma_a^{j\pm1})$ respectively. Therefore, we have the variational formulation satisfied by (0.22):

Find $(p^b, \varphi^0, \varphi^1, \varphi^2, \varphi^3) \in V$ such that $\forall (q, \psi^0, \psi^1, \psi^2, \psi^3) \in V$

$$
\int_{\Omega_b} \nabla p^b \cdot \nabla \bar{q} - \omega^2 p^b \bar{q} - \sum_{j=0}^3 \int_{\Sigma_{bb}^j} \Lambda^j \varphi^j \bar{q}
$$
$$
+ \sum_{j=0}^3 \int_{\Sigma_a^j \cap \Omega_a^{j\pm1}} \varphi^j \bar{\psi}^j - D^{j\pm1,j}\varphi^{j\pm1}\bar{\psi}^j = \int_{\Omega_b} f\bar{q}. \tag{0.24}
$$

To discretize the variational formulation, we introduce an approximation to the unknowns. First, it is necessary to truncate the infinite lines Σ_a^j where the traces live and we define the segments:

$$
\Sigma_{a,T}^j = \{(x^j = a, y^j),\ -T < y^j < T\},
$$

with $T > a$. Then, we approximate the φ^j's with 1D P1 Lagrange elements with h as the discretization step. For the volume unknown p^b, we approximate it with 2D P1 Lagrange elements. We look for an approximate solution:

$$
p_h^b(x, y) = \sum_{k=1}^{N_b} P_{h,k}^b u_k(x, y) \text{ in } \Omega_b,
$$

$$\varphi_h^j(y^j) = \sum_{k=1}^{N_j} \Phi_{h,k}^j w_k(y^j) \text{ in } \Sigma_a^j,$$

where u_k and w_k are the basis functions of the Lagrange elements, $P_{h,k}$, $\Phi_{h,k}^j \in \mathbb{C}$, and N_b and N_j are the numbers of discretization points in Ω_b and on Σ_a^j respectively. We define an approximation space of (0.23):

$$V_h := \left\{ (q_h, \psi_h^0, \psi_h^1, \psi_h^2, \psi_h^3), \ q_h(x,y) = \sum_{k=1}^{N_b} Q_{h,k} u_k(x,y), \right. \tag{0.25}$$

$$\left. \forall j \in \{0,1,2,3\}, \ \psi_h^j(y^j) = \sum_{k=1}^{N_j} \Phi_{h,k}^j w_k(y^j), q_h = \psi_h^j \text{ on } \Sigma_{aa}^j, \text{ where } Q_{h,k}, \Phi_{h,k}^j \in \mathbb{C} \right\}.$$

Finally, we also need to approximate the integral operators by truncating the Fourier integral which appears in several operators Λ^j and $D^{j,j\pm1}$. These integrals on $\xi \in \mathbb{R}$ are replaced by integrals on $\xi \in [-\hat{T}, \hat{T}]$ with $\hat{T} > 0$:

$$D_{\hat{T}}^{j,j\pm1} \psi(x^j, \pm a) = \frac{1}{\sqrt{2\pi}} \int_{-\hat{T}}^{\hat{T}} \hat{\psi}(\xi) \, e^{\imath\sqrt{\omega^2-\xi^2}(x^j-a)} e^{\pm\imath\xi a} \mathrm{d}\xi,$$

$$\Lambda_{\hat{T}}^j \psi(b, y^j) = \frac{1}{\sqrt{2\pi}} \int_{-\hat{T}}^{\hat{T}} \hat{\psi}(\xi) \, \imath\sqrt{\omega^2-\xi^2} e^{\imath\sqrt{\omega^2-\xi^2}\ell} e^{\imath\xi y^j} \mathrm{d}\xi.$$

To compute these Fourier integrals, we implement a quadrature formula:

$$D_{\hat{T},\mathcal{Q}}^{j,j\pm1} \psi(x^j, \pm a) = \frac{1}{\sqrt{2\pi}} \sum_{\xi_k \in \mathcal{Q}} w_k \, \hat{\psi}(\xi_k) \, e^{\imath\sqrt{\omega^2-\xi_k^2}(x^j-a)} e^{\pm\imath\xi_k a},$$

$$\Lambda_{\hat{T},\mathcal{Q}}^j \psi(b, y^j) = \frac{1}{\sqrt{2\pi}} \sum_{\xi_k \in \mathcal{Q}} w_k \, \hat{\psi}(\xi_k) \imath\sqrt{\omega^2-\xi_k^2} e^{\imath\sqrt{\omega^2-\xi_k^2}\ell} e^{\imath\xi_k y^j}.$$

where ξ_k denotes the quadrature point in a set $\mathcal{Q}$ and w_k denotes the weight. Remark that these integral operators lead to dense blocks in the matrix.

0.4 Numerical Validation

To validate the method, we consider a domain Ω with a unit disk as an obstacle

$$\left| \begin{array}{ll} -\Delta p(\mathbf{x}) - \omega^2 p(\mathbf{x}) = 0 & \text{in } \Omega := \mathbb{R}^2 \backslash \mathcal{O}, \\ p = \dfrac{1}{4\imath} H_0^{(1)}\left(\omega\sqrt{x^2+y^2}\right) & \text{on } \partial\Omega, \end{array} \right.$$

where $H_0^{(1)}$ is the Hankel function of the first kind. The exact solution of this problem is

$$p = \frac{1}{4\imath} H\left(\omega\sqrt{x^2+y^2}\right),$$

which is the fundamental solution of the Helmholtz equation in the plane. We take $\omega = 1 + 0.1\imath$, $a = 4$, $b = 6$, $T = 10$, and $\hat{T} = 10$ and 3rd Gauss-Lagrange quadrature in 1000 intervals. In Figure 4 we show the numerical solution obtained by the HSM method. We compute the relative error on $\Sigma_{a,T}^j$ as

$$err_{rel} = \left\| \frac{\varphi_h^j - \varphi_{exact}^j}{\varphi_{exact}^j} \right\|_{L^2([-T,T])},$$
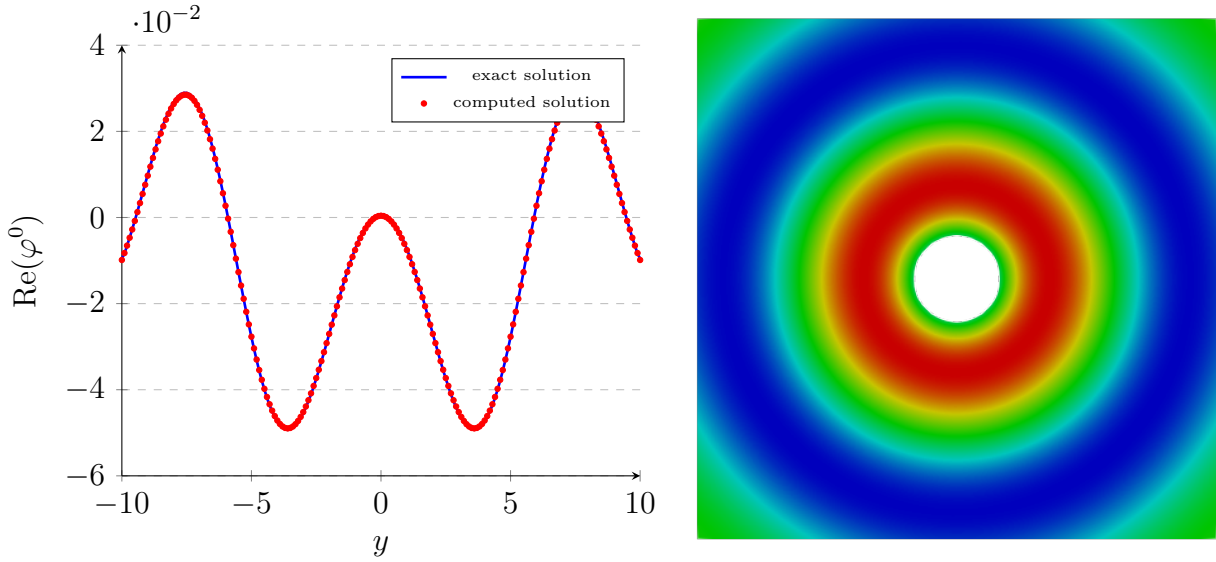
Figure 4: On the left: the real part of φ^0, both the exact solution and the computed solution. On the right: the real part of p^b in Ω_b.

and similarly for p^b in Ω_b. In Figure 4 (a) we compare the real part of the computed solution and the exact solution. Visually, the computed solution of φ_h^0 matches the exact solution φ^0. The relative error for φ^j is 0.82%. In Figure 4 (b), we show the real part of the solution in Ω_b. We obtain a relative L^2 error 1.71%.

Once we obtain the traces φ_h^j, we can use Formula (0.6) to reconstruct the solution in each half-plane. In the overlapping zone, we have 2 possible choices of representations, for example in $\Omega_a^0 \cap \Omega_a^1$ we can reconstruct the solution by using either $P^0(\varphi^0)$ or $P^1(\varphi^1)$. We show that these different representations give the same results, up to a discretization error. In Figure 5, we show the representations in Ω_a^0, Ω_a^1, and the modulus of the difference in $\Omega_a^0 \cap \Omega_a^1$. The values of solutions are in the range $[-0.23, 0.31]$ while the modulus of the difference $|P^0 - P^1|$ is in the range $[0, 0.05]$. We conclude that the representations coincide in the quarter plane.
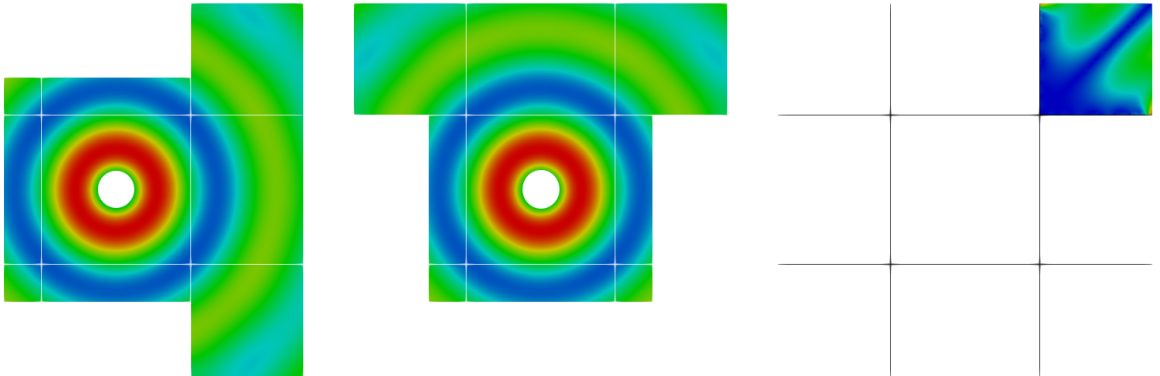
Figure 5: The real part of the representations of the solution in Ω_b and (a) Ω_a^0, (b) Ω_a^1. The modulus of the difference $P^0 - P^1$ is shown in (c).

Finally, we can reconstruct the solution in the whole domain Ω, as shown in Figure 6.

The convergence of this method based on the discretization parameters is studied in Chapter 1.
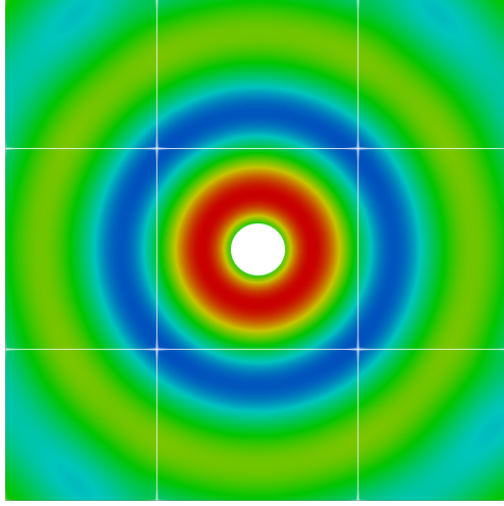
Figure 6: The real part of the representations of the solution in Ω.

0.5   Extension to the anisotropic case

In this last section, we show that the HSM method developed previously can be easily extended to anisotropic problems. We consider the anisotropic Helmholtz equation

$$\left| \begin{aligned} -\nabla \cdot (A\nabla p) - \omega^2 p &= f \text{ in } \Omega := \mathbb{R}\backslash\mathcal{O}, \\ \nabla p \cdot n &= 0 \text{ on } \partial\Omega, \end{aligned} \right. \tag{0.26}$$

where A is a 2×2 symmetric positive definite matrix which models the anisotropy. This matrix satisfies

$$A = \begin{pmatrix} c_1 & c_3 \\ c_3 & c_2 \end{pmatrix}, \text{ where } c_1, c_2 > 0 \text{ and } c_1 c_2 - (c_3)^2 > 0,$$

and it is supposed to be constant in the exterior domain Ω_a^c. By having this condition, Problem (0.26) is well-posed for $\text{Im}(\omega) > 0$.

The half-space representation is derived in a similar manner as the one in the isotropic case. Given any $\psi \in H^{1/2}(\Sigma_a^j)$, $j \in \{0, 1, 2, 3\}$, the solution $P^j \in H^1(\Omega_a^j)$ satisfies the half-space problem

$$\left| \begin{aligned} \nabla \cdot (A\nabla P^j) + \omega^2 P^j &= 0 \text{ in } \Omega^j \\ P^j &= \psi \text{ on } \Sigma_a^j. \end{aligned} \right. \tag{0.27}$$

By applying Fourier transform and taking the $H^1(\Omega_a^j)$ solution, we have a unique solution

$$P^j(x^j, y^j) = \frac{1}{\sqrt{2\pi}} \int_{\mathbb{R}} \hat{\psi}(\xi) e^{\imath r^j(\xi)(x^j - a)} e^{\imath \xi y^j} \mathrm{d}\xi, \tag{0.28}$$

where the r^j's are defined as:

$$\begin{aligned} r^0 = r^2 &= \frac{-\imath\xi c_3}{c_1} + \imath\sqrt{d_1(\xi)} \text{ with } d_1(\xi) = \frac{\omega^2 c_1 - (c_1 c_2 - (c_3)^2)\xi^2}{(c_1)^2}, \\ r^1 = r^3 &= \frac{\imath\xi c_3}{c_1} + \imath\sqrt{d_2(\xi)} \text{ with } d_2(\xi) = \frac{\omega^2 c_2 - (c_1 c_2 - (c_3)^2)\xi^2}{(c_2)^2}. \end{aligned} \tag{0.29}$$

We derive the definition of the operators $D^{j,j\pm1}$ and Λ^j in the same manner as before:

$$D^{j,j\pm1}\varphi^j(x^j, y^j = \pm a) = \frac{1}{\sqrt{2\pi}} \int_{\mathbb{R}} \hat{\varphi}^j(\xi) e^{\imath r^j(\xi)(x^j - a)} e^{\pm\imath\xi a} \mathrm{d}\xi, \tag{0.30}$$

and

$$\Lambda^j \varphi^j(x^j = b, y^j) = \frac{1}{\sqrt{2\pi}} \int_{\mathbb{R}} \hat{\varphi}^j(\xi) r^j(\xi) e^{\imath r^j(\xi)b} e^{\imath \xi y^j} \, \mathrm{d}\xi. \tag{0.31}$$

Finally, we obtain the same formulation, (0.22). The well-posedness of this formulation is shown in [19].

To show that the method works for the anisotropic case, we consider the matrix:

$$A = \begin{pmatrix} 1 & -0.6 \\ -0.6 & 1 \end{pmatrix},$$

and a source term $f = 1$ in a disk centered at $(0,0)$ with a radius of 1, without any obstacle. In Figure 7, we represent the solution in Ω_b and the reconstructed solution in Ω_a^j.
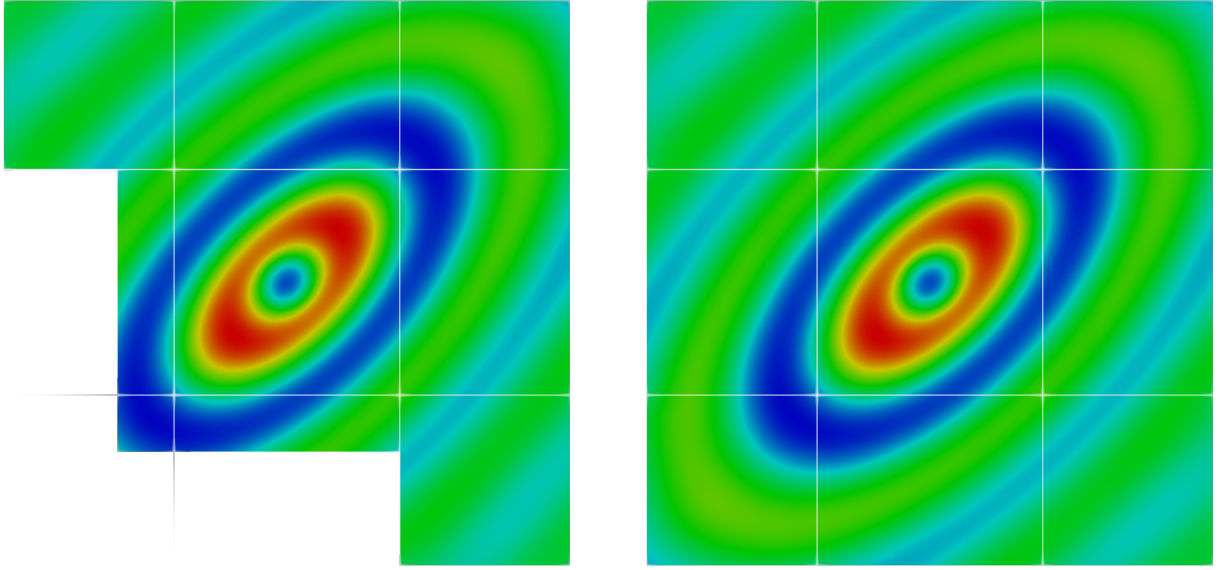
Figure 7: Representations of the real part of the solution in Ω_b and (a) Ω_a^0 and Ω_a^1, (b) in all 4 reconstruction domains.

Chapter 1

Numerical analysis of the HSM method

Summary

1.1 Introduction

1.1.1 Motivation

This study takes place in the general framework of the development of numerical methods for the simulation and the optimization of ultrasonic Non-Destructive Testing (NDT) experiments. NDT consists in detecting defects in an elastic structure by measuring the ultrasonic echoes produced by these defects, when they are illuminated by some incident ultrasonic wave. In particular, one needs to simulate the interaction of a given incident wave with a compactly

supported defect in an infinite medium. When this medium is homogeneous and isotropic, there exist several efficient methods to solve this problem, like Perfectly Matched Layers or integral equations. However, difficulties arise in more complex configurations [18, 70, 14]. Among them, one important case which remains unsolved is the case where the infinite medium is an infinite elastic plate made of an anisotropic homogeneous material.

A new method called the Half-Space Matching (HSM) method (inspired by [32]) has been introduced recently in view of tackling this problem. As a first step, the method has been applied in [19] to the acoustic scalar problem in $\mathbb{R}^2$, showing that anisotropy can be taken into account easily, without any additional cost. The method mainly relies on a decomposition of the infinite domain, exterior to the obstacle, into the union of several overlapping half-spaces, where a Fourier-integral representation of the solution is available.

In this first version of the method, the unknowns of the Fourier-integral equations are the Dirichlet traces of the field on the boundaries of the different half-spaces. But with this choice, the method cannot be extended to the case of the elastic plate, where both the traces of the displacement and of the normal stress are required to derive the half-plate representations. This is a first motivation of the present paper where we consider still a scalar problem but with different types of traces, including Neumann, Dirichlet, and Robin traces.

The content of the present paper is the following. We first derive the HSM formulation for general types of traces. Then we prove the well-posedness of the continuous problem by adapting the arguments used in [19]. More importantly, the main contribution of this paper is the numerical analysis of the discretized formulation which is not straightforward and has never been addressed in previous works.

The model problem that we consider is presented in the next subsection. The corresponding HSM formulation is the object of Section 1.2. Section 1.3 is devoted to the theoretical analysis of the formulation: we use Fredholm theory, the main tools being the Mellin transform [29, 52] and Hilbert-Schmidt operators [58, p.210]. The discretization aspects are detailed in Section 1.4 and error estimates are derived for an appropriate Fourier discretization. Some numerical results are finally presented in Section 1.5.

1.1.2   The model problem

The problem that we consider is the 2D Helmholtz equation in the exterior of a compact convex polygonal obstacle $\mathcal{O}$, with a boundary condition of Robin type. More precisely, the problem takes the following form where ω, α and β are some complex constants whose characteristics are specified below, ν denotes the outgoing normal to $\mathcal{O}$ and the data is a given function g defined on the boundary of the obstacle $\partial\mathcal{O}$:

$$\left|\begin{array}{ll} \Delta p + \omega^2 p = 0 & \text{in } \Omega = \mathbb{R}^2 \backslash \mathcal{O}, \\[2mm] \alpha p + \beta \dfrac{\partial p}{\partial \nu} = g & \text{on } \partial\mathcal{O}. \end{array}\right. \tag{1.1}$$

In the sequel, we will use the following assumptions:

$$\text{Im}\,\omega > 0,\ \beta \neq 0, \text{Im}\left(\frac{\alpha}{\beta\omega}\right) \geq 0,\ \text{and } g \in L^2(\partial\mathcal{O}), \tag{1.2}$$

which lead to several results as follows.

1. Since $\text{Im}\,\omega > 0$ (which can be justified in a dissipative medium), we will look for a solution p which belongs to $H^1(\Omega)$. More precisely, p is exponentially decaying at infinity and satisfies

$$\forall \varepsilon < \text{Im}(\omega), \quad (x, y) \mapsto p(x, y)\, e^{\varepsilon \sqrt{x^2+y^2}} \in H^1(\Omega). \tag{1.3}$$

However, we emphasize that the numerical method also works in the non-dissipative case, that is when $\omega \in \mathbb{R}^+$. In this latter case, p is chosen as the outgoing solution of (1.1) (defined as the unique solution satisfying the Sommerfeld condition) .

2. As $\beta \neq 0$, the problem (1.1) admits the following variational formulation:

$$\left| \begin{array}{l} \text{Find } p \in H^1(\Omega) \text{ such that for all } q \in H^1(\Omega) \\ \displaystyle\int_\Omega \nabla p \cdot \overline{\nabla q} - \omega^2 \int_\Omega p\,\bar{q} - \frac{\alpha}{\beta} \int_{\partial\mathcal{O}} p\,\bar{q} = \frac{-1}{\beta} \int_{\partial\mathcal{O}} g\,\bar{q}. \end{array} \right. \tag{1.4}$$

Using the fact that for $p \in H^1(\Omega)$:

$$\text{Im}\left(\frac{-1}{\omega} \left(\int_\Omega |\nabla p|^2 - \omega^2 |p|^2 - \frac{\alpha}{\beta} \int_{\partial\mathcal{O}} |p|^2 \right) \right) =$$
$$\frac{\text{Im}(\omega)}{|\omega|^2} \int_\Omega |\nabla p|^2 + \text{Im}(\omega) \int_\Omega |p|^2 + \text{Im}\left(\frac{\alpha}{\beta\omega} \right) \int_{\partial\mathcal{O}} |p|^2,$$

one deduces, due to the assumption that $\text{Im}\left(\dfrac{\alpha}{\beta\omega} \right) \geq 0$, that the bilinear form is coercive. Then the problem is well-posed by Lax-Milgram theorem.

Remark 1.1.1. *For the data g on the boundary, we make the assumption $g \in L^2(\partial\mathcal{O})$, which is convenient for our approach, and which differs from the natural one ($g \in H^{-\frac{1}{2}}(\partial\mathcal{O})$) that would be used in a variational approach. In particular, since $g \in L^2(\partial\mathcal{O})$, we know from classical regularity results [35] that $p \in H^{3/2}(\Omega)$.*

Remark 1.1.2 (The Dirichlet case)**.** *Taking $\beta = 0$ and $\alpha \neq 0$ in (1.1), one simply recovers a Dirichlet boundary condition (a case which has been already treated in [19]). In that case, the natural hypothesis in a variational approach would be $g \in H^{\frac{1}{2}}(\partial\mathcal{O})$. We point out that our approach allows to consider more general Dirichlet data which are only in $L^2(\partial\mathcal{O})$. As a consequence, the solution may not be in H^1 up to the boundary (see [4] for a similar problem). Note that the numerical analysis performed in Section 1.4 is also valid in the Dirichlet case, which is illustrated numerically in Section 1.5.3.*

1.2 The Half-Space Matching formulation

The Half-Space Matching method consists in coupling several analytical representations of the solution in half-planes surrounding the obstacle.

1.2.1   Geometry and notations

Let us consider a convex polygon $\mathcal{O}$ with n edges $\Sigma_{\mathcal{O}}^j$, $j = 0, \ldots, n-1$. For convenience, we introduce $\mathbb{Z}/n\mathbb{Z}$ the ring of integers modulo n. For $j \in \mathbb{Z}/n\mathbb{Z}$, the angle between $\Sigma_{\mathcal{O}}^j$ and $\Sigma_{\mathcal{O}}^{j+1}$ is denoted as $\theta^{j,j+1}$ or equivalently $\theta^{j+1,j}$. Because of the convexity, one has

$$0 < \theta^{j,j+1} < \pi. \tag{1.5}$$
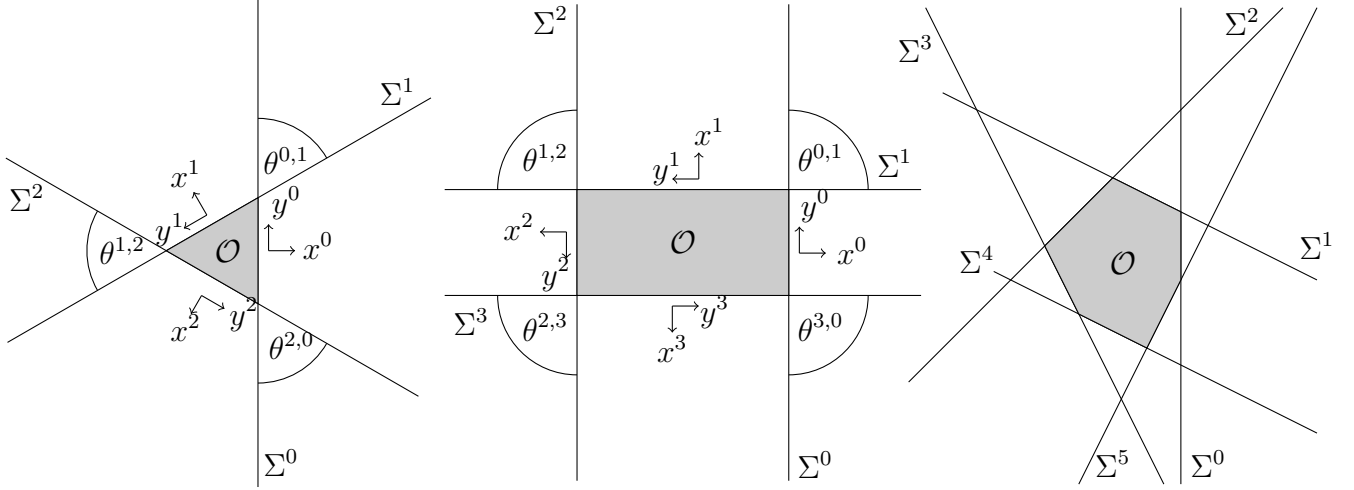
Figure 1.1: Examples of polygons $\mathcal{O}$ for $n = 3, 4$ and 6 and associated notations.

To define the half-spaces, we introduce several local coordinate systems (x^j, y^j). The origin of all of them is the centroid O of the polygon $\mathcal{O}$. We choose the reference Cartesian coordinate system $(O, \mathbf{e}_x^0, \mathbf{e}_y^0)$ such that $\mathbf{e}_x^0$ is orthogonal to $\Sigma_{\mathcal{O}}^0$ and oriented to the exterior of the polygon, while the axis $\mathbf{e}_y^0$ is $\pi/2$ counter clockwise to $\mathbf{e}_x^0$. The other local coordinate systems $(O, \mathbf{e}_x^j, \mathbf{e}_y^j)$ are defined recursively as follows:

$$\forall j \in \mathbb{Z}/n\mathbb{Z}, \quad \left| \begin{array}{l} \mathbf{e}_x^{j+1} = -\cos\theta^{j,j+1}\mathbf{e}_x^j + \sin\theta^{j,j+1}\mathbf{e}_y^j, \\ \mathbf{e}_y^{j+1} = -\sin\theta^{j,j+1}\mathbf{e}_x^j - \cos\theta^{j,j+1}\mathbf{e}_y^j. \end{array} \right. \tag{1.6}$$

If we define l^j as the distance of the centroid of the polygon to the edge $\Sigma_{\mathcal{O}}^j$, each half-plane Ω^j is defined in the local coordinate system $(O, \mathbf{e}_x^j, \mathbf{e}_y^j)$ as

$$\forall j \in \mathbb{Z}/n\mathbb{Z},, \quad \Omega^j = \{x^j \geq l^j\} \times \{y^j \in \mathbb{R}\},$$

and its boundary denoted by Σ^j is given by

$$\Sigma^j = \{x^j = l^j\} \times \{y^j \in \mathbb{R}\}.$$

1.2.2   Half-space problems

The jth half-space problem is defined as follows: given $\psi^j \in L^2(\Sigma^j)$, $P^j(\psi^j)$ is the unique solution in $H^1(\Omega^j)$ of

$$\left| \begin{array}{ll} \Delta P^j + \omega^2 P^j = 0, & \text{in } \Omega^j, \\ \alpha P^j + \beta \dfrac{\partial P^j}{\partial x^j} = \psi^j & \text{on } \Sigma^j. \end{array} \right. \tag{1.7}$$

This problem is well-posed under assumptions (1.2) for the same reasons than the ones detailed in Section 1.1.2. Remark again that in the usual framework, we would take $\psi^j \in H^{-1/2}(\Sigma^j)$, but here we take $\psi^j \in L^2(\Sigma^j)$. Applying the Fourier transform in y^j defined as

$$\forall \psi^j \in L^2(\Sigma^j), \quad \hat{\psi}^j(\xi) = \frac{1}{\sqrt{2\pi}} \int_{\mathbb{R}} \psi^j(y^j) e^{-\imath \xi y^j} \mathrm{d}y^j, \tag{1.8}$$

we obtain the following ordinary differential equation in x^j, parametrized by the Fourier variable ξ:

$$\left| \begin{array}{ll} \dfrac{\partial^2 \hat{P}^j}{(\partial x^j)^2} + (\omega^2 - \xi^2)\hat{P}^j = 0, & x^j > l^j, \\[4mm] \alpha \hat{P}^j + \beta \dfrac{\partial \hat{P}^j}{\partial x^j} = \hat{\psi}^j, & x^j = l^j, \end{array} \right. \tag{1.9}$$

whose unique L^2 solution is given by

$$\hat{P}^j(x^j, \xi) = A(\xi) e^{\imath \sqrt{\omega^2 - \xi^2}(x^j - l^j)}, \tag{1.10}$$

where $\mathrm{Im}\sqrt{\omega^2 - \xi^2} > 0$ and

$$\left(\alpha + \imath\beta\sqrt{\omega^2 - \xi^2} \right) A(\xi) = \hat{\psi}^j(\xi). \tag{1.11}$$

One can check that, thanks to assumptions (1.2), the quantity $\alpha + \imath\beta\sqrt{\omega^2 - \xi^2}$ never vanishes for $\xi \in \mathbb{R}$. Finally, by taking the inverse Fourier transform, the solution $P^j(\psi^j)$ of (1.7) is given by

$$P^j(x^j, y^j) = \frac{1}{\sqrt{2\pi}} \int_{\mathbb{R}} \frac{\hat{\psi}^j(\xi)}{\alpha + \imath\beta\sqrt{\omega^2 - \xi^2}} e^{\imath\sqrt{\omega^2 - \xi^2}(x^j - l^j)} e^{i\xi y^j} \mathrm{d}\xi. \tag{1.12}$$

1.2.3 Half-space matching integral equations

For the solution p of problem (1.1), let us define the Robin traces

$$\forall j \in \mathbb{Z}/n\mathbb{Z}, \quad \varphi^j := \left(\alpha p + \beta \frac{\partial p}{\partial x^j} \right)\bigg|_{\Sigma^j}. \tag{1.13}$$

Note that $\varphi^j \in L^2(\Sigma^j)$ since $p \in H^{3/2}(\Omega)$. Our objective is to derive integral equations linking the φ^j by using half-space representations of Section 2.2 and the fact that the half-spaces Ω^j overlap. First, the restriction of p in Ω^j is the solution of (1.7) for $\psi = \varphi^j$. By uniqueness,

$$p|_{\Omega^j} = P^j(\varphi^j). \tag{1.14}$$

Then the quantity

$$\left(\alpha p + \beta \frac{\partial p}{\partial x^{j\pm 1}} \right)\bigg|_{\Sigma^{j\pm 1} \cap \Omega^j} \tag{1.15}$$

is equal both to

$$\varphi^{j\pm 1}|_{\Sigma^{j\pm 1} \cap \Omega^j} \quad (\text{ by definition of } \varphi^{j\pm 1})$$

and to

$$\alpha P^j(\varphi^j) + \beta \frac{\partial P^j(\varphi^j)}{\partial x^{j\pm 1}}\bigg|_{\Sigma^{j\pm 1} \cap \Omega^j} \quad (\text{ by } (1.14)).$$

This provides the compatibility relations

$$\varphi^{j\pm 1} = \alpha P^j(\varphi^j) + \beta \frac{\partial P^j(\varphi^j)}{\partial x^{j\pm 1}} \text{ on } \Sigma^{j\pm 1} \cap \Omega^j, \quad \forall j \in \mathbb{Z}/n\mathbb{Z}. \tag{1.16}$$
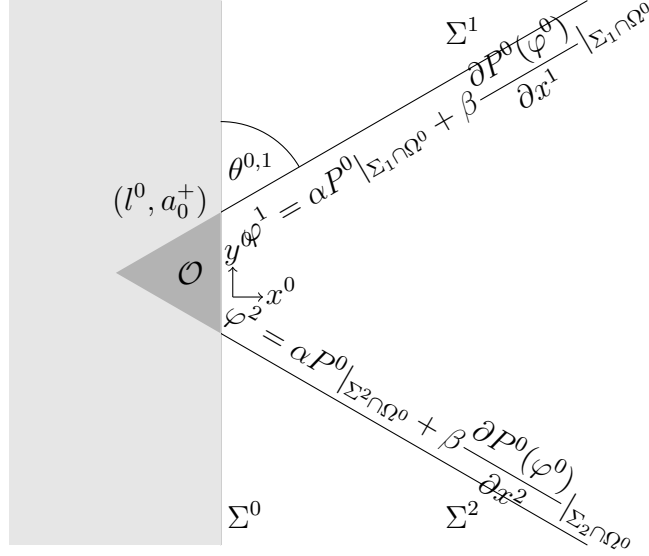
Figure 1.2: Robin traces on $\Sigma^1 \cap \Omega^0$ and $\Sigma^2 \cap \Omega^0$.

Remark 1.2.1.   • *Such compatibility relations have been firstly introduced in [32, 16] for Dirichlet traces in the case of periodic media.*

• *Here we have used the overlap of two consecutive half-spaces Ω^j and $\Omega^{j\pm1}$. This will be sufficient for our formulation, even for polygons with more than four edges where non-consecutive half-spaces may overlap (see Figure 1.1 on the right).*

This leads to introducing the following integral operator

$$D^{j,j\pm1} : L^2(\Sigma^j) \to L^2(\Sigma^{j\pm1} \cap \Omega^j) \tag{1.17}$$

$$\psi \to \alpha P^j(\psi) + \beta \frac{\partial P^j(\psi)}{\partial x^{j\pm1}}\bigg|_{\Sigma^{j\pm1}\cap\Omega^j}, \tag{1.18}$$

which can be expressed, using (1.12), as a kernel operator acting on the Fourier transform

$$\left[D^{j,j\pm1}\psi\right](r) = \frac{1}{\sqrt{2\pi}} \int_{\mathbb{R}} k^{j,j\pm1}(r,\xi)\, \hat{\psi}(\xi)\, \mathrm{d}\xi, \quad r \geq 0 \tag{1.19}$$

with the following kernel

$$k^{j,j\pm1}(r,\xi) = \frac{\alpha + \beta(-\cos(\theta^{j,j\pm1})\imath\sqrt{\omega^2-\xi^2} + \sin(\theta^{j,j\pm1})\imath\xi)}{\alpha + \imath\beta\sqrt{\omega^2-\xi^2}} e^{\imath\sqrt{\omega^2-\xi^2}r\sin(\theta^{j,j\pm1})} e^{\imath\xi(a_j^{\pm}+r\cos(\theta^{j,j\pm1}))}. \tag{1.20}$$

Here, $a_j^{\pm}$ denotes the ordinate of the intersection point of Σ^j and $\Sigma^{j\pm1}$ in (x^j, y^j) local coordinates and r is the radial variable of the polar coordinates centered at this intersection point. If $\theta^{j,j+1} = \pi/2$ (which holds for instance for all j when $\mathcal{O}$ is a rectangle), the previous operator has the simpler form

$$\left[D^{j,j\pm1}\psi\right](r) = \frac{1}{\sqrt{2\pi}} \int_{\mathbb{R}} \frac{\alpha + \imath\beta\xi}{\alpha + \imath\beta\sqrt{\omega^2-\xi^2}} e^{\imath\sqrt{\omega^2-\xi^2}r} e^{\imath\xi a_j^{\pm}} \hat{\psi}(\xi)\mathrm{d}\xi. \tag{1.21}$$

It is not so difficult to see that the operator $D^{j,j\pm1}$ is continuous from $L^2(\Sigma^j)$ to $L^2(\Omega^j \cap \Sigma^{j\pm1})$. Indeed, if $\psi \in L^2(\Sigma^j)$, we can show that $P^j(\psi)$, the solution of the half-space problem (1.7) in

Ω^j, is in $H^{3/2}(\Omega^j)$. It suffices then to use the continuity of the trace operators. Let us remark that it is less obvious when using directly the expression (1.19-1.20) of $D^{j,j\pm1}$, but this will be a by-product of the next section.

Summing up, we have finally the following system of coupled equations satisfied by the φ^j's:

$$\varphi^j = \begin{cases} D^{j-1,j}\varphi^{j-1} & \text{on } \Sigma^j \cap \Omega^{j-1} \\ g & \text{on } \Sigma^j_{\mathcal{O}} \qquad \forall j \in \mathbb{Z}/n\mathbb{Z} \\ D^{j+1,j}\varphi^{j+1} & \text{on } \Sigma^j \cap \Omega^{j+1}, \end{cases} \tag{1.22}$$

where we have used the boundary condition satisfied by p on $\partial\mathcal{O}$. The system of equations (1.22) can be written in a matricial form as

$$(\mathbb{I} - \mathbb{D})\,\Phi = G, \tag{1.23}$$

where

$$\Phi \in V := \{(\varphi^0, \varphi^1, \ldots, \varphi^{n-1}) \in \prod_{j=0}^{n-1} L^2(\Sigma^j)\}, \tag{1.24}$$

$\mathbb{I}$ corresponds to the identity operator, G is given by

$$G := (g^0, g^1, \ldots, g^{n-1}) \in V \quad \text{where } g^j = \begin{cases} g & \text{on } \Sigma^j_{\mathcal{O}}, \\ 0 & \text{otherwise,} \end{cases} \tag{1.25}$$

and $\mathbb{D}$ is given by

$$\mathbb{D} := \begin{bmatrix} 0 & D^{1,0} & 0 & \ldots & 0 & D^{n-1,0} \\ D^{0,1} & 0 & D^{2,1} & \ldots & 0 & 0 \\ 0 & D^{1,2} & 0 & \ldots & 0 & 0 \\ \vdots & \vdots & \vdots & \ddots & \vdots & \vdots \\ 0 & 0 & 0 & \ldots & 0 & D^{n-1,n-2} \\ D^{0,n-1} & 0 & 0 & \ldots & D^{n-2,n-1} & 0 \end{bmatrix}, \tag{1.26}$$

where for all $j \in \mathbb{Z}/n\mathbb{Z}$ we have identified a function of $L^2(\Sigma^j \cap \Omega^{j\pm1})$ to a function of $L^2(\Sigma^j)$ by extending it by 0. Remark then that for all Φ in V, $\mathbb{D}\,\Phi$ is in $\tilde{V}$ where

$$\tilde{V} := \{\tilde{\Phi} = (\tilde{\varphi}^0, \tilde{\varphi}^1, \ldots, \tilde{\varphi}^{n-1}) \in V, \ \tilde{\varphi}^j = 0 \text{ on } \Sigma^j_{\mathcal{O}} \quad \forall j \in \mathbb{Z}/n\mathbb{Z}\}. \tag{1.27}$$

Remark 1.2.2. *If we want to make the extension by 0 explicit, we have to replace in $\mathbb{D}$, $D^{j,j\pm1}$ by $E^{j,j\pm1}D^{j,j\pm1}$ where*

$$\begin{aligned} E^{j,j\pm1} : L^2(\Sigma^{j\pm1} \cap \Omega^j) &\to L^2(\Sigma^{j\pm1}) \\ \psi &\mapsto E^{j,j\pm1}\psi \end{aligned} \tag{1.28}$$

with

$$E^{j,j\pm1}\psi = \begin{cases} \psi \text{ on } \Sigma^{j\pm1} \cap \Omega^j \\ 0 \text{ on } \Sigma^{j\pm1} \setminus (\Sigma^{j\pm1} \cap \Omega^j). \end{cases}$$

All the properties of $D^{j,j\pm1}$ also hold trivially for $E^{j,j\pm1}D^{j,j\pm1}$. In order to enhance readability, we have chosen to drop these extension operators.

Lemma 1.2.3 (Equivalence)*. Let $g \in L^2(\partial\mathcal{O})$. If $p \in H^1(\Omega)$ is solution of (1.1) then $\Phi = (\varphi^0, \varphi^1, \ldots, \varphi^{n-1})$ where φ^j is defined by (1.13) belongs to V and is a solution of (1.23).*

Conversely, if $\Phi \in V$ is a solution of (1.23), then p satisfying (1.14) for all $j \in \mathbb{Z}/n\mathbb{Z}$ is a function defined "unequivocally" in Ω. Moreover, $p \in H^1(\Omega)$ and is solution of (1.1).

Proof. The first assertion is true by construction. Conversely, suppose that $\Phi = (\varphi^0, \ldots, \varphi^{n-1}) \in V$ is solution of (1.23). This implies that the φ^j's satisfy the system of coupled equations (1.22). Now, let us introduce $P^j(\varphi^j) \in H^1(\Omega^j)$ for all $j \in \mathbb{Z}/n\mathbb{Z}$, the solution of the half-space problem (1.7) with $\psi = \varphi^j$. By definition:

$$\varphi^j = \alpha P^j(\varphi^j) + \beta \frac{\partial P^j(\varphi^j)}{\partial x^j}\Big|_{\Sigma^j}. \tag{1.29}$$

Because the φ^j's satisfy the first set of equations of (1.22), we have by definition of $D^{j\pm1,j}$ that

$$\varphi^j = \alpha P^{j\pm1}(\varphi^{j\pm1}) + \beta \frac{\partial P^{j\pm1}(\varphi^{j\pm1})}{\partial x^j} \quad \text{on } \Sigma^j \cap \Omega^{j\pm1}, \quad \forall j \in \mathbb{Z}/n\mathbb{Z}. \tag{1.30}$$

From (1.29) and (1.30), we have that

$$\alpha P^j(\varphi^j) + \beta \frac{\partial P^j(\varphi^j)}{\partial x^j}\Big|_{\Sigma^j \cap \Omega^{j\pm1}} = \alpha P^{j\pm1}(\varphi^{j\pm1}) + \beta \frac{\partial P^{j\pm1}(\varphi^{j\pm1})}{\partial x^j}\Big|_{\Sigma^j \cap \Omega^{j\pm1}}.$$

In particular, the previous relations for $j = 0$ and $\pm = +$ and for $j = 1$ and $\pm = -$ yield to

$$\alpha P^0(\varphi^0) + \beta \frac{\partial P^0(\varphi^0)}{\partial x^0}\Big|_{\Sigma^0 \cap \Omega^1} = \alpha P^1(\varphi^1) + \beta \frac{\partial P^1(\varphi^1)}{\partial x^0}\Big|_{\Sigma^0 \cap \Omega^1}$$

and

$$\alpha P^1(\varphi^1) + \beta \frac{\partial P^1(\varphi^1)}{\partial x^1}\Big|_{\Sigma^1 \cap \Omega^0} = \alpha P^0(\varphi^0) + \beta \frac{\partial P^0(\varphi^0)}{\partial x^1}\Big|_{\Sigma^1 \cap \Omega^0}.$$

Let

$$Q = P^0(\varphi^0) - P^1(\varphi^1) \quad \text{in } \Omega^0 \cap \Omega^1.$$

Because $P^0(\varphi^0)$ and $P^1(\varphi^1)$ satisfy the same Helmholtz equation and because of the previous relations, Q satisfies the problem

$$\left|\begin{array}{ll} \Delta Q + \omega^2 Q = 0 & \text{in } \Omega^0 \cap \Omega^1, \\ \alpha Q + \beta \dfrac{\partial Q}{\partial \nu} = 0 & \text{on } \partial(\Omega^0 \cap \Omega^1), \end{array}\right.$$

where ν is the interior normal to $\Omega^0 \cap \Omega^1$. This problem is well-posed under assumptions (1.2) for the same reasons as the ones detailed in Section 1.1.2. So $Q = 0$ in $\Omega^0 \cap \Omega^1$ which means that $P^0(\varphi^0)$ and $P^1(\varphi^1)$ coincide in the overlapping zone $\Omega^0 \cap \Omega^1$.

Similar arguments enable us to show that for all $j \in \mathbb{Z}/n\mathbb{Z}$, $P^j(\varphi^j)$ and $P^{j+1}(\varphi^{j+1})$ coincide in the overlapping zone $\Omega^j \cap \Omega^{j+1}$. We can then define unequivocally a function p by

$$\forall j \in \mathbb{Z}/n\mathbb{Z}, \quad p|_{\Omega^j} = P^j(\varphi^j).$$

Because the half-space solutions coincide two by two in the overlapping zones, the function p is in $H^1(\Omega)$ and is solution of the Helmholtz equation in Ω. Moreover, by definition

$$\forall j \in \mathbb{Z}/n\mathbb{Z}, \quad \left(\alpha p + \beta \frac{\partial p}{\partial x^j}\right)\Big|_{\Sigma_\mathcal{O}^j} = \left(\alpha P^j(\varphi^j) + \beta \frac{\partial P^j(\varphi^j)}{\partial x^j}\right)\Big|_{\Sigma_\mathcal{O}^j} = \varphi^j\Big|_{\Sigma_\mathcal{O}^j} = g,$$

where the last equality is obtained by using the second set of equations of (1.22). Hence, the function p is then solution of (1.1). $\qquad\square$

Writing

$$\Phi = G + \tilde{\Phi} \tag{1.31}$$

where $\tilde{\Phi}$ is in $\tilde{V}$, we obtain an equivalent system

$$(\mathbb{I} - \mathbb{D})\,\tilde{\Phi} = \mathbb{D}\,G. \tag{1.32}$$

This system constitutes the Half-Space Matching formulation which will be analyzed in Section 1.3.

1.3 Analysis of the continuous formulation

In this section, we consider the general problem

$$\text{Find } \tilde{\Phi} \in \tilde{V}, \quad (\mathbb{I} - \mathbb{D}) \tilde{\Phi} = F, \tag{1.33}$$

where $\tilde{V}$ is defined in (1.27), $\mathbb{D}$ is defined in (1.26), and $F \in \tilde{V}$. Denoting $\mathcal{L}(A)$ as the set of bounded linear operators of a vector space A, we show in this section the following main results.

Theorem 1.3.1. *The operator* $(\mathbb{I} - \mathbb{D}) \in \mathcal{L}(\tilde{V})$ *is the sum of a coercive operator and a compact one. Moreover, Problem* (1.33) *is well-posed.*

A naive idea would be that $\mathbb{D} \in \mathcal{L}(\tilde{V})$ is compact, but it is not. However, it can be decomposed as the sum of an operator of norm strictly less than 1 and a compact operator. This decomposition is linked to a similar decomposition of the operators $D^{j,j\pm 1}$. Inspired by the proofs for the Dirichlet case shown in [19], we prove the properties of the operators for the Robin case in Section 1.3.1 and finally show the theorem in Section 1.3.2.

1.3.1 Properties of the operators $D^{j,j\pm 1}$

Let us concentrate first on the operator $D^{0,1}$ and similar properties will be given, without proof, for all the operators $D^{j,j\pm 1}$ at the end of this section. To simplify the notation, we denote in this section, $D^{0,1} = D$, $x^0 = x$, $y^0 = y$. We will identify, when necessary, Σ^0 to $\mathbb{R}$, its upper part $\Sigma^0 \cap \Omega^1$ to $(a_0^+, +\infty)$, its lower part $\Sigma^0 \cap \Omega^{n-1}$ to $(-\infty, a_0^-)$ and finally $\Sigma^1 \cap \Omega^0$ to $\mathbb{R}^+$. Let us also introduce for any open interval I included in J, an open interval of $\mathbb{R}$, the restriction operator χ_I

$$
\begin{array}{rcl}
\chi_I : L^2(J) & \to & L^2(J) \\
\varphi & \mapsto & \left|
\begin{array}{l}
\chi_I \varphi = \varphi \text{ on } I \\
\chi_I \varphi = 0 \text{ on } J \setminus I
\end{array}
\right.
\end{array}
$$

In the sequel, we are going to decompose the operator D progressively in order to isolate a compact part and a part for which we get the norm explicitly.

First, from the definition (1.17), we can decompose simply D as

$$D = D_D + D_N \tag{1.34}$$

where

$$
\begin{array}{rclcrcl}
D_D : L^2(\Sigma^0) & \to & L^2(\Sigma^1 \cap \Omega^0) & & D_N : L^2(\Sigma^0) & \to & L^2(\Sigma^1 \cap \Omega^0) \\
\psi & \mapsto & \alpha P^0(\psi)\big|_{\Sigma^1 \cap \Omega^0} & \text{and} & \psi & \mapsto & \beta \dfrac{\partial P^0(\psi)}{\partial x^1}\Big|_{\Sigma^1 \cap \Omega^0}.
\end{array} \tag{1.35}
$$

Lemma 1.3.2. *The operator* $D_D : L^2(\Sigma^0) \to L^2(\Sigma^1 \cap \Omega^0)$ *is compact.*

Proof. By definition of D_D, we have

$$\forall \psi \in L^2(\Sigma^0), \quad D_D \psi\,(r) = \int_{\mathbb{R}} k_D(\xi, r) \hat{\psi}(\xi) \, \mathrm{d}\xi$$

with

$$k_D(\xi, r) = \frac{\alpha}{\alpha + \imath \beta \sqrt{\omega^2 - \xi^2}} \, e^{\imath \sqrt{\omega^2 - \xi^2}\, r \sin \theta^{0,1}} \, e^{\imath \xi (a_0^+ + r \cos \theta^{0,1})}.$$

Using Fubini's theorem, we obtain

$$\|k_D(\xi, r)\|^2_{L^2(\mathbb{R} \times \mathbb{R}^+)} = \int_{\mathbb{R}} \int_{\mathbb{R}^+} \frac{|\alpha|^2}{\left|\alpha + \imath\beta\sqrt{\omega^2 - \xi^2}\right|^2} e^{-2\,\mathrm{Im}(\sqrt{\omega^2 - \xi^2})r\sin\theta^{0,1}} \mathrm{d}r\mathrm{d}\xi$$

$$= \int_{\mathbb{R}} \frac{|\alpha|^2}{2\,\mathrm{Im}(\sqrt{\omega^2 - \xi^2})\,\sin\theta\,\left|\alpha + \imath\beta\sqrt{\omega^2 - \xi^2}\right|^2} \mathrm{d}\xi$$

$$< +\infty.$$

This proves that D_D is the composition of the Fourier operator $\psi \mapsto \hat{\psi}$ and of a Hilbert-Schmidt operator [61]. The lemma follows. $\square$

Let us focus now on D_N. For all ψ, $D_N\psi$ is, up to the parameter β, the normal trace on $\Sigma^1 \cap \Omega^0$ of the half-space solution $P^0(\psi)$ in Ω^0 with a Robin data ψ on the boundary Σ^0. Because the half-line $\Sigma^1 \cap \Omega^0$ touches Σ^0, the operator D_N is not compact. The lack of compactness is precisely due to the intersection point. So let us isolate the intersection point by decomposing D_N thanks to restriction operators:

$$D_N = \chi_{(0,b)}D_N + \chi_{(b,+\infty)}D_N, \quad \text{with } b > 0. \tag{1.36}$$
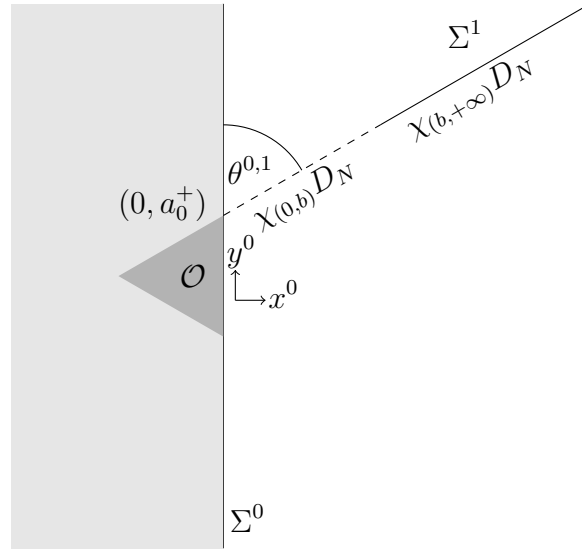
Figure 1.3: Decomposition of the operator D_N into $\chi_{(0,b)}D_N$ and $\chi_{(b,+\infty)}D_N$ with a regular triangle as the obstacle.

Lemma 1.3.3. *For any $b > 0$, the operator $\chi_{(b,+\infty)}D_N : L^2(\Sigma^0) \to L^2(\Omega^0 \cap \Sigma^1)$ is compact.*

Proof. By definition of D_N, we have

$$\forall \psi \in L^2(\Sigma^0), \quad D_N\psi\,(r) = \int_{\mathbb{R}} k_N(\xi, r)\hat{\psi}(\xi)\,\mathrm{d}\xi$$

with

$$k_N(\xi, r) = \frac{\beta\left(-\imath\sqrt{\omega^2 - \xi^2}\cos\theta^{0,1} + \imath\xi\sin\theta^{0,1}\right)}{\alpha + \imath\beta\sqrt{\omega^2 - \xi^2}} e^{\imath\sqrt{\omega^2 - \xi^2}r\sin\theta^{0,1}} e^{\imath\xi(a_0^+ + r\cos\theta^{0,1})}. \tag{1.37}$$

Again by Fubini's theorem, we get for $b > 0$

$$\|k_N(\xi, r)\|^2_{L^2(\mathbb{R}\times(b,+\infty))} = \int_\mathbb{R} \int_b^{+\infty} \frac{|\beta|^2 \left| -\imath\sqrt{\omega^2 - \xi^2} \cos\theta^{0,1} + \imath\xi \sin\theta^{0,1} \right|^2}{\left| \alpha + \imath\beta\sqrt{\omega^2 - \xi^2} \right|^2} e^{-2\operatorname{Im}(\sqrt{\omega^2-\xi^2})r\sin\theta^{0,1}} \mathrm{d}r\mathrm{d}\xi$$

$$= \int_\mathbb{R} \frac{|\beta|^2 \left| -\imath\sqrt{\omega^2 - \xi^2}\cos\theta^{0,1} + \imath\xi\sin\theta^{0,1} \right|^2}{2\operatorname{Im}(\sqrt{\omega^2 - \xi^2})\sin\theta^{0,1} \left| \alpha + \imath\beta\sqrt{\omega^2 - \xi^2} \right|^2} e^{-2\operatorname{Im}(\sqrt{\omega^2-\xi^2})b\sin\theta^{0,1}} \mathrm{d}\xi$$

$$< +\infty.$$

We conclude as in the proof of Lemma 1.3.2. $\qquad\square$

As you can notice, this proof requires that $b > 0$. To analyse the non compact part $\chi_{(0,b)}D_N$, inspired by the Dirichlet case [19] and more generally by the singularity theory [52], we decompose finally $\chi_{(0,b)}D_N$ as

$$\chi_{(0,b)} D_N = \chi_{(0,b)} L_N + \chi_{(0,b)} (D_N - L_N)$$

where L_N is obtained by taking $\omega = 0$ and $\alpha = 0$ in the expression (1.37) of $k_N(\xi, r)$

$$L_N\psi(r) = \frac{1}{\sqrt{2\pi}} \int_\mathbb{R} \hat{\psi}(\xi)(-\cos\theta^{0,1} - \imath\operatorname{sgn}(\xi)\sin\theta^{0,1})e^{-|\xi|r\sin\theta^{0,1}}e^{\imath\xi(a_0^+ + r\cos\theta^{0,1})}\mathrm{d}\xi, \quad r > 0. \quad (1.38)$$

The operator L_N is similar to D_N, but it is associated with the Laplace operator. Indeed, it can also be defined as

$$L_N : L^2(\Sigma^0) \to L^2(\Sigma^1 \cap \Omega^0),$$

$$L_N\psi := \beta \left. \frac{\partial}{\partial x^1} v(\psi) \right|_{\Sigma^1 \cap \Omega^0}, \qquad (1.39)$$

where, for all $\psi \in L^2(\Sigma^0)$, $v(\psi)$ is the solution (at least in the distributional sense) to

$$\left|\begin{array}{ll} -\Delta v = 0 & \text{in } \Omega^0, \\ \beta\dfrac{\partial v}{\partial x} = \psi & \text{on } \Sigma^0. \end{array}\right.$$

We refer to Appendix A for the precise definition of the appropriate functional framework for this problem.

Lemma 1.3.4. *The operator $\chi_{(0,b)}(D_N - L_N)$ is compact.*

Proof. It is a kernel operator whose kernel is given by

$$k(\xi, r) = \left(c_1(\xi)e^{\imath\sqrt{\omega^2-\xi^2}r\sin\theta^{0,1}} - c_2(\xi)e^{-|\xi|r\sin\theta^{0,1}} \right) e^{\imath\xi(a^+ + r\cos\theta^{0,1})}$$

where from (1.37) and (1.38), we have that

$$c_1, c_2, 1/c_2 \in L^\infty(\mathbb{R}), \quad \text{and} \quad \left|\frac{c_1(\xi)}{c_2(\xi)}\right| \to 1 \text{ when } \xi \to +\infty$$

Consequently

$$|k(\xi, r)| = |c_2(\xi)| e^{-|\xi|r\sin\theta^{0,1}} \left| \frac{c_1(\xi)}{c_2(\xi)} e^{-q(\xi) r\sin\theta^{0,1}} - 1 \right|$$

where
$$q(\xi) = \sqrt{\xi^2 - \omega^2} - |\xi| = \frac{-\omega^2}{\sqrt{\xi^2 - \omega^2} + |\xi|} = \mathcal{O}(\frac{1}{\xi}).$$

We deduce that
$$|k(\xi, r)| \leq C|q(\xi)| \, e^{-|\xi| r \sin \theta^{0,1}}$$

which enables us to conclude as in the proof of Lemma 1.3.2.   □

Finally, let us focus on the properties of L_N which are summarized in this fundamental lemma.

Lemma 1.3.5. *The operator L_N is continuous from $L^2(\Sigma^0)$ to $L^2(\Sigma^1 \cap \Omega^0)$ and its norm is bounded by 1. Moreover, we have*

- $\exists C \in (0, 1), \quad \forall \varphi \in L^2(\Sigma^0), \quad \|L_N \chi_{(a_0^+, +\infty)} \varphi\| \leq C \|\chi_{(a_0^+, +\infty)} \varphi\|;$

- $L_N \chi_{(-\infty, a_0^-)}$ *is a compact operator.*

We give the proof which is quite technical in Appendix A. As we will see in the proof of Theorem 1.3.1, it is not sufficient to know that the norm of L_N is bounded by 1. This is the second part of the lemma which will enable us to conclude that $\mathbb{I} - \mathbb{D}$ is a sum of a coercive operator and a compact one. As indicated in Appendix A, the constant C is linked to the angle $\theta^{0,1}$ between Σ^0 and $\Sigma^1 \cap \Omega^0$:
$$C = \cos(\theta^{0,1}/2).$$

When $\theta^{0,1}$ tends to 0, this constant tends to 1.

Gathering all the results of this section, we can show the following properties of D.

Proposition 1.3.6. *The operator D is such that $D - L$ is a compact operator from $L^2(\Sigma^0)$ to $L^2(\Sigma^1 \cap \Omega^0)$ where L is a continuous operator from $L^2(\Sigma^0)$ to $L^2(\Sigma^1 \cap \Omega^0)$ which satisfies*

- $\exists C \in (0, 1), \quad \forall \varphi \in L^2(\Sigma^0), \quad \|L \chi_{(a_0^+, +\infty)} \varphi\| \leq C \|\chi_{(a_0^+, +\infty)} \varphi\|;$

- $L \chi_{(-\infty, a_0^-)}$ *is a compact operator.*

Proof. The operator L is nothing else but $\chi_{(0,b)} L_N$. Indeed, using all the operators introduced in this section, we write
$$D - \chi_{(0,b)} L_N = \chi_{(0,b)} (D_N - L_N) + \chi_{(b, +\infty)} D_N + D_D.$$

From Lemmas 1.3.2, 1.3.3 and 1.3.4, we have that the operator $D - \chi_{(0,b)} L_N$ is compact. As L_N satisfies Lemma 1.3.5, the operator $\chi_{(0,b)} L_N$ inherits similar properties.   □

Finally, we have obviously similar results for all the operators $D^{j,j\pm1}$ for $j \in \mathbb{Z}/n\mathbb{Z}$. Again, we will identify, when necessary, Σ^j to $\mathbb{R}$, its upper part $\Sigma^j \cap \Omega^{j+1}$ to $(a_j^+, +\infty)$, its lower part $\Sigma^j \cap \Omega^{j-1}$ to $(-\infty, a_j^-)$. Finally, in order to give a short statement of the following theorem, we use the notation
$$\forall j, \quad (a_j^-, -\infty) = (-\infty, a_j^-).$$

Theorem 1.3.7. *The operator $D^{j,j\pm1}$ is such that $D^{j,j\pm1} - L^{j,j\pm1}$ is a compact operator from $L^2(\Sigma^j)$ to $L^2(\Sigma^{j\pm1} \cap \Omega^j)$ where $L^{j,j\pm1}$ is a continuous operator from $L^2(\Sigma^j)$ to $L^2(\Sigma^{j\pm1} \cap \Omega^j)$ which satisfies*

- $\exists C^{j,j\pm1} \in (0,1)$, $\forall \varphi \in L^2(\Sigma^j)$, $\quad \|L^{j,j\pm1}\chi_{(a_j^\pm,\pm\infty)}\varphi\| \leq C^{j,j\pm1}\|\chi_{(a_j^\pm,\pm\infty)}\varphi\|$;

- $L^{j,j\pm1}\chi_{(a_j^\mp,\mp\infty)}$ is a compact operator from $L^2(\Sigma^j)$ to $L^2(\Sigma^{j\pm1} \cap \Omega^j)$.

Remark 1.3.8. *The constant $C^{j,j\pm1}$ is linked to the angle $\theta^{j,j\pm1}$ between Σ^j and $\Sigma^{j\pm1} \cap \Omega^j$. More precisely, we can show, as in Appendix A, that*

$$C^{j,j\pm1} = \cos(\theta^{j,j\pm1}/2).$$

Remark 1.3.9. *Theorem 1.3.7 has links with classical analysis for second kind boundary equations on non-smooth domains. Indeed, using the notation $\mathbf{x}^j = (x^j, y^j)$, $D^{j,j\pm1}$ can be written in layer-potential form as*

$$D^{j,j\pm1}\psi^j(\mathbf{x}) = -\frac{1}{\beta}\int_{\Sigma^j}\left(\alpha G(\mathbf{x},\mathbf{x}^j) + \beta\frac{\partial G}{\partial x^{j\pm1}}(\mathbf{x},\mathbf{x}^j)\right)\psi^j(\mathbf{x}^j)\mathrm{d}\mathbf{x}^j, \quad \mathbf{x} \in \Sigma^{j\pm1}\cap\Omega^j, \quad (1.40)$$

where G is the Green's function for the Helmholtz equation satisfying the Robin condition on Σ^j (see for instance [24] for a characterization of G). Formula (1.19) is nothing else but the Plancherel equality applied to (1.40). As G is a smooth perturbation of the Green's function of the Laplace equation with Neumann boundary condition on Σ^j [49], and as $\mathrm{Im}(\omega) > 0$, the properties of $D^{j,j\pm1}$ can be deduced from those of the double layer potential operator defined by

$$\int_{\Sigma^j}\frac{\partial G_0}{\partial x^{j\pm1}}(\mathbf{x},\mathbf{x}^j)\psi^j(\mathbf{x}^j)\mathrm{d}\mathbf{x}^j, \quad \mathbf{x} \in \Sigma^{j\pm1}\cap\Omega^j,$$

where

$$G_0(\mathbf{x},\mathbf{x}') = \frac{1}{2\pi}\log(|\mathbf{x}-\mathbf{x}'|).$$

This operator, as an operator acting on L^2 functions on the sides of a bounded polygon has been discussed and analyzed in [23, 7]. Let us mention that in [23, Lemma 1], the same bound for the norm of the operator $L^{j,j\pm1}$ has been found.

1.3.2 Proof of Theorem 1.3.1

Let us prove now that the operator $\mathbb{I} - \mathbb{D}$ is the sum of a coercive operator and a compact one in $\tilde{V}$. Using Theorem 1.3.7, and the following obvious decomposition

$$\forall\tilde{\Phi} = (\tilde{\varphi}^0, \tilde{\varphi}^1, \ldots, \tilde{\varphi}^{n-1}) \in \tilde{V}, \quad \forall j \in \mathbb{Z}/n\mathbb{Z}, \quad \tilde{\varphi}^j = \chi_{(-\infty,a_j^-)}\tilde{\varphi}^j + \chi_{(a_j^+,+\infty)}\tilde{\varphi}^j$$

we can decompose the operator $\mathbb{D}$ as follows

$$\forall\tilde{\Phi} \in \tilde{V}, \quad \mathbb{D}\tilde{\Phi} = \mathbb{L}\tilde{\Phi} + \mathbb{K}\tilde{\Phi}, \quad (1.41)$$

where

$$\mathbb{L} := \begin{bmatrix} 0 & L^{1,0}\chi_{(-\infty,a_1^-)} & 0 & \ldots & 0 & L^{n-1,0}\chi_{(a_{n-1}^+,+\infty)} \\ L^{0,1}\chi_{(a_0^+,+\infty)} & 0 & L^{2,1}\chi_{(-\infty,a_2^-)} & \ldots & 0 & 0 \\ 0 & L^{1,2}\chi_{(a_1^+,+\infty)} & 0 & \ldots & 0 & 0 \\ \vdots & \vdots & \vdots & \ddots & \vdots & \vdots \\ 0 & 0 & 0 & \ldots & 0 & L^{n-1,n-2}\chi_{(-\infty,a_{n-1}^-)} \\ L^{0,n-1}\chi_{(-\infty,a_0^-)} & 0 & 0 & \ldots & L^{n-2,n-1}\chi_{(a_{n-2}^+,+\infty)} & 0 \end{bmatrix},$$

$$(1.42)$$

and

$$\mathbb{K} := \begin{bmatrix} 0 & K^{1,0} & 0 & \dots & 0 & K^{n-1,0} \\ K^{0,1} & 0 & K^{2,1} & \dots & 0 & 0 \\ 0 & K^{1,2} & 0 & \dots & 0 & 0 \\ \vdots & \vdots & \vdots & \ddots & \vdots & \vdots \\ 0 & 0 & 0 & \dots & 0 & K^{n-1,n-2} \\ K^{0,n-1} & 0 & 0 & \dots & K^{n-2,n-1} & 0 \end{bmatrix}, \tag{1.43}$$

with

$$\forall j \in \mathbb{Z}/n\mathbb{Z}, \quad K^{j\pm 1,j} = (D^{j\pm 1,j} - L^{j\pm 1,j}) + L^{j\pm 1,j} \chi_{(a_{j\pm 1}^\pm, \pm\infty)} \tag{1.44}$$

From Theorem 1.3.7, we get easily that the operator $\mathbb{K}$ is compact in $\tilde{V}$.

Moreover, by Theorem 1.3.7, for all $j \in \mathbb{Z}/n\mathbb{Z}$, we have that for all $\tilde{\varphi}^j \in L^2(\Sigma^j)$ such that $\tilde{\varphi}^j\big|_{\Sigma_\mathcal{O}^j} = 0$

$$\|L^{j,j-1}\chi_{(-\infty,a_j^-)}\tilde{\varphi}^j\|^2 + \|L^{j,j+1}\chi_{(a_j^+,+\infty)}\tilde{\varphi}^j\|^2 \leq C_j^2 \left[\|\chi_{(-\infty,a_j^-)}\tilde{\varphi}^j\|^2 + \|\chi_{(a_j^+,+\infty)}\tilde{\varphi}^j\|^2 \right]$$

$$= C_j^2 \|\tilde{\varphi}^j\|_{L^2(\Sigma^j)}^2,$$

where $C_j = \max(\cos(\theta^{j,j-1}/2), \cos(\theta^{j,j+1}/2))$. Consequently the norm of the operator $\mathbb{L}$ is strictly less than 1. This implies that the operator $\mathbb{I} - \mathbb{L}$ is coercive in $\tilde{V}$, its coercivity constant being given by

$$\alpha = 1 - \max_{j \in \mathbb{Z}/n\mathbb{Z}} \cos \frac{\theta^{j,j+1}}{2}. \tag{1.45}$$

Let us now show that Problem (1.33) is well-posed. Since it is Fredholm of index 0, it is sufficient to show the uniqueness. We will suppose that $F = 0$ and show that the corresponding solution $\tilde{\Phi} \in \tilde{V}$ necessarily vanishes. By Lemma 1.2.3, we can define unequivocally a function p satisfying (1.14) for all $j \in \mathbb{Z}/n\mathbb{Z}$. Moreover, $p \in H^1(\Omega)$ and is solution of (1.1) with $g = 0$. Problem (1.1) being well-posed, $p = 0$ and then $P^j(\varphi^j) = 0$ for all j. Consequently $\varphi^j = 0$ for all $j \in \mathbb{Z}/n\mathbb{Z}$.

1.4 Discretization

1.4.1 The discrete problem

To get a discrete problem that we can solve numerically, we use three main ingredients:

1. We truncate the integrals which appear in the definition of the integral operators $D^{j,j\pm 1}$: the integral for $\xi \in \mathbb{R}$ is replaced by an integral for $|\xi| \leq \hat{T}$ for some $\hat{T} \in \mathbb{R}^+$.

2. Then, we introduce finite dimensional subspaces $\tilde{V}_\mathbf{h}$ of $\tilde{V}$ on which a Galerkin approximation is computed. To define the space $\tilde{V}_\mathbf{h}$, we truncate the infinite lines Σ^j as follows:

$$\Sigma_T^j = \{(x^j = l^j, y^j), -T_j < y^j < T_j\} \tag{1.46}$$

and we mesh these truncated lines into segments $[M_i^j, M_{i+1}^j]$, $i \in \{1, \dots, N_j\}$ whose maximum length is h_j. Let $T = \min_j T_j$ and $h = \max_j h_j$. Finally, the space $V_\mathbf{h}$ with $\mathbf{h} = (T, h)$ built with Lagrange finite elements of degree l ($l \in \mathbb{N}^*$) is given by:

$$\left\{ (\psi_\mathbf{h}^0, \dots, \psi_\mathbf{h}^{n-1}) \in V, \quad \forall j, \ \psi_\mathbf{h}^j \text{ is polynomial of degree } l \text{ on } [M_i^j, M_{i+1}^j], \ i \in \{1, \dots, N_j\} \right\}, \tag{1.47}$$

and $\tilde{V}_{\mathbf{h}} = V_{\mathbf{h}} \cap \tilde{V}$. Let us emphasize that of course

$$\forall \Psi \in V, \quad \inf_{\Psi_{\mathbf{h}} \in V_{\mathbf{h}}} \| \Psi - \Psi_{\mathbf{h}} \| \xrightarrow[\mathbf{h} \to (+\infty, 0)]{} 0. \tag{1.48}$$

3. Finally, quadrature formulae have to be used to evaluate the Fourier integrals which appear in the variational formulation.

In what follows, we will study the error due to points 1 and 2 but not the quadrature formulae.

For this purpose, we consider the three following variational problems:

0. The exact problem:
   Find $\tilde{\Phi} \in \tilde{V}$ such that

   $$(\mathbb{B}\,\tilde{\Phi}, \tilde{\Psi}) = (\mathbb{D}\,G, \tilde{\Psi}), \quad \forall \tilde{\Psi} \in \tilde{V}, \tag{1.49}$$

   where $\mathbb{B} = \mathbb{I} - \mathbb{D}$, $\mathbb{D}$ is defined by (1.26), $\tilde{V}$ by (1.27), G by (1.25), and $(\cdot, \cdot)$ denotes the L^2 scalar product in V. We have the expression

   $$\forall (\Phi, \Psi) \in V, \quad (\mathbb{D}\,\Phi, \Psi) = \sum_{j \in \mathbb{Z}/n\mathbb{Z}} \left(\int_{\Sigma^j \cap \Omega^{j+1}} \left[D^{j+1,j} \varphi^{j+1} \right] \psi^j + \int_{\Sigma^j \cap \Omega^{j-1}} \left[D^{j-1,j} \varphi^{j-1} \right] \psi^j \right). \tag{1.50}$$

   with

   $$\forall j \in \mathbb{Z}/n\mathbb{Z}, \quad \forall \psi \in L^2(\Sigma^j), \quad \left[D^{j\pm1,j}\,\psi \right](r) = \frac{1}{\sqrt{2\pi}} \int_{\mathbb{R}} k^{j\pm1,j}(r, \xi)\,\hat{\psi}(\xi)\,\mathrm{d}\xi, \quad r \geq 0,$$

   and $k^{j\pm1,j}(r, \xi)$ is given by (1.20).

1. The semi-discrete problem (truncation of the integrals):
   Find $\tilde{\Phi}_{\hat{T}} \in \tilde{V}$ such that

   $$(\mathbb{B}_{\hat{T}}\,\tilde{\Phi}_{\hat{T}}, \tilde{\Psi}) = (\mathbb{D}_{\hat{T}}\,G, \tilde{\Psi}), \quad \forall \tilde{\Psi} \in \tilde{V}, \tag{1.51}$$

   where $\mathbb{B}_{\hat{T}} = \mathbb{I} - \mathbb{D}_{\hat{T}}$ and $\mathbb{D}_{\hat{T}}$ is defined by

   $$\forall (\Phi, \Psi) \in V, \quad (\mathbb{D}_{\hat{T}}\,\Phi, \Psi) = \sum_{j \in \mathbb{Z}/n\mathbb{Z}} \left(\int_{\Sigma^j \cap \Omega^{j+1}} \left[D_{\hat{T}}^{j+1,j} \varphi^{j+1} \right] \psi^j + \int_{\Sigma^j \cap \Omega^{j-1}} \left[D_{\hat{T}}^{j-1,j} \varphi^{j-1} \right] \psi^j \right), \tag{1.52}$$

   where

   $$\left[D_{\hat{T}}^{j\pm1,j}\,\psi \right](r) = \frac{1}{\sqrt{2\pi}} \int_{-\hat{T}}^{\hat{T}} k^{j\pm1,j}(r, \xi)\,\hat{\psi}(\xi)\,\mathrm{d}\xi, \quad r \geq 0. \tag{1.53}$$

2. The discrete problem (truncation of the infinite lines Σ^j and meshing):
   Find $\tilde{\Phi}_{\hat{T}, \mathbf{h}} \in \tilde{V}_{\mathbf{h}}$ such that

   $$(\mathbb{B}_{\hat{T}}\,\tilde{\Phi}_{\hat{T}, \mathbf{h}}, \tilde{\Psi}_{\mathbf{h}}) = (\mathbb{D}_{\hat{T}}\,G_{\mathbf{h}}, \tilde{\Psi}_{\mathbf{h}}), \quad \forall \tilde{\Psi}_{\mathbf{h}} \in \tilde{V}_{\mathbf{h}}, \tag{1.54}$$

   where $G_{\mathbf{h}} \in V_{\mathbf{h}}$ is the interpolate of G.

Our first objective is to prove that for $\hat{T}$ and T large enough, and for h small enough, the above discrete problem is well-posed. The second objective is to prove that the error $\| \Phi - \Phi_{\hat{T}, \mathbf{h}} \|$ (where $\Phi_{\hat{T}, \mathbf{h}} = \tilde{\Phi}_{\hat{T}, \mathbf{h}} + G_{\mathbf{h}}$) tends to 0 when $\hat{T} \to +\infty$, $T \to +\infty$, and $h \to 0$. And finally if the φ^j's are regular enough (whose precise definition will be given later), we will also estimate the convergence rate.

Remark 1.4.1. *As in [55], the difficulty of the numerical analysis comes from the fact that the operator appearing in the discrete problem is the sum of a coercive part and a compact part, which both depend on $\hat{T}$.*

As a first step, we will derive the same type of result but only for the semi-discrete problem.

1.4.2   Numerical analysis of the semi-discrete problem

For $\hat{T} > 0$, we denote by $\Pi_{\hat{T}}$ the projection operator on $L^2(\mathbb{R})$ defined by

$$\forall \psi \in L^2(\mathbb{R}), \quad \Pi_{\hat{T}}\psi(y) = \frac{1}{\sqrt{2\pi}} \int_{-\hat{T}}^{\hat{T}} \hat{\psi}(\xi)e^{i\xi y}\mathrm{d}\xi. \tag{1.55}$$

In other words,

$$\forall \psi \in L^2(\mathbb{R}), \quad \widehat{\Pi_{\hat{T}}\psi}(\xi) = \chi_{[-\hat{T},\hat{T}]}(\xi)\hat{\psi}(\xi). \tag{1.56}$$

Then, we denote by $\mathbb{\Pi}_{\hat{T}}$ the projection operator on V defined by

$$\forall \Phi = (\varphi^0, \ldots, \varphi^{n-1}) \in V, \quad \mathbb{\Pi}_{\hat{T}}\Phi = (\Pi_{\hat{T}}\varphi^0, \ldots, \Pi_{\hat{T}}\varphi^{n-1}). \tag{1.57}$$

Using Plancherel and Lebesgue theorems, one can easily check the following properties that will be used in the sequel:

$$\|\mathbb{\Pi}_{\hat{T}}\Phi\|_V \leq \|\Phi\|_V, \tag{1.58}$$

$$\forall \Phi, \Psi \in V, \quad (\mathbb{\Pi}_{\hat{T}}\Phi, \Psi) = (\Phi, \mathbb{\Pi}_{\hat{T}}\Psi), \tag{1.59}$$

$$\forall \Phi \in V, \quad \|\mathbb{\Pi}_{\hat{T}}\Phi - \Phi\|_V \to 0 \quad \text{when } \hat{T} \to +\infty. \tag{1.60}$$

Using this definition, we have $\mathbb{D}_{\hat{T}} = \mathbb{D}\,\mathbb{\Pi}_{\hat{T}}$, where $\mathbb{D}_{\hat{T}}$ is defined by (1.52). The main results of this section are given in the following theorem.

Theorem 1.4.2.   *1. [**Stability**] There exists $\hat{T}_{\min}$ such that the semi-discrete problem (1.51) is well-posed for $\hat{T} \geq \hat{T}_{\min}$.*

   *2. [**Convergence**] The solution $\tilde{\Phi}_{\hat{T}}$ of the semi-discrete problem (1.51) tends to the exact solution $\tilde{\Phi}$ of (1.49) when $\hat{T}$ tends to infinity.*

   *3. [**Error estimates**] Let $\Phi = \tilde{\Phi} + G = (\varphi^0, \ldots, \varphi^{n-1})$, where $\tilde{\Phi}$ is the solution of (1.49). If there exists $s > 0$ such that for all $j \in \mathbb{Z}/n\mathbb{Z}$, $\varphi^j \in H^s(\Sigma^j)$, we have*

$$\|\tilde{\Phi} - \tilde{\Phi}_{\hat{T}}\|_V \leq \frac{C}{\hat{T}^s} \sum_{j \in \mathbb{Z}/n\mathbb{Z}} \left(\frac{1}{\sqrt{\sin(\theta^{j,j+1})}} \|\varphi^{j+1}\|_{H^s(\Sigma^{j+1})} + \frac{1}{\sqrt{\sin(\theta^{j,j-1})}} \|\varphi^{j-1}\|_{H^s(\Sigma^{j-1})} \right) \tag{1.61}$$

The rest of this section is dedicated to the proof of this theorem. To do so, we will need several lemmas:

- the two first lemmas give properties of the operators $L^{j\pm1,j}\Pi_{\hat{T}}$ for the $L^{j\pm1,j}$ appearing in (1.42). These results are the equivalent of the two properties stated in Theorem 1.3.7, but they are not a straightforward consequence of this theorem. The difficulty comes from the fact that, in general, for a function ψ, the support of $\Pi_{\hat{T}}\psi$ is not the same than the one of ψ. These lemmas enable us to deduce properties of the operator $\mathbb{D}\,\mathbb{\Pi}_{\hat{T}}$, used in Lemma 1.4.6 as a basic tool for the stability and the convergence result.

- To establish the error estimates, we will use finally Lemma 1.4.7.

Lemma 1.4.3. *For all $j \in \mathbb{Z}/n\mathbb{Z}$, the operator $L^{j\pm1,j}$ appearing in Theorem 1.3.7 satisfies*

$$\exists \tilde{C}^{j\pm1,j} \in (0,1), \forall \varphi \in L^2(\Sigma^{j\pm1}), \quad \|L^{j\pm1,j}\Pi_{\hat{T}}\chi_{(a_{j\pm1}^\mp, \mp\infty)}\varphi\| \leq \tilde{C}^{j\pm1,j}\|\chi_{(a_{j\pm1}^\mp, \mp\infty)}\varphi\|;$$

where $\tilde{C}^{j\pm1,j} = \max\left(\sin\left(\theta^{j\pm1,j}/2\right), \cos\left(\theta^{j\pm1,j}/2\right)\right)$.

Proof. As explained in the proof of Lemma 1.3.6, $L^{0,1} = \chi_{(0,b)}L_N$ where L_N is defined by (1.39). It suffices then to show that

$$\forall \hat{T} > 0, \ \forall \psi \in L^2(\Sigma^0) \quad \|L_N \Pi_{\hat{T}} \chi_{(a_0^+,+\infty)} \psi\| \le C \|\chi_{(a_0^+,+\infty)} \psi\| \tag{1.62}$$

with

$$C = \max\left(\sin\left(\theta^{0,1}/2\right), \cos\left(\theta^{0,1}/2\right)\right)$$

to obtain the result for $L^{0,1}$. A similar proof can be applied to other $L^{j\pm1,j}$.

We stress again that (1.62) is not a direct consequence of Lemma 1.3.5 since $\Pi_{\hat{T}} \chi_{(a_0^+,+\infty)} \psi$ is not supported in $(a_0^+, +\infty)$.

We introduce the linear operators S and A of $\mathcal{L}(L^2(\mathbb{R}))$ defined by

$$\forall \psi \in L^2(\mathbb{R}), \quad S\psi(y) = \frac{1}{2}\left(\psi(y) + \psi(2a_0^+ - y)\right) \quad \text{and} \quad A\psi(y) = \frac{1}{2}\left(\psi(y) - \psi(2a_0^+ - y)\right)$$

We have obviously $S + A = Id$.

The key point is that $\Pi_{\hat{T}}$ commutes with S and A. Indeed, from

$$\widehat{S\psi}(\xi)\, e^{i2a_0^+\xi} = \widehat{S\psi}(-\xi),$$

we deduce that $\Pi_{\hat{T}}S\psi$ is symmetric with respect to a_0^+:

$$\begin{aligned}
\Pi_{\hat{T}}S\psi(2a_0^+ - y) &= \frac{1}{\sqrt{2\pi}} \int_{-\hat{T}}^{\hat{T}} \widehat{S\psi}(\xi) e^{i(2a_0^+ - y)\xi} d\xi \\
&= \frac{1}{\sqrt{2\pi}} \int_{-\hat{T}}^{\hat{T}} \widehat{S\psi}(-\xi) e^{-iy\xi} d\xi \\
&= \frac{1}{\sqrt{2\pi}} \int_{-\hat{T}}^{\hat{T}} \widehat{S\psi}(\xi) e^{iy\xi} d\xi \\
&= \Pi_{\hat{T}}S\psi(y).
\end{aligned}$$

Similarly, we prove that $\Pi_{\hat{T}}A\psi$ is anti-symmetric with respect to a_0^+:

$$\Pi_{\hat{T}}A\psi(2a_0^+ - y) = -\Pi_{\hat{T}}A\psi(y).$$

Finally, gathering all these properties, we get

$$\begin{aligned}
S\Pi_{\hat{T}}\psi(y) &= \frac{1}{2}\left(\Pi_{\hat{T}}\psi(y) + \Pi_{\hat{T}}\psi(2a_0^+ - y)\right) \\
&= \frac{1}{2}\left(\Pi_{\hat{T}}S\psi(y) + \Pi_{\hat{T}}A\psi(y) + \Pi_{\hat{T}}S\psi(2a_0^+ - y) + \Pi_{\hat{T}}A\psi(2a_0^+ - y)\right) \\
&= \Pi_{\hat{T}}S\psi(y),
\end{aligned}$$

and the same result can be obtained for A. To summarize, we have

$$\Pi_{\hat{T}}S\psi = S\Pi_{\hat{T}}\psi \quad \text{and} \quad \Pi_{\hat{T}}A\psi = A\Pi_{\hat{T}}\psi. \tag{1.63}$$

Now let us apply all these properties to our purpose. Since $S + A = Id$, $S^2 = S$ and $A^2 = A$:

$$\begin{aligned}
L_N\Pi_{\hat{T}} &= L_N\Pi_{\hat{T}}(S + A) \\
&= L_N\Pi_{\hat{T}}(S^2 + A^2)
\end{aligned}$$

$$= L_N S \Pi_{\hat{T}} S + L_N A \Pi_{\hat{T}} A$$

so that

$$\forall \psi \in L^2(\Sigma^0), \quad \left\| L_N \Pi_{\hat{T}} \chi_{(a_0^+, +\infty)} \psi \right\| \le \|L_N S\| \|\Pi_{\hat{T}}\| \|S \chi_{(a_0^+, +\infty)} \psi\| + \|L_N A\| \|\Pi_{\hat{T}}\| \|A \chi_{(a_0^+, +\infty)} \psi\|.$$
(1.64)

Moreover, since for any $\psi \in L^2(\mathbb{R})$,

$$\|\Pi_{\hat{T}}\| \le 1 \text{ and} \tag{1.65}$$

$$\left\| S \chi_{(a_0^+, +\infty)} \psi \right\|_{L^2(\mathbb{R})} = \left\| A \chi_{(a_0^+, +\infty)} \psi \right\|_{L^2(\mathbb{R})} = \frac{1}{\sqrt{2}} \left\| \chi_{(a_0^+, +\infty)} \psi \right\|_{L^2(\mathbb{R})}, \tag{1.66}$$

we get

$$\left\| L_N \Pi_{\hat{T}} \chi_{(a_0^+, +\infty)} \psi \right\| \le \frac{1}{\sqrt{2}} \left(\|L_N S\| + \|L_N A\| \right) \|\chi_{(a_0^+, +\infty)} \psi\|, \tag{1.67}$$

Finally, the estimates (A.12) and (A.13) proven in Appendix A enables us to show (1.62).

<div style="text-align: right">□</div>

Remark 1.4.4. *Let us emphasize that the key property (1.63) is true because in the definition of $\Pi_{\hat{T}}$, the Fourier integral has been truncated to a symmetric interval $[-\hat{T}, \hat{T}]$.*

Lemma 1.4.5. *For all $\hat{T}$, the operator $L^{j\pm1,j} \Pi_{\hat{T}} \chi_{(a_{j\pm1}^\pm, \pm\infty)}$ is compact.*

Moreover, let ψ_n be a sequence of $L^2(\Sigma^{j\pm1})$, for $\hat{T}_n \to +\infty$ and for $j \in \mathbb{Z}/n\mathbb{Z}$ such that ψ_n converges weakly to 0 in $L^2(\Sigma^{j\pm1})$, then

$$L^{j\pm1,j} \Pi_{\hat{T}_n} \chi_{(a_{j\pm1}^\pm, \pm\infty)} \psi_n \to 0 \quad \text{in } L^2(\Sigma^j \cap \Omega^{j\pm1}).$$

Proof. As explained in the proof of the previous lemma, it suffices to show the result replacing $L^{j\pm1,j}$ by L_N to deduce the one for $L^{0,1}$ and in a similar way the one for the other $L^{j\pm1,j}$.

Again, the difficulty is that, in general, for a function ψ, $\Pi_{\hat{T}} \chi_{(-\infty, a_0^-)} \psi$ is not supported in $(-\infty, a_0^-)$, so that the results cannot be deduced from the second point of Lemma 1.3.5.

We decompose
$$L_N \Pi_{\hat{T}} \chi_{(-\infty, a_0^-)} = L_N \chi_{(-\infty, a_0^-)} + L_N \left(\Pi_{\hat{T}} - I \right) \chi_{(-\infty, a_0^-)}$$
From Lemma 1.3.5 we know that $L_N \chi_{(-\infty, a_0^-)}$ is compact. We show in the rest of the proof that $L_N \left(\Pi_{\hat{T}} - I \right) \chi_{(-\infty, a_0^-)}$ is a Hilbert Schmidt operator and that $L_N \left(\Pi_{\hat{T}} - I \right) \chi_{(-\infty, a_0^-)} \to 0$ when $\hat{T} \to +\infty$, and the results of the lemma follow.

Using the expression of L_N in (1.38), we get:

$$L_N \left(\Pi_{\hat{T}} - I \right) \chi_{(-\infty, a_0^-)} = R_{\hat{T}}^+ e^{\iota \theta^{0,1}} + R_{\hat{T}}^- e^{-\iota \theta^{0,1}},$$

where, for $\psi \in L^2(\Sigma^0)$

$$R_{\hat{T}}^+ \psi(r) = \frac{1}{2\pi} \int_{\xi > \hat{T}} d\xi \int_{-\infty}^{a_0^-} dy \, e^{-\xi r \sin \theta^{0,1}} \, e^{\iota \xi (a_0^+ - y + r \cos \theta^{0,1})} \psi(y),$$

$$R_{\hat{T}}^- \psi(r) = \frac{1}{2\pi} \int_{\xi < -\hat{T}} d\xi \int_{-\infty}^{a_0^-} dy \, e^{\xi r \sin \theta^{0,1}} \, e^{\iota \xi (a_0^+ - y + r \cos \theta^{0,1})} \psi(y).$$

By Fubini's Theorem, we deduce that

$$R_{\hat{T}}^{\pm}\psi(r) = \frac{1}{2\pi}\int_{-\infty}^{a_0^-} k_{\hat{T}}^{\pm}(r,y)\,\psi(y)\,\mathrm{d}y$$

with

$$k_{\hat{T}}^{\pm}(r,y) = \frac{e^{-\hat{T}(r\sin\theta^{0,1}\pm\iota(a_0^+ - y + r\cos\theta^{0,1}))}}{r\sin\theta^{0,1} \mp \iota(a_0^+ - y + r\cos\theta^{0,1})}.$$

Since the denominator never vanishes for $r \geq 0$ and $y < a_0^- < a_0^+$, one can easily check that

$$\int_0^{+\infty}\int_{-\infty}^{a_0^-}\left|k_{\hat{T}}^{\pm}(r,y)\right|^2\,\mathrm{d}y\,\mathrm{d}r$$

is finite and tends to 0 when $\hat{T} \to +\infty$. $\qquad\square$

From these two lemmas, we deduce the following result.

Lemma 1.4.6. *For all $\hat{T} > 0$, the operator $\mathbb{B}_{\hat{T}}$ is the sum of a coercive operator and a compact operator in $\tilde{V}$.*

Moreover, there exists $\gamma > 0$ and $\hat{T}_{min}$ such that for $\hat{T} \geq \hat{T}_{min}$

$$\forall\tilde{\Phi} \in \tilde{V} \quad \|\mathbb{B}_{\hat{T}}\tilde{\Phi}\| \geq \gamma\|\tilde{\Phi}\| \tag{1.68}$$

Proof. Let $\hat{T} > 0$. Let us remind that $\mathbb{B}_{\hat{T}} = \mathbb{I} - \mathbb{D}\,\mathbb{\Pi}_{\hat{T}}$. By the definitions (1.26) of $\mathbb{D}$ and (1.57) of $\mathbb{\Pi}_{\hat{T}}$, the operator $\mathbb{D}\,\mathbb{\Pi}_{\hat{T}}$ is nothing else but (1.26) with the terms $D^{j\pm1,j}$ replaced by $D^{j\pm1,j}\,\mathbb{\Pi}_{\hat{T}}$. Finally, as in (1.41-1.42-1.43), we have the decomposition

$$\mathbb{B}_{\hat{T}} = \mathbb{I} - \mathbb{D}\,\mathbb{\Pi}_{\hat{T}} \quad \text{where} \quad \mathbb{D}\,\mathbb{\Pi}_{\hat{T}} = \mathbb{L}_{\hat{T}} + \mathbb{K}_{\hat{T}}$$

with

- $\mathbb{L}_{\hat{T}}$ having the form of (1.42) where the terms $L^{j\pm1,j}\,\chi_{(a_{j\pm1}^{\mp},\mp\infty)}$ are replaced by $L^{j\pm1,j}\,\mathbb{\Pi}_{\hat{T}}\,\chi_{(a_{j\pm1}^{\mp},\mp\infty)}$. Using Lemma 1.4.3 and the same arguments as in Section 1.3.2, we can show that the norm of $\mathbb{L}_{\hat{T}}$ is strictly less than 1, the norm being independent of $\hat{T}$. Therefore $\mathbb{I} - \mathbb{L}_{\hat{T}}$ is coercive in $\tilde{V}$ with a coercive constant $\tilde{\gamma}$ independent of $\hat{T}$.

- $\mathbb{K}_{\hat{T}}$ has the form of (1.43) where the terms $K^{j\pm1,j}$ are replaced by $K_{\hat{T}}^{j\pm1,j}$ with

$$K_{\hat{T}}^{j\pm1,j} = (D^{j\pm1,j} - L^{j\pm1,j})\,\mathbb{\Pi}_{\hat{T}} + L^{j\pm1,j}\,\mathbb{\Pi}_{\hat{T}}\,\chi_{(a_{j\pm1}^{\pm},\pm\infty)}. \tag{1.69}$$

  By using Theorem 1.3.7 and Lemma 1.4.5, $K_{\hat{T}}^{j\pm1,j}$ is compact. The operator $\mathbb{K}_{\hat{T}}$ is then also compact in $\tilde{V}$.

We have then proven the first part of the lemma. We show the second part of the lemma by contradiction. We suppose the existence of a sequence $\tilde{\Phi}_n \in \tilde{V}$ and a sequence $\hat{T}_n \to +\infty$ such that $\|\tilde{\Phi}_n\|_V = 1$ and $\mathbb{B}_{\hat{T}_n}\tilde{\Phi}_n \to 0$ in $\tilde{V}$. Using the first part of the proof, we have

$$\mathbb{B}_{\hat{T}_n} = (\mathbb{I} - \mathbb{L}_{\hat{T}_n}) - \mathbb{K}_{\hat{T}_n},$$

where the operator $(\mathbb{I} - \mathbb{L}_{\hat{T}_n})$ is coercive with a coercivity constant $\tilde{\gamma}$ independent of n and $\mathbb{K}_{\hat{T}_n}$ is compact. Rearranging the terms and taking the scalar product, we have

$$(\mathbb{B}_{\hat{T}_n}\tilde{\Phi}_n, \tilde{\Phi}_n) + (\mathbb{K}_{\hat{T}_n}\tilde{\Phi}_n, \tilde{\Phi}_n) = ((\mathbb{I} - \mathbb{L}_{\hat{T}_n})\tilde{\Phi}_n, \tilde{\Phi}_n) \geq \tilde{\gamma} > 0, \tag{1.70}$$

and we will show that the left hand side tends to 0 with n to establish the contradiction.

Since $\tilde{\Phi}_n$ is bounded in the Hilbert space $\tilde{V}$, it admits a weakly convergent subsequence that we denote also by $\tilde{\Phi}_n$: $\tilde{\Phi}_n \rightharpoonup \tilde{\Phi}$ in $\tilde{V}$. By (1.59) and (1.60),

$$\forall \tilde{\Psi} \in \tilde{V}, \quad (\Pi_{\hat{T}_n}\tilde{\Phi}_n, \tilde{\Psi}) = (\tilde{\Phi}_n, \Pi_{\hat{T}_n}\tilde{\Psi} - \tilde{\Psi}) + (\tilde{\Phi}_n, \tilde{\Psi}) \to (\tilde{\Phi}, \tilde{\Psi}),$$

which means that $\Pi_{\hat{T}_n}\tilde{\Phi}_n \rightharpoonup \tilde{\Phi}$. As a consequence,

$$\mathbb{B}_{\hat{T}_n}\tilde{\Phi}_n = \tilde{\Phi}_n - \mathbb{D}\Pi_{\hat{T}_n}\tilde{\Phi}_n \rightharpoonup \tilde{\Phi} - \mathbb{D}\tilde{\Phi} = \mathbb{B}\tilde{\Phi}.$$

Since by hypothesis, $\mathbb{B}_{\hat{T}_n}\tilde{\Phi}_n \to 0$, we conclude that $\mathbb{B}\tilde{\Phi} = 0$ which implies $\tilde{\Phi} = 0$ because $\mathbb{B}$ is invertible (see Theorem 1.3.1).

On the other hand, as written in (1.69), each operator $K_{\hat{T}_n}^{j\pm1,j}$ involved in the definition of $\mathbb{K}_{\hat{T}_n}$ is the sum of two operators such that

- $(D^{j\pm1,j} - L^{j\pm1,j})\Pi_{\hat{T}_n}\tilde{\varphi}_n \to 0$ when $\tilde{\varphi}_n \rightharpoonup 0$ since $\Pi_{\hat{T}_n}\tilde{\varphi}_n \rightharpoonup 0$ because of (1.60) and $(D^{j\pm1,j} - L^{j\pm1,j})$ is compact because of Theorem 1.3.7;

- $L^{j\pm1,j}\Pi_{\hat{T}_n}\chi_{(a_{j\pm1}^{\pm},\pm\infty)}\tilde{\varphi}_n \to 0$ when $\tilde{\varphi}_n \rightharpoonup 0$ because of Lemma 1.4.5.

Consequently, as $\tilde{\Phi}_n \rightharpoonup 0$, we have $\mathbb{K}_{\hat{T}_n}\tilde{\Phi}_n \to 0$ in $\tilde{V}$ when n tends to $+\infty$.

Gathering all these results, we have $(\mathbb{B}_{\hat{T}_n}\tilde{\Phi}_n, \tilde{\Phi}_n) + (\mathbb{K}_{\hat{T}_n}\tilde{\Phi}_n, \tilde{\Phi}_n)$ tends to 0 with n. This contradiction finishes the proof.

$\square$

To establish the error estimates of Theorem 1.4.2, we need the following lemma.

Lemma 1.4.7. *Let $s > 0$ and $\psi \in H^s(\Sigma^j)$. There exists a constant $C > 0$ independent of ψ and $\hat{T}$ such that*

$$\left\| D^{j,j\pm1}(I - \Pi_{\hat{T}})\psi \right\|_{L^2} \leq \frac{C}{\hat{T}^s\sqrt{\sin(\theta^{j,j\pm1})}}\|\psi\|_{H^s(\Sigma^j)}. \tag{1.71}$$

Proof. By definition (1.19-1.20) of $D^{j,j\pm1}$, we have, by Cauchy-Schwarz inequality, Fubini's Theorem, and by the Fourier definition of the Sobolev spaces [1]:

$$\left\| D^{j,j\pm1}(I - \Pi_{\hat{T}})\psi \right\|^2 \leq \|\psi\|_{H^s(\Sigma^j)}^2 \int_{|\xi|>\hat{T}} \int_0^{+\infty} \frac{|k^{j,j\pm1}(r,\xi)|^2}{(1+\xi^2)^s}\mathrm{d}\xi\,\mathrm{d}r, \tag{1.72}$$

Moreover, an easy calculation gives

$$\int_{|\xi|>\hat{T}} \int_0^{+\infty} \frac{|k^{j,j\pm1}(r,\xi)|^2}{(1+\xi^2)^s}\mathrm{d}\xi\,\mathrm{d}r = \int_{|\xi|>\hat{T}} F(\xi)\mathrm{d}\xi,$$

where

$$F(\xi) = \frac{\left|\alpha + \beta(-\cos(\theta^{j,j\pm1})i\sqrt{\omega^2 - \xi^2} + \sin(\theta^{j,j\pm1})i\xi)\right|^2}{2\left|\alpha + i\beta\sqrt{\omega^2 - \xi^2}\right|^2 \mathrm{Im}(\sqrt{\omega^2 - \xi^2})\sin(\theta^{j,j\pm1})(1+\xi^2)^s}$$

is such that

$$F(\xi) \leq \frac{C}{\xi^{2s+1}\sin(\theta^{j,j\pm1})}$$

for some constant C depending only on $\alpha, \beta, \omega,$ and s. The result follows. $\square$

Proof of Theorem 1.4.2.

1. By Lemma 1.4.6, $\mathbb{B}_{\hat{T}}$ is the sum of a coercive and a compact operators. By Fredholm alternative, it is invertible if and only if it is injective. Again by lemma 1.4.6, we have that there exists $\hat{T}_{\min}$ such that for $\hat{T} \geq \hat{T}_{\min}$, $\mathbb{B}_{\hat{T}}$ is injective.

2. From $\mathbb{B}\tilde{\Phi} = \mathbb{D}G$ and $\mathbb{B}_{\hat{T}}\tilde{\Phi}_{\hat{T}} = \mathbb{D}\mathrm{III}_{\hat{T}}G$, we deduce:

$$\mathbb{B}_{\hat{T}}(\tilde{\Phi} - \tilde{\Phi}_{\hat{T}}) = \mathbb{B}\tilde{\Phi} - (\mathbb{B} - \mathbb{B}_{\hat{T}})\tilde{\Phi} - \mathbb{B}_{\hat{T}}\tilde{\Phi}_{\hat{T}}$$
$$= \mathbb{D}(\mathbb{I} - \mathrm{III}_{\hat{T}})(\tilde{\Phi} + G)$$
$$= \mathbb{D}(\mathbb{I} - \mathrm{III}_{\hat{T}})\Phi$$

which tends to 0 when $\hat{T}$ tends to $+\infty$ by (1.60). Lemma 1.4.6 then implies that

$$\left\|\tilde{\Phi} - \tilde{\Phi}_{\hat{T}}\right\| \leq \frac{1}{\gamma}\left\|\mathbb{B}_{\hat{T}}(\tilde{\Phi} - \tilde{\Phi}_{\hat{T}})\right\|,$$

which proves that $\tilde{\Phi}_{\hat{T}}$ tends to $\tilde{\Phi}$ when $\hat{T}$ tends to $+\infty$.

3. The previous step provides also the following inequality:

$$\|\tilde{\Phi} - \tilde{\Phi}_{\hat{T}}\| \leq \frac{1}{\gamma}\|\mathbb{D}(\mathbb{I} - \mathrm{III}_{\hat{T}})\Phi\|. \tag{1.73}$$

Combined with Lemma 1.4.7, we get the estimate (1.61).

1.4.3 Error estimate for the discrete problem

The main result of this section is given in the following theorem.

Theorem 1.4.8. *1. There exist $\hat{T}_{\min}$, $T_{\min}$ and $h_{\max}$ such that the discrete problem (1.54) is well-posed for $\hat{T} \geq \hat{T}_{\min}$, $T \geq T_{\min}$ and $h \leq h_{\max}$.*

2. The solution $\tilde{\Phi}_{\hat{T},\mathbf{h}}$ of the discrete problem (1.54) tends to the exact solution $\tilde{\Phi}$ of (1.49) when $\hat{T} \to +\infty$ and $\mathbf{h} = (T, h) \to (+\infty, 0)$.

3. If $\Phi = \tilde{\Phi} + G$ is such that $\varphi^j \in H^s(\Sigma^j)$ for $j \in \mathbb{Z}/n\mathbb{Z}$ with $s > 0$, there exists $C > 0$ such that

$$\|\tilde{\Phi} - \tilde{\Phi}_{\hat{T},\mathbf{h}}\| \leq \frac{C}{\hat{T}^s} + Ce^{-\varepsilon T} + C\,h^{\min(s,l+1)} \tag{1.74}$$

where ε is given by (1.3).

To show this theorem, we will use the following lemma (which is the discrete equivalent of Lemma 1.4.6).

Lemma 1.4.9. *There exists $\gamma' > 0$, $\hat{T}_{\min}$, $T_{\min}$ and $h_{\max}$ such that for $\hat{T} \geq \hat{T}_{\min}$, $T \geq T_{\min}$ and $h \leq h_{\max}$,*

$$\forall \tilde{\Phi}_{\mathbf{h}} \in \tilde{V}_{\mathbf{h}} \quad \sup_{\tilde{\Psi}_{\mathbf{h}} \in \tilde{V}_{\mathbf{h}}, \tilde{\Psi}_{\mathbf{h}} \neq 0} \frac{|(\mathbb{B}_{\hat{T}}\tilde{\Phi}_{\mathbf{h}}, \tilde{\Psi}_{\mathbf{h}})|}{\|\tilde{\Psi}_{\mathbf{h}}\|} \geq \gamma'\|\tilde{\Phi}_{\mathbf{h}}\|.$$

Proof. We proceed as in the proof of Lemma 1.4.6 and prove the result by contradiction. We consider a sequence $h_n, h_n \to 0$, a sequence $T_n, T_n \to +\infty$, a sequence $\hat{T}_n, \hat{T}_n \to +\infty$, and a sequence $\tilde{\Phi}_{\hat{T}_n, \mathbf{h}_n} \in \tilde{V}_{\hat{T}_n, \mathbf{h}_n}$, $\mathbf{h}_n = (h_n, T_n)$ such that

$$\|\tilde{\Phi}_{\hat{T}_n, \mathbf{h}_n}\| = 1 \quad \text{and} \quad \forall \tilde{\Psi}_{\mathbf{h}_n} \in \tilde{V}_{\mathbf{h}_n}, \ \left| (\mathbb{B}_{\hat{T}_n} \tilde{\Phi}_{\hat{T}_n, \mathbf{h}_n}, \tilde{\Psi}_{\mathbf{h}_n}) \right| \leq \frac{1}{n} \|\tilde{\Psi}_{\mathbf{h}_n}\|.$$

Since $\tilde{\Phi}_{\hat{T}_n, \mathbf{h}_n}$ is bounded in $\tilde{V}$, it admits a weakly convergent subsequence that we denote also by $\tilde{\Phi}_{\hat{T}_n, \mathbf{h}_n} : \tilde{\Phi}_{\hat{T}_n, \mathbf{h}_n} \rightharpoonup \tilde{\Phi}$. Moreover, for all $\tilde{\Psi} \in \tilde{V}$ and all $\tilde{\Psi}_{\mathbf{h}_n} \in \tilde{V}_{\mathbf{h}_n}$ we have

$$|(\mathbb{B}_{\hat{T}_n} \tilde{\Phi}_{\hat{T}_n, \mathbf{h}_n}, \tilde{\Psi})| \leq |(\mathbb{B}_{\hat{T}_n} \tilde{\Phi}_{\hat{T}_n, \mathbf{h}_n}, \tilde{\Psi}_{\mathbf{h}_n})| + |(\mathbb{B}_{\hat{T}_n} \tilde{\Phi}_{\hat{T}_n, \mathbf{h}_n}, \tilde{\Psi} - \tilde{\Psi}_{\mathbf{h}_n})|$$
$$\leq \frac{1}{n} \|\tilde{\Psi}_{\mathbf{h}_n}\| + \|\mathbb{B}_{\hat{T}_n}\| \|\tilde{\Psi} - \tilde{\Psi}_{\mathbf{h}_n}\|.$$

Since $\|\mathbb{B}_{\hat{T}_n}\|$ is bounded by a constant independent of n, we deduce from (1.48) that

$$\mathbb{B}_{\hat{T}_n} \tilde{\Phi}_{\hat{T}_n, \mathbf{h}_n} \rightharpoonup 0 \quad \text{in } \tilde{V}.$$

We can then continue the proof as in Lemma 1.4.6 which results in the contradiction. $\square$

Proof of Theorem 1.4.8.

1. This is a direct consequence of Lemma 1.4.9.

2. Let $\tilde{\Phi}$ be the solution of the original problem (1.49), $\tilde{\Phi}_{\hat{T}}$ the solution of the semi discrete problem (1.51) and $\tilde{\Phi}_{\hat{T}, \mathbf{h}}$ the solution of the discrete problem (1.54). We have that

$$\forall \tilde{\Upsilon}_{\mathbf{h}} \in \tilde{V}_{\mathbf{h}}, \quad \|\tilde{\Phi} - \tilde{\Phi}_{\hat{T}, \mathbf{h}}\| \leq \|\tilde{\Phi} - \tilde{\Upsilon}_{\mathbf{h}}\| + \|\tilde{\Upsilon}_{\mathbf{h}} - \tilde{\Phi}_{\hat{T}, \mathbf{h}}\| \tag{1.75}$$

For all $\tilde{\Upsilon}_{\mathbf{h}} \in \tilde{V}_{\mathbf{h}}$ and all $\tilde{\Psi}_{\mathbf{h}} \in \tilde{V}_{\mathbf{h}}$, we have

$$(\mathbb{B}_{\hat{T}}(\tilde{\Upsilon}_{\mathbf{h}} - \tilde{\Phi}_{\hat{T}, \mathbf{h}}), \tilde{\Psi}_{\mathbf{h}}) = (\mathbb{B}_{\hat{T}}(\tilde{\Upsilon}_{\mathbf{h}} - \tilde{\Phi}_{\hat{T}}), \tilde{\Psi}_{\mathbf{h}}) + (\mathbb{D}_{\hat{T}}(G - G_{\mathbf{h}}), \tilde{\Psi}_{\mathbf{h}}).$$

By Lemma 1.4.9 and by the continuity of $\mathbb{D}_{\hat{T}}$ and $\mathbb{B}_{\hat{T}}$, we get

$$\gamma' \|\tilde{\Upsilon}_{\mathbf{h}} - \tilde{\Phi}_{\hat{T}, \mathbf{h}}\| \leq C \left(\|G - G_{\mathbf{h}}\|_V + \|\tilde{\Phi}_{\hat{T}} - \tilde{\Upsilon}_{\mathbf{h}}\| \right). \tag{1.76}$$

Gathering (1.75-1.76), we deduce that there exists $C > 0$, such that

$$\|\tilde{\Phi} - \tilde{\Phi}_{\hat{T}, \mathbf{h}}\| \leq C \left(\|\tilde{\Phi} - \tilde{\Phi}_{\hat{T}}\| + \|G - G_{\mathbf{h}}\|_V + \inf_{\tilde{\Upsilon}_{\mathbf{h}} \in \tilde{V}_{\mathbf{h}}, \ \tilde{\Upsilon}_{\mathbf{h}} \neq 0} \|\tilde{\Phi} - \tilde{\Upsilon}_{\mathbf{h}}\| \right). \tag{1.77}$$

By Theorem 1.4.2, the first term of the right hand side tends to 0. $G_{\mathbf{h}}$ being the interpolant of G in $\tilde{V}_{\mathbf{h}}$, (1.48) ensures that the two last terms tend to 0 when $\mathbf{h} \to (+\infty, 0)$.

3. Let now suppose that $\Phi = \tilde{\Phi} + G = (\varphi^0, \ldots, \varphi^{n-1})$ the solution of (1.49) is such that for all $j \in \mathbb{Z}/n\mathbb{Z}$, $\varphi^j \in H^s(\Sigma^j)$ for a certain $s > 0$. Then we deduce from Theorem 1.4.2 an estimation of the first term of the right hand side of (1.77). For the second term, it suffices to use classical results of the interpolation error for Lagrange FE of order l:

$$\exists C > 0, \quad \|G - G_{\mathbf{h}}\|_V \leq C h^{\min(s, l+1)}.$$

Finally for the last term, let us introduce the function $\tilde{\Phi}_T \in \tilde{V}$ defined by

$$\tilde{\Phi}_T = \Phi_T - G \quad \text{where} \quad \Phi_T = (\chi_{(-T_0, T_0)} \varphi^0, \ldots, \chi_{(-T_{n-1}, T_{n-1})} \varphi^{n-1}).$$

We get
$$\inf_{\tilde{\Upsilon}_{\mathbf{h}} \in \tilde{V}_{\mathbf{h}}, \, \tilde{\Upsilon}_{\mathbf{h}} \neq 0} \|\tilde{\Phi} - \tilde{\Upsilon}_{\mathbf{h}}\| \leq \|\tilde{\Phi} - \tilde{\Phi}_T\| + \inf_{\tilde{\Upsilon}_{\mathbf{h}} \in \tilde{V}_{\mathbf{h}}, \, \tilde{\Upsilon}_{\mathbf{h}} \neq 0} \|\tilde{\Phi}_T - \tilde{\Upsilon}_{\mathbf{h}}\|$$

where using (1.3), we can show that

$$\|\tilde{\Phi} - \tilde{\Phi}_T\| \leq C \, e^{-\varepsilon T}$$

and using again the results on interpolation error of Lagrange FE

$$\inf_{\tilde{\Upsilon}_{\mathbf{h}} \in \tilde{V}_{\mathbf{h}}, \, \tilde{\Upsilon}_{\mathbf{h}} \neq 0} \|\tilde{\Phi}_T - \tilde{\Upsilon}_{\mathbf{h}}\| \leq C \, h^{\min(s,l+1)}.$$

This ends the proof of the theorem.

Remark 1.4.10. *This error estimate has been obtained for simple regular mesh. A more sophisticated discretization method could be used as done in [25] for scattering problems.*

1.5 Numerical results

The numerical results presented in this section are obtained using the Finite Element library XLiFE++ [50].

1.5.1 Qualitative validation of the method

In order to validate the method, we consider a particular data on a triangle given by

$$g = \frac{1}{4\imath} \left(\alpha H(\omega \sqrt{x^2 + y^2}) + \beta \frac{\partial H}{\partial x^j}(\omega \sqrt{x^2 + y^2}) \right) \Bigg|_{\Sigma_{\mathcal{O}}^j}$$

with $\omega = 1 + 0.1\imath$, $\alpha = 2$, $\beta = -0.5$ and $H(.)$ denotes the zeroth Hankel function of the first kind [2]. The exact solution of this problem is

$$p = \frac{1}{4\imath} H(\omega \sqrt{x^2 + y^2}).$$

On Figure 1.4 we represent on the interval $(-T, T)$ the real and imaginary parts of the exact solution φ^0 (blue line) and of the solution $\varphi^0_{\hat{T},\mathbf{h}}$ (red dots) computed by using P1 finite elements with $h = 0.1$, $T = 20$, $\hat{T} = 10$, and a 3rd order Gauss quadrature with 1000 intervals. We get an L^2 relative error:

$$\frac{\|\varphi^0 - \varphi^0_{\hat{T},\mathbf{h}}\|_{L^2(\Sigma_T^0)}}{\|\varphi^0\|_{L^2(\Sigma_T^0)}}$$

of 0.090%. On Figure 1.5 (left), we represent the Fourier transform of the computed solution. Remark that the behavior of this Fourier transform justifies the truncation of the Fourier integral and requires a precise quadrature especially near $\xi = \omega$.

Once we obtained the $\varphi^j_{\hat{T},\mathbf{h}}$'s, we can reconstruct an approximation of the solution p of (1.1) in each Ω^j by Formula (1.12). Here, we compute the solution in the domain Ω' represented in Figure 1.5 (right), where the white lines represent the position of the Σ^j. In the overlapping
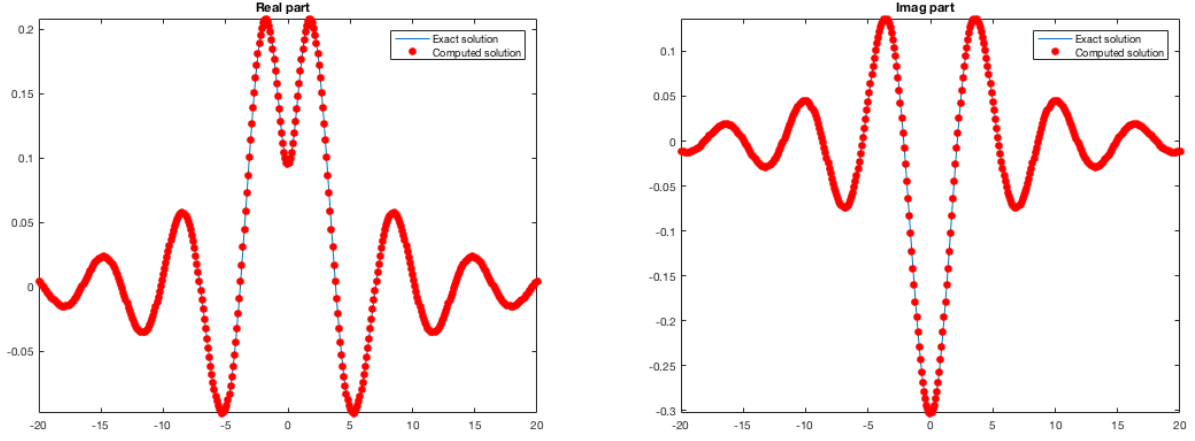
Figure 1.4: Real (left) and imaginary (right) part of the computed solution $\varphi^0_{\hat{T},\mathbf{h}}$ (red points) and the exact solution (blue line) on Σ^0.
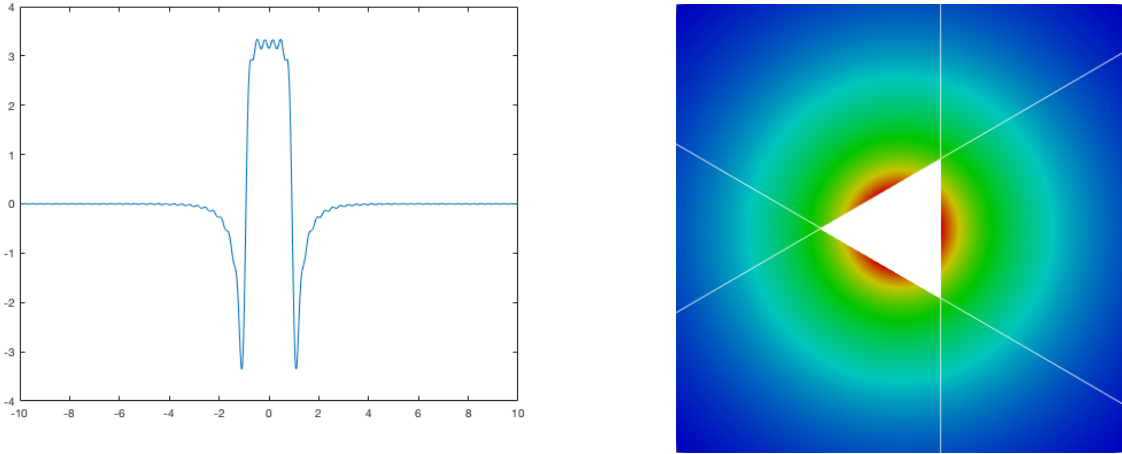
Figure 1.5: On the left: real part of the Fourier transform $\hat{\varphi}^0_{\hat{T},\mathbf{h}}$. On the right: reconstruction of the solution in Ω'.

zones, we can choose indifferently one of the available half-plane representations, since they coincide up to the discretization error. Remark that although the solutions φ^j are not close to zero at $y^j = \pm T$, the reconstructed solution is accurate, with an $L^2(\Omega')$ relative error equal to 0.030%.

The same results can also be obtained when the obstacle is a rectangle or a pentagon. The reconstruction results are shown in Figure 1.6. For a rectangle obstacle, the L^2 relative error for the lines is 0.042% and the L^2 error on the reconstructed domain is 0.043%, while for a pentagon, we get 0.074% L^2 relative error on the lines and 0.054% L^2 relative error on the reconstructed domain.
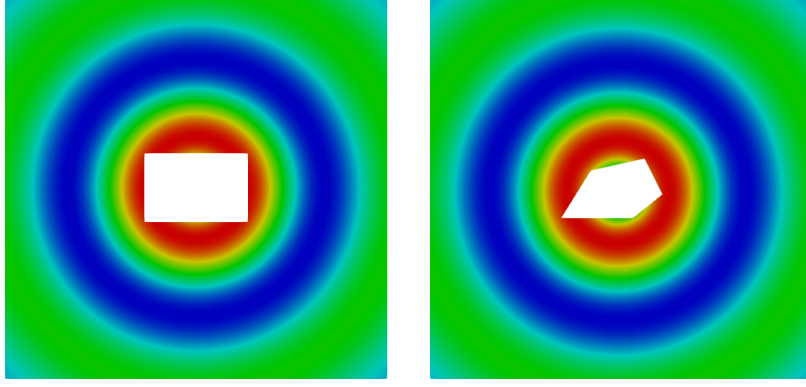
Figure 1.6: Reconstruction of the solution in Ω with rectangle and pentagon.

1.5.2 Quantitative validation of the error estimation

After this qualitative validation, we validate the error estimation derived in Section 1.4 by studying the influence of the different parameters. Since the triangle is regular, it suffices, by symmetry, to only consider the error on Σ^0. We still consider $\alpha = 2$, $\beta = -0.5$, and except in Section 1.5.2, $\omega = 1 + 0.1\imath$.

Influence of the length of the lines (parameter T)

From (1.74), we expect that the error will decay like $e^{-\varepsilon T}$, where ε is the imaginary part of the frequency. That is why, in this section (and only in this section), we consider different values of $\varepsilon \in \{0.05, 0.1, 0.2\}$. We fix the other parameters to $h = 0.025$, $\hat{T} = 10$ and use a 3rd order Gauss quadrature with 1000 intervals.
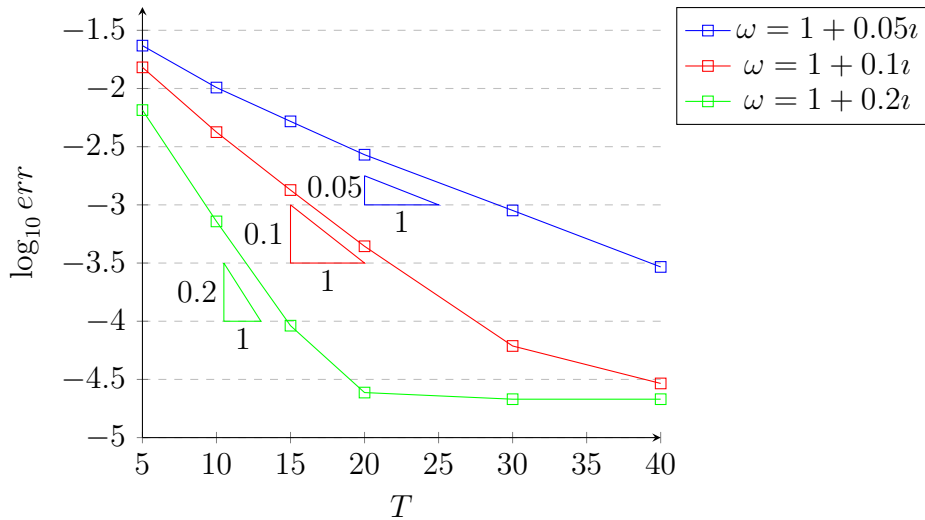
Figure 1.7: Influence of the length of the lines T for various values of $\varepsilon = \mathrm{Im}(\omega)$.

In Figure 1.7, we represent $\log\left(\left\|\varphi^0 - \varphi^0_{\hat{T},\mathbf{h}}\right\|\right)$ as a function of T. The errors $\left\|\varphi^0 - \varphi^0_{\hat{T},\mathbf{h}}\right\|$ decrease exponentially, depending on ε with the following behavior

$$err := \left\|\varphi^0 - \varphi^0_{T,\mathbf{h}}\right\|_{L^2(\Sigma^0_T)} \sim e^{-\varepsilon T},$$

before finally becoming constant, which is due to the other discretization parameters.

Influence of the discretization in space (parameter h)

We plot the error $\log\left(\left\|\varphi^0 - \varphi^0_{\hat{T},\mathbf{h}}\right\|\right)$ as a function of $\log h$. We use the P1 and P2 finite elements and the following parameters:

$$T = 40, \ \hat{T} = 10,$$

and a 3rd order quadrature with 1000 intervals.
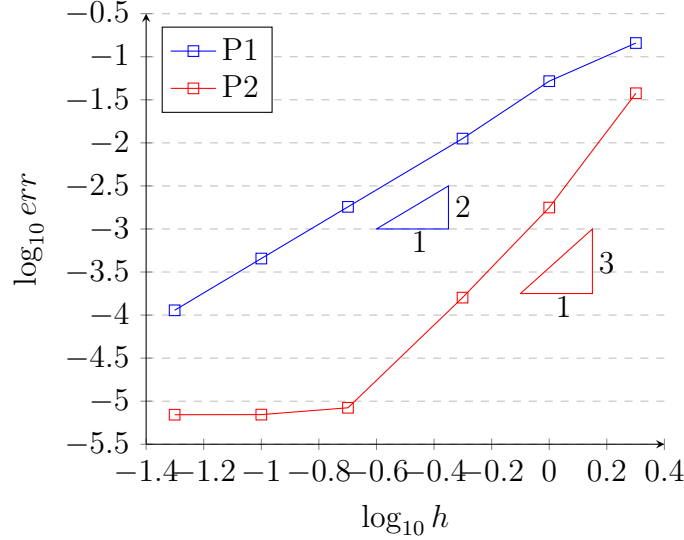
Figure 1.8: Influence of the space discretization h.

Figure 1.8 shows that the error decreases following

$$err \sim h^{l+1},$$

before becoming constant because of the other discretization parameters.

Influence of the truncation of the Fourier integrals (parameter $\hat{T}$)

Finally, we plot the error $\log\left(\left\|\varphi^0 - \varphi^0_{\hat{T},\mathbf{h}}\right\|\right)$ with respect to $\hat{T}$ and we use $T = 40$, $h = 0.1$, and a 3rd order quadrature with $100 \times \hat{T}$ intervals.

From Figure 1.9, we see that the error decreases exponentially due to the $\mathcal{C}^\infty$ regularity of the Hankel function.

The influence of the angles of the polygon

Refering to the Theorem 1.3.7, we investigate the influence of the angles of the polygon on the computation of the solution. Remember that the coercivity constant tends to zero when one of the angles tends to zero (see (1.45)).

We represent the reconstruction of the solution around three different triangles with one angle becoming smaller and smaller ($\min(\theta^{j,j+1}) = 0.33\pi, 0.16\pi, 0.03\pi$). Qualitatively, the results look similar and the L^2 relative error are of the same order (respectively 1.01%, 0.88%, and 1.23%). The condition number of the finite element matrices are 1617.27, 2482.05, and 4647.19 respectively, meaning that it is only slightly affected by the smallness of one of the angles.
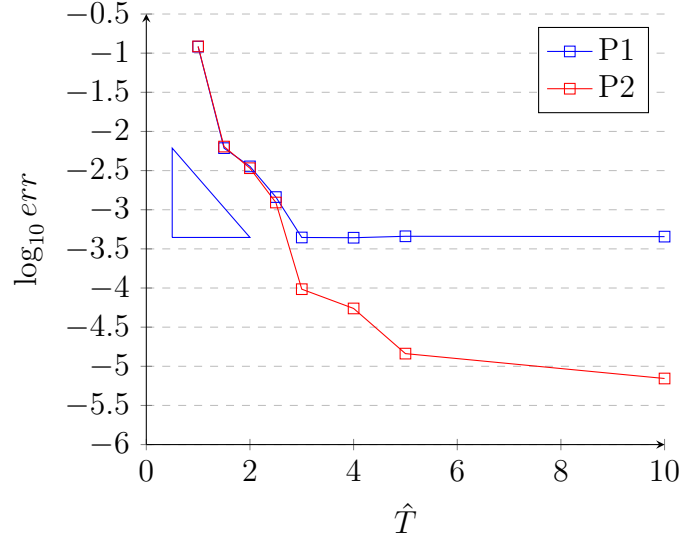
Figure 1.9: Influence of the length of the Fourier integral $\hat{T}$.
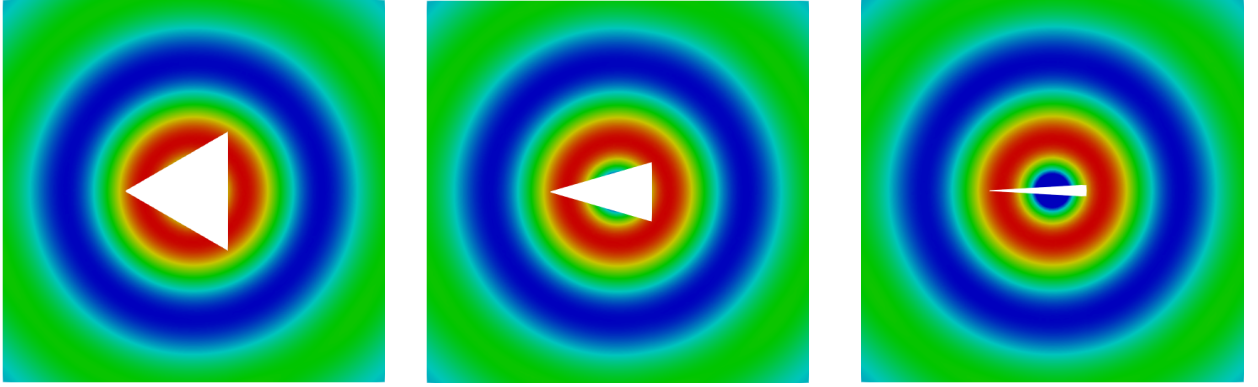
Figure 1.10: Reconstruction of the solution in Ω with triangles that becomes more and more flat.

1.5.3 Extension cases

Non-regular Dirichlet data

In this section, we consider the Dirichlet case, namely (1.1) with $\alpha = 1, \beta = 0$ and we use the Half-Space Matching formulation (1.22) where the φ^j's correspond to the Dirichlet traces of p on the Σ^j's. As mentioned in Section 1.1.2, our formulation allows to consider a data $g \in L^2(\partial\mathcal{O})$ but $g \notin H^{1/2}(\partial\mathcal{O})$. In the following test, we take

$$g = \begin{cases} 1 & \text{if } x^0 = 0, y^0 > 0 \text{ or } x^1 = 0, y^1 < 0, \\ 0 & \text{otherwise.} \end{cases} \tag{1.78}$$

We use P1 discontinuous finite elements since we have a discontinuous boundary condition on $\partial\mathcal{O}$. The real part of the $\varphi^0_{T,\mathbf{h}}$ and the Fourier transform are given in Figure 1.11. As the data is less regular than the previous example, the Fourier transform $\hat{\varphi}^0_{T,\mathbf{h}}$ decays more slowly than in the previous example (pay attention to the scale).
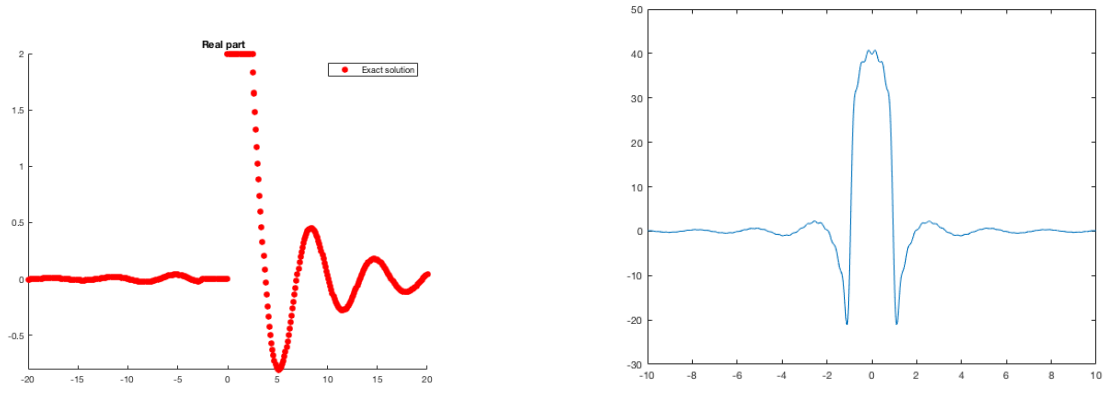
Figure 1.11: On the left: real part of the computed solution φ_h^0 (red points) on Σ^0. On the right: the Fourier transform $\hat{\varphi}^0$ for g defined in (1.78).

The reconstruction in Ω is shown in Figure 1.12. The result is good as there is no visible jump on different reconstructions from different φ^j.
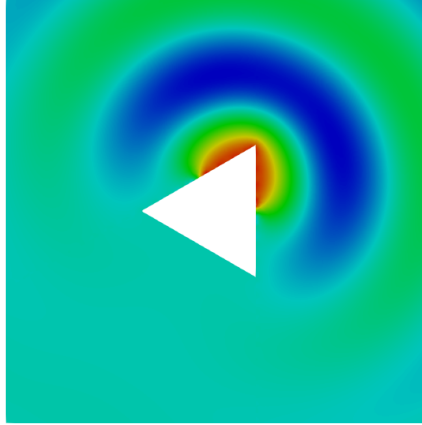
Figure 1.12: Real part of p with $\alpha = 1, \beta = 0, \omega = 1$, with g given defined in (1.78).

Chapter 2

Scattering problem in 2D plane

Summary

This chapter focuses on the 2D acoustic scattering problem by localized obstacles in the non-dissipative case. We revisit several aspects of the HSM formulation and point out several difficulties compared to the dissipative case. Although we are not able to show the well-posedness of the HSM formulation, we still derive the formulations formally. The scattering problem can be written with either the total field or the scattered field as the unknowns. Several HSM formulations are constructed depending on this choice and validated numerically. Finally, based on the direction of the incident field, it is outgoing in some half-spaces and ingoing in the others. We can then develop some formulations where we consider the total field in some half-spaces, and scattered field in the others. We show that the numerical solutions obtained are compatible up to a finer discretization compared to the dissipative case.

2.1 Introduction

The problem setting in this chapter is the following: given an incident field, we are interested in the perturbation induced by some localized obstacles, denoted by $\mathcal{O}$. We take a plane wave for the incident field

$$p_{inc}(\mathbf{x}) = e^{\imath \omega \mathbf{x} \cdot \mathbf{n}} \text{ in } \Omega := \mathbb{R}^2 \backslash \mathcal{O}, \tag{2.1}$$

where $\mathbf{n}$ is the direction of the propagation and $\omega \in \mathbb{R}^+$. The perturbation wave is called the *scattered field*, denoted as p. The *total field* p_{tot} is defined as the superposition of the incident field p_{inc} and the scattered field p

$$p_{tot} = p + p_{inc}. \tag{2.2}$$
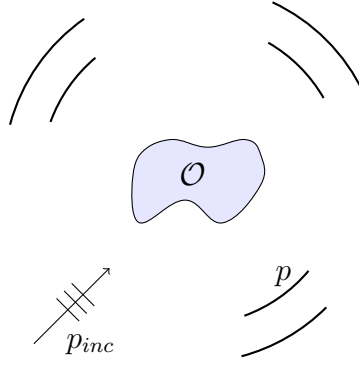
Figure 2.1: Scattering problem in infinite 2D domain.

The total field satisfies the homogeneous Helmholtz equation

$$\left|\begin{array}{l} -\Delta p_{tot} - \omega^2 p_{tot} = 0 \text{ in } \Omega, \\ \quad\quad\quad\quad p_{tot} = 0 \text{ on } \partial\mathcal{O}. \end{array}\right. \tag{2.3}$$

Remark that the boundary condition on $\partial\mathcal{O}$ can be replaced by another boundary condition (for example a Neumann or Robin boundary condition) without any additional difficulty.

This problem as it is now is not well-posed since there exist infinitely many solutions. A condition at infinity should be added to make this problem well-posed. Classically, we impose the *Sommerfeld radiation condition* defined as

$$\lim_{r \to +\infty} \sqrt{r} \left(\frac{\partial}{\partial r} - \imath\omega \right) p \left(r \frac{\mathbf{x}}{\|\mathbf{x}\|} \right) = 0, \tag{2.4}$$

with $r = \|\mathbf{x}\|$, $\mathbf{x} = (x, y) \in \Omega$. Remark that this radiation condition is satisfied by the scattered field p. This condition makes sure that the scattered field is unique and *physical* in the sense that the energy scattered from the obstacles must go to infinity and that there is no source at infinity [64]. Completed with this radiation condition, the problem is well-posed for $p_{tot} \in H^1_{loc}(\Omega)$.

If we rewrite the Sommerfeld radiation condition for the total field, we get

$$\lim_{r \to +\infty} \sqrt{r} \left(\frac{\partial}{\partial r} - \imath\omega \right) (p_{tot} - p_{inc}) \left(r \frac{\mathbf{x}}{\|\mathbf{x}\|} \right) = 0.$$

Notice that the incident field p_{inc} which is the given data, appears only in the radiation condition.

If we write a formulation with the scattered field p as the unknown, we find

$$\left|\begin{array}{ll} \text{Find } p \in H^1_{loc}(\Omega) \text{ such that} \\ \quad\quad\quad -\Delta p - \omega^2 p = 0 & \text{in } \Omega, \\ \quad\quad\quad\quad\quad\quad\quad p = -p_{inc} & \text{on } \partial\mathcal{O}, \\ \lim_{r \to +\infty} \sqrt{r} \left(\frac{\partial}{\partial r} - \imath\omega \right) p \left(r \frac{\mathbf{x}}{\|\mathbf{x}\|} \right) = 0. \end{array}\right. \tag{2.5}$$

By using the scattered field p as the unknown, the incident field p_{inc} appears as a source term. Thus, we have two possible formulations to model the scattering problem.

2.2 The Half-Space Matching Method

To solve this scattering problem, we couple a Finite Element (FE) representation and 4 half-space representations, as described in Chapter 0. We also use the same notations as in Chapter 0

(see Figure 2.2). In the following, we show that there are several difficulties that arise in the non-dissipative case that we did not encounter in the dissipative case. We derive the formulation formally and show some numerical results in the end.
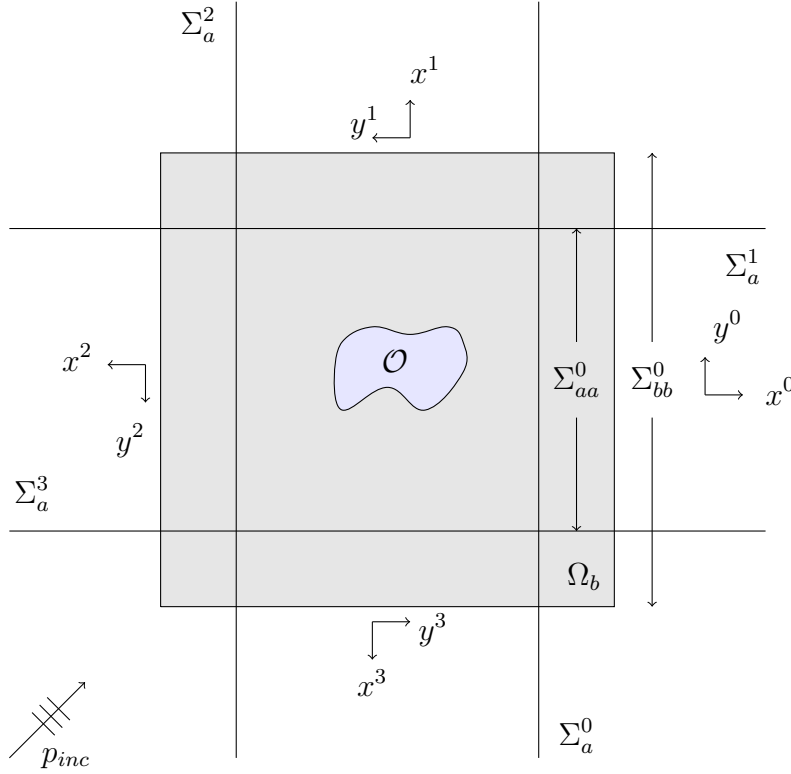
Figure 2.2: Geometry of the problem.

2.2.1 Half-space representation

In this section, we revisit the half-space problem for the scattered field p. We denote again φ^j the trace of the solution p on $\Sigma_a^j, \forall j \in \{0, 1, 2, 3\}$. Since now p is only in $H_{loc}^1(\Omega)$ and not in $H^1(\Omega)$, the trace φ^j is only in $H_{loc}^{1/2}(\Sigma_a^j)$ and not in $H^{1/2}(\Sigma_a^j)$, and it is not even in $L^2(\Sigma_a^j)$ due to its slow decay at infinity (it behaves like $\dfrac{e^{\imath\omega r}}{\sqrt{r}}$ at infinity). Furthermore, since φ^j is not in L^2, the Fourier transform φ^j is not in L^2 either. From the property of the fundamental solution of the Helmholtz equation i.e. the Hankel function of the first kind, $\hat{\varphi}^j$ tends to infinity as ξ tends to $\pm\omega$. However, $\hat{\varphi}^j$ is still integrable in ξ.

We consider now the following problem: for all $\psi^j \in H_{loc}^{1/2}(\Sigma_a^j)$ such that $\hat{\psi}^j \in L^1(\mathbb{R})$, $P^j(\psi^j)$ satisfies

$$\left|\begin{array}{ll} \Delta P^j + \omega^2 P^j = 0, & \text{in } \Omega_a^j, \\ P^j = \psi^j & \text{on } \Sigma_a^j. \end{array}\right. \tag{2.6}$$

For simplicity we consider the half-space Ω_a^0, the same computation can be done in all the other half-spaces. Taking the Fourier transform, we obtain an ODE in x, and the general solution is given by

$$\hat{P}^0(x, \xi) = Ae^{\imath\sqrt{\omega^2 - \xi^2}(x-a)} + Be^{-\imath\sqrt{\omega^2 - \xi^2}(x-a)},$$

where we take the convention

$$\imath\sqrt{\omega^2 - \xi^2} = \begin{cases} \imath\sqrt{\omega^2 - \xi^2} & \text{for } \omega^2 - \xi^2 \geq 0, \\ -\sqrt{\xi^2 - \omega^2} & \text{for } \omega^2 - \xi^2 < 0. \end{cases}$$

To choose the outgoing solution in x direction, we take $B = 0$ and finally take the inverse Fourier transform to obtain

$$P^0(\psi^0)(x, y) = \frac{1}{\sqrt{2\pi}} \int_{\mathbb{R}} \hat{\psi}^0(\xi) e^{i\sqrt{\omega^2 - \xi^2}(x-a)} e^{i\xi y} d\xi \text{ in } \Omega_a^0, \tag{2.7}$$

Remark that formula (2.7) is well-defined because $\hat{\psi}^0$ is integrable in ξ.

2.2.2 The half-space matching formulation

To obtain the HSM formulation, we derive compatibility conditions thanks to the overlap as it is done in Chapter 0. Again, we take different restrictions of the solution:

$$p^b := p \text{ in } \Omega_b$$
$$p^j := p \text{ in } \Omega_a^j, \quad \forall j \in \{0, 1, 2, 3\},$$

and we define φ^j as the trace of p on Σ_a^j:

$$\varphi^j := p|_{\Sigma_a^j}, \quad \forall j \in \{0, 1, 2, 3\}. \tag{2.8}$$

The half-space restriction p^j can be written in terms of its trace φ^j by Formula (2.7). We define the same operators $D^{j,j\pm 1}$ and Λ^j as in Chapter 0 to establish the compatibility conditions between the different representations. We obtain the following formulation:

for a given p_{inc}, find $(p^b, \varphi^0, \varphi^1, \varphi^2, \varphi^3)$ such that

$$\left|\begin{array}{ll} -\Delta p^b - \omega^2 p^b = 0 & \text{in } \Omega_b \\[4pt] \qquad\quad p^b = -p_{inc} & \text{on } \partial\mathcal{O} \\[4pt] \left.\dfrac{\partial p^b}{\partial n}\right|_{\Sigma_{bb}^j} = \Lambda^j \varphi^j & \text{on } \Sigma_{bb}^j \\[8pt] \left.\varphi^j\right|_{\Sigma_{aa}^j} = \left.p^b\right|_{\Sigma_{aa}^j} & \text{on } \Sigma_{aa}^j \\[4pt] \qquad \varphi^{j\pm 1} = D^{j,j\pm 1}\varphi^j & \text{on } \Sigma_a^{j\pm 1} \cap \Omega_a^j. \end{array}\right. \tag{2.9}$$

This formulation poses several difficulties. First, the operators $D^{j,j\pm 1}$'s are not from $L^2(\Sigma_a^j)$ to $L^2(\Sigma_a^{j\pm 1} \cap \Omega_a^j)$. Thus, the analysis done in Chapter 1 does not extend to the non-dissipative case. Another difficulty of this formulation in the non-dissipative case is that we have not been able to show the equivalence of the HSM formulation with the original problem. By construction, we know that if p is the solution of (2.5), then $(p^b, \varphi^0, \varphi^1, \varphi^2, \varphi^3)$ is the solution of (2.9). However, we cannot show the converse statement. The difficulty comes from the inability to show that $P^j(\varphi^j) = P^{j\pm 1}(\varphi^{j\pm 1})$ in $\Omega_a^j \cap \Omega_a^{j\pm 1}$. Indeed, for example taking the difference $v := P^0 - P^1$, it satisfies the Helmholtz equation in $\Omega^0 \cap \Omega^1$ with homogeneous Dirichlet boundary condition

$$\left|\begin{array}{l} \Delta v + \omega^2 v = 0 \text{ in } \Omega_a^0 \cap \Omega_a^1 \\ \qquad\quad v = 0 \text{ on } \Sigma_a^1 \cap \Omega_a^0 \\ \qquad\quad v = 0 \text{ on } \Sigma_a^0 \cap \Omega_a^1. \end{array}\right.$$

Unfortunately, this problem is not coercive in the non-dissipative case. Moreover, P^0 satisfies the radiation condition only in the direction of positive x, and P^1 satisfies it in the direction of positive y. To obtain $v = 0$, we need to have the radiation condition in all outgoing direction of the quarter plane $\Omega_a^0 \cap \Omega_a^1$. Due to the lack of this condition, we cannot conclude to the equivalence. The same difficulties are also encountered in the other formulations that we develop in the following sections. Despite these difficulties, we show that numerically it works well.
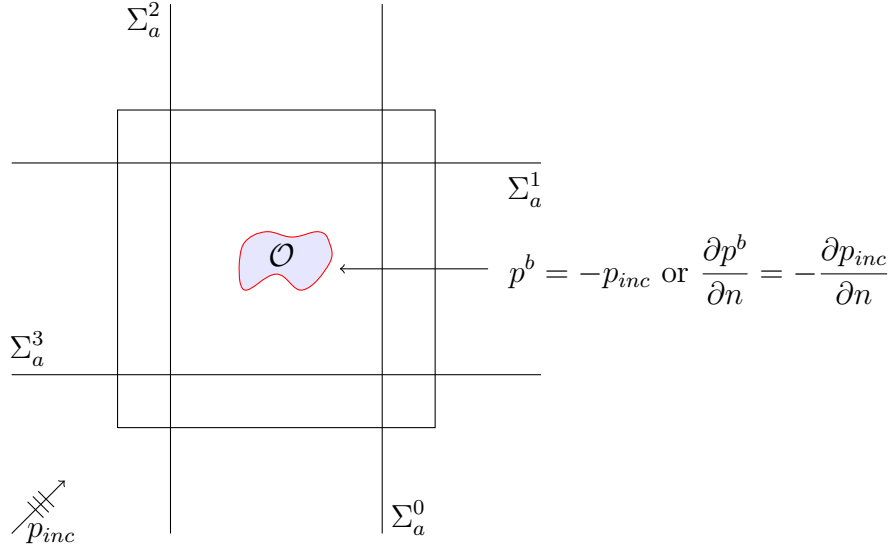
Figure 2.3: The incident field appears as the source term on the boundary of the obstacle for Formulation (2.9).

2.2.3 Different choices of representation

As the scattering problem can be written with the total field p_{tot} or the scattered field p as the unknown, the HSM formulation can also be written with different unknowns. The simplest formulation is the one where we take the scattered field for all of the unknowns (p^b, φ^j) which is given by (2.9). In this formulation, the incident field p_{inc} appears as the source term at the boundary of the obstacles. In many more complicated configurations, it is usually not easy to define the incident field (for example in a junction of waveguides). In such cases, we have no choice but to use the total field as the unknown. With this motivation, we would like to derive some formulations with the total field as the unknowns.

Total-scattered formulation

Let us now start by constructing an HSM formulation with the total field p_{tot}^b on the bounded domain Ω_b but the scattered field φ^j on the lines as the unknowns. The restriction p_{tot}^b satisfies the same problem as p_{tot}

$$\left|\begin{array}{rl} -\Delta p_{tot}^b - \omega^2 p_{tot}^b = 0 & \text{in } \Omega_b \\ p_{tot}^b = 0 & \text{on } \partial\mathcal{O}. \end{array}\right. \tag{2.10}$$

Since we take the scattered field traces on the lines, they satisfy the same equations as the one from Formulation (2.9)

$$\varphi^{j\pm1} = D^{j,j\pm1}\varphi^j \text{ on } \Sigma_a^{j\pm1} \cap \Omega_a^j.$$

However, the compatibility relations between p_{tot}^b and φ^j are a little bit different. We have

$$\varphi^j\big|_{\Sigma_{aa}^j} = p_{tot}^b\big|_{\Sigma_{aa}^j} - p_{inc}\big|_{\Sigma_{aa}^j}.$$

To write the compatibility relation involving the operator Λ^j on Σ_{bb}^j, we should first notice that this operator is defined from the operator P^j, which only gives the outgoing solution in the half-space Ω^j. By definition, the scattered field is outgoing in all half-spaces. On the other hand, the incident field is only outgoing in some half-spaces depending on the direction of the propagation $\mathbf{n}$. Therefore, the total field, which is the superposition of the scattered field

and the incident field, is not always outgoing in all half-spaces either. Hence, we write the compatibility relation for the scattered field

$$\frac{\partial}{\partial n}\left(\left.p^b_{tot}\right|_{\Sigma^j_{bb}} - \left.p_{inc}\right|_{\Sigma^j_{bb}}\right) = \left.\frac{\partial P^j}{\partial n}\right|_{\Sigma^j_{bb}}.$$

The right hand side can then be written by using the operator Λ^j and we obtain

$$\frac{\partial}{\partial n}\left(\left.p^b_{tot}\right|_{\Sigma^j_{bb}} - \left.p_{inc}\right|_{\Sigma^j_{bb}}\right) = \Lambda^j\varphi^j \text{ on } \Sigma^j_{bb}.$$

Finally, we obtain the total-scattered formulation

find $(p^b_{tot}, \varphi^0, \varphi^1, \varphi^2, \varphi^3)$ such that

$$\left|\begin{aligned} -\Delta p^b_{tot} - \omega^2 p^b_{tot} &= 0 && \text{in } \Omega_b \\ p^b_{tot} &= 0 && \text{on } \partial\mathcal{O} \\ \frac{\partial}{\partial n}\left(\left.p^b_{tot}\right|_{\Sigma^j_{bb}} - \left.p_{inc}\right|_{\Sigma^j_{bb}}\right) &= \Lambda^j\varphi^j && \text{on } \Sigma^j_{bb} \\ \left.\varphi^j\right|_{\Sigma^j_{aa}} &= \left.p^b_{tot}\right|_{\Sigma^j_{aa}} - \left.p_{inc}\right|_{\Sigma^j_{aa}} && \text{on } \Sigma^j_{aa} \\ \varphi^{j\pm1} &= D^{j,j\pm1}\varphi^j && \text{on } \Sigma^{j\pm1}_a \cap \Omega^j. \end{aligned}\right. \tag{2.11}$$
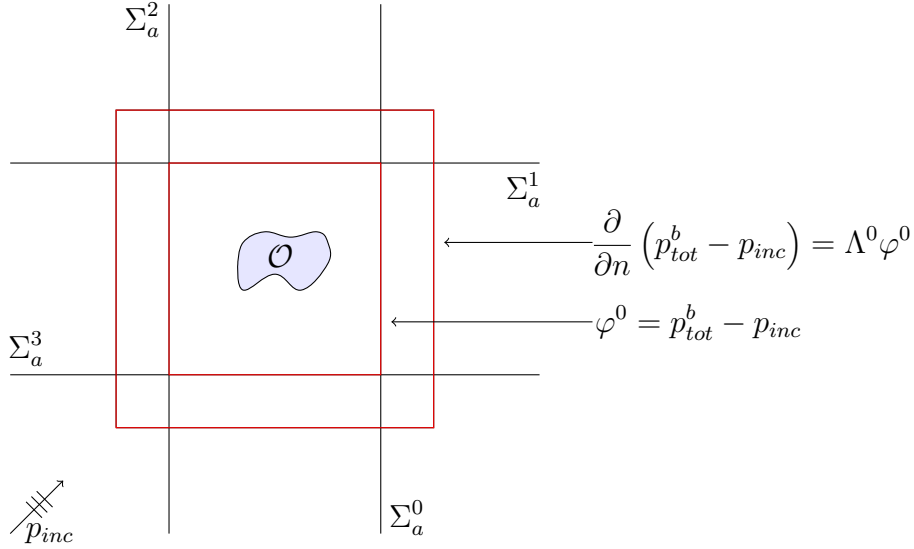
Figure 2.4: The incident field appears on the squares Σ_{aa} and Σ_{bb} in the compatibility relations in the total-scattered HSM formulation.

Total-total formulation

We can take one step further by considering the trace of the total field φ^j_{tot} on the lines too. The equations satisfied by p^b_{tot} is (2.10). Remark again that the half-space representation P^j is defined for outgoing solutions. We write the compatibility relations between the traces for the scattered field

$$\varphi^{j\pm1}_{tot} - \left.p_{inc}\right|_{\Sigma^{j\pm1}_a \cap \Omega^j_a} = D^{j,j\pm1}\left(\varphi^j_{tot} - \left.p_{inc}\right|_{\Sigma^j_a}\right) \text{ on } \Sigma^{j\pm1}_a \cap \Omega^j_a.$$

From the same reasoning, the compatibility relations involving the operator Λ^j is

$$\frac{\partial}{\partial n}\left(p^b_{tot}\big|_{\Sigma^j_{bb}} - p_{inc}\big|_{\Sigma^j_{bb}}\right) = \Lambda^j(\varphi^j_{tot} - p_{inc}\big|_{\Sigma^j_a}) \text{ on } \Sigma^j_{bb}.$$

Finally, we also have

$$\varphi^j_{tot}\big|_{\Sigma^j_{aa}} = p^b_{tot}\big|_{\Sigma^j_{aa}}.$$

Summing up, the total-total formulation is

find $(p^b_{tot}, \varphi^0_{tot}, \varphi^1_{tot}, \varphi^2_{tot}, \varphi^3_{tot})$ such that

$$\left|\begin{array}{ll}
\qquad -\Delta p^b_{tot} - \omega^2 p^b_{tot} = 0 & \text{in } \Omega_b \\[4pt]
\qquad\qquad\qquad p^b_{tot} = 0 & \text{on } \partial\mathcal{O} \\[4pt]
\frac{\partial}{\partial n}\left(p^b_{tot}\big|_{\Sigma^j_{bb}} - p_{inc}\big|_{\Sigma^j_{bb}}\right) = \Lambda^j(\varphi^j_{tot} - p_{inc}\big|_{\Sigma^j_a}) & \text{on } \Sigma^j_{bb} \\[4pt]
\qquad\qquad \varphi^j_{tot}\big|_{\Sigma^j_{aa}} = p^b_{tot}\big|_{\Sigma^j_{aa}} & \text{on } \Sigma^j_{aa} \\[4pt]
\varphi^{j\pm1}_{tot} - p_{inc}\big|_{\Sigma^{j\pm1}_a \cap \Omega^j_a} = D^{j,j\pm1}\left(\varphi^j_{tot} - p_{inc}\big|_{\Sigma^j_a}\right) & \text{on } \Sigma^{j\pm1}_a \cap \Omega^j_a.
\end{array}\right. \tag{2.12}$$

Figure 2.5: The incident field appears on the squares Σ_{bb} and the half-lines $\Sigma^{j\pm1}_a \cap \Omega^j_a$ in the compatibility relations in the total-total HSM formulation.

2.3 Numerical aspects

2.3.1 Discretization

In order to solve the HSM formulation numerically, we write the variational formulation and then discretize it. The variational formulation for the scattered-scattered formulation (2.9) is

find $(p^b, \varphi^0, \varphi^1, \varphi^2, \varphi^3)$, $p^b = \varphi^j$ on Σ^j_{aa} and $p^b = -p_{inc}$ on $\partial\mathcal{O}$, such that for all $(q, \psi^0, \psi^1, \psi^2, \psi^3)$, $q = \psi^j$ on Σ^j_{aa} and $q = 0$ on $\partial\mathcal{O}$,

$$\left|\begin{array}{l}
\displaystyle\int_{\Omega_b} \nabla p^b \cdot \nabla q - \omega^2 p^b q - \int_{\Sigma^j_{bb}} \Lambda^j \varphi^j q = 0, \\[12pt]
\displaystyle\int_{\Sigma^{j\pm1}_a \cap \Omega^j_a} \varphi^{j\pm1} \psi^{j\pm1} - D^{j,j\pm1} \varphi^j \psi^{j\pm1} = 0, \quad \forall j \in \mathbb{Z}/4\mathbb{Z}.
\end{array}\right. \tag{2.13}$$

The variational formulation for the total-scattered formulation is

find $(p_{tot}^b, \varphi^0, \varphi^1, \varphi^2, \varphi^3)$, $p_{tot}^b - p_{inc} = \varphi^j$ on Σ_{aa}^j and $p_{tot}^b = 0$ on $\partial\mathcal{O}$, such that for all $(q, \psi^0, \psi^1, \psi^2, \psi^3)$, $q - p_{inc} = \psi^j$ on Σ_{aa}^j and $q = 0$ on $\partial\mathcal{O}$,

$$
\left|
\begin{aligned}
&\int_{\Omega_b} \nabla p_{tot}^b \cdot \nabla q - \omega^2 p_{tot}^b q - \int_{\Sigma_{bb}^j} \Lambda^j \varphi^j q = \sum_{j=0}^3 \int_{\Sigma_{bb}^j} \frac{\partial p_{inc}}{\partial n} q, \\
&\int_{\Sigma_a^{j\pm1} \cap \Omega_a^j} \varphi^{j\pm1} \psi^{j\pm1} - D^{j,j\pm1} \varphi^j \psi^{j\pm1} = 0.
\end{aligned}
\right.
\tag{2.14}
$$

Finally, the variational formulation for total-total formulation is

find $(p_{tot}^b, \varphi_{tot}^0, \varphi_{tot}^1, \varphi_{tot}^2, \varphi_{tot}^3)$, $p_{tot}^b = \varphi_{tot}^j$ on Σ_{aa}^j and $p_{tot}^b = 0$ on $\partial\mathcal{O}$, such that for all $(q, \psi^0, \psi^1, \psi^2, \psi^3)$, $q = \psi^j$ on Σ_{aa}^j and $q = 0$ on $\partial\mathcal{O}$,

$$
\left|
\begin{aligned}
&\int_{\Omega_b} \nabla p_{tot}^b \cdot \nabla q - \omega^2 p_{tot}^b q - \int_{\Sigma_{bb}^j} \Lambda^j \varphi_{tot}^j q = \sum_{j=0}^3 \int_{\Sigma_{bb}^j} \frac{\partial p_{inc}}{\partial n} q - \int_{\Sigma_{bb}^j} \Lambda^j p_{inc} q, \\
&\int_{\Sigma_a^{j\pm1} \cap \Omega_a^j} \varphi_{tot}^{j\pm1} \psi^{j\pm1} - D^{j,j\pm1} \varphi_{tot}^j \psi^{j\pm1} = \int_{\Sigma_a^{j\pm1} \cap \Omega_a^j} p_{inc} \psi^{j\pm1} - D^{j,j\pm1} p_{inc} \psi^{j\pm1}.
\end{aligned}
\right.
\tag{2.15}
$$

For the discretization, we use the same ingredients as in Chapter 0:

- we truncate the lines Σ_a^j to a segment $\Sigma_{a,T}^j$ and discretize the traces with 1D P1 Lagrange elements with h as the discretization step,

- we discretize p^b with 2D P1 Lagrange elements,

- we truncate the Fourier integrals from $\mathbb{R}$ to $[-\hat{T}, \hat{T}]$ and apply a quadrature formula to approximate the integral operators.

Remark that the total-total formulation is a little bit more intricate due to the incident field data that appears in the integral operators $\Lambda^j \left(p_{inc}|_{\Sigma_a^j} \right)$ and $D^{j,j\pm1} \left(p_{inc}|_{\Sigma_a^j} \right)$, in which its Fourier transform has to be computed. For example, let us consider the operator $D^{0,1}$

$$
D^{0,1} \left(p_{inc}|_{\Sigma_a^0} \right)(x, a) = \frac{1}{\sqrt{2\pi}} \int_{\mathbb{R}} \widehat{p_{inc}|_{\Sigma_a^0}}(\xi) e^{i\sqrt{\omega^2 - \xi^2}(x-a)} e^{i\xi a} d\xi.
$$

The incident field is a plane wave as given in (2.1). Taking $\mathbf{n} = (\cos\theta, \sin\theta)^T$, we obtain

$$
p_{inc}(a, y) = e^{i\omega a \cos\theta} e^{i\omega y \sin\theta} \text{ on } \Sigma_a^0,
$$

and its Fourier transform is a Dirac distribution

$$
\widehat{p_{inc}|_{\Sigma_a^0}}(\xi) = \sqrt{2\pi} e^{i\omega a \cos\theta} \delta(\xi - \omega \sin\theta).
$$

A priori, we cannot compute this distribution numerically. However, due to the truncation of the line Σ_a^0, the approximate Fourier transform becomes regular

$$
\begin{aligned}
\widehat{p_{inc}|_{\Sigma_{a,T}^0}}(\xi) &= \frac{1}{\sqrt{2\pi}} e^{i\omega a \cos\theta} \int_{-T}^{T} e^{i y \sin\theta} e^{-i\xi y} dy \\
&= \frac{2}{\sqrt{2\pi}} e^{i\omega a \cos\theta} \frac{\sin(\xi - \omega \sin\theta)T}{\xi - \omega \sin\theta}.
\end{aligned}
$$

In Figure 2.6 we illustrate the Fourier transform $\widehat{p_{inc}|_{\Sigma_{a,T}^0}}$ for different values of T. As T tends to infinity, the peak of the Fourier transform at $\xi = \omega \sin\theta$ also tends to infinity as it is approaching a Dirac distribution. Thus, thanks to the discretization, the Fourier transform of the truncated incident field can be computed but a finer discretization in ξ around $\omega \sin\theta$ is needed when larger T is used.
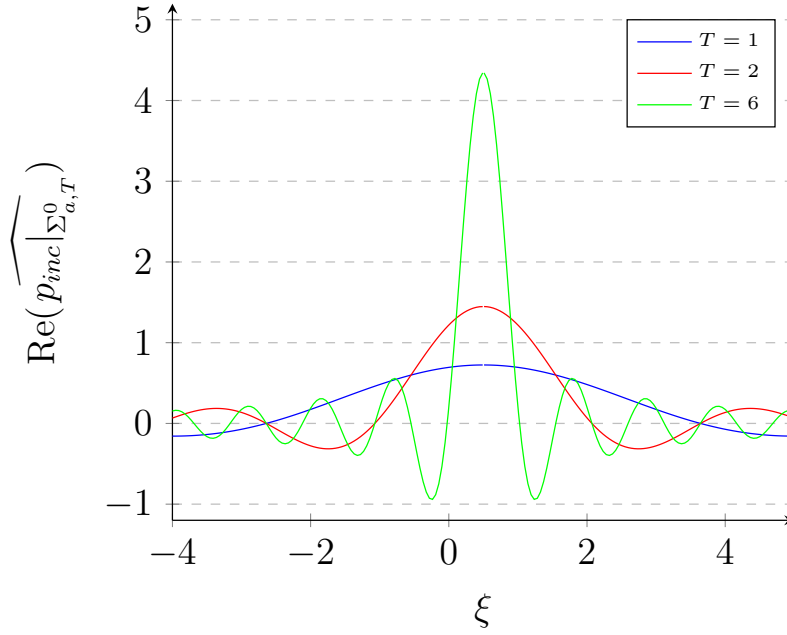
Figure 2.6: The Fourier transform of the truncated incident field for different values of the truncation parameter T.

2.3.2 Numerical results

For a numerical simulation, we consider a unit disk centered in $(-1, 1)$ and a square centered in $(1.5, -1.5)$ with sides of length 1 as the obstacles $\mathcal{O}$. For the geometry, we take $a = 4$, $b = 6$, and the lines are truncated into segments with $T = 10$ and discretized with $h = 0.1$. We take $\hat{T} = 10$ and a 3rd order Gauss quadrature with 1000 intervals to compute the Fourier integrals. Furthermore, we consider an incident field with $\mathbf{n} = (\cos \pi/3, \sin \pi/3)^T$ and $\omega = 1$. This parameters are used for all formulations, unless stated otherwise. Since we do not have the exact solution of this problem, we will only show several numerical results for different formulations and compare them qualitatively.

Scattered-scattered formulation

In Figure 2.7 (a), we show the diffracted field obtained by Formulation (2.9). By simply superposing the diffracted field and the incident field, we obtain the total field in Ω_b as given in Figure 2.7 (b).

In addition to the scattered field in Ω_b, we also obtain $\varphi_{T,h}^j$ on Σ^j. In Figure 2.8 we show the trace $\varphi_{T,h}^0$ and its Fourier transform $\hat{\varphi}_{T,h}^0$. The Fourier transform spikes higher than the one for the dissipative case, which means that a finer quadrature is needed for the non-dissipative case. These peaks theoretically tend to infinity as T tends to infinity.

Once the traces $\varphi_{T,h}^j$ are obtained, we can reconstruct the scattered field in the half-spaces Ω^j by using Formula (2.7). By simply adding the incident field, we can also obtain the total field in the whole domain Ω. We reconstruct the solution in

$$\Omega' := [-10, 10]^2 \backslash \mathcal{O}.$$

In each overlap zone (for example in $\Omega^b \cap \Omega^j$ or in $\Omega^j \cap \Omega^{j\pm1}$), we can choose any representation that we like because they coincide up to some discretization error. In the following results,
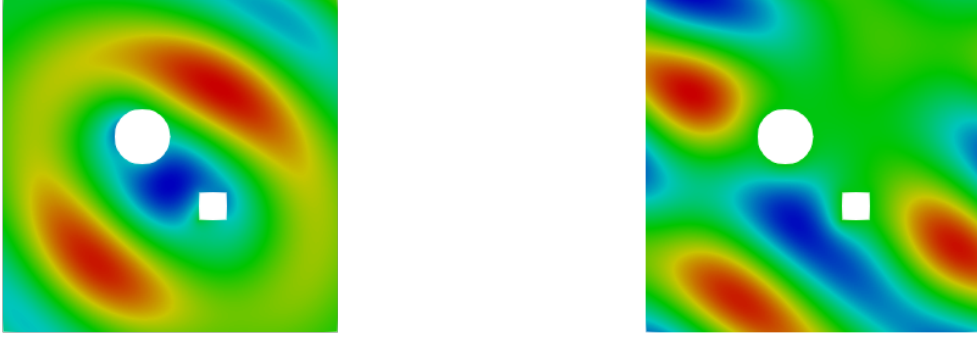
Figure 2.7: Real part of the (a) scattered field and the (b) total field in Ω_b obtained by Formulation (2.9).
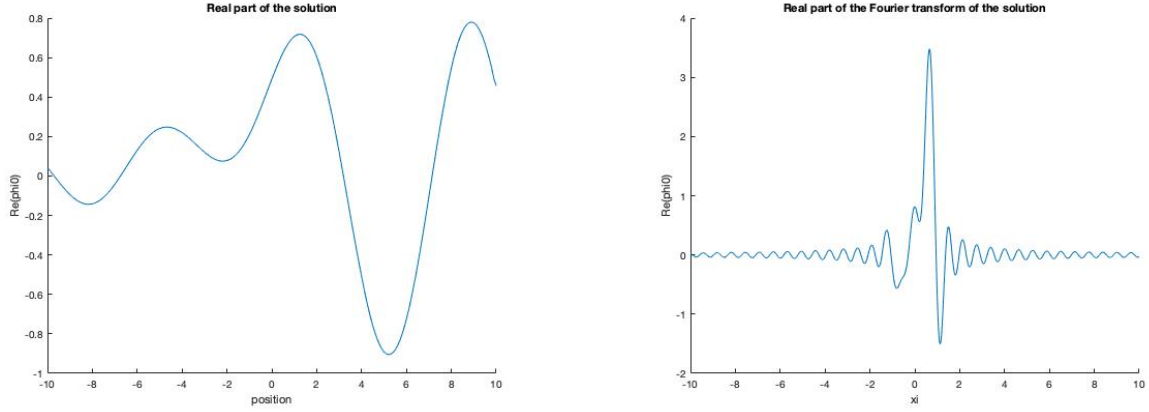
Figure 2.8: (a) Real part of the scattered field $\varphi_{T,h}^0$ and (b) the real part of the Fourier transform $\hat{\varphi}_{T,h}^0$.

we choose the representation in Ω^b (in the overlap $\Omega^b \cap \Omega^j$), the representations in Ω^0 (in the overlap $\Omega^0 \cap \Omega^1$ and $\Omega^0 \cap \Omega^3$) and Ω^2 (in the overlap $\Omega^2 \cap \Omega^1$ and $\Omega^2 \cap \Omega^3$).

Figure 2.9 shows the scattered field and total field completed with the half-space representations obtained from the traces $\varphi_{T,h}^j$ in Ω'. Remark that there is no apparent discontinuity in the solutions between two different representations in two different half-planes. We conclude that the representations coincide in the overlapping zone.

Comparison with total-scattered and total-total formulations

For the total-scattered formulation, once we solve (2.14), we obtain the total field in Ω_b and the scattered field on Σ_a^j. The scattered field in Ω_b can be obtained by simply subtracting the incident field p_{inc} from the computed total field p_{tot}^b. To reconstruct the scattered field in the half-space Ω_a^j from the scattered field trace φ^j, we use the same formula (2.7), and the total field is obtained again by adding the incident field in the half-space.

For the total-total formulation, we do the same thing to obtain the scattered field in Ω_b.
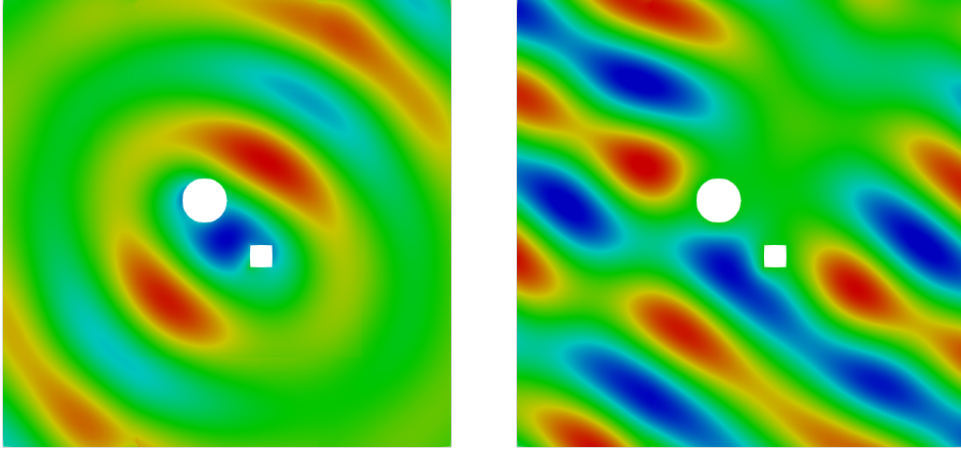
Figure 2.9: Real part of the (a) scattered field and (b) total field obtained in Ω' for the scattered-scattered formulation.

Contrary to the total-scattered formulation, now we directly obtain the total field trace on Σ_a^j. However, to obtain the total field in the half-space, we a priori cannot use directly the operator P^j due to the same reason i.e. the operator P^j only produces outgoing solutions while the total field is not always outgoing. Thus, we need to first reconstruct the scattered field in the half-space by taking the scattered field trace

$$P^j(\varphi_{tot}^j)(x^j, y^j) = \frac{1}{\sqrt{2\pi}} \int_{\mathbb{R}} \widehat{(\varphi_{tot}^j - p_{inc}|_{\Sigma_a^j})}(\xi) e^{i\sqrt{\omega^2 - \xi^2}(x^j - a)} e^{i\xi y^j} \mathrm{d}\xi. \qquad (2.16)$$

The total field can then be obtained by adding the incident field

$$P_{tot}^j(\varphi_{tot}^j)(x^j, y^j) = \frac{1}{\sqrt{2\pi}} \int_{\mathbb{R}} \widehat{(\varphi_{tot}^j - p_{inc}|_{\Sigma_a^j})}(\xi) e^{i\sqrt{\omega^2 - \xi^2}(x^j - a)} e^{i\xi y^j} \mathrm{d}\xi + p_{inc}(x^j, y^j). \qquad (2.17)$$

In Figure 2.10 we show the real part of the scattered field and in Figure 2.11 the total field for all 3 formulations in Ω'. Qualitatively, there is no apparent difference from these 3 formulations and there is no apparent jump between different representations. Once again we conclude that the representations coincide in the overlapping zones.
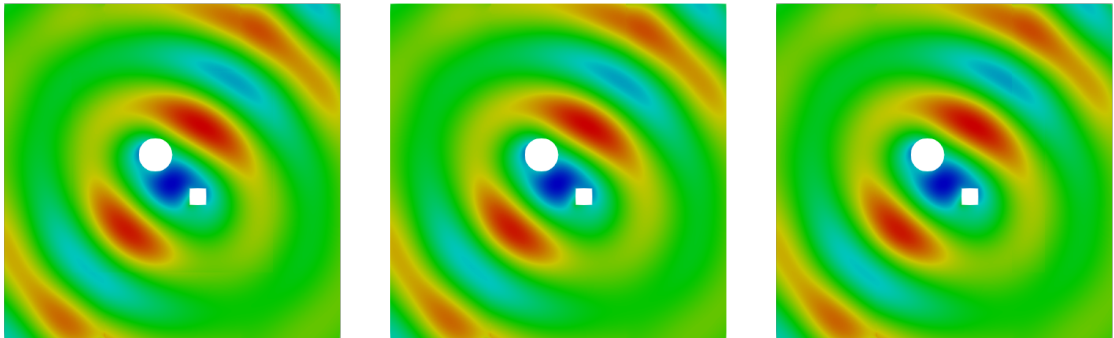
Figure 2.10: Real part of the scattered field for the (a) scattered-scattered, (b) total-scattered, and (c) total-total formulations.
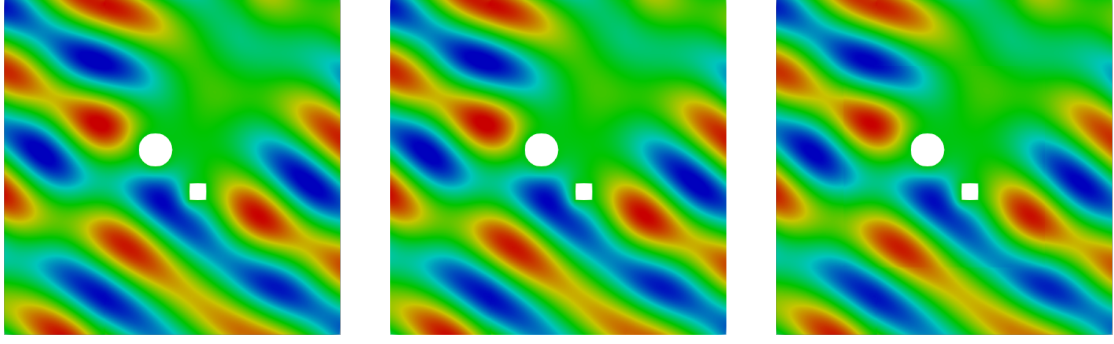
Figure 2.11: Real part of the total field the (a) scattered-scattered, (b) total-scattered, and (c) total-total formulations.

2.4 Extension: mixed formulation

As it is mentioned before, the incident field is outgoing in some half-spaces depending on the direction of the propagation. Indeed, if we take for example the direction

$$\mathbf{n} = (\cos\theta, \sin\theta)^T, \text{ where } 0 < \theta < \frac{\pi}{2}, \tag{2.18}$$

p_{inc} is then outgoing in Ω_a^0 and Ω_a^1, but ingoing in Ω_a^2 and Ω_a^3. Thus, taking for example the
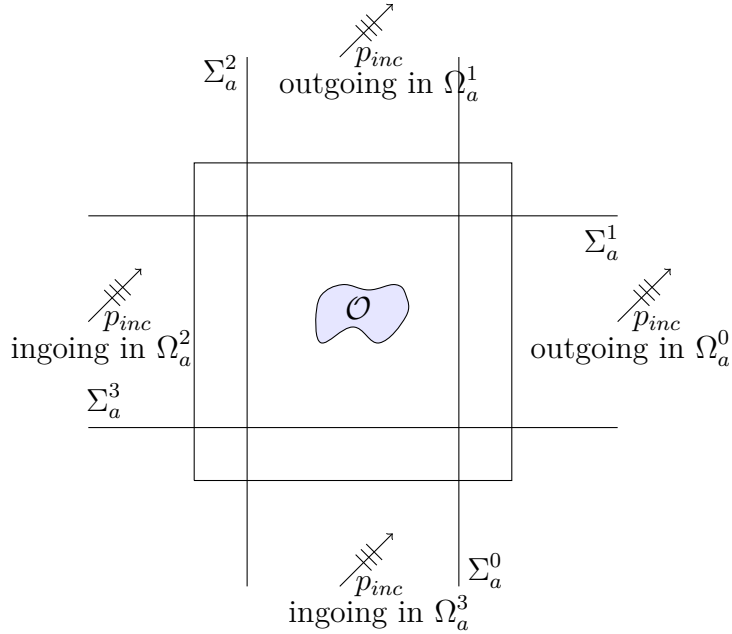
Figure 2.12: The incident field with $\mathbf{n} = (\cos\theta, \sin\theta)^T$ for $0 < \theta < \frac{\pi}{2}$. It is outgoing in Ω_a^0 and Ω_a^1 but ingoing in Ω_a^2 and Ω_a^3.

trace of the incident field on Σ_a^0 and plugging it in P^0, we want to obtain p_{inc} in Ω_a^0. Indeed, direct calculation shows (with an abuse of notation by treating a distribution as a function)

$$P^0(p_{inc}|_{\Sigma_a^0})(x,y) = \frac{1}{\sqrt{2\pi}} \int_{\mathbb{R}} \widehat{p_{inc}|_{\Sigma_a^0}}(\xi) e^{\imath\sqrt{\omega^2-\xi^2}(x-a)} e^{\imath\xi y} \mathrm{d}\xi$$

$$= \frac{1}{\sqrt{2\pi}} \int_{\mathbb{R}} \sqrt{2\pi} e^{\imath\omega a\cos\theta} \delta(\xi - \omega\sin\theta) e^{\imath\sqrt{\omega^2-\xi^2}(x-a)} e^{\imath\xi y} \mathrm{d}\xi$$

$$= e^{\imath\omega x\cos\theta} e^{\imath\omega y\sin\theta}$$

$$= p_{inc}(x, y) \text{ in } \Omega_a^0.$$

However, in Ω_a^3, we have

$$P^3(p_{inc}|_{\Sigma_a^3})(x, y) = \frac{1}{\sqrt{2\pi}} \int_{\mathbb{R}} \widehat{p_{inc}|_{\Sigma_a^3}}(\xi) e^{\imath \sqrt{\omega^2 - \xi^2}(-x-a)} e^{\imath \xi y} d\xi$$

$$= \frac{1}{\sqrt{2\pi}} \int_{\mathbb{R}} \sqrt{2\pi} e^{-\imath \omega a \cos\theta} \delta(\xi - \omega \sin\theta) e^{\imath \sqrt{\omega^2 - \xi^2}(-x-a)} e^{\imath \xi y} d\xi$$

$$= e^{-\imath \omega(x+2a)\cos\theta} e^{\imath \omega y \sin\theta}$$

$$\neq p_{inc}(x, y) \text{ in } \Omega_a^3.$$

Thus, plugging the trace of the incident field to P^3, we obtain a wrong solution in Ω_a^3.

Since p_{inc} is outgoing in Ω_a^0 and Ω_a^1, we can establish a mixed formulation where we take the total field trace as the unknowns on Σ_a^0 and Σ_a^1, but the scattered field trace on Σ_a^2 and Σ_a^3. Furthermore, since φ_{tot}^0 and φ_{tot}^1 are outgoing, the compatibility relations can be written in terms of the total field

$$\begin{aligned} \varphi_{tot}^0 &= D^{1,0}\varphi_{tot}^1 & \text{on } \Sigma^0 \cap \Omega^1, \\ \varphi_{tot}^1 &= D^{0,1}\varphi_{tot}^0 & \text{on } \Sigma^1 \cap \Omega^0. \end{aligned}$$

The compatibility relations involving the operator Λ^j can also be written as

$$\frac{\partial}{\partial n} p_{tot}^b = \Lambda^j \varphi_{tot}^j \qquad \text{on } \Sigma_{bb}^j, j \in \{0, 1\}.$$

The other compatibility relations are written for the scattered field as before.

Therefore, we obtain the following mixed formulation

$$\left| \begin{aligned} -\Delta p_{tot}^b - \omega^2 p_{tot}^b &= 0 & \text{in } \Omega_b \\ p_{tot}^b &= 0 & \text{on } \partial\mathcal{O} \\ \frac{\partial}{\partial n} p_{tot}^b &= \Lambda^j \varphi_{tot}^j & \text{on } \Sigma_{bb}^j, j \in \{0, 1\} \\ \frac{\partial}{\partial n}(p_{tot}^b - p_{inc}) &= \Lambda^j \varphi^j & \text{on } \Sigma_{bb}^j, j \in \{2, 3\} \\ \varphi_{tot}^j &= p_{tot}^b & \text{on } \Sigma_{aa}^j, j \in \{0, 1\} \\ \varphi^j &= p_{tot}^b - p_{inc} & \text{on } \Sigma_{aa}^j, j \in \{2, 3\} \\ \varphi_{tot}^0 &= D^{1,0}\varphi_{tot}^1 & \text{on } \Sigma_a^0 \cap \Omega_a^1 \\ \varphi_{tot}^1 &= D^{0,1}\varphi_{tot}^0 & \text{on } \Sigma_a^1 \cap \Omega_a^0 \\ \varphi_{tot}^1 - p_{inc} &= D^{2,1}\varphi^2 & \text{on } \Sigma_a^1 \cap \Omega_a^2 \\ \varphi_{tot}^0 - p_{inc} &= D^{3,0}\varphi^3 & \text{on } \Sigma_a^0 \cap \Omega_a^3 \\ \varphi^2 &= D^{1,2}\left(\varphi_{tot}^1 - p_{inc}\right) & \text{on } \Sigma_a^2 \cap \Omega_a^1 \\ \varphi^3 &= D^{0,3}\left(\varphi_{tot}^0 - p_{inc}\right) & \text{on } \Sigma_a^3 \cap \Omega_a^0 \\ \varphi^2 &= D^{3,2}\varphi^3 & \text{on } \Sigma_a^2 \cap \Omega_a^3 \\ \varphi^3 &= D^{2,3}\varphi^2 & \text{on } \Sigma_a^3 \cap \Omega_a^2. \end{aligned} \right. \tag{2.19}$$

In Figure 2.14, we show the scattered field and the total field obtained by mixed formulation (2.19), but the solution in the half-spaces are reconstructed by using (2.16 - 2.17). Contrary to what we expected, we see that the solution has a slight discontinuity between different

$$\varphi^2 = D^{1,2}\left(\varphi^1_{tot} - p_{inc}|_{\Sigma^1_a}\right)$$

$$\varphi^0_{tot} = D^{1,0}\varphi^1_{tot}$$

$$\Sigma^2_a$$

$$\varphi^1_{tot} - p_{inc} = D^{2,1}\varphi^2$$

$$\Sigma^1_a$$

$$\varphi^1_{tot} = D^{0,1}\varphi^0_{tot}$$

$$\mathcal{O}$$

$$\Sigma^3_a$$

$$\varphi^3 = D^{2,3}\varphi^2$$

$$\varphi^3 = D^{0,3}\left(\varphi^0_{tot} - p_{inc}|_{\Sigma^0_a}\right)$$

$$p_{inc}$$

$$\varphi^2 = D^{3,2}\varphi^3$$

$$\Sigma^0_a$$

$$\varphi^0_{tot} - p_{inc}|_{\Sigma^3_a} = D^{3,0}\varphi^3$$

Figure 2.13: The compatibility relations for the traces on $\Sigma^j_a \cap \Omega^{j\pm1}_a$.

representations. This is due to the incident field trace on Σ^0_a and Σ^1_a which are truncated. We do not have the equality on the discrete level

$$\frac{\partial}{\partial n}\left(p_{inc,T,h}|_{\Sigma^j_{bb}}\right) \neq \Lambda^j_{\hat{T}}\left(p_{inc,T,h}|_{\Sigma^j_{bb}}\right) \quad \text{on } \Sigma^j_{bb}, j \in \{0,1\}$$

$$p_{inc,T,h}|_{\Sigma^0_a \cap \Omega^1_a} \neq D^{1,0}\left(p_{inc,T,h}|_{\Sigma^1_a}\right) \quad \text{on } \Sigma^0 \cap \Omega^1$$

$$p_{inc,T,h}|_{\Sigma^1_a \cap \Omega^0_a} \neq D^{0,1}\left(p_{inc,T,h}|_{\Sigma^0_a}\right) \quad \text{on } \Sigma^1 \cap \Omega^0.$$

Finally, based on the same argument that p_{inc} is outgoing in Ω^0_a and Ω^1_a, we can a priori directly use φ^j_{tot} to obtain the total field in the half-space instead of (2.17) by using

$$P^j_{tot}(\varphi^j_{tot})(x^j, y^j) = \frac{1}{\sqrt{2\pi}}\int_{\mathbb{R}} \hat{\varphi}^j_{tot}(\xi)e^{i\sqrt{\omega^2-\xi^2}(x^j-a)}e^{i\xi y^j}\,\mathrm{d}\xi. \tag{2.20}$$

Figure 2.14: Real part of the (a) scattered field and (b) total field obtained in Ω' obtained by mixed formulation (2.19).

We want to verify whether this reconstruction formulation works. In Figure 2.15, we represent the total field in (a) $\Omega_b \cup \Omega^0$ and (b) $\Omega_b \cup \Omega^3$. Again, we see a discontinuity between p^b and the
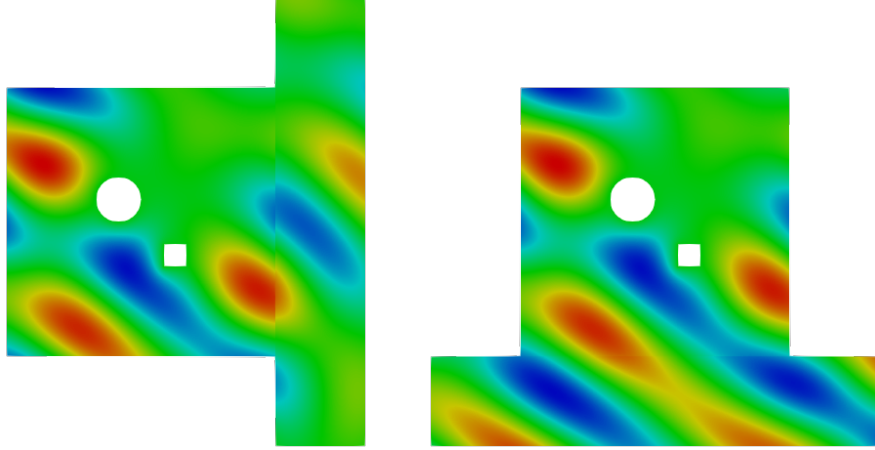
Figure 2.15: Real part of the total field in (a) $\Omega_b \cup \Omega_a^0$ and (b) $\Omega_b \cup \Omega_a^3$ obtained by Formula (2.20).

half-space solution $P^j(\varphi^j)$. Notice in particular that the representations do not match in the overlapping zone $\Omega^0 \cap \Omega^3$. Compared to the results obtained by the previous formulations, the representation $P_{tot}^3(\varphi^3)$ is a better solution than $P_{tot}^0(\varphi_{tot}^0)$ in $\Omega_a^0 \cap \Omega_a^3$. This is because the incident field in $P_{tot}^3(\varphi^3)$ is taken into account exactly, while the incident field in the representation $P_{tot}^0(\varphi_{tot}^0)$ is approximated.

In conclusion, for the same discretization parameters, the formulations in which we use the trace of the scattered field yield better results compared to the ones obtained from the trace of the total field. We suppose that to obtain similar solutions by using the total field trace, it is necessary to take finer discretization to capture the incident field. Thus, when the incident field of the problem is known, it is more advantageous to consider a formulation for the scattered field and superpose it with the incident field.

In the end of Chapter 4 and in the perspectives, we mention a scattering problem for which a hybrid formulation as above can be useful. It is the case of the scattering of a plane wave by the "stair" boundary of a "half-plane". In that case, the scattered field satisfies a non-homogeneous boundary condition on an infinite boundary (the "stair" boundary). To get a compactly supported data, one has to modify the definition of the incident wave, introducing different incident fields in the different half-planes.

Chapter 3

Elasticity problem in 3D plates

Summary

This chapter is dedicated to describe in details the elasticity problem in 3D plates. We consider a time-harmonic elastic wave equation posed in a locally perturbed plate which is infinite in 2 directions and bounded in the direction of the thickness. To treat this problem, we will adapt the Half-Space Matching method. In this 3D case, the 2D half-planes introduced in the previous chapters will be replaced by 3D half-plates. The main difficulty is to derive an explicit representation of the solution in these half-plates. The idea is to combine a Fourier transform in the infinite direction with a modal decomposition in the thickness. Whereas in the 2D case only one trace of the solution is used to express its restriction in a half-space, two traces will be used in the 3D case: the trace of the displacement and the trace of the normal stress. As we will see in Section 3.3.2, this is due to the lack of orthogonality relation between the elastic modes. However, bi-orthogonal relations which involves both the displacement and the normal stress can be used to determine the modal amplitudes in the modal expansion of the half-plate solutions.

We start the chapter by briefly introducing the problem and the notations. Afterwards, we have a short section about the modes in elastic plates since they have a central role in the problem. Indeed, the half-plate representations are obtained by combining a Fourier transform in the direction parallel to the plate and a modal decomposition in the width of the plate. The modes involved in the representation correspond to the Lamb modes described in Section 3.2, considered in a direction given by the Fourier variable. With these half-plate representations involving the traces of the displacement and the normal stress on the boundary, we establish the complete formulation by exploiting some compatibility relations between different representations. We finish the chapter with some numerical results.

3.1   Introduction

In this chapter, we are interested in solving the time-harmonic elastic wave equation completed with a free-surface boundary condition in a perturbed 3D plate $\Omega := \mathbb{R}^2 \times (-d, d)\backslash\mathcal{O}, d > 0$ (see Figure 3.1) where $\mathcal{O}$ is a localized defect.
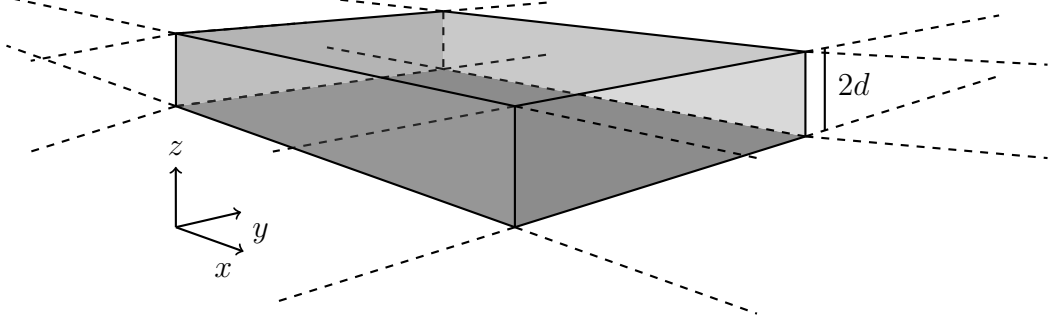
Figure 3.1: The geometry of the unperturbed plate.

More precisely, for a given frequency $\omega \in \mathbb{R}^+$, the displacement field, denoted by $\mathbf{u} = (u_x, u_y, u_z)$, satisfies the equation (see [59])

$$\left|\begin{aligned} -\mathbf{div}(\sigma(\mathbf{u})) - \rho\omega^2\mathbf{u} &= \mathbf{f} \quad \text{in } \Omega, \\ (\sigma(\mathbf{u}))n &= \mathbf{0} \quad \text{on } z = \pm d \text{ and } \partial\mathcal{O}, \end{aligned}\right. \tag{3.1}$$

where n is the outgoing normal, ρ is the density of the medium, $\mathbf{f}$ is the volume source term, and $\sigma(\mathbf{u})$ is the stress tensor which is given by:

$$\sigma(\mathbf{u})_{ij} = \sum_{k,l\in\{x,y,z\}} \mathbf{C}_{ijkl}\epsilon_{kl}, \text{ with } i, j \in \{x, y, z\}, \tag{3.2}$$

where ϵ and $\mathbf{C}$ are the strain and the rigidity tensors. By using the small deformation model, we have

$$\begin{aligned} \epsilon &= \frac{1}{2}\left(\nabla\mathbf{u} + \nabla^T\mathbf{u}\right) \\ &= \begin{pmatrix} \partial_x u_x & \dfrac{\partial_x u_y + \partial_y u_x}{2} & \dfrac{\partial_x u_z + \partial_z u_x}{2} \\ \dfrac{\partial_x u_y + \partial_y u_x}{2} & \partial_y u_y & \dfrac{\partial_y u_z + \partial_z u_y}{2} \\ \dfrac{\partial_x u_z + \partial_z u_x}{2} & \dfrac{\partial_y u_z + \partial_z u_y}{2} & \partial_z u_z \end{pmatrix}. \end{aligned} \tag{3.3}$$

Due to physics laws, the rigidity tensor $\mathbf{C}$ verifies the symmetry property

$$\mathbf{C}_{ijkl} = \mathbf{C}_{klij} = \mathbf{C}_{jilk}, \text{ where } i, j, k, l \in \{x, y, z\}, \tag{3.4}$$

and it is positive definite:

$$\forall\xi \in \mathbb{R}^{3\times3}, \exists\alpha > 0 \text{ such that } \mathbf{C}_{ijkl}\xi_{ij}\xi_{kl} \geq \alpha\|\xi\|^2 = \alpha|\xi_{ij}|^2. \tag{3.5}$$

By using the symmetry property, the writing of the rigidity tensor can be simplified by using a 6×6 matrix $\tilde{\mathbf{C}}$ with *the Voigt notation*

$$\tilde{\mathbf{C}}_{p(i,j),p(k,l)} = \mathbf{C}_{ijkl}, \tag{3.6}$$

where $p(i,j) = p(j,i)$ and

$$p(x,x) = 1, \ p(y,y) = 2, \ p(z,z) = 3,$$
$$p(x,y) = 6, \ p(x,z) = 5, \ p(y,z) = 4. \tag{3.7}$$

By using the same notation, the deformation and stress tensors can as well be simplified and be written as vectors

$$\tilde{\epsilon}(\mathbf{u}) = \begin{pmatrix} \epsilon_{xx} & \epsilon_{yy} & \epsilon_{zz} & 2\epsilon_{yz} & 2\epsilon_{xz} & 2\epsilon_{xy} \end{pmatrix}^T, \text{ and}$$
$$\tilde{\sigma}(\mathbf{u}) = \begin{pmatrix} \sigma_{xx} & \sigma_{yy} & \sigma_{zz} & \sigma_{yz} & \sigma_{xz} & \sigma_{xy} \end{pmatrix}^T. \tag{3.8}$$

In the following we will consider 3 types of material: isotropic, orthotropic, and anisotropic. The rigidity tensor $\tilde{\mathbf{C}}$ for each type is given in Figure 3.2. Thanks to the symmetry, the

c_{11}	c_{12}	c_{13}	c_{14}	c_{15}	c_{16}
c_{12}	c_{22}	c_{23}	c_{24}	c_{25}	c_{26}
c_{13}	c_{23}	c_{33}	c_{34}	c_{35}	c_{36}
c_{14}	c_{24}	c_{34}	c_{44}	c_{45}	c_{46}
c_{15}	c_{25}	c_{35}	c_{45}	c_{55}	c_{56}
c_{16}	c_{26}	c_{36}	c_{46}	c_{56}	c_{66}

Anisotropic

c_{11}	c_{12}	c_{13}	0	0	0
c_{12}	c_{22}	c_{23}	0	0	0
c_{13}	c_{23}	c_{33}	0	0	0
0	0	0	c_{44}	0	0
0	0	0	0	c_{55}	0
0	0	0	0	0	c_{66}

Orthotropic

c_{11}	c_{12}	c_{12}	0	0	0
c_{12}	c_{11}	c_{12}	0	0	0
c_{12}	c_{12}	c_{11}	0	0	0
0	0	0	c_{44}	0	0
0	0	0	0	c_{44}	0
0	0	0	0	0	c_{44}

Isotropic

Figure 3.2: The rigidity tensor $\tilde{\mathbf{C}}$ for different materials.

rigidity tensor for anisotropic, orthotropic, and isotropic materials depend only on 21, 9, and 2 parameters respectively. More precisely for isotropic material, we have

$$c_{11} = \lambda + 2\mu, \quad c_{12} = \lambda, \text{ and } c_{44} = \mu,$$

where λ and μ are called *Lamé parameters*. These parameters can also be represented as

$$\lambda = \frac{E\nu}{(1+\nu)(1-2\nu)} \text{ and } \mu = \frac{E}{2(1+\nu)},$$

where E is the Young modulus and ν is the Poisson ratio of the elastic material. In more details, the operators $\sigma(\mathbf{u})$ and $\mathbf{div}(\sigma(\mathbf{u}))$ for isotropic media are given by

$$\tilde{\sigma}(\mathbf{u}) = \begin{pmatrix} \lambda(\partial_x u_x + \partial_y u_y + \partial_z u_z) + 2\mu\partial_x u_x \\ \lambda(\partial_x u_x + \partial_y u_y + \partial_z u_z) + 2\mu\partial_y u_y \\ \lambda(\partial_x u_x + \partial_y u_y + \partial_z u_z) + 2\mu\partial_z u_z \\ \mu(\partial_y u_z + \partial_z u_y) \\ \mu(\partial_x u_z + \partial_z u_x) \\ \mu(\partial_x u_y + \partial_y u_x) \end{pmatrix}, \tag{3.9}$$

$$\mathbf{div}(\sigma(\mathbf{u})) = \begin{pmatrix} \mu(\partial_{xx} u_x + \partial_{yy} u_x + \partial_{zz} u_x) + (\lambda+\mu)\partial_x(\partial_x u_x + \partial_y u_y + \partial_z u_z) \\ \mu(\partial_{xx} u_y + \partial_{yy} u_y + \partial_{zz} u_y) + (\lambda+\mu)\partial_y(\partial_x u_x + \partial_y u_y + \partial_z u_z) \\ \mu(\partial_{xx} u_z + \partial_{yy} u_z + \partial_{zz} u_z) + (\lambda+\mu)\partial_z(\partial_x u_x + \partial_y u_y + \partial_z u_z) \end{pmatrix}. \tag{3.10}$$

Equivalently to the Helmholtz problem in Chapter 2, Problem (3.1) should be completed with a radiation condition at infinity to make it well-posed. Indeed, we have to select the outgoing solution. This can be done through a radiation condition (see [24] for the isotropic case). In our approach, it will be done in the definition of half-plate representations.

In the following, we impose several hypotheses:

1. the source term $\mathbf{f}$ is compactly supported,

2. the rigidity tensor $\mathbf{C}$ is constant in the exterior of a bounded domain,

3. the density ρ is strictly positive in Ω and constant in the exterior of a bounded domain.

Remark that our method is easily generalizable to stratified plates, where C and ρ in the exterior of a bounded domain are functions of z only.

3.2   Modes in elastic plates

First, let us consider a homogeneous elastic plate without any defect

$$\left|\begin{aligned} \mathbf{div}(\sigma(\mathbf{U})) + \rho\omega^2\mathbf{U} &= \mathbf{0} \quad \text{in } \mathbb{R}^2 \times (-d, d), \\ \sigma(\mathbf{U})n &= \mathbf{0} \quad \text{on } z = \pm d. \end{aligned}\right. \tag{3.11}$$

The modes are particular solutions of (3.11) of the form:

$$\mathbf{U}(x, y, z) = \mathcal{U}(z)e^{\imath\alpha_x x + \imath\alpha_y y}, \quad \mathcal{U} \neq 0. \tag{3.12}$$

If α_x and α_y are real, the associated mode propagates in the direction $(\alpha_x, \alpha_y)^T$ without attenuating. We call such mode a *propagative* mode. Otherwise, the associated mode vanishes at least in one direction. It is called an *evanescent* mode.

Plugging this form into (3.11), we obtain

$$\left|\begin{aligned} \mathbf{div}^{\alpha_x,\alpha_y}(\sigma^{\alpha_x,\alpha_y}(\mathcal{U})) + \rho\omega^2\mathcal{U} &= \mathbf{0} \quad \text{for } z \in S := (-d, d), \\ \sigma^{\alpha_x,\alpha_y}(\mathcal{U})n &= \mathbf{0} \quad \text{on } z = \pm d, \end{aligned}\right. \tag{3.13}$$

where $\sigma^{\alpha_x,\alpha_y}$ and $\mathbf{div}^{\alpha_x,\alpha_y}$ are the operators σ and $\mathbf{div}$ with the derivative with respect to x and y replaced respectively by $\imath\alpha_x$ and $\imath\alpha_y$. Looking for the modes corresponds then to looking for $(\alpha_x, \alpha_y) \in \mathbb{C}^2$ such that

$$\exists \mathcal{U} \neq 0, \quad \mathcal{A}(\alpha_x, \alpha_y)\mathcal{U} = 0, \tag{3.14}$$

where the operator $\mathcal{A}(\alpha_x, \alpha_y)$ is given by

$$\left|\begin{aligned} \mathcal{A}(\alpha_x, \alpha_y)\mathcal{V} &= \mathbf{div}^{\alpha_x,\alpha_y}(\sigma^{\alpha_x,\alpha_y}(\mathcal{V})) + \rho\omega^2\mathcal{V}, \\ D(\mathcal{A}(\alpha_x, \alpha_y)) &= \left\{\mathcal{V} \in H^2((-d, d)), \sigma^{\alpha_x,\alpha_y}(\mathcal{V})n = 0\right\}. \end{aligned}\right.$$

It can be written by using (3.2 - 3.3) as

$$\mathcal{A}(\alpha_x, \alpha_y) = \mathbf{c_1}\partial_z^2 + \imath\mathbf{c_2}\alpha_x\partial_z + \imath\mathbf{c_3}\alpha_y\partial_z - \mathbf{c_4}\alpha_x^2 - \mathbf{c_5}\alpha_y^2 - \mathbf{c_6}\alpha_x\alpha_y + \rho\omega^2 I_3, \tag{3.15}$$

where $\mathbf{c_1}, \mathbf{c_2}, \mathbf{c_3}, \mathbf{c_4}, \mathbf{c_5}$, and $\mathbf{c_6}$ are symmetric 3×3 matrices depending on $\mathbf{C}$. Let us remark that for instance, for a fixed α_y and a fixed ω, (3.14) corresponds to a quadratic eigenvalue problem in α_x. In the sequel, when (α_x, α_y) is such that (3.14) is satisfied, we say that $(\alpha_x, \alpha_y, \mathcal{U})$ defines a mode by using (3.12).

Proposition 3.2.1. *If $(\alpha_x, \alpha_y, \mathcal{U})$ is a mode, then $(-\overline{\alpha}_x, -\overline{\alpha}_y, \overline{\mathcal{U}})$ is also a mode. Moreover, there exists $\mathcal{V}$ such that $(\overline{\alpha}_x, \overline{\alpha}_y, \mathcal{V})$ and $(-\alpha_x, -\alpha_y, \overline{\mathcal{V}})$ are also modes.*

Proof. If $(\alpha_x, \alpha_y, \mathcal{U})$ is a mode, then

$$\mathcal{A}(\alpha_x, \alpha_y)\mathcal{U} = \mathbf{0}.$$

It suffices to take the conjugate of the previous expression and to use (3.15) which implies

$$\overline{\mathcal{A}(\alpha_x, \alpha_y)} = \mathcal{A}(-\overline{\alpha}_x, -\overline{\alpha}_y)$$

to conclude that $(-\overline{\alpha}_x, -\overline{\alpha}_y, \overline{\mathcal{U}})$ is also a mode. It can be shown that for all (α_x, α_y), $\mathcal{A}(\alpha_x, \alpha_y)$ is a Fredholm operator. Consequently,

$$\ker\left(\mathcal{A}(\alpha_x, \alpha_y)\right) \neq 0 \text{ implies } \ker\left(\mathcal{A}(\alpha_x, \alpha_y)\right)^* \neq 0.$$

By using (3.15), we can show that

$$\left(\mathcal{A}(\alpha_x, \alpha_y)\right)^* = \mathcal{A}(\overline{\alpha}_x, \overline{\alpha}_y).$$

This suffices to conclude that there exists $\mathcal{V}$ such that $(\overline{\alpha}_x, \overline{\alpha}_y, \mathcal{V})$ is a mode. By using the first part of the proposition, we obtain that $(-\alpha_x, -\alpha_y, \overline{\mathcal{V}})$ is also a mode. $\qquad\square$

The particular case of the isotropic plate

In the isotropic case, the operator $\mathcal{A}(\alpha_x, \alpha_y)$ can be written by using (3.2 - 3.3) as

$$
\begin{aligned}
\mathcal{A}(\alpha_x, \alpha_y) = &\begin{pmatrix} \mu & 0 & 0 \\ 0 & \mu & 0 \\ 0 & 0 & \lambda + 2\mu \end{pmatrix} \partial_z^2 + \begin{pmatrix} 0 & 0 & (\lambda+\mu)\alpha_x \\ 0 & 0 & (\lambda+\mu)\alpha_y \\ (\lambda+\mu)\alpha_x & (\lambda+\mu)\alpha_y & 0 \end{pmatrix} \imath\partial_z \\
&- \begin{pmatrix} (\lambda+2\mu)\alpha_x^2 + \mu\alpha_y^2 - \omega^2 & (\lambda+\mu)\alpha_x\alpha_y & 0 \\ (\lambda+\mu)\alpha_x\alpha_y & (\lambda+2\mu)\alpha_y^2 + \mu\alpha_x^2 - \omega^2 & 0 \\ 0 & 0 & \mu(\alpha_x^2 + \alpha_y^2) - \omega^2 \end{pmatrix}
\end{aligned}
\tag{3.16}
$$

The particular feature of the isotropic case is the fact that knowledge of the modes in one direction enables us to construct the modes in any direction.

Proposition 3.2.2. *Suppose that $(k, 0, \mathcal{U})$ is a mode with $k \neq 0$. Then, $\forall(\alpha_x, \alpha_y)$ such that $\alpha_x^2 + \alpha_y^2 = k^2$, $(\alpha_x, \alpha_y, \mathcal{V})$ is a mode where*

$$\mathcal{V} = R\mathcal{U},$$

with

$$R = \begin{pmatrix} \alpha_x/k & -\alpha_y/k & 0 \\ \alpha_y/k & \alpha_x/k & 0 \\ 0 & 0 & 1 \end{pmatrix}.$$

Proof. This proposition is due to the fact that

$$\mathcal{A}(\alpha_x, \alpha_y)R = R\mathcal{A}(k, 0),$$

which can be obtained by a simple computation.
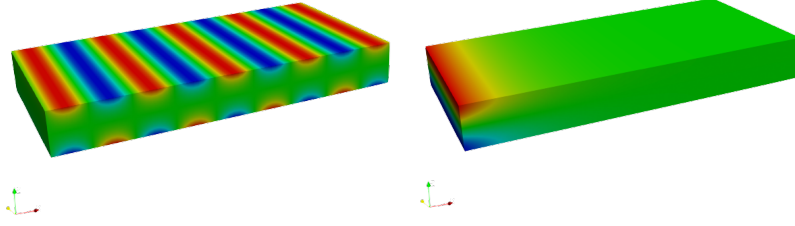
$\qquad\square$

Figure 3.3: The real part of the $x-$component of (left) a propagative and (right) an evanescent mode.

Note that thanks to this proposition, we can deduce other properties on the modes than the ones obtained in Proposition 3.2.1. Indeed, we see easily that if $(\alpha_x, \alpha_y, \mathcal{U})$ is a mode, $(\alpha_x, -\alpha_y, \mathcal{V})$, $(-\alpha_x, \alpha_y, \mathcal{W})$ are also modes, where $\mathcal{V}$ and $\mathcal{W}$ can be obtained easily from $\mathcal{U}$.

Thus, thanks to Proposition 3.2.2, in order to compute all the modes of the isotropic plate, it suffices to solve Problem (3.14) replacing α_y by 0 which corresponds to a quadratic eigenvalue problem in α_x. In Figure 3.3, we represent an example of a propagative and an evanescent mode for $\alpha_y = 0$.

Finally, we can categorize the modes thanks to their polarization:

1. The SH (from *shear horizontal*) or transversal modes, which are polarized in the horizontal direction.

2. The *Lamb* or P-SV wave (from *pressure - shear vertical*) modes, which are polarized in the vertical plane (which contains e_z and the propagation direction). Lamb modes can be classified into two different families relative to the symmetry of the displacement in the thickness of the plate: symmetric (S) and antisymmetric (A) modes [53, 54].

In Figure 3.4 we represent the different types of modes by representing the deformation of the plate.

Remark 3.2.3. *This kind of computation can be used to compute explicitly the waves radiated by a localized source in unperturbed elastic isotropic plates [69] and its far-field [70].*

Slowness diagram and dispersion curves

In this section, we focus on the propagative modes, i.e. the solutions of (3.14)

$$\ker \mathcal{A}(\alpha_x, \alpha_y) \neq 0 \text{ such that } (\alpha_x, \alpha_y) \in \mathbb{R}^2.$$

For a given ω, the set

$$\mathcal{S} := \left\{ \left(\frac{\alpha_x}{\omega}, \frac{\alpha_y}{\omega} \right) \in \mathbb{R}^2, \ker \mathcal{A}(\alpha_x, \alpha_y) \neq 0 \right\} \tag{3.17}$$

is called the *slowness diagram*. Figure 3.5 shows slowness diagrams associated to various materials (the isotropic, orthotropic, and anisotropic materials) whose characteristics are given in Table 3.1.

Figure 3.5(a) shows that the slowness diagram for an isotropic material consists of circles, which illustrates Proposition 3.2.2. For the orthotropic case, some of the curves are not circles

(a)

(b)

(c)
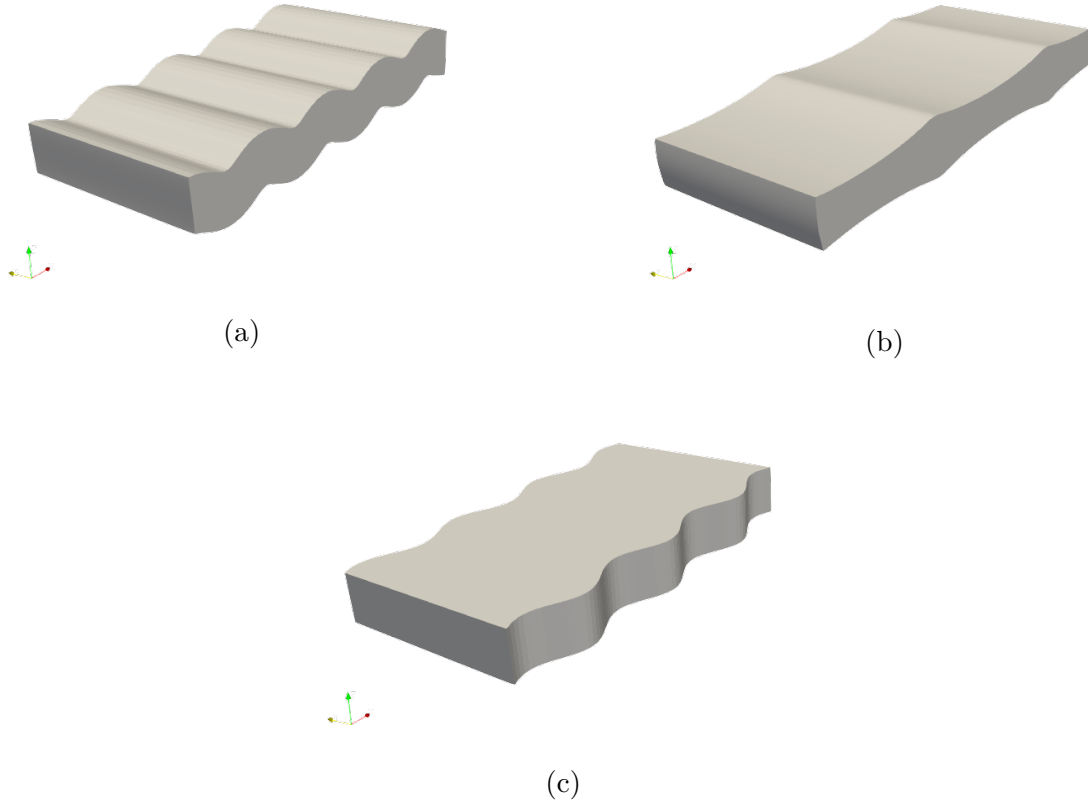
Figure 3.4: Different types of modes based on the polarization: (a) antisymmetric Lamb mode, (b) symmetric Lamb mode, (c) SH mode.

Material	Density (ρ)	Rigidity tensor ($\tilde{\mathbf{C}}$) parameters		
Sil (isotropic)	2.329	$\lambda = 6.39$ $\mu = 7.95$		
Bar [59] (orthotropic)	5.3	$c_{11} = 23.9,$ $c_{22} = 24.7,$ $c_{44} = 6.5,$	$c_{12} = 10.4,$ $c_{23} = 5.2,$ $c_{55} = 6.6,$	$c_{13} = 5.0$ $c_{33} = 13.5$ $c_{66} = 7.6$
Alb [21] (anisotropic)	2.623	$c_{11} = 69.1,$ $c_{14} = 5.1,$ $c_{22} = 183.5,$ $c_{25} = -7.7,$ $c_{34} = -8.7,$ $c_{44} = 24.9,$ $c_{55} = 26.8,$	$c_{12} = 34.0,$ $c_{15} = -2.4,$ $c_{23} = 5.5,$ $c_{26} = -5.8,$ $c_{35} = 7.1,$ $c_{45} = -2.4,$ $c_{56} = 0.5,$	$c_{13} = 30.8$ $c_{16} = -0.9$ $c_{24} = -3.9$ $c_{33} = 179.5$ $c_{36} = -9.8$ $c_{46} = -7.2$ $c_{66} = 33.5$

Table 3.1: Parameters list of the materials.
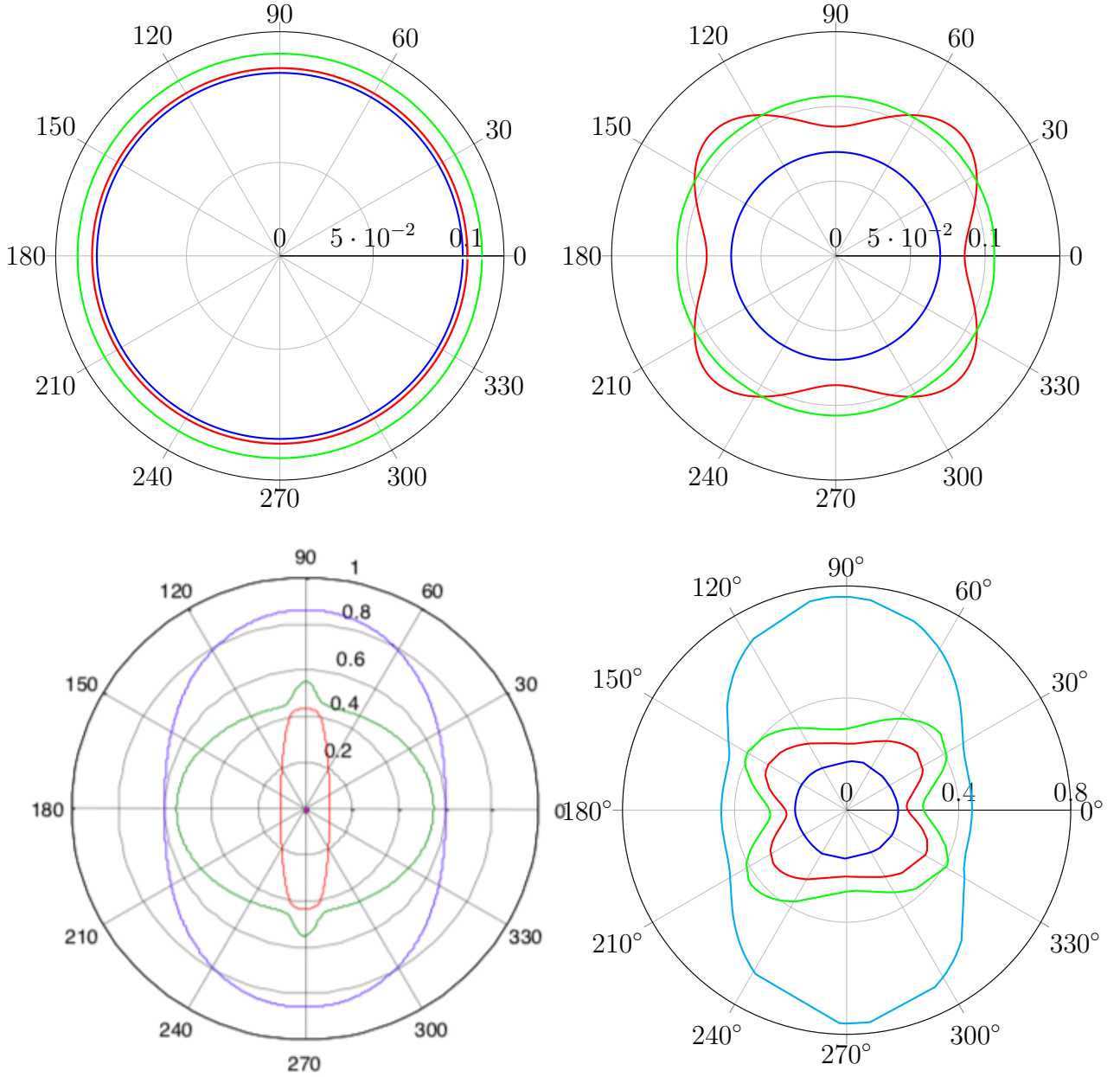
Figure 3.5: Slowness diagram for (a) isotropic, (b) orthotropic, (c) orthotropic (taken from [67]) and (d) anisotropic plate with $\omega^2 = 10$ for (a), (b), (d) and $\omega = 300$ KHz for (c).

anymore but the diagram is still symmetric with respect to the vertical and horizontal axes. Finally for the anisotropic case, we only have the symmetry by rotation of π radians (if $(\alpha_x, \alpha_y) \in \mathcal{S}, (-\alpha_x, -\alpha_y)$ is too).

The number of the curves constituting the slowness diagram and their forms depend on ω. This corresponds to the dispersive characteristic of the problem. In order to point out the dispersion, we fix $\alpha_y \in \mathbb{R}$ and consider all the solutions α_x of (3.14) which depend on ω. We can show that there exist only a finite number of them which are real and we denote them as $\alpha_x^{(1)}(\omega), \ldots, \alpha_x^{(N)}(\omega)$. It corresponds to taking a horizontal cut on α_y in the slowness diagram for a given $\omega,$. This number N depends on α_y. As we can see in Figure 3.5, for large values of α_y, $N = 0$ and for $\alpha_y = 0$, $N = 6$, but this number depends also on ω. We denote $N = N(\omega, \alpha_y)$ when necessary.

We represent the so called *dispersion curves* $\omega \mapsto \alpha_x^{(j)}(\omega), j \in [1, \ldots, N(\omega, \alpha_y)]$, when

$\alpha_x^{(j)}(\omega) > 0$, for the isotropic material described in Table 3.1 (see Figure 3.6). In the isotropic case, we represent the curves with the category of the associated modes as it is described previously (A and S denote the antisymmetric and symmetric Lamb modes respectively, and SH denotes the SH modes). The numbering of the modes refers to the order of the apparition of the modes as the frequency increases (the negative numbering is linked to the group velocity as it is explained below). For the isotropic or the anisotropic case, we see that as the frequency increases, there are more and more modes that propagate in the plate. Remark that even for a low frequency, there exist 3 modes.

For a fixed α_y, we define for each $\alpha_x^{(j)}(\omega), j \in [1, \ldots, N(\omega, \alpha_y)]$ the *phase velocity* $V_\phi^{(j)}$ of the associated propagative mode as

$$V_\phi^{(j)} = \frac{\omega}{\alpha_x^{(j)}(\omega)}. \tag{3.18}$$

We represent the curves $\omega \mapsto V_\phi^{(j)}(\omega), j \in [1, \ldots, N(\omega, \alpha_y)]$, when $\alpha_x^{(j)}(\omega) > 0$, for an isotropic case (see Figure 3.7) and an anisotropic case (see Figure 3.8 taken from [12, 67])

Finally, we define for each $\alpha_x^{(j)}(\omega), j \in [1, \ldots, N(\omega, \alpha_y)]$ the *group velocity* of the associated propagative mode as

$$V_g^{(j)} = \left[\frac{\partial \alpha_x^{(j)}}{\partial \omega} \right]^{-1}. \tag{3.19}$$

When $V_g^{(j)}$ is positive (or the associated dispersion curve is increasing), the energy of the associated propagative mode goes towards $+\infty$ in the $x-$direction. When $V_g^{(j)}$ is negative (or the associated dispersion curve is decreasing), the energy of the associated propagative mode goes towards $-\infty$ in the $x-$direction. The Figure 3.6 representing the dispersion curves in the isotropic case show that some modes have positive phase velocity but negative group velocity. That is why the corresponding dispersion curves have a negative numbering. These modes are called *backward modes* in the $x-$direction.
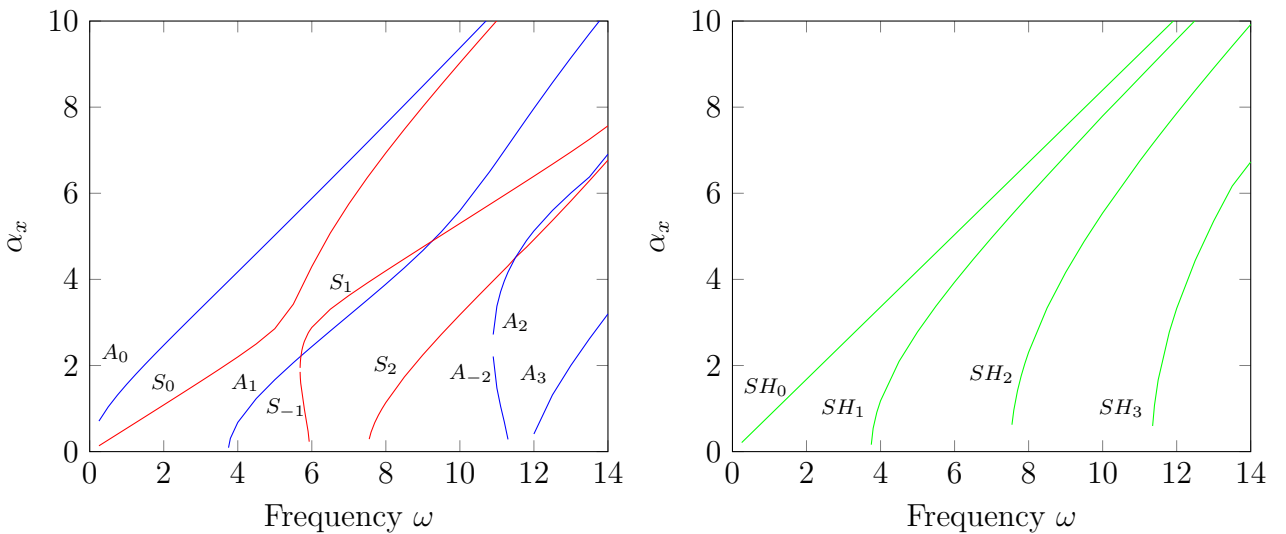
Figure 3.6: Curves for α_x of the symmetric, antisymmetric Lamb modes, and SH modes with respect to the frequency for **Sil** material.
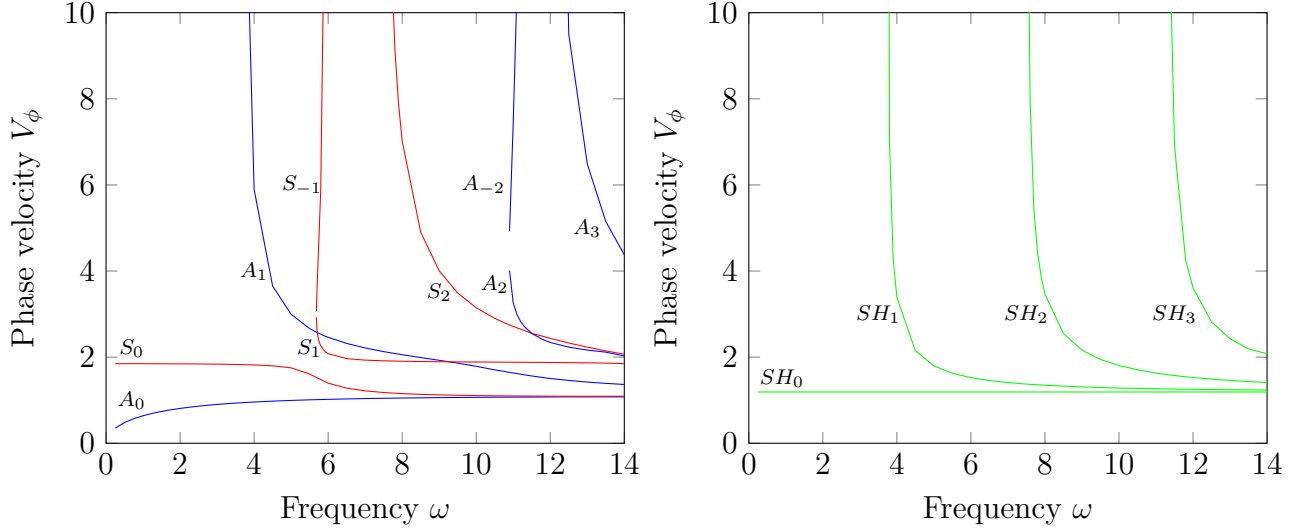
Figure 3.7: Curves for phase velocity of the SH, symmetric, and antisymmetric Lamb modes with respect to the frequency for **Sil** material.
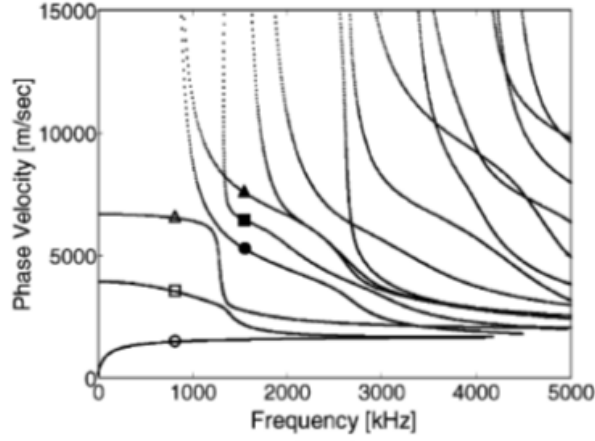
Figure 3.8: Phase velocity for an anisotropic material (taken from [12]).

3.3   The Half-Space Matching method

3.3.1   Some notations

For the rest of the chapter, we use some notations described here. Let us note

$$\Omega_a = \left((-a, a)^2 \times (-d, d)\right) \backslash \mathcal{O} \text{ and } \Omega_a^c = \left(\mathbb{R}^2 \backslash (-a, a)^2\right) \times (-d, d),$$
$$\Omega_b = \left((-b, b)^2 \times (-d, d)\right) \backslash \mathcal{O} \text{ and } \Omega_b^c = \left(\mathbb{R}^2 \backslash (-b, b)^2\right) \times (-d, d), \quad (3.20)$$

where a and b are strictly positive real numbers with $a < b$, $\mathcal{O} \subset (-a, a)^2 \times (-d, d)$, $\mathrm{supp}(\mathbf{f}) \subset (-a, a)^2 \times (-d, d)$, ρ and $\mathbf{C}$ are constant in Ω_a^c. We denote the domain Ω_b the *interior domain* where all the defects and source terms are located, and Ω_a^c the *exterior domain*. Remark that, as for the scalar case explained in Chapter 0, there is an overlap between the interior and the exterior domains.

The exterior domain is recovered by four overlapping half-plates. To precisely define the half-plates, we use local coordinates systems for $j \in \{0, 1, 2, 3\}$:
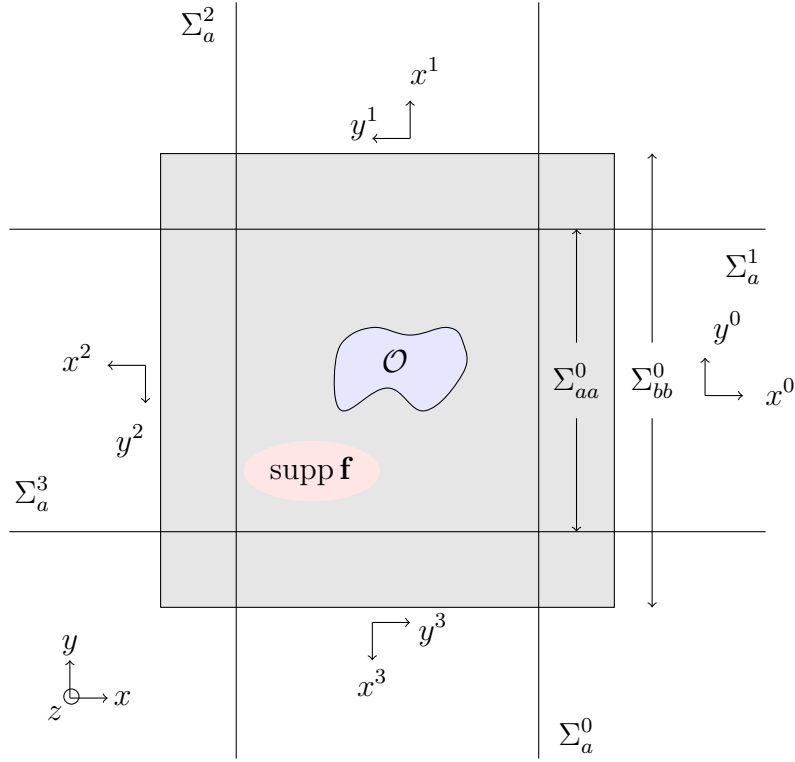
Figure 3.9: Geometry of the problem viewed from the above.

$$\begin{bmatrix} x^j \\ y^j \\ z^j \end{bmatrix} = \begin{bmatrix} \cos\theta^j & \sin\theta^j & 0 \\ -\sin\theta^j & \cos\theta^j & 0 \\ 0 & 0 & 1 \end{bmatrix} \begin{bmatrix} x \\ y \\ z \end{bmatrix}, \text{ where } \theta^j = \frac{j\pi}{2}. \tag{3.21}$$

Using the local coodinate systems, we define the half-plates as:

$$\Omega_a^j = \{x^j \geq a\} \times \{y^j \in \mathbb{R}\} \times \{z^j \in (-d, d)\}, \tag{3.22}$$

and the bands that border the half-plates:

$$\Sigma_a^j = \{x^j = a\} \times \{y^j \in \mathbb{R}\} \times \{z^j \in (-d, d)\}. \tag{3.23}$$

Furthermore, we also define

$$\begin{aligned} \Sigma_{aa}^j &= \{x^j = a\} \times \{y^j \in [-a, a]\} \times \{z^j \in (-d, d)\}, \\ \Sigma_{bb}^j &= \{x^j = b\} \times \{y^j \in [-b, b]\} \times \{z^j \in (-d, d)\}, \end{aligned} \tag{3.24}$$

and the union of these segments are denoted as

$$\Sigma_{aa} = \bigcup_{j=0}^{3} \Sigma_{aa}^j$$

$$\Sigma_{bb} = \bigcup_{j=0}^{3} \Sigma_{bb}^j.$$

In the sequel, we will use $\mathbf{x}$ and (x, y, z) interchangeably.

3.3.2 The half-plate representation

Consider $\mathbf{u}$ the solution of (3.1), we denote the restriction in each half-plate $\mathbf{u}^j(\mathbf{x}) := \mathbf{u}(\mathbf{x})|_{\Omega_a^j}$, $j \in \mathbb{Z}/4\mathbb{Z}$. Each restriction $\mathbf{u}^j$ satisfies

$$\left|\begin{array}{ll} \mathbf{div}(\sigma(\mathbf{u}^j)) + \rho\omega^2\mathbf{u}^j = \mathbf{0} & \text{in } \Omega_a^j, \\ (\sigma(\mathbf{u}^j))n = \mathbf{0} & \text{on } z = \pm d. \end{array}\right. \tag{3.25}$$

To simplify the presentation, we will only consider the restriction $\mathbf{u}^0$ in the half-plate Ω_a^0, the other restrictions are treated similarly. We also drop the superscript 0 to lighten the notation. We define the Fourier transform $\hat{\mathbf{u}}$ as

$$\hat{\mathbf{u}}(x, \xi, z) = \frac{1}{\sqrt{2\pi}} \int_{\mathbb{R}} \mathbf{u}(x, y, z) e^{-\iota\xi y} \mathrm{d}y, \tag{3.26}$$

which is the Fourier transform taken in only one direction. Thus, $\hat{\mathbf{u}}$ satisfies

$$\left|\begin{array}{ll} \mathbf{div}^\xi(\sigma^\xi(\hat{\mathbf{u}})) + \rho\omega^2\hat{\mathbf{u}} = \mathbf{0} & \text{in } \hat{\Omega}_a := (a, +\infty) \times (-d, d), \\ (\hat{\sigma}(\hat{\mathbf{u}}))n = \mathbf{0} & \text{on } z = \pm d, \end{array}\right. \tag{3.27}$$

where σ^ξ et $\mathbf{div}^\xi$ are the operators σ and $\mathbf{div}$ with the derivatives on y replaced by $i\xi$. Contrary to the 2D acoustic problem where for a fixed ξ we have an ordinary differential equation which is easy to solve, in this case we have a 2D problem (but with 3 components) on the half strip $\hat{\Omega}_a$ that we will solve by using a modal decomposition.

Description of the modes in a strip

Now we fix $\xi \in \mathbb{R}$ and we consider a strip $\hat{\Omega} := \mathbb{R} \times (-d, d)$ where we have the equation

$$\left|\begin{array}{ll} \mathbf{div}^\xi(\sigma^\xi(\hat{\mathbf{U}})) + \rho\omega^2\hat{\mathbf{U}} = \mathbf{0} & \text{in } \hat{\Omega}, \\ (\sigma^\xi(\hat{\mathbf{U}}))n = \mathbf{0} & \text{on } z = \pm d. \end{array}\right. \tag{3.28}$$

The modes of this problem are particular solutions, given by

$$\hat{\mathbf{U}}_k(\xi; x, z) = \hat{\mathcal{U}}_k(\xi; z) e^{\iota\beta_k(\xi)x}. \tag{3.29}$$

Then, $(\beta_k(\xi), \hat{\mathcal{U}}_k(\xi; z))$ are solutions of the quadratic eigenvalue problem

$$\left|\begin{array}{ll} \mathbf{div}^{\beta,\xi}(\sigma^{\beta,\xi}(\hat{\mathcal{U}})) + \rho\omega^2\hat{\mathcal{U}} = \mathbf{0} & \in S := (-h, h), \\ \sigma^{\beta,\xi}(\hat{\mathcal{U}})n = \mathbf{0} & \text{on } z = \pm d, \end{array}\right. \tag{3.30}$$

which is the same as (3.13) with $\alpha_x = \beta$ and $\alpha_y = \xi$, but now α_y is fixed.

From a numerical point of view, we use a numerical method called the SAFE (Semi Analytical Finite Element) method. The variational formulation is discretized using 1D Finite Elements and a new unknown is introduced to change the quadratic eigenvalue problem to a linear eigenvalue problem of double size.

Once $(\beta_k(\xi), \hat{\mathcal{U}}_k(\xi; z))$ is computed, the associated mode $\hat{\mathbf{U}}_k(\xi; x, z) = \hat{\mathcal{U}}_k(\xi; z) e^{\iota\beta_k(\xi)x}$ can be constructed and its normal stress in the $x-$direction can be obtained by using

$$\hat{\mathbf{T}}_k(\xi; x, z) := \sigma^\xi(\hat{\mathbf{U}}_k)e_x = \hat{\mathcal{T}}_k(\xi; z)e^{\iota\beta_k(\xi)x}. \tag{3.31}$$

The modes are classified into two different categories:

1. if $\beta_k(\xi)$ is real, the associated $\hat{\mathbf{U}}_k$ is the *propagative* mode. Remark that this $\beta_k(\xi)$ corresponds also to one intersection between the slowness diagram and the horizontal line $y = \dfrac{\xi}{\omega}$. There exists as many propagative modes as intersection points. This number is denoted $N(\omega, \xi)$. Such a mode is said to be rightgoing if it propagates to positive x and leftgoing if it propagates to negative x. We define the direction of propagation of this mode by using the energy flux in a section S

$$\mathrm{Im}\left(\int_S \overline{\hat{\mathbf{U}}_k} \cdot \hat{\mathbf{T}}_k \right). \tag{3.32}$$

   If the flux is positive (negative, respectively), the mode is rightgoing (leftgoing, respectively). The sign of the flux can be linked to the group velocity defined in (3.19).

2. if $\mathrm{Im}(\beta_k(\xi)) \neq 0$, the associated mode $\hat{\mathbf{U}}_k$ is an *evanescent* mode. Such mode decays exponentially as $\mathrm{sgn}(\mathrm{Im}(\beta_k(\xi)))x \to +\infty$. This mode is said to be rightgoing if $\mathrm{Im}(\beta_k(\xi)) > 0$ and leftgoing otherwise.

Remark that in certain literature, some authors may make a distinction for the evanescent mode between the ones with $\mathrm{Re}(\beta_k(\xi)) = 0$ (which are called the evanescent modes) and $\mathrm{Re}(\beta_k(\xi)) \neq 0$ (which are called the inhomogeneous modes). In this thesis, we do not find this distinction important.

It can be shown that there is a finite number of propagative modes and an infinite number of evanescent and inhomogeneous modes. Remark that in the dissipative case, all modes are evanescent.

In the sequel, we denote $\hat{\mathbf{U}}_k^+(\xi; x, z)$ the *rightgoing* modes and $\hat{\mathbf{U}}_k^-(\xi; x, z)$ the *leftgoing* ones and $\beta_k^+(\xi)$ and $\beta_k^-(\xi)$ the associated rightgoing and leftgoing wavenumbers. We represent for different values of ω and for the isotropic material of Table 3.1 the $\beta_k(\xi)$'s in the complex plane for $\xi = 0$.
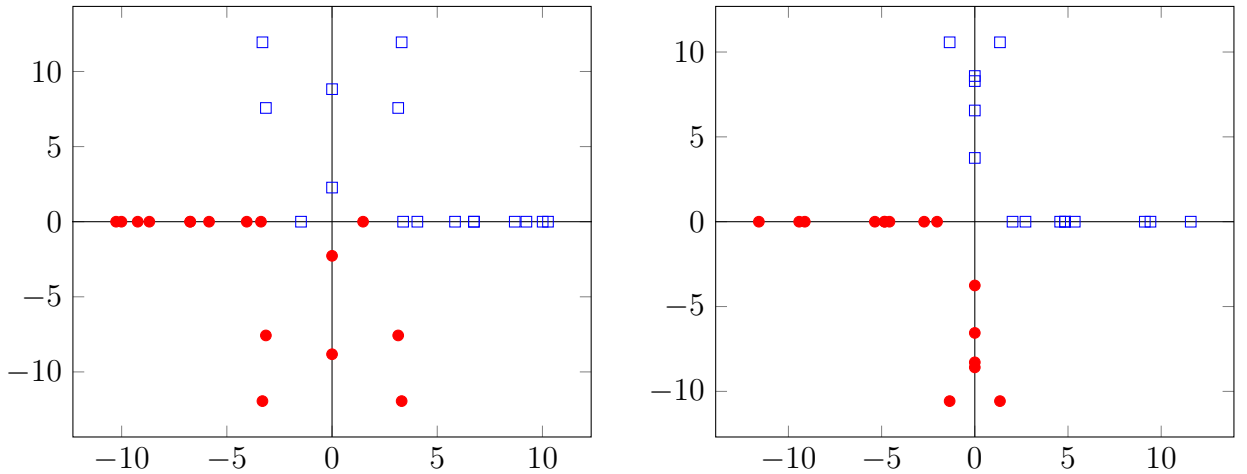
Figure 3.10: The $\beta_k(\xi)$'s in complex plane for a strip $\hat{\Omega}(\xi = 0)$ of (a) an isotropic medium **Sil** and (b) an orthotropic medium **Bar** with $\omega = 11$ and $h = 0.5$. Blue dots represent the rightgoing modes and red dots represent the leftgoing ones.

We suppose that a function satisfying (3.28) that is rightgoing can be decomposed in terms of the rightgoing modes:

$$\hat{\mathbf{U}}(\xi; x, z) = \sum_{k>0} A_k(\xi)\hat{\mathbf{U}}_k^+(\xi; x, z). \tag{3.33}$$

The difficulty now is to determine the modal amplitudes A_k in terms of $\hat{\mathbf{U}}$. In the isotropic scalar case, as the trace of the modes in a section S are orthogonal in $L^2(S)$, the modal amplitudes A_k are simply the scalar product in $L^2(S)$ between the trace of $\hat{\mathbf{U}}$ and the trace of $\hat{\mathbf{U}}_k$. However, the trace of the elastic modes are not orthogonal and therefore we need to use bi-orthogonal properties that are described in the next paragraph.

Properties of the elastic modes

In this paragraph, we show several properties of the modes. We begin with some symmetry properties of the $\beta_k(\xi)$. In the following, in order to emphasize the dependence on ξ and to simplify the presentation, we will say when $(\beta(\xi), \hat{\mathcal{U}})$ defines a mode by (3.29) that $(\beta = \beta(\xi), \hat{\mathcal{U}})$ is a ξ-mode.

By using Proposition 3.2.1 for $\alpha_y \in \mathbb{R}$ it is easy to show the following property.

Proposition 3.3.1. *If $(\beta, \hat{\mathcal{U}})$ is a ξ-mode, then $(-\overline{\beta}, \overline{\hat{\mathcal{U}}})$ is a $(-\xi)$-mode. Moreover, there exists $\hat{\mathcal{V}}$ such that $(\overline{\beta}, \hat{\mathcal{V}})$ is a ξ-mode and $(-\beta, \overline{\hat{\mathcal{V}}})$ is a $(-\xi)$-mode.*

Let us make some remarks on this important proposition. First, we deduce in particular for $\xi = 0$ that if $(\beta, \hat{\mathcal{U}})$ is a 0-mode, then $(-\overline{\beta}, \overline{\hat{\mathcal{U}}})$, $(\overline{\beta}, \hat{\mathcal{V}})$, $(-\beta, \overline{\hat{\mathcal{V}}})$ are also 0-modes for a particular $\hat{\mathcal{V}}$. This was used for instance in [10, 68]. But this property is not true for $\xi \neq 0$ in general.

If $(\beta^+, \hat{\mathcal{U}}^+)$ is a rightgoing and evanescent or inhomogeneous ξ-mode, this proposition show that there exists an associated ξ-mode defined by $(\overline{\beta^+}, \hat{\mathcal{V}})$ which is leftgoing (if $\text{Im}(\beta^+) > 0$, then $\text{Im}(\overline{\beta^+}) < 0$). Moreover, there exists also an associated $(-\xi)$-mode defined by $(-\beta^+, \overline{\hat{\mathcal{V}}})$ which is leftgoing (if $\text{Im}(\beta^+) > 0$, then $\text{Im}(-\beta^+) < 0$). We can then choose the numbering of the evanescent/inhomogeneous modes such that

$$\beta_k^-(\xi) = \overline{\beta_k^+(\xi)} \quad \text{and} \quad \beta_k^-(-\xi) = -\beta_k^+(\xi).$$

Concerning the rightgoing propagative ξ-modes $(\beta^+, \hat{\mathcal{U}}^+)$, i.e. they satisfy $\beta^+ \in \mathbb{R}$ and

$$\text{Im}\left(\int_S \overline{\hat{\mathbf{U}}^+(\xi; x, z)} \cdot \hat{\mathbf{T}}^+(\xi; x, z) \mathrm{d}z \right) > 0,$$

with $\hat{\mathbf{U}}$ and $\hat{\mathbf{T}}$ defined from $(\beta^+, \hat{\mathcal{U}}^+)$ by (3.29 - 3.31), this proposition shows that there exists a propagative $(-\xi)$-mode defined by $(-\beta^+, \overline{\hat{\mathcal{U}}^+})$ which is leftgoing. We can then choose the numbering of the propagative modes such that

$$\beta_k^-(-\xi) = -\beta_k^+(\xi) \quad \text{and} \quad \hat{\mathbf{U}}_k^-(-\xi; x, z) = \overline{\hat{\mathbf{U}}_k^+(\xi; x, z)}. \tag{3.34}$$

Finally, let us mention that for isotropic materials, by using Proposition 3.2.2, it suffices to compute the modes for $\xi = 0$ to deduce the modes for all $\xi \in \mathbb{R}$. More precisely, we deduce from this proposition that

Proposition 3.3.2. *For isotropic media, if $(k, \hat{\mathcal{U}})$ is a 0-mode, then $\forall \beta$ such that $\beta^2 + \xi^2 = k^2$, $(\beta, \mathcal{V})$ is a ξ-mode where*

$$\mathcal{V} = R(\xi)\,\mathcal{U},$$

with

$$R(\xi) = \begin{pmatrix} \beta/k & -\xi/k & 0 \\ \xi/k & \beta/k & 0 \\ 0 & 0 & 1 \end{pmatrix}.$$

Now, we derive bi-orthogonality relations between the modes which will be useful to determine the modal amplitudes in the modal decomposition (3.33).

Proposition 3.3.3 (Bi-orthogonality relation)*. For a fixed $\xi \in \mathbb{R}$, let us denote $(\beta_k(\xi), \hat{\mathcal{U}}_k(\xi))$ a ξ-mode and $(\beta_l(-\xi), \hat{\mathcal{U}}_l(-\xi))$ a $(-\xi)$-mode. We define respectively $\hat{\mathcal{T}}_k(\xi)$ and $\hat{\mathcal{T}}_l(-\xi)$ their associated normal stress as explained in (3.31). These modes verify the bi-orthogonality relation*

$$\forall \xi \in \mathbb{R}, \quad \int_S \left(\hat{\mathcal{U}}_k(\xi; z) \cdot \hat{\mathcal{T}}_l(-\xi; z) - \hat{\mathcal{U}}_l(-\xi; z) \cdot \hat{\mathcal{T}}_k(\xi; z) \right) \mathrm{d}z = 0 \ \text{for } \beta_k(\xi) \neq -\beta_l(-\xi), \quad (3.35)$$

where $S := [0,1]$.

Proof. This property can be shown by a simple Green's formula in any portion $\hat{\Omega}_{(x_1, x_2)}$ of the strip $\hat{\Omega}$ defined by

$$\hat{\Omega}_{(x_1, x_2)} := \{(x, z) \in \hat{\Omega}, x_1 < x < x_2\},$$

with $x_1 < x_2$. The left and right boundaries of $\hat{\Omega}_{(x_1, x_2)}$ are denoted respectively S_1 and S_2. As $(\beta_k(\xi), \hat{\mathcal{U}}_k(\xi))$ a ξ-mode, the mode $\hat{\mathbf{U}}_k(\xi)$ defined from $(\beta_k(\xi), \hat{\mathcal{U}}_k(\xi))$ by (3.29) satisfies by definition (3.28)

$$\int_{\hat{\Omega}_{(x_1, x_2)}} \left(\mathbf{div}^\xi(\sigma^\xi(\hat{\mathbf{U}}_k(\xi; x, z))) + \rho \omega^2 \hat{\mathbf{U}}_k(\xi; x, z) \right) \cdot \hat{\mathbf{U}}_l(-\xi; x, z) \mathrm{d}z = 0.$$

By using twice the Green's formula, we obtain

$$- \int_{S_1} (\sigma^\xi(\hat{\mathbf{U}}_k(\xi; x_1, z))\mathbf{e}_x) \cdot \hat{\mathbf{U}}_l(-\xi; x_1, z) - (\sigma^{-\xi}(\hat{\mathbf{U}}_l(-\xi; x_1, z))\mathbf{e}_x) \cdot \hat{\mathbf{U}}_k(\xi; x_1, z) \mathrm{d}z$$

$$+ \int_{S_2} (\sigma^\xi(\hat{\mathbf{U}}_k(\xi; x_2, z))\mathbf{e}_x) \cdot \hat{\mathbf{U}}_l(-\xi; x_2, z) - (\sigma^{-\xi}(\hat{\mathbf{U}}_l(-\xi; x_2, z))\mathbf{e}_x) \cdot \hat{\mathbf{U}}_k(\xi; x_2, z) \mathrm{d}z$$

$$+ \int_{\hat{\Omega}_{(x_1, x_2)}} \hat{\mathbf{U}}_k(\xi; x, z) \cdot \left(\mathbf{div}^{-\xi}(\sigma^{-\xi}(\hat{\mathbf{U}}_l(-\xi; x, z))) + \rho \omega^2 \hat{\mathbf{U}}_l(-\xi; x, z) \right) \mathrm{d}z = 0.$$

As $(\hat{\mathbf{U}}_l(-\xi; x, z))$ satisfies (3.28) for $-\xi$, the volume integral vanishes and we obtain

$$\int_{S_1} \hat{\mathbf{T}}_k(\xi; x_1, z) \cdot \hat{\mathbf{U}}_l(-\xi; x_1, z) - \hat{\mathbf{T}}_l(-\xi; x_1, z) \cdot \hat{\mathbf{U}}_k(\xi; x_1, z) \mathrm{d}z$$

$$= \int_{S_2} \hat{\mathbf{T}}_k(\xi; x_2, z) \cdot \hat{\mathbf{U}}_l(-\xi; x_2, z) - \hat{\mathbf{T}}_l(-\xi; x_2, z) \cdot \hat{\mathbf{U}}_k(\xi; x_2, z) \mathrm{d}z,$$

where the normal traces $\hat{\mathbf{T}}_k(\xi; x, z)$ and $\hat{\mathbf{T}}_l(-\xi; x, z)$ are defined according to (3.31).

By definition of the modes, we deduce that

$$\left(e^{\imath(\beta_k(\xi) + \beta_l(-\xi))(x_1 - x_2)} - 1 \right) \int_S \left(\hat{\mathcal{U}}_k(\xi; z) \cdot \hat{\mathcal{T}}_l(-\xi; z) - \hat{\mathcal{U}}_l(-\xi; z) \cdot \hat{\mathcal{T}}_k(\xi; z) \right) \mathrm{d}z = 0.$$

As x_1 and x_2 can be chosen arbitrarily, we deduce the bi-orthogonality relation except if $\beta_k(\xi) = -\beta_l(-\xi)$. $\qquad \square$

From this proposition and proposition 3.3.1, and the discussion above about the numbering, we deduce that

$$\forall \xi \in \mathbb{R}, \forall k \neq l \in \mathbb{N}, \quad \int_S \left(\hat{\mathcal{U}}_k^+(\xi; z) \cdot \hat{\mathcal{T}}_l^-(-\xi; z) - \hat{\mathcal{U}}_l^-(-\xi; z) \cdot \hat{\mathcal{T}}_k^+(\xi; z) \right) \mathrm{d}z = 0.$$

We denote

$$\forall \xi \in \mathbb{R}, \forall k \in \mathbb{N}, \quad J_k(\xi) = \int_S \left(\hat{\mathcal{U}}_k^+(\xi; z) \cdot \hat{\mathcal{T}}_k^-(-\xi; z) - \hat{\mathcal{U}}_k^-(-\xi; z) \cdot \hat{\mathcal{T}}_k^+(\xi; z) \right) \mathrm{d}z. \quad (3.36)$$

For propagative modes, by (3.34),

$$J_k(\xi) = 2\imath \, \mathrm{Im} \left(\int_S \hat{\mathcal{U}}_k^+(\xi; z) \cdot \overline{\hat{\mathcal{T}}_k^+(\xi; z)} \mathrm{d}z \right).$$

We suppose that the frequency ω is such that $J_k(\xi) \neq 0$ for all $k \in \mathbb{N}$ and almost every ξ.

Modal decomposition

Let us go back to the restriction of the solution of the original problem (3.1). We have seen that the Fourier transform of its restriction in Ω^0 (it is similar for the other half-plates) satisfies (3.27). We suppose that this function decomposes as a superposition of the rightgoing modes (and only the rightgoing ones) for all ξ

$$\hat{\mathbf{u}}(\xi; x, z) = \sum_{k \in \mathbb{N}} A_k(\xi) \,\hat{\mathcal{U}}_k^+(\xi; z) e^{\iota \beta_k (x-a)}. \tag{3.37}$$

This is in some sense our definition of the outgoing solution of the original problem. The amplitude is then obtained by using the bi-orthogonality relation:

$$A_k(\xi) = A_k(\xi; \mathbf{u}|_{\Sigma_a^0}, (\sigma(\mathbf{u}))n|_{\Sigma_a^0}) = \frac{1}{J_k(\xi)} \int_S \widehat{\mathbf{u}|_{\Sigma_a^0}}(\xi; z) \cdot \hat{\mathcal{T}}_k^-(-\xi; z) - \hat{\mathcal{U}}_k^-(-\xi; z) \cdot \widehat{(\sigma(\mathbf{u}))n|_{\Sigma_a^0}}(\xi; z) \mathrm{d}z. \tag{3.38}$$

Taking the inverse Fourier transform of (3.37), we obtain

$$\mathbf{u}(x, y, z) = \frac{1}{\sqrt{2\pi}} \int_\mathbb{R} \sum_{k \in \mathbb{N}} A_k(\xi; \mathbf{u}|_{\Sigma_a^0}, (\sigma(\mathbf{u}))n^j\big|_{\Sigma_a^0}) \,\hat{\mathcal{U}}_k^+(\xi; z) e^{\iota \beta_k^+(\xi)(x-a)} e^{\iota \xi y} \mathrm{d}\xi.$$

Finally, we denote the trace of the displacement and normal stress field of the solution

$$\forall j \in \{0, 1, 2, 3\} \left| \begin{aligned} \mathbf{d}^j &:= \mathbf{u} && \text{on } \Sigma_a^j, \\ \mathbf{s}^j &:= (\sigma(\mathbf{u}))n^j && \text{on } \Sigma_a^j. \end{aligned} \right. \tag{3.39}$$

The restriction $\mathbf{u}^j$ of $\mathbf{u}$ in Ω_a^j for all $j \in \{0, 1, 2, 3\}$ satisfies (3.25) and can be represented in terms of $\mathbf{d}^j$ and $\mathbf{s}^j$ as

$$\mathbf{u}^j(x^j, y^j, z^j) = \frac{1}{\sqrt{2\pi}} \int_\mathbb{R} \sum_{k \in \mathbb{N}} A_k^j(\xi; \mathbf{d}^j, \mathbf{s}^j) \,\hat{\mathcal{U}}_k^{j,+}(\xi; z^j) e^{\iota \beta_k^{j,+}(\xi)(x^j-a)} e^{\iota \xi y^j} \mathrm{d}\xi. \tag{3.40}$$

From Formula (3.40), we define an operator $\boldsymbol{u}^j$ as

$$\forall (\boldsymbol{d}^j, \boldsymbol{s}^j), \quad \boldsymbol{u}^j(\boldsymbol{d}^j, \boldsymbol{s}^j)(x^j, y^j, z^j) = \frac{1}{\sqrt{2\pi}} \int_\mathbb{R} \sum_{k \in \mathbb{N}} A_k^j(\xi; \boldsymbol{d}^j, \boldsymbol{s}^j) \,\hat{\mathcal{U}}_k^{j,+}(\xi; z^j) e^{\iota \beta_k^{j,+}(\xi)(x^j-a)} e^{\iota \xi y^j} \mathrm{d}\xi, \tag{3.41}$$

for any arbitrary couple $(\boldsymbol{d}^j, \boldsymbol{s}^j)$ on Σ_a^j. Naturally, we have (pay attention to the difference of $\mathbf{u}^j$ and $\boldsymbol{u}^j$)

$$\mathbf{u}^j = \boldsymbol{u}^j(\mathbf{d}^j, \mathbf{s}^j) \text{ in } \Omega_a^j, \ j \in \{0, 1, 2, 3\}.$$

3.3.3 The Half-Space Matching formulation

The objective of this section is to derive some compatibility relations linking $\mathbf{u}^b$ in Ω^b and $(\mathbf{d}^j, \mathbf{s}^j)$ on Σ_a^j, $j \in \mathbb{Z}/4\mathbb{Z}$. By using Formula (3.41), we have the restrictions $\mathbf{u}^j$ in terms of $(\mathbf{d}^j, \mathbf{s}^j)$ on Σ_a^j. Remark that two functions are needed to obtain $\mathbf{u}^j$, while in the 2D acoustic case we only need to know the trace on the boundary of the half-space. Thus, there are twice as many equations as for the 2D acoustic case.

First, we derive the compatibility relations between the traces. On parts of the strips $\Sigma_a^{j\pm1} \cap \Omega_a^j$ for $j \in \mathbb{Z}/4\mathbb{Z}$, we impose

$$\mathbf{d}^{j\pm1} = \boldsymbol{u}^j(\mathbf{d}^j, \mathbf{s}^j) \qquad \text{on } \Sigma_a^{j\pm1} \cap \Omega_a^j, \tag{3.42}$$

$$\mathbf{s}^{j\pm1} = (\sigma(\boldsymbol{u}^j(\mathbf{d}^j, \mathbf{s}^j)))n^{j\pm1} \quad \text{on } \Sigma_a^{j\pm1} \cap \Omega_a^j, \ j \in \mathbb{Z}/4\mathbb{Z}. \tag{3.43}$$

These compatibility relations lead us to define the operators $D^{j,j\pm1}$'s and $N^{j,j\pm1}$'s as

$$\forall(\mathbf{d}^j, \mathbf{s}^j), \quad D^{j,j\pm1}(\mathbf{d}^j, \mathbf{s}^j) = \boldsymbol{u}^j(\mathbf{d}^j, \mathbf{s}^j) \qquad \text{on } \Sigma_a^{j\pm1} \cap \Omega_a^j, \tag{3.44}$$

$$\forall(\mathbf{d}^j, \mathbf{s}^j), \quad N^{j,j\pm1}(\mathbf{d}^j, \mathbf{s}^j) = (\sigma(\boldsymbol{u}^j(\mathbf{d}^j, \mathbf{s}^j)))n^{j\pm1} \qquad \text{on } \Sigma_a^{j\pm1} \cap \Omega_a^j. \tag{3.45}$$
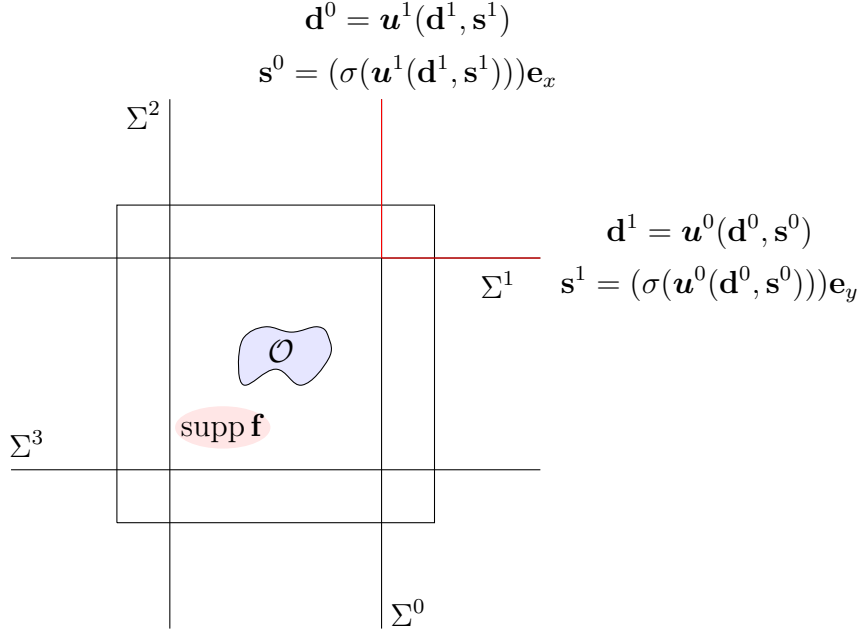
Figure 3.11: Compatibility relations between the traces on $\Sigma_a^1 \cap \Omega_a^0$ and $\Sigma_a^0 \cap \Omega_a^1$.

The operators $D^{j,j\pm1}$ and $N^{j,j\pm1}$ have explicit expressions, for example the expressions of $D^{0,1}$ and $N^{0,1}$ are $\forall(\mathbf{d}^j, \mathbf{s}^j)$,

$$D^{0,1}(\mathbf{d}^0, \mathbf{s}^0)(x, z) = \frac{1}{\sqrt{2\pi}} \int_{\mathbb{R}} \sum_{k \in \mathbb{N}} A_k^0(\xi; \mathbf{d}^0, \mathbf{s}^0) \,\hat{\mathcal{U}}_k^{0,+}(\xi; x, z) e^{\imath \beta_k^{0,+}(\xi)(x-a)} e^{\imath \xi a} \mathrm{d}\xi, \tag{3.46}$$

$$N^{0,1}(\mathbf{d}^0, \mathbf{s}^0)(x, z) = \frac{1}{\sqrt{2\pi}} \int_{\mathbb{R}} \sum_{k \in \mathbb{N}} A_k^0(\xi; \mathbf{d}^0, \mathbf{s}^0) \left(\sigma^{\beta_k^{0,+},\xi} \left(\hat{\mathcal{U}}_k^{0,+}(\xi; x, z)\right)\right) \mathbf{e}_y \, e^{\imath \beta_k^{0,+}(\xi)(x-a)} e^{\imath \xi a} \mathrm{d}\xi. \tag{3.47}$$

Using the operators $D^{j,j\pm1}$ and $N^{j,j\pm1}$, the compatibility relations (3.42 - 3.43) can be written in terms of the displacement and normal stress traces

$$\mathbf{d}^{j\pm1} = D^{j,j\pm1}(\mathbf{d}^j, \mathbf{s}^j) \text{ on } \Omega^j \cap \Sigma^{j\pm1}, \tag{3.48}$$

$$\mathbf{s}^{j\pm1} = N^{j,j\pm1}(\mathbf{d}^j, \mathbf{s}^j) \text{ on } \Omega^j \cap \Sigma^{j\pm1}, \ j \in \mathbb{Z}/4\mathbb{Z}. \tag{3.49}$$

Second, we derive some compatibility relations linking $\mathbf{u}^b$ and $(\mathbf{d}^j, \mathbf{s}^j)$ on Σ_{bb}. We have

$$(\sigma(\mathbf{u}^b))n^j = (\sigma(\boldsymbol{u}^j(\mathbf{d}^j, \mathbf{s}^j)))n^j \qquad \text{on } \Sigma_{bb}^j, \ j \in \{0, 1, 2, 3\}, \tag{3.50}$$

which then leads us to define the operators Λ^j's as

$$\forall(\mathbf{d}^j, \mathbf{s}^j), \quad \Lambda^j(\mathbf{d}^j, \mathbf{s}^j) = (\sigma(\boldsymbol{u}^j(\mathbf{d}^j, \mathbf{s}^j)))n \text{ on } \Sigma_{bb}^j. \tag{3.51}$$
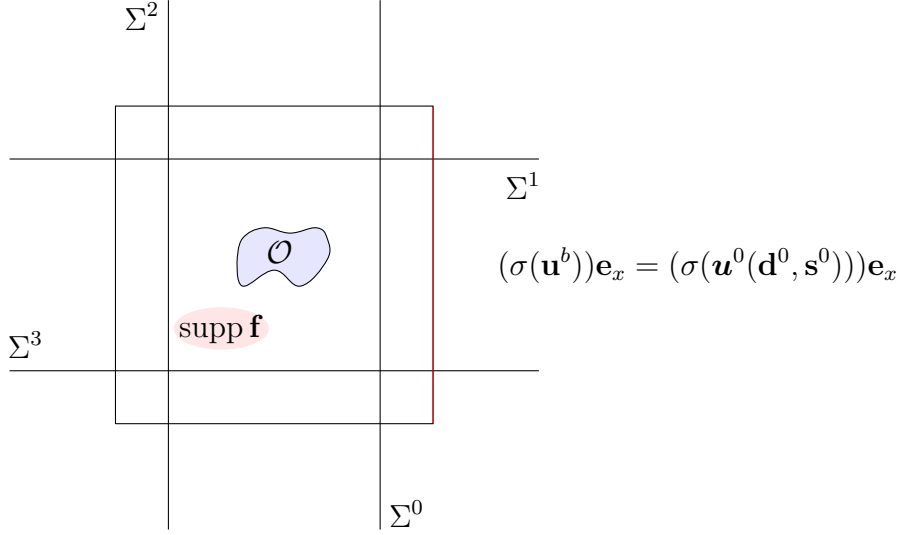
Figure 3.12: Compatibility relation between $\mathbf{u}^b$ and $\boldsymbol{u}^0(\mathbf{d}^0, \mathbf{s}^0)$ on Σ^0_{bb}.

The operators Λ^j also have an explicit expression. For example, the expression of Λ^0 is $\forall(\boldsymbol{d}^j, \boldsymbol{s}^j)$,

$$\Lambda^0(\boldsymbol{d}^0, \boldsymbol{s}^0)(y, z) = \frac{1}{\sqrt{2\pi}} \int_{\mathbb{R}} \sum_{k \in \mathbb{N}} A_k^0(\xi; \boldsymbol{d}^0, \boldsymbol{s}^0) \left(\sigma^{\beta_k^{0,+}, \xi} \left(\hat{\mathcal{U}}_k^{0,+}(\xi; x, z) \right) \right) \mathbf{e}_x \, e^{\imath \beta_k^{0,+}(\xi)\ell} e^{\imath \xi y} \mathrm{d}\xi, \quad (3.52)$$

where $\ell = b - a > 0$. We can then write the compatibility relation (3.50) as

$$(\sigma(\mathbf{u}^b))n^j = \Lambda^j(\mathbf{d}^j, \mathbf{s}^j) \text{ on } \Sigma^j_{bb}, \; j \in \mathbb{Z}/4\mathbb{Z}. \tag{3.53}$$

Finally, we impose some conditions for $\mathbf{d}^j$ and $\mathbf{s}^j$ on the segments $\Sigma^j_{aa}, j \in \{0, 1, 2, 3\}$. For the displacement field traces $\mathbf{d}^j$, we have

$$\mathbf{d}^j = \mathbf{u}^b \text{ on } \Sigma^j_{aa}, j \in \{0, 1, 2, 3\}. \tag{3.54}$$

For the normal stress field traces, we have two possibilities. We can impose

$$\mathbf{d}^j = \boldsymbol{u}^j(\mathbf{d}^j, \mathbf{s}^j) \text{ on } \Sigma^j_{aa}, \tag{3.55}$$

or

$$(\sigma(\mathbf{u}^b))n^j = (\sigma(\boldsymbol{u}^j(\mathbf{d}^j, \mathbf{s}^j)))n^j \text{ on } \Sigma^j_{aa}. \tag{3.56}$$

Remark 3.3.4. *Equations* (3.54) *and* (3.55) *seem to be redundant since both express the value of $\boldsymbol{d}^j$. However, these two equations are only equal for the trace of the solution $(\mathbf{d}^j, \mathbf{s}^j)$*

$$\mathbf{u}^b = \boldsymbol{u}^j(\mathbf{d}^j, \mathbf{s}^j) \text{ on } \Sigma^j_{aa}, \quad j \in \{0, 1, 2, 3\},$$

but they are different for arbitrary functions $(\boldsymbol{d}^j, \boldsymbol{s}^j)$

$$\mathbf{u}^b \neq \boldsymbol{u}^j(\boldsymbol{d}^j, \boldsymbol{s}^j) \text{ on } \Sigma^j_{aa}, \quad j \in \{0, 1, 2, 3\}.$$

More details concerning this compatibility relations are discussed in Chapter 4.

Equations (3.55 - 3.56) lead to the definition of the operators K^j's and Γ^j's as

$$\forall(\boldsymbol{d}^j, \boldsymbol{s}^j), \quad K^j(\boldsymbol{d}^j, \boldsymbol{s}^j) = \boldsymbol{u}^j(\boldsymbol{d}^j, \boldsymbol{s}^j)n^j \qquad\qquad \text{on } \Sigma^j_{aa}, \tag{3.57}$$

$$\forall(\boldsymbol{d}^j, \boldsymbol{s}^j), \quad \Gamma^j(\boldsymbol{d}^j, \boldsymbol{s}^j) = (\sigma(\boldsymbol{u}^j(\boldsymbol{d}^j, \boldsymbol{s}^j)))n^j \qquad \text{on } \Sigma_{aa}^j. \qquad (3.58)$$

Again, the operators K^j and Γ^j have explicit expressions, for example K^0 and Γ^0 are expressed as

$$K^0(\boldsymbol{d}^0, \boldsymbol{s}^0)(y, z) = \frac{1}{\sqrt{2\pi}} \int_{\mathbb{R}} \sum_{k\in\mathbb{N}} A_k^0(\xi; \boldsymbol{d}^0, \boldsymbol{s}^0) \, \hat{\mathcal{U}}_k^{0,+}(\xi; x, z) \, e^{\imath\xi y} \mathrm{d}\xi,$$

$$\Gamma^0(\boldsymbol{d}^0, \boldsymbol{s}^0)(y, z) = \frac{1}{\sqrt{2\pi}} \int_{\mathbb{R}} \sum_{k\in\mathbb{N}} A_k^0(\xi; \boldsymbol{d}^0, \boldsymbol{s}^0) \left(\sigma^{\beta_k^{0,+},\xi}\left(\hat{\mathcal{U}}_k^{0,+}(\xi; x, z)\right)\right) \mathbf{e}_x \, e^{\imath\xi y} \mathrm{d}\xi.$$
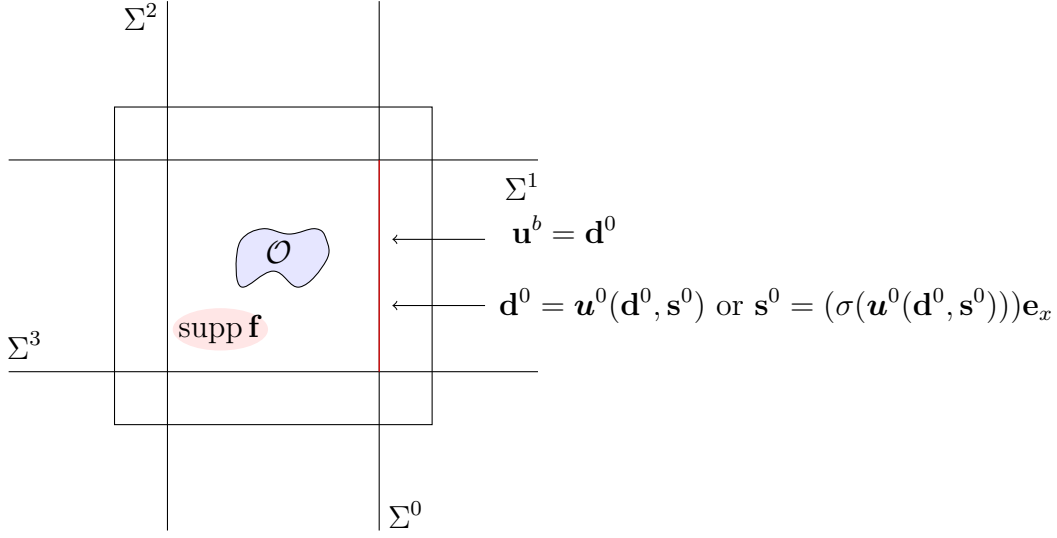
Figure 3.13: Compatibility relations on Σ_{aa}^0.

Summing up, we have two HSM formulations

$$\left| \begin{array}{ll} -\mathbf{div}(\sigma(\mathbf{u}^b)) - \rho\omega^2\mathbf{u}^b = \mathbf{f} & \text{in } \Omega_b, \\ \sigma(\mathbf{u}^b)n = \mathbf{0} & \text{on } z = \pm h \text{ and } \partial\mathcal{O}, \\ \sigma(\mathbf{u}^b)n = \Lambda^j(\mathbf{d}^j, \mathbf{s}^j) & \text{on } \Sigma_{bb}^j, \\ \mathbf{d}^j = \mathbf{u}^b & \text{on } \Sigma_{aa}^j, \\ \mathbf{d}^j = D^{j\pm1,j}(\mathbf{d}^{j\pm1}, \mathbf{s}^{j\pm1}) & \text{on } \Sigma_a^j \cap \Omega^{j\pm1}, \\ \mathbf{s}^j = N^{j\pm1,j}(\mathbf{d}^{j\pm1}, \mathbf{s}^{j\pm1}) & \text{on } \Sigma_a^j \cap \Omega^{j\pm1}, \end{array} \right. \qquad (3.59)$$

with

$$\mathbf{d}^j = K^j(\mathbf{d}^j, \mathbf{s}^j) \text{ on } \Sigma_{aa}^j, \qquad (3.60)$$

or

$$\mathbf{s}^j = \Gamma^j(\mathbf{d}^j, \mathbf{s}^j) \text{ on } \Sigma_{aa}^j. \qquad (3.61)$$

3.4 Numerical aspects

3.4.1 Variational formulation of the multi-unknown problem

In the rest of the chapter, we will use only Formulation (3.59) with (3.61), while the one with (3.60) can be treated similarly. Remember that the unknowns of the problem consist of a volume

unknown $\mathbf{u}^b$ and several unknowns $(\mathbf{d}^j, \mathbf{s}^j)$ on the strips Σ_a^j. In Ω^b, $\mathbf{u}^b$ satisfies

$$\left|\begin{array}{ll} -\mathbf{div}(\sigma(\mathbf{u}^b)) - \rho\omega^2\mathbf{u}^b = \mathbf{f} & \text{in } \Omega^b, \\ \qquad\qquad (\sigma(\mathbf{u}^b))n = \mathbf{0} & \text{on } z = \pm d \text{ and } \partial\mathcal{O}. \end{array}\right. \tag{3.62}$$

Taking test functions $\mathbf{v}$, we get classically the following identity

$$\int_{\Omega_b} \sigma(\mathbf{u}^b) : \epsilon(\mathbf{v}) - \rho\omega^2\mathbf{u}^b \cdot \mathbf{v} - \int_{\Sigma_{bb}} (\sigma(\mathbf{u}^b))n^j \cdot \mathbf{v} = \int_{\Omega_b} \mathbf{f} \cdot \mathbf{v},$$

The term on Σ_{bb} can be replaced by (3.53) and thus we obtain

$$\int_{\Omega_b} \sigma(\mathbf{u}^b) : \epsilon(\mathbf{v}) - \rho\omega^2\mathbf{u}^b \cdot \mathbf{v} - \sum_{j=0}^{3} \int_{\Sigma_{bb}^j} \Lambda^j(\mathbf{d}^j, \mathbf{s}^j) \cdot \mathbf{v} = \int_{\Omega_b} \mathbf{f} \cdot \mathbf{v}$$

For the traces, we take test functions $\tilde{\boldsymbol{d}}_t^j$ and $\tilde{\boldsymbol{s}}_t^j$. We obtain the following identities

$$\int_{\Sigma_a^{j\pm1} \cap \Omega_a^j} \mathbf{d}^{j\pm1} \cdot \tilde{\boldsymbol{d}}_t^{j\pm1} - D^{j,j\pm1}(\mathbf{d}^j, \mathbf{s}^j) \cdot \tilde{\boldsymbol{d}}_t^{j\pm1} = 0, \text{ for } j \in \mathbb{Z}/4\mathbb{Z},$$

$$\int_{\Sigma_a^{j\pm1} \cap \Omega_a^j} \mathbf{s}^{j\pm1} \cdot \tilde{\boldsymbol{s}}_t^{j\pm1} - N^{j,j\pm1}(\mathbf{d}^j, \mathbf{s}^j) \cdot \tilde{\boldsymbol{s}}_t^{j\pm1} = 0, \text{ for } j \in \mathbb{Z}/4\mathbb{Z},$$

$$\int_{\Sigma_{aa}^j} \mathbf{s}^j \cdot \tilde{\boldsymbol{s}}_t^j - \Gamma^j(\mathbf{d}^j, \mathbf{s}^j) \cdot \tilde{\boldsymbol{s}}_t^j = 0, \text{ for } j \in \{0, 1, 2, 3\}.$$

Finally, the equation

$$\mathbf{u}^b = \mathbf{d}^j \text{ on } \Sigma_{aa}^j$$

is taken into account as an essential condition. The variational formulation of (3.59) is

Find $\left(\mathbf{u}^b, \prod_{j=0}^{3} \mathbf{d}^j, \prod_{j=0}^{3} \mathbf{s}^j\right)$, $\mathbf{u}^b = \mathbf{d}^j$ on $\Sigma_{bb}^j, \forall j \in \{0, 1, 2, 3\}$ such that $\forall \left(\mathbf{v}, \prod_{j=0}^{3} \tilde{\boldsymbol{d}}^j, \prod_{j=0}^{3} \tilde{\boldsymbol{s}}^j\right)$, $\mathbf{v} = \tilde{\boldsymbol{d}}^j$ on $\Sigma_{bb}^j, \forall j \in \{0, 1, 2, 3\}$

$$\left|\begin{array}{l} \int_{\Omega_b} \sigma(\mathbf{u}^b) : \epsilon(\mathbf{v}) - \rho\omega^2\mathbf{u}^b \cdot \mathbf{v} - \sum_{j=0}^{3} \int_{\Sigma_{bb}^j} \Lambda^j(\mathbf{d}^j, \mathbf{s}^j) \cdot \mathbf{v} = \int_{\Omega_b} \mathbf{f} \cdot \mathbf{v}, \\[4mm] \qquad \int_{\Sigma_a^{j\pm1} \cap \Omega_a^j} \mathbf{d}^{j\pm1} \cdot \tilde{\boldsymbol{d}}_t^{j\pm1} - D^{j,j\pm1}(\mathbf{d}^j, \mathbf{s}^j) \cdot \tilde{\boldsymbol{d}}_t^{j\pm1} = 0, \text{ for } j \in \mathbb{Z}/4\mathbb{Z}, \\[4mm] \qquad \int_{\Sigma_a^{j\pm1} \cap \Omega_a^j} \mathbf{s}^{j\pm1} \cdot \tilde{\boldsymbol{s}}_t^{j\pm1} - N^{j,j\pm1}(\mathbf{d}^j, \mathbf{s}^j) \cdot \tilde{\boldsymbol{s}}_t^{j\pm1} = 0, \text{ for } j \in \mathbb{Z}/4\mathbb{Z}, \\[4mm] \qquad\qquad\qquad \int_{\Sigma_{aa}^j} \mathbf{s}^j \cdot \tilde{\boldsymbol{s}}_t^j - \Gamma^j(\mathbf{d}^j, \mathbf{s}^j) \cdot \tilde{\boldsymbol{s}}_t^j = 0, \text{ for } j \in \{0, 1, 2, 3\}. \end{array}\right. \tag{3.63}$$

Let us take a detailed look in one of the bilinear forms involving a Fourier integral, for example the one involving the operator $D^{0,1}$. Expanding the definition of the operator, we obtain

$$\int_{\Sigma_a^1 \cap \Omega_a^0} D^{0,1}(\boldsymbol{d}^0, \boldsymbol{s}^0)(x, z) \cdot \boldsymbol{d}^1(x, z) \, \mathrm{d}x \, \mathrm{d}z$$

$$= \int_{\Sigma_a^1 \cap \Omega_a^0} \left(\frac{1}{\sqrt{2\pi}} \int_{\mathbb{R}} \sum_{k \in \mathbb{N}} A_k^0(\xi; \boldsymbol{d}^0, \boldsymbol{s}^0) \, \hat{\mathcal{U}}_k^{0,+}(\xi; z) e^{\imath\beta_k^{0,+}(\xi)(x-a)} e^{\imath\xi a} \mathrm{d}\xi \cdot \boldsymbol{d}^1(x, z)\right) \, \mathrm{d}x \, \mathrm{d}z.$$

The modal amplitudes $A_k^0(\xi; \boldsymbol{d}^0, \boldsymbol{s}^0)$ can be rewritten as

$$A_k^0(\xi; \boldsymbol{d}^0, \boldsymbol{s}^0) = \frac{1}{J_k(\xi)} \int_S \hat{\boldsymbol{d}}^0(\xi; z') \cdot \hat{\mathcal{T}}_k^-(-\xi; z') - \hat{\boldsymbol{s}}^0(\xi; z') \cdot \hat{\mathcal{U}}_k^-(-\xi; z') \, \mathrm{d}z'$$

$$= \frac{1}{\sqrt{2\pi}} \frac{1}{J_k(\xi)} \int_S \int_{\mathbb{R}} \left(\boldsymbol{d}^0(y', z') \cdot \hat{\mathcal{T}}_k^-(-\xi; z') - \boldsymbol{s}^0(y', z') \cdot \hat{\mathcal{U}}_k^-(-\xi; z') \right) e^{-\imath \xi y'} \, \mathrm{d}y' \, \mathrm{d}z'$$

$$= \frac{1}{\sqrt{2\pi}} \frac{1}{J_k(\xi)} \int_{\Sigma_a^0} \left(\boldsymbol{d}^0(y', z') \cdot \hat{\mathcal{T}}_k^-(-\xi; z') - \boldsymbol{s}^0(y', z') \cdot \hat{\mathcal{U}}_k^-(-\xi; z') \right) e^{-\imath \xi y'} \, \mathrm{d}y' \, \mathrm{d}z'.$$

Plugging this expanded expression of the modal amplitude, the bilinear form can then be decomposed into two forms

$$\left| \begin{aligned} & \int_{\Sigma_a^1 \cap \Omega_a^0} D^{0,1}(\boldsymbol{d}^0, \boldsymbol{s}^0)(x, z) \cdot \boldsymbol{d}^1(x, z) \, \mathrm{d}x \, \mathrm{d}z \\ & = \frac{1}{2\pi} \int_{\Sigma_a^1 \cap \Omega_a^0} \int_{\Sigma_a^0} \left(\boldsymbol{d}^0(y', z') \right)^T \, k_{DD}^{0,1}(x, z, y', z') \, \boldsymbol{d}^1(x, z) \, \mathrm{d}x \, \mathrm{d}z \, \mathrm{d}y' \, \mathrm{d}z' \\ & - \frac{1}{2\pi} \int_{\Sigma_a^1 \cap \Omega_a^0} \int_{\Sigma_a^0} \left(\boldsymbol{s}^0(y', z') \right)^T \, k_{DN}^{0,1}(x, z, y', z') \, \boldsymbol{d}^1(x, z) \, \mathrm{d}x \, \mathrm{d}z \, \mathrm{d}y' \, \mathrm{d}z', \end{aligned} \right. \tag{3.64}$$

where the kernels are 3×3 matrices given by

$$\left| \begin{aligned} k_{DD}^{0,1}(x, z, y', z') &= \int_{\mathbb{R}} \frac{1}{J_k(\xi)} \sum_{k \in \mathbb{N}} \hat{\mathcal{T}}_k^{0,-}(-\xi; z') \otimes \hat{\mathcal{U}}_k^{0,+}(\xi; z) \, e^{\imath \beta_k^{0,+}(\xi)(x-a)} e^{\imath \xi(a-y')} \mathrm{d}\xi, \\ k_{DN}^{0,1}(x, z, y', z') &= \int_{\mathbb{R}} \frac{1}{J_k(\xi)} \sum_{k \in \mathbb{N}} \hat{\mathcal{U}}_k^{0,-}(-\xi; z') \otimes \hat{\mathcal{U}}_k^{0,+}(\xi; z) \, e^{\imath \beta_k^{0,+}(\xi)(x-a)} e^{\imath \xi(a-y')} \mathrm{d}\xi, \end{aligned} \right. \tag{3.65}$$

with $\otimes$ denotes the outer product of two vectors. We conclude from (3.64 - 3.65) that each bilinear form can be written as the sum of two forms, each with a kernel that produces 3×3 matrices.

3.4.2 Discretization of the variational formulation

To solve the HSM formulation numerically, we discretize the variational formulation (3.63) with the following ingredients:

1. We truncate the strip Σ_a^j to a bounded strip

$$\Sigma_{a,T}^j = \{ (x^j = a, y^j, z^j), -T < y^j < T, -d < z^j < d \}.$$

2. We discretize the unknowns by taking 3D P1 Lagrange elements for the volume unknown in the bounded domain $\mathbf{u}_h^b$, 2D P1 Lagrange element for the trace unknowns $\boldsymbol{d}_\mathbf{h}^j$, where $\mathbf{h} = (T, h)$ and 2D P0 Lagrange element for the normal trace unknowns $\boldsymbol{s}_\mathbf{h}^j$ with h as the discretization step. With these discretization elements, the discretized unknowns are $\mathbf{u}_h^b, \boldsymbol{d}_\mathbf{h}^j, \boldsymbol{s}_\mathbf{h}^j$, such that $\mathbf{u}_h^b = \boldsymbol{d}_\mathbf{h}^j$ on $\Sigma_{aa}^j, \quad \forall j \in \{0, 1, 2, 3\}$.

3. We truncate the modal series expansion for each half-plate and for each ξ by keeping N modes, where N is an integer greater than the number of propagative modes in all half-plates.

4. We truncate the Fourier integrals which appear in several operators Λ^j's, K^j's, Γ^j's, $D^{j,j\pm1}$'s, $N^{j,j\pm1}$'s: the integral for $\xi \in \mathbb{R}$ is replaced by an integral for $\xi \in [-\hat{T}, \hat{T}]$;

5. we apply a quadrature formula $\mathcal{Q}$ to compute the Fourier integrals explicitly. The quadrature can be optimized by applying the Generalized Gaussian quadrature as described in Appendix B (see also [20, 22]).

For example, the bilinear form (3.64) becomes

$$
\begin{aligned}
&\left| \int_{\Sigma^1_{a,\mathbf{h}}\cap\Omega^0_a} D^{0,1}_{\hat{T},\mathcal{Q}}(\boldsymbol{d}^0_{\mathbf{h}}, \boldsymbol{s}^0_{\mathbf{h}})(x,z) \cdot \boldsymbol{d}^1_{\mathbf{h}}(x,z)\, \mathrm{d}y'\mathrm{d}z' \right. \\
&= \frac{1}{2\pi} \int_{\Sigma^1_{a,\mathbf{h}}\cap\Omega^0_a} \int_{\Sigma^0_{a,\mathbf{h}}} \left(\boldsymbol{d}^0_{\mathbf{h}}(y',z')\right)^T k^{0,1}_{DD,\hat{T},\mathcal{Q},N}(x,z,y',z')\, \boldsymbol{d}^1_{\mathbf{h}}(x,z)\, \mathrm{d}x\, \mathrm{d}z\, \mathrm{d}y'\, \mathrm{d}z' \\
&\left. - \frac{1}{2\pi} \int_{\Sigma^1_{a,\mathbf{h}}\cap\Omega^0_a} \int_{\Sigma^0_{a,\mathbf{h}}} \left(\boldsymbol{s}^0_{\mathbf{h}}(y',z')\right)^T k^{0,1}_{DN,\hat{T},\mathcal{Q},N}(x,z,y',z')\, \boldsymbol{d}^1_{\mathbf{h}}(x,z)\, \mathrm{d}x\, \mathrm{d}z\, \mathrm{d}y'\, \mathrm{d}z', \right.
\end{aligned}
\tag{3.66}
$$

where the kernels are 3×3 matrices given by

$$
\begin{aligned}
&\left| k^{0,1}_{DD,\hat{T},\mathcal{Q},N}(x,z,y',z') = \sum_{\xi\in\mathcal{Q}} \frac{w_\xi}{J_k(\xi)} \sum_{k=1}^N \hat{\mathcal{T}}^{0,-}_k(-\xi;z') \otimes \hat{\mathcal{U}}^{0,+}_k(\xi;z)\, e^{\imath\beta^{0,+}_k(\xi)(x-a)} e^{\imath\xi(a-y')}, \right. \\
&\left| k^{0,1}_{DN,\hat{T},\mathcal{Q},N}(x,z,y',z') = \sum_{\xi\in\mathcal{Q}} \frac{w_\xi}{J_k(\xi)} \sum_{k=1}^N \hat{\mathcal{U}}^{0,-}_k(-\xi;z') \otimes \hat{\mathcal{U}}^{0,+}_k(\xi;z)\, e^{\imath\beta^{0,+}_k(\xi)(x-a)} e^{\imath\xi(a-y')}. \right.
\end{aligned}
\tag{3.67}
$$

Finally, the whole computation can be summarized into Algorithm 3.1

Algorithm 3.1 HSM formulation for the elastic plate

1: **Input:** problem parameters $(\omega, \rho, \mathbf{C})$, domain parameters (a, b, d), and discretization parameters $(T, h, \hat{T})$
2: Construct the discretized domain: the box Ω^b_h and the strips $\Sigma^j_{T,h}$.
3: Compute the Fourier quadrature points ξ and weights w_ξ (either by standard Gauss-Legendre quadrature or by the optimized one described in Appendix B).
4: For each half-plate j: compute the modes $(\mathcal{U}^j_k, \mathcal{T}^j_k)$ and the constants J^j_k for all ξ by the SAFE method.
5: Construct the kernels of the integral operators.
6: Construct the FE matrices of the discretized variational formulation and solve the linear system for $\mathbf{u}^b$ and $\forall j \in \{0,1,2,3\}$ $\boldsymbol{d}^j_{\mathbf{h}}$ and $\boldsymbol{s}^j_{\mathbf{h}}$.
7: Compute the Fourier transform $\hat{\boldsymbol{d}}^j_{\mathbf{h}}$ and $\hat{\boldsymbol{s}}^j_{\mathbf{h}}$.
8: Compute the solution in each half-plate by Formula (3.40).
9: **Output:** $\mathbf{u}$ in Ω.

3.4.3   Numerical validation

We validate the method only for isotropic media. However, the method should work well also for anisotropic media. The only difference is that the modes of an anisotropic plate have to be computed for all $\xi \in \mathbb{R}$, while for isotropic media it is enough to compute the modes for $\xi = 0$ and use the Proposition (3.3.2) to obtain the modes for other ξ.

As far as we know, there is no known fundamental solution for an elastic plate, even for isotropic medium. Therefore, we validate the method only by showing that the different representations are compatible in the zone where they coexist.

We consider again a **Sil** plate with $a = 1$, $b = 2$, and $d = 0.5$ with a sphere whose center is $(0, 0, 0)$ and radius is 0.25 as the obstacle $\mathcal{O}$. We consider

$$
\left|
\begin{aligned}
-\mathbf{div}(\sigma(\mathbf{u})) - \rho\omega^2\mathbf{u} &= \mathbf{0} && \text{in } \Omega, \\
(\sigma(\mathbf{u}))n &= 0 && \text{on } z = \pm d, \\
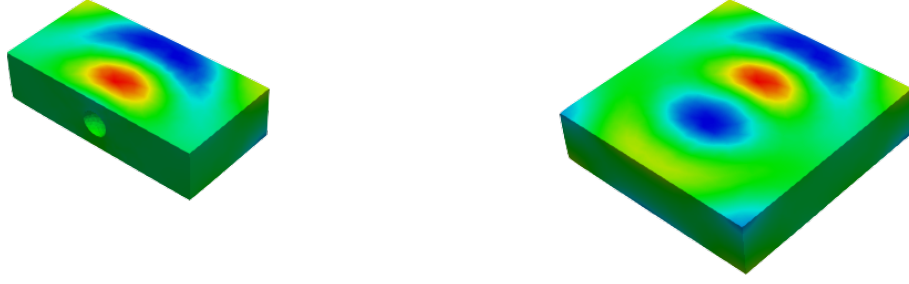\mathbf{u}(x,y,z) &= (x,y,z)^T && \text{on } \partial\mathcal{O},
\end{aligned}
\right.
$$

Figure 3.14: The x-component of the solution in (a) $\Omega^b \cap \{x \geq 0\}$ and in (b) Ω^b.

with $\omega^2 = 10$. As for the discretization parameters, we use $T = 5$, $\hat{T} = 4.15$, 3rd Gauss-Legendre quadrature with 250 intervals, and we take only 5 first modes of which 3 are propagative. Solving the variational formulation related to this problem, we obtain $\mathbf{u}_h^b$ in Ω^b and the traces $\boldsymbol{d}_{\mathbf{h}}^j$ and $\boldsymbol{s}_{\mathbf{h}}^j$ on Σ_a^j. To show the defect in the middle of the plate, we show the x-component $\mathbf{u}_h^b$ in $\Omega^b \cap \{x \geq 0\}$ and in Ω^b in Figure 3.14. In Figure 3.15 we show the y and z-components of the solution in Ω^b as well.

Figure 3.15: The y, and z-components of the solution in Ω^b.

Finally, by using the traces $\boldsymbol{d}_{\mathbf{h}}^j$ and $\boldsymbol{s}_{\mathbf{h}}^j$ on Σ_a^j, we can reconstruct the solution in the half-plates by using Formula (3.40). We show in Figure 3.16 the x, y, and z-components of the solution in Ω^b and in the half-plates Ω_a^j. Due to the limited parameters, some discontinuities might be seen (see for example the y-component in Figure 3.16 (b)). However, in Figure 3.16 (a) and (c), we see that there is no apparent jump on the overlapping zone. We conclude that the different representations coincide provided that the discretization parameters are taken fine enough.

Scattering problem in the plate

Finally, we consider here a scattering problem where $\mathbf{u}$ represents the scattered field and we take an incident wave $\mathbf{u}_{inc}$ such that

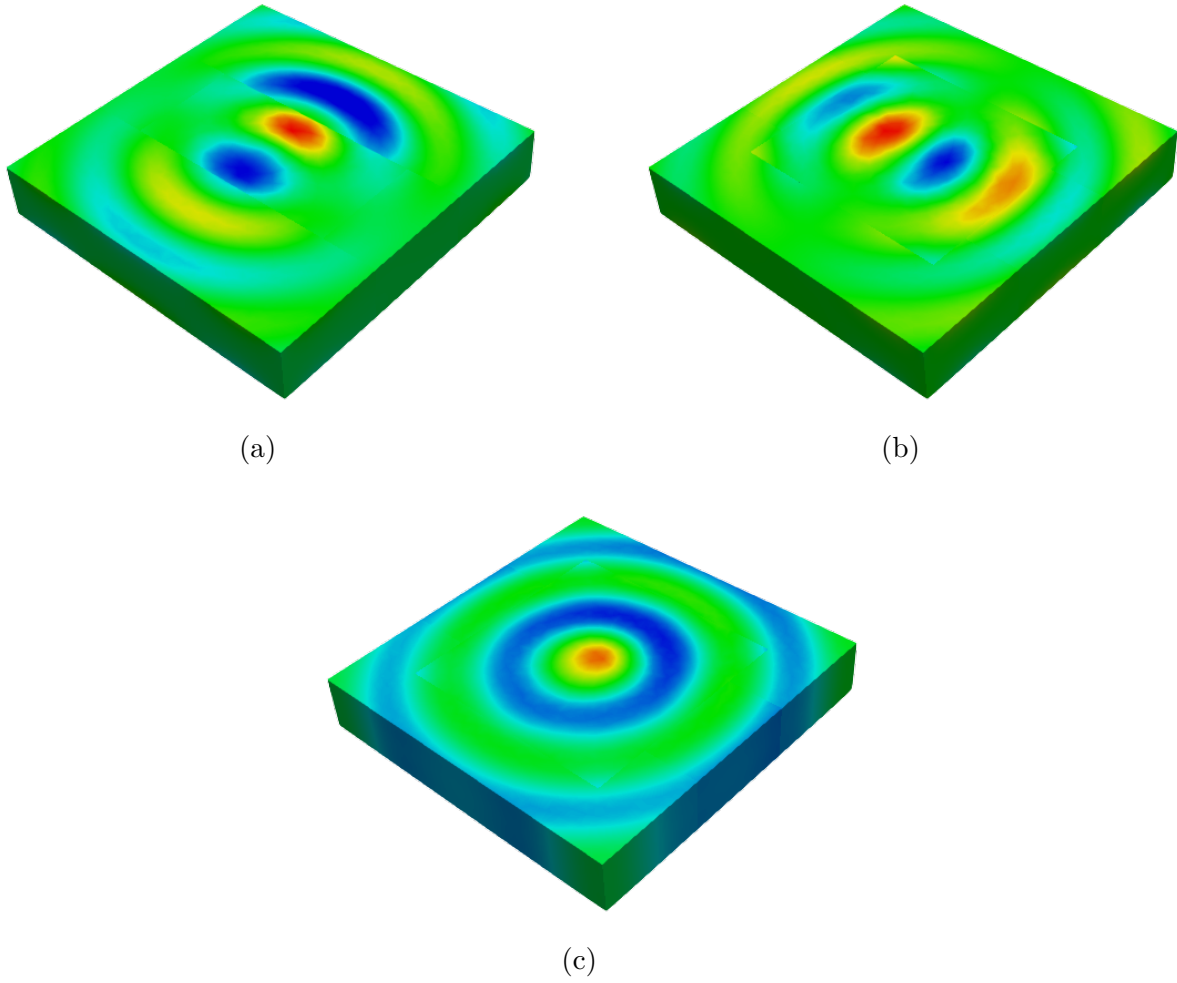$$\hat{\mathbf{u}}_{inc}(\xi = 0; x, z) = \hat{\mathcal{U}}_1^0(\xi = 0; z)e^{i\beta_1^{0,+}(x+a)}, \tag{3.68}$$

(a)   (b)

(c)

Figure 3.16: The (a) x, (b) y, and (c) z-components of the solution in Ω

.

where $(\mathcal{U}_1^{0,+}, \beta_1^{0,+})$ is the first propagative mode in the half-strip $\hat{\Omega} = \mathbb{R} \times (-d, d)$. Since we consider an isotropic medium, $\hat{\boldsymbol{u}}_{inc}(\xi; x, z)$ can be obtained by Proposition 3.3.2. The scattered field satisfies

$$\left|\begin{aligned}-\mathbf{div}(\sigma(\mathbf{u})) - \rho\omega^2\mathbf{u} &= \mathbf{0} && \text{in } \Omega, \\ (\sigma(\mathbf{u}))n &= 0 && \text{on } z = \pm d, \\ \mathbf{u} &= -\mathbf{u}_{inc} && \text{on } \partial\mathcal{O},\end{aligned}\right.$$

where we have the same defect as in the previous case. We take the scattered-scattered formulation equivalent to (2.9) for the 2D scalar case.

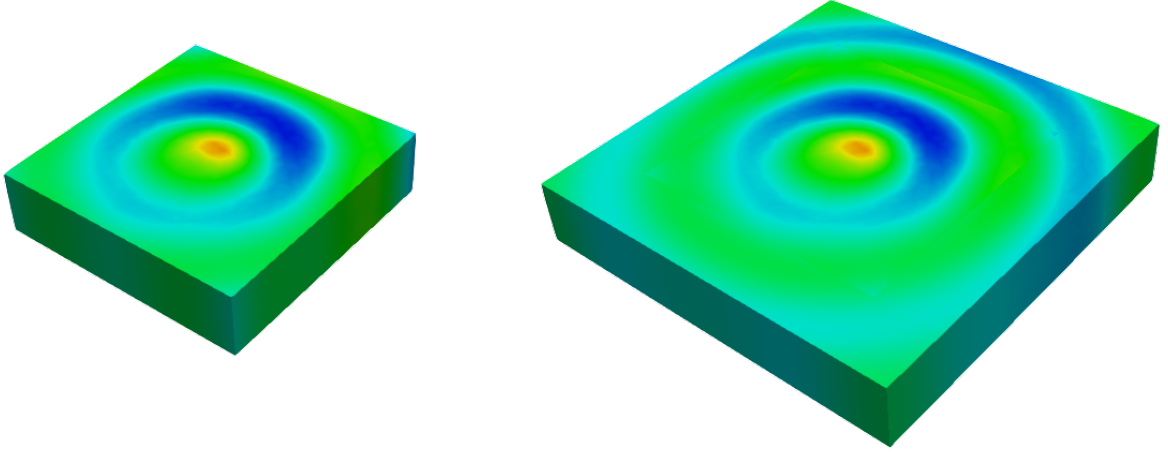Figure 3.17: The z-component of the solution in (a) Ω^b and (b) the reconstructed solution in Ω.

In Figure 3.17(a) we show the scattered field in Ω^b, and again in (b) the reconstructed solution in Ω. Visually, there is no visible discontinuity of the solution between different representations. We conclude that the representations are compatible at the overlapping zones.

Chapter 4

Multi-unknown Half-Space Matching Method

Summary

4.1   **A first model problem** **94**

4.2   **Multi-trace Half-Space Matching Formulations** **95**

4.3   **Variational formulations** **98**

     4.3.1   Variational formulation for System (4.16) 100

     4.3.2   Variational formulation for System (4.17) 107

4.4   **Generalization to a general exterior problem** **111**

4.5   **Numerical validation** **113**

4.6   **Formulations involving Green's functions** **115**

     4.6.1   The multi-unknown formulation set on curves instead of lines 115

     4.6.2   Configurations where a global Green's function is not available 117

The motivation of this chapter is to answer several theoretical questions that arise, notably from Chapter 3. In the said chapter, we developed a Half-Space Matching formulation for the anisotropic elastic plate by using as unknowns both the displacement and the normal stress fields, because both of them were necessary to obtain the half-plate representations. However, the questions about the well-posedness and the appropriate functional spaces of the multi-unknown HSM method were not addressed. As a first step, we give partial answers to these questions in a simpler acoustic problem in 2D where we have in each half-plane Ω^j representations of the solution with both the trace and normal trace on the boundary Σ^j used. We show the equivalence of the multi-unknown formulations to the original problem and the uniqueness in Section 4.3, while the stability is still an open question. Multi trace boundary integral equations studied in [26, 27, 28, 44] also involve traces and normal traces unknowns and similar difficulties appear in the analysis.

The half-space representation in each half-space Ω^j in terms of the trace and the normal trace can be rewritten using the Green's function instead of using the Fourier transform. With this formulation, we can propose a representation of the solution in subdomains which are not necessarily half-spaces. The method can then be used in configurations when the Green's function is not known globally but only subdomain by subdomain. This is explained in Section 4.6.

4.1 A first model problem

In order to simplify the presentation, we consider first a problem where only 2 half-spaces are involved. Let us then consider a simple model problem in a three-quarter plane:

$$\Omega := \{\mathbf{x} = (x_1, x_2), x_1 > 0 \text{ or } x_2 > 0\}.$$

The problem that we are interested in is still the Helmholtz equation with Dirichlet boundary condition in the dissipative case:

Find $p \in H^1(\Omega)$ such that

$$\left|\begin{aligned} \Delta p + \omega^2 p &= 0 \text{ in } \Omega, \\ p &= g \text{ on } \partial\Omega, \end{aligned}\right. \tag{4.1}$$

where $g \in H^{1/2}(\partial\Omega)$ is given and $\operatorname{Im}\omega > 0$. We define two half-spaces Ω^1 and Ω^2 that cover Ω

$$\Omega^1 := \{(x_1, x_2), x_1 \in \mathbb{R}^+, x_2 \in \mathbb{R}\}, \qquad \Omega^2 := \{(x_1, x_2), x_1 \in \mathbb{R}, x_2 \in \mathbb{R}^+\},$$

and the lines that border these half-spaces

$$\Sigma^1 := \{(0, x_2), x_2 \in \mathbb{R}\}, \qquad \Sigma^2 := \{(x_1, 0), x_1 \in \mathbb{R}\}.$$

These lines can be decomposed further into

$$\Sigma^1_+ := \{(0, x_2), x_2 \in \mathbb{R}^+\}, \qquad \Sigma^1_- := \{(0, x_2), x_2 \in \mathbb{R}^-\},$$

$$\Sigma^2_+ := \{(x_1, 0), x_1 \in \mathbb{R}^+\}, \qquad \Sigma^2_- := \{(x_1, 0), x_1 \in \mathbb{R}^-\}.$$

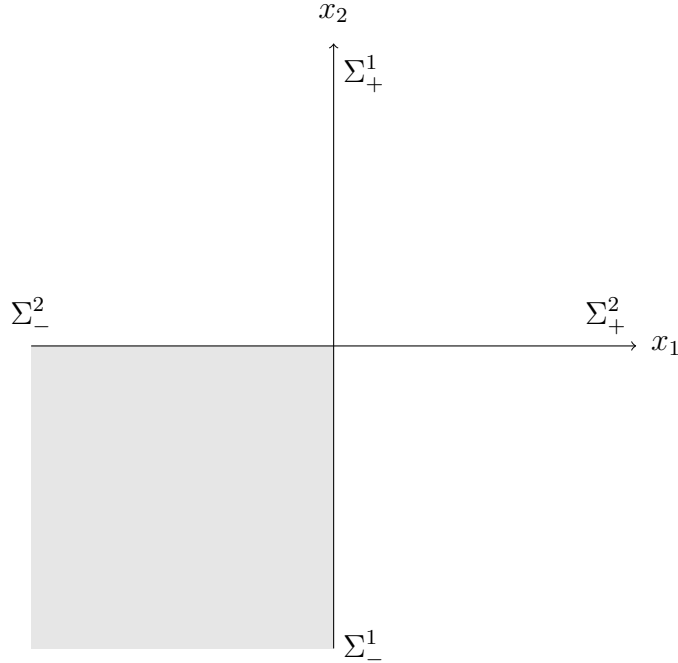
Figure 4.1: The three-quarter plane completed with notations.

Finally, we denote the traces and the normal traces

$$\forall j \in \{1, 2\}, \quad \varphi^j := p \qquad \text{on } \Sigma^j,$$

$$\psi^j := \frac{\partial p}{\partial x_j} \quad \text{on } \Sigma^j. \tag{4.2}$$

4.2 Multi-trace Half-Space Matching Formulations

In this section, we develop half-space matching formulations satisfied by the trace and normal trace and show that these formulations are equivalent to (4.1).

We consider the restriction of p in the half-space $\Omega^j, j \in \{1, 2\}$ and derive a representation formula of the restriction in terms of φ^j and ψ^j. In some sense, we are looking for a formula analog to Formula (3.40) for the elastic plate where we represent the restriction in the half-plate in terms of the Lamb modes and the Fourier transform of the displacement and the normal stress traces. Let us consider the case of the half-space Ω^1, the formula for Ω^2 is obtained similarly. The restriction of p in Ω^1 satisfies the homogeneous Helmholtz equation

$$\left| \Delta p + \omega^2 p = 0 \quad \text{in } \Omega^1. \right. \tag{4.3}$$

Taking the Fourier transform in x_2 of (4.3), we obtain an ODE parametrized by the Fourier variable ξ

$$\text{for a.e. } \xi \in \mathbb{R}, \quad \frac{\mathrm{d}^2 \hat{p}}{\mathrm{d}x_1^2} + (\omega^2 - \xi^2)\hat{p} = 0 \quad \text{for } x_1 \in (a, +\infty).$$

Solving the equation for x_1 gives us the general solution

$$\hat{p}(x_1, \xi) = A e^{i\sqrt{\omega^2 - \xi^2} x_1} + B e^{-i\sqrt{\omega^2 - \xi^2} x_1}.$$

On the boundary, we know that the trace and the normal trace are given by

$$p = \varphi^1 \quad \text{on } \Sigma^1,$$

$$\frac{\partial p}{\partial x_1} = \psi^1 \quad \text{on } \Sigma^1,$$

which then lead to

$$\text{for a.e. } \xi \in \mathbb{R}, \quad \hat{p}(a, \xi) = \hat{\varphi}^1(\xi),$$

$$\frac{\mathrm{d}\hat{p}}{\mathrm{d}x_1}(a, \xi) = \hat{\psi}^1(\xi),$$

We then have an ODE with 2 boundary conditions. The coefficients A and B can be expressed in terms of these boundary conditions as

$$A = \frac{1}{2}\left(\hat{\varphi}^1 + \frac{\hat{\psi}^1}{i\sqrt{\omega^2 - \xi^2}}\right) \text{ and } B = \frac{1}{2}\left(\hat{\varphi}^1 - \frac{\hat{\psi}^1}{i\sqrt{\omega^2 - \xi^2}}\right).$$

Since p is in $H^1(\Omega^1)$, B has to be 0. Therefore, we have

$$\hat{p}(x_1, \xi) = \frac{1}{2}\left(\hat{\varphi}^1 + \frac{\hat{\psi}^1}{i\sqrt{\omega^2 - \xi^2}}\right) e^{i\sqrt{\omega^2 - \xi^2} x_1}. \tag{4.4}$$

Remark that $B = 0$ is equivalent to

$$\forall \xi \in \mathbb{R}, \quad \hat{\varphi}^1(\xi) = \frac{\hat{\psi}^1(\xi)}{i\sqrt{\omega^2 - \xi^2}}. \tag{4.5}$$

Thus, (4.4) can be written more generally as

$$\hat{p}(x_1, \xi) = \left(r\hat{\varphi}^1(\xi) + (1 - r)\frac{\hat{\psi}^1(\xi)}{i\sqrt{\omega^2 - \xi^2}}\right) e^{i\sqrt{\omega^2 - \xi^2} x_1}, \tag{4.6}$$

for $r \in \mathbb{R}$. For $r = 1$, we obtain the usual formula where we only have the trace in the formulation, while formula (4.4) is the case where $r = 1/2$. We use (4.7) for the rest of the chapter, but similar results could be obtained for any $r \in \mathbb{R}$.

Taking the inverse Fourier transform, the restriction of p in Ω^1 is expressed in terms of the trace φ^1 and normal trace ψ^1 as

$$p(x_1, x_2) = \frac{1}{2\sqrt{2\pi}} \int_{\mathbb{R}} \left(\hat{\varphi}^1(\xi) + \frac{\hat{\psi}^1(\xi)}{\imath\sqrt{\omega^2 - \xi^2}} \right) e^{\imath\sqrt{\omega^2-\xi^2}x_1} e^{\imath\xi x_2} \mathrm{d}\xi, \quad \text{for } (x_1, x_2) \in \Omega^1. \qquad (4.7)$$

Based on the form of Formula (4.7), we define integral operators $P^j, j \in \{1, 2\}$ that take two arbitrary boundary data (φ^j, ψ^j) on Σ^j and give

$$P^1(\varphi^1, \psi^1)(x_1, x_2) = \frac{1}{2\sqrt{2\pi}} \int_{\mathbb{R}} \left(\hat{\varphi}^1(\xi) + \frac{\hat{\psi}^1(\xi)}{\imath\sqrt{\omega^2 - \xi^2}} \right) e^{\imath\sqrt{\omega^2-\xi^2}x_1} e^{\imath\xi x_2} \mathrm{d}\xi, \quad \text{for } (x_1, x_2) \in \Omega^1,$$

$$P^2(\varphi^2, \psi^2)(x_1, x_2) = \frac{1}{2\sqrt{2\pi}} \int_{\mathbb{R}} \left(\hat{\varphi}^2(\xi) + \frac{\hat{\psi}^2(\xi)}{\imath\sqrt{\omega^2 - \xi^2}} \right) e^{\imath\sqrt{\omega^2-\xi^2}x_2} e^{\imath\xi x_1} \mathrm{d}\xi, \quad \text{for } (x_1, x_2) \in \Omega^2,$$

$$\qquad (4.8)$$

and of course we have

$$\forall j \in \{1, 2\}, \quad p = P^j(\varphi^j, \psi^j) \text{ in } \Omega^j.$$

We note in the following $\forall j \in \{1, 2\}$, (φ^j, ψ^j) the trace and normal trace of p on Σ^j as defined in (4.2), and (φ^j, ψ^j) arbitrary data.

We have $P^j(\varphi^j, \psi^j) = p$ in Ω^j only for the couple of trace and normal trace of the solution (φ^j, ψ^j). If we take any couple of two arbitrary functions (φ^j, ψ^j), a priori the trace of $P^j(\varphi^j, \psi^j)$ is not φ^j, and the normal trace is not ψ^j

$$\forall j \in \{1, 2\}, \quad \begin{cases} P^j(\varphi^j, \psi^j)\big|_{\Sigma^j} \neq \varphi^j, \\ \dfrac{\partial}{\partial x_j} P^j(\varphi^j, \psi^j)\bigg|_{\Sigma^j} \neq \psi^j, \end{cases} \qquad (4.9)$$

and

$$\forall j \in \{1, 2\}, \quad \begin{vmatrix} P^j(\varphi^j, \psi^j)\big|_{\Sigma^j} = \varphi^j \\ \dfrac{\partial}{\partial x_j} P^j(\varphi^j, \psi^j)\bigg|_{\Sigma^j} = \psi^j \end{vmatrix} \Leftrightarrow \hat{\varphi}^j(\xi) = \frac{\hat{\psi}^j(\xi)}{\imath\sqrt{\omega^2 - \xi^2}}. \qquad (4.10)$$

In the following, we say that the couple (φ^j, ψ^j) is compatible if it satisfies this relation.

As in previous chapters, the idea of the method is to derive a system of equations satisfied by the couples of traces and normal traces $(\varphi^j, \psi^j), j \in \{1, 2\}$. These equations are obtained again by exploiting the overlap of the half-spaces. By definition of the traces, we have

$$p = \varphi^2 \quad \text{and} \quad \frac{\partial p}{\partial x_2} = \psi^2 \quad \text{on } \Sigma^2.$$

On the other hand, the representation in Ω^1 gives

$$p = P^1(\varphi^1, \psi^1) \quad \text{and} \quad \frac{\partial p}{\partial x_2} = \frac{\partial}{\partial x_2} P^1(\varphi^1, \psi^1) \quad \text{in } \Omega^1.$$

In particular on $\Sigma_+^2 = \Sigma^2 \cap \Omega^1$, we obtain the compatibility relations

$$\varphi^2 = P^1(\varphi^1, \psi^1) \quad \text{and } \psi^2 = \frac{\partial}{\partial x_2} P^1(\varphi^1, \psi^1) \quad \text{on } \Sigma_+^2. \qquad (4.11)$$

Similar compatibility relations are obtained on $\Sigma^1_+ = \Sigma^1 \cap \Omega^2$:

$$\varphi^1 = P^2(\varphi^2, \psi^2) \quad \text{and} \quad \psi^1 = \frac{\partial}{\partial x_1} P^2(\varphi^2, \psi^2) \quad \text{on } \Sigma^1_+. \tag{4.12}$$
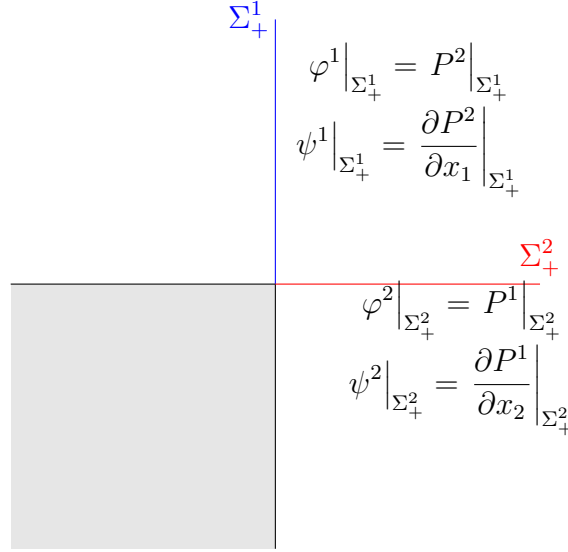

$$\varphi^1\big|_{\Sigma^1_+} = P^2\big|_{\Sigma^1_+}$$
$$\psi^1\big|_{\Sigma^1_+} = \frac{\partial P^2}{\partial x_1}\bigg|_{\Sigma^1_+}$$

$$\varphi^2\big|_{\Sigma^2_+} = P^1\big|_{\Sigma^2_+}$$
$$\psi^2\big|_{\Sigma^2_+} = \frac{\partial P^1}{\partial x_2}\bigg|_{\Sigma^2_+}$$

Figure 4.2: Compatibility conditions on Σ^1_+ and Σ^2_+.

Now, we need to derive the compatibility relations for $(\varphi^j, \psi^j), j \in \{1, 2\}$ on Σ^j_-'s. The boundary condition of (4.1) implies that

$$\varphi^1 = g \text{ on } \Sigma^1_-,$$
$$\varphi^2 = g \text{ on } \Sigma^2_-. \tag{4.13}$$

It is then natural to impose these conditions on φ^1 and φ^2. Equations are missing for the ψ^j's on Σ^j_-'s. There are several possible equations:

1. we impose another compatibility conditions on the traces

$$\varphi^1 = P^1(\varphi^1, \psi^1) \text{ on } \Sigma^1_-,$$
$$\varphi^2 = P^2(\varphi^2, \psi^2) \text{ on } \Sigma^2_-, \tag{4.14}$$

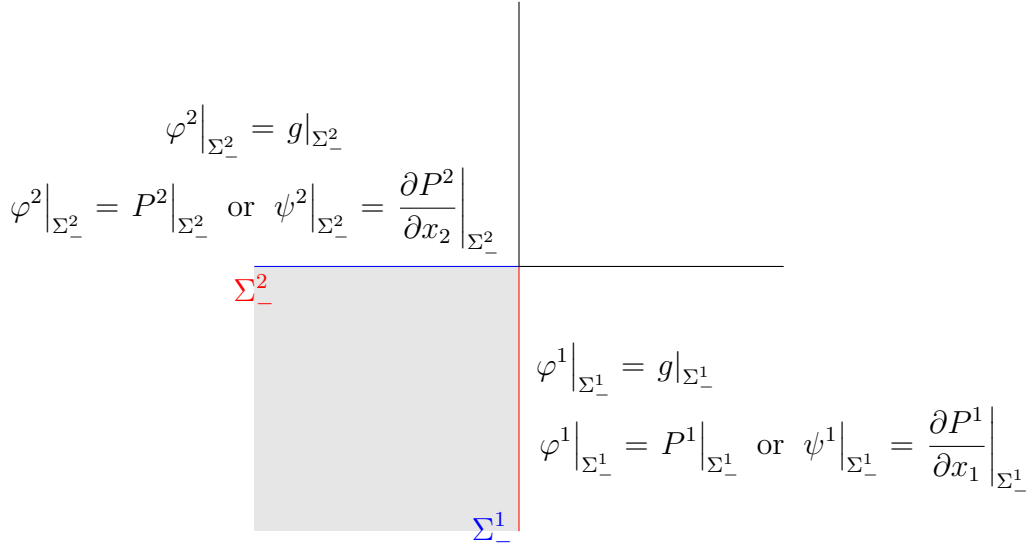2. we impose another compatibility conditions on the normal traces

$$\psi^1 = \frac{\partial}{\partial x_1} P^1(\varphi^1, \psi^1) \text{ on } \Sigma^1_-,$$
$$\psi^2 = \frac{\partial}{\partial x_2} P^2(\varphi^2, \psi^2) \text{ on } \Sigma^2_-. \tag{4.15}$$

Remark 4.2.1. *Adding Equation* (4.14) *seems redundant because we have Equation* (4.13) *on Σ^j_-. However, for any function φ^j, these two equations are different. Indeed, for the traces and normal traces of the solution, we have*

$$P^j(\varphi^j, \psi^j) = g \text{ on } \Sigma^j_-,$$

but for general functions,

$$P^j(\varphi^j, \psi^j) \neq g \text{ on } \Sigma^j_-.$$

$$\varphi^2\big|_{\Sigma_-^2} = g\big|_{\Sigma_-^2}$$

$$\varphi^2\big|_{\Sigma_-^2} = P^2\big|_{\Sigma_-^2} \quad \text{or} \quad \psi^2\big|_{\Sigma_-^2} = \frac{\partial P^2}{\partial x_2}\bigg|_{\Sigma_-^2}$$

$$\Sigma_-^2$$

$$\varphi^1\big|_{\Sigma_-^1} = g\big|_{\Sigma_-^1}$$

$$\varphi^1\big|_{\Sigma_-^1} = P^1\big|_{\Sigma_-^1} \quad \text{or} \quad \psi^1\big|_{\Sigma_-^1} = \frac{\partial P^1}{\partial x_1}\bigg|_{\Sigma_-^1}$$

$$\Sigma_-^1$$

Figure 4.3: Compatibility conditions on Σ_-^1 and Σ_-^2.

Summing up, the traces $(\varphi^1, \varphi^2, \psi^1, \psi^2)$ satisfy these systems of equations

$$
\left|
\begin{array}{lll}
\varphi^1 & = P^2(\varphi^2, \psi^2) & \text{on } \Sigma_+^1, \\
\varphi^2 & = P^1(\varphi^1, \psi^1) & \text{on } \Sigma_+^2, \\
\psi^1 & = \dfrac{\partial}{\partial x_1} P^2(\varphi^2, \psi^2) & \text{on } \Sigma_+^1, \\
\psi^2 & = \dfrac{\partial}{\partial x_2} P^1(\varphi^1, \psi^1) & \text{on } \Sigma_+^2, \\
\varphi^1 & = g & \text{on } \Sigma_-^1, \\
\varphi^2 & = g & \text{on } \Sigma_-^2, \\
\varphi^1 & = P^1(\varphi^1, \psi^1) & \text{on } \Sigma_-^1, \\
\varphi^2 & = P^2(\varphi^2, \psi^2) & \text{on } \Sigma_-^2,
\end{array}
\right.
\tag{4.16}
$$

or

$$
\left|
\begin{array}{lll}
\varphi^1 & = P^2(\varphi^2, \psi^2) & \text{on } \Sigma_+^1, \\
\varphi^2 & = P^1(\varphi^1, \psi^1) & \text{on } \Sigma_+^2, \\
\psi^1 & = \dfrac{\partial}{\partial x_1} P^2(\varphi^2, \psi^2) & \text{on } \Sigma_+^1, \\
\psi^2 & = \dfrac{\partial}{\partial x_2} P^1(\varphi^1, \psi^1) & \text{on } \Sigma_+^2, \\
\varphi^1 & = g & \text{on } \Sigma_-^1, \\
\varphi^2 & = g & \text{on } \Sigma_-^2, \\
\psi^1 & = \dfrac{\partial}{\partial x_1} P^1(\varphi^1, \psi^1) & \text{on } \Sigma_-^1, \\
\psi^2 & = \dfrac{\partial}{\partial x_2} P^2(\varphi^2, \psi^2) & \text{on } \Sigma_-^2.
\end{array}
\right.
\tag{4.17}
$$

4.3   Variational formulations

The natural functional spaces for the unknowns are

$$\forall j \in \{1, 2\}, \quad \varphi^j \in H_g^{1/2}(\Sigma^j) := \left\{ \varphi^j \in H^{1/2}(\Sigma^j), \varphi^j = g \text{ on } \Sigma_-^j \right\},$$
$$\psi^j \in H^{-1/2}(\Sigma^j).$$

In the sequel, we denote $\Phi := (\varphi^1, \varphi^2, \psi^1, \psi^2)$ and the variational space is

$$V := H_g^{1/2}(\Sigma^1) \times H_g^{1/2}(\Sigma^2) \times H^{-1/2}(\Sigma^1) \times H^{-1/2}(\Sigma^2).$$

Remark that it is intricate to write the variational formulations of (4.16) or (4.17) because the unknowns are defined piecewisely. We know that if $\varphi^1\big|_{\Sigma^1_-} \in L^2(\Sigma^1_-)$ and $\varphi^1\big|_{\Sigma^1_+} \in L^2(\Sigma^1_+)$, then $\varphi^1\big|_{\Sigma^1} \in L^2(\Sigma^1)$. However, it is a priori not true for $H^{1/2}$ traces. Moreover, we know that if $\psi^1 \in H^{-1/2}(\Sigma^1)$, $\psi^1\big|_{\Sigma^1_+} \notin \left(H^{1/2}(\Sigma^1_+)\right)'$ but $\psi^1\big|_{\Sigma^1_+} \in (H_0^{1/2}(\Sigma^1_+))'$ where

$$\forall j \in \{1, 2\}, \quad H_0^{1/2}(\Sigma^j_+) := \left\{ \varphi^j\big|_{\Sigma^j_+} \,\middle|\, \varphi^j \in H^{1/2}(\Sigma^j), \, \varphi^j\big|_{\Sigma^j_-} = 0 \right\}.$$

Thus, we have to find appropriate test functions in order to write the variational formulations.

The idea is to write the compatibility conditions weakly, using duality products $H^{1/2}, H^{-1/2}$. For instance, in (4.16) the second equation

$$\varphi^2 = P^1(\varphi^1, \psi^1) \text{ on } \Sigma^2_+$$

can be joined to the seventh one

$$\varphi^1 = P^1(\varphi^1, \psi^1) \text{ on } \Sigma^1_-$$

by taking a test function living on $\Sigma^1_- \cup \Sigma^2_+$. The set of test functions is then naturally different from the one of the unknowns.

We need then to introduce the two following curves

$$\begin{aligned} \tilde{\Sigma}^1 &:= \Sigma^1_- \cup \Sigma^2_+, \\ \tilde{\Sigma}^2 &:= \Sigma^2_- \cup \Sigma^1_+. \end{aligned} \tag{4.18}$$

These curves $\tilde{\Sigma}^j$ are a simple swap (see Figure 4.4) of the two lines Σ^j and we have

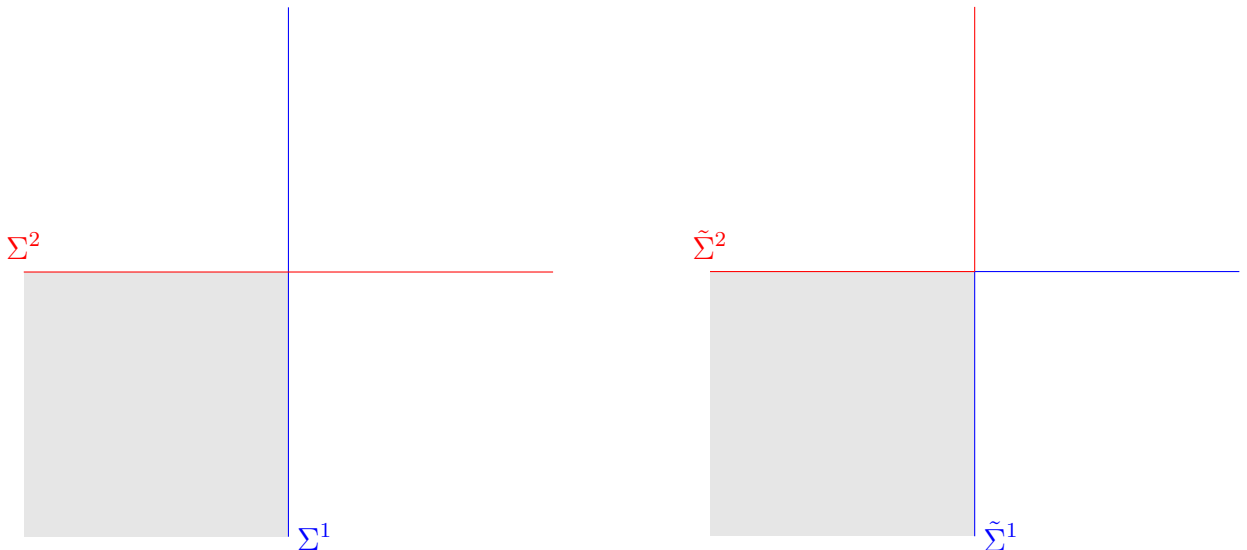$$\Sigma^1 \cup \Sigma^2 = \tilde{\Sigma}^1 \cup \tilde{\Sigma}^2.$$

Figure 4.4: Illustration of the different curves: on the left Σ^1 and Σ^2, on the right $\tilde{\Sigma}^1$ and $\tilde{\Sigma}^2$.

Moreover, we define operators to pass functions defined on $\Sigma^1 \cup \Sigma^2$ to ones defined on $\tilde{\Sigma}^j$

$$\left| \begin{aligned} &E^1 : L^2(\Sigma^1) \times L^2(\Sigma^2) \to L^2(\tilde{\Sigma}^1), \\ &E^1(\varphi^1, \varphi^2) = \begin{cases} \varphi^1 & \text{on } \Sigma^1_-, \\ \varphi^2 & \text{on } \Sigma^2_+, \end{cases} \end{aligned} \right. \tag{4.19}$$

$$\left| \begin{aligned} &E^2 : L^2(\Sigma^1) \times L^2(\Sigma^2) \to L^2(\tilde{\Sigma}^2), \\ &E^2(\varphi^1, \varphi^2) = \begin{cases} \varphi^2 & \text{on } \Sigma^2_-, \\ \varphi^1 & \text{on } \Sigma^1_+. \end{cases} \end{aligned} \right. \tag{4.20}$$

We can show easily that if (φ^1, φ^2) are in $H_g^{1/2}(\Sigma^1) \times H_g^{1/2}(\Sigma^2)$, then $\forall j \in \{1, 2\}$, $E^j(\varphi^1, \varphi^2)$ is in $H_g^{1/2}(\tilde{\Sigma}^j)$ where

$$H_g^{1/2}(\tilde{\Sigma}^j) := \left\{ \varphi \in H^{1/2}(\tilde{\Sigma}^j), \varphi = g \text{ on } \Sigma^j_- \right\}.$$

This is true because the traces are compatible at the crossing point

$$\varphi^1 = \varphi^2 \text{ on } \Sigma^1 \cap \Sigma^2,$$

by definition of $H_g^{1/2}(\Sigma^j)$.

We propose the variational formulation associated to each system in separate sections: System (4.16) is studied in Section 4.3.1 and System (4.17) is studied in Section 4.3.2.

4.3.1   Variational formulation for System (4.16)

We will first derive the variational formulation for the first formulation, which is

$$\left| \begin{aligned} \varphi^1 &= P^2(\varphi^2, \psi^2) & &\text{on } \Sigma^1_+, \\ \varphi^2 &= P^1(\varphi^1, \psi^1) & &\text{on } \Sigma^2_+, \\ \psi^1 &= \frac{\partial}{\partial x_1} P^2(\varphi^2, \psi^2) & &\text{on } \Sigma^1_+, \\ \psi^2 &= \frac{\partial}{\partial x_2} P^1(\varphi^1, \psi^1) & &\text{on } \Sigma^2_+, \\ \varphi^1 &= g & &\text{on } \Sigma^1_-, \\ \varphi^2 &= g & &\text{on } \Sigma^2_-, \\ \varphi^1 &= P^1(\varphi^1, \psi^1) & &\text{on } \Sigma^1_-, \\ \varphi^2 &= P^2(\varphi^2, \psi^2) & &\text{on } \Sigma^2_-, \end{aligned} \right.$$

First, notice that the fifth and sixth lines are taken as essential conditions. Next, we consider the equations for the traces φ^j. The second and the seventh lines are

$$\varphi^2 = P^1(\varphi^1, \psi^1) \text{ on } \Sigma^2_+,$$
$$\varphi^1 = P^1(\varphi^1, \psi^1) \text{ on } \Sigma^1_-.$$

We know that the right hand side $P^1(\varphi^1, \psi^1)\big|_{\tilde{\Sigma}^1}$ is in $H^{1/2}(\tilde{\Sigma}^1)$. For the left hand side, we can combine them by using the operator (4.19), and it leads to

$$E^1(\varphi^1, \varphi^2) = P^1(\varphi^1, \psi^1) \text{ on } \tilde{\Sigma}^1.$$

Taking the test functions $\tilde{\psi}_t^1 \in H^{-1/2}(\tilde{\Sigma}^1)$, this is equivalent to

$$\langle E^1(\varphi^1, \varphi^2), \tilde{\psi}_t^1 \rangle_{\tilde{\Sigma}^1} = \langle P^1(\varphi^1, \psi^1), \tilde{\psi}_t^1 \rangle_{\tilde{\Sigma}^1}, \tag{4.21}$$
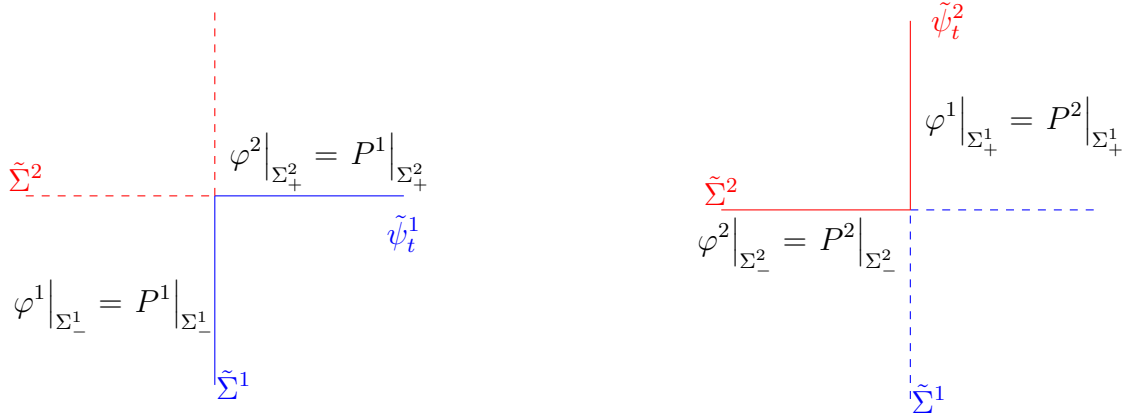
Figure 4.5: Combination of φ^1 and φ^2 on $\tilde{\Sigma}^1$ and $\tilde{\Sigma}^2$ to obtain (4.21) (left figure) and (4.22) (right figure).

where $\langle \cdot, \cdot \rangle_{\tilde{\Sigma}^j}$ is the duality product between $H^{1/2}(\tilde{\Sigma}^j)$ and $H^{-1/2}(\tilde{\Sigma}^j)$. Similarly, by permuting 1 and 2, we combine the first and the eighth lines

$$\varphi^1 = P^2(\varphi^2, \psi^2) \text{ on } \Sigma_+^1,$$
$$\varphi^2 = P^2(\varphi^2, \psi^2) \text{ on } \Sigma_-^2.$$

For all $\tilde{\psi}_t^2 \in H^{-1/2}(\tilde{\Sigma}^2)$ we obtain

$$\langle E^2(\varphi^1, \varphi^2), \tilde{\psi}_t^2 \rangle_{\tilde{\Sigma}^2} = \langle P^2(\varphi^2, \psi^2), \tilde{\psi}_t^2 \rangle_{\tilde{\Sigma}^2}. \tag{4.22}$$

Finally, we consider the equations for ψ^j's. The third line of (4.16) is

$$\psi^1 = \frac{\partial}{\partial x_1} P^2(\varphi^2, \psi^2) \text{ on } \Sigma_+^1.$$

For this equation, we take the test functions φ_t^1 in $H_0^{1/2}(\Sigma_+^1)$. We obtain

$$\langle \varphi_t^1, \psi^1 \big|_{\Sigma_+^1} \rangle_{\Sigma_+^1} = \langle \varphi_t^1, \frac{\partial}{\partial x_1} P^2(\varphi^2, \psi^2) \big|_{\Sigma_+^1} \rangle_{\Sigma_+^1}. \tag{4.23}$$

A similar equation is obtained for all $\varphi_t^2 \in H_0^{1/2}(\Sigma_+^2)$

$$\langle \varphi_t^2, \psi^2 \big|_{\Sigma_+^2} \rangle_{\Sigma_+^2} = \langle \varphi_t^2, \frac{\partial}{\partial x_2} P^1(\varphi^1, \psi^1) \big|_{\Sigma_+^2} \rangle_{\Sigma_+^2}. \tag{4.24}$$

Summing up, we take the test functions

$$\forall j \in \{1, 2\}, \quad \varphi_t^j \in H_0^{1/2}(\Sigma_+^j),$$
$$\tilde{\psi}_t^j \in H^{-1/2}(\tilde{\Sigma}^j).$$

We denote $\Phi_t := (\varphi_t^1, \varphi_t^2, \tilde{\psi}_t^1, \tilde{\psi}_t^2)$ and

$$V_D := H_0^{1/2}(\Sigma_+^1) \times H_0^{1/2}(\Sigma_+^2) \times H^{-1/2}(\tilde{\Sigma}^1) \times H^{-1/2}(\tilde{\Sigma}^2).$$

The variational formulation associated to (4.16) is

find Φ in V such that for all $\tilde{\Phi}_t$ in V_D,

$$\left| \begin{array}{l} \langle E^1(\varphi^1, \varphi^2), \tilde{\psi}_t^1 \rangle_{\tilde{\Sigma}^1} = \langle P^1(\varphi^1, \psi^1), \tilde{\psi}_t^1 \rangle_{\tilde{\Sigma}^1}, \\[2mm] \langle \varphi_t^1, \psi^1 \big|_{\Sigma_+^1} \rangle_{\Sigma_+^1} = \langle \varphi_t^1, \dfrac{\partial}{\partial x_1} P^2(\varphi^2, \psi^2) \big|_{\Sigma_+^1} \rangle_{\Sigma_+^1}, \\[3mm] \langle E^2(\varphi^1, \varphi^2), \tilde{\psi}_t^2 \rangle_{\tilde{\Sigma}^2} = \langle P^2(\varphi^2, \psi^2), \tilde{\psi}_t^2 \rangle_{\tilde{\Sigma}^2}, \\[2mm] \langle \varphi_t^2, \psi^1 \big|_{\Sigma_+^2} \rangle_{\Sigma_+^2} = \langle \varphi_t^2, \dfrac{\partial}{\partial x_2} P^1(\varphi^1, \psi^1) \big|_{\Sigma_+^2} \rangle_{\Sigma_+^2}. \end{array} \right. \qquad (4.25)$$

The following theorem states that Formula (4.25) is equivalent to the original problem (4.1).

Theorem 4.3.1. *Let $g \in H^{1/2}(\partial\Omega)$. If $p \in H^1(\Omega)$ is solution of (4.1) then $(\varphi^1, \varphi^2, \psi^1, \psi^2)$ defined by (4.2) belongs to V and is a solution of (4.25).*

Conversely, if $(\varphi^1, \varphi^2, \psi^1, \psi^2) \in V$ is a solution of (4.25), then $p := P^j(\varphi^j, \psi^j)$ satisfying (4.8) for $j \in \{1, 2\}$ is a function defined "unequivocally" in Ω. Moreover, $p \in H^1(\Omega)$ and is solution of (4.1).

Proof. The first assertion is true by construction. Conversely, suppose that $(\varphi^1, \varphi^2, \psi^1, \psi^2) \in V$ is solution of (4.25). For $j \in \{1, 2\}$, we have the representation $P^j(\varphi^j, \psi^j)$ as given by (4.8). In order to alleviate the notation, we denote $P^j = P^j(\varphi^j, \psi^j)$ in the sequel. We are going to show that

$$P^1 = P^2 \text{ in } \Omega^1 \cap \Omega^2.$$

Why the proof of Lemma 1.2.3 does not work

To show $P^1 = P^2$ in $\Omega^1 \cap \Omega^2$, we have to use a significantly different reasoning from the one used in Lemma 1.2.3. Let us try to proceed as done in Lemma 1.2.3 and see why it does not work. Indeed, the difference $v := P^1 - P^2$ in $\Omega^1 \cap \Omega^2$ satisfies the Helmholtz equation

$$\Delta v + \omega^2 v = 0 \text{ in } \Omega^1 \cap \Omega^2.$$

In Lemma 1.2.3, the compatibility conditions allow us to conclude that $v = 0$ on $\partial(\Omega^1 \cap \Omega^2)$. Here, this is not true a priori. For instance,

$$\begin{aligned} v &= P^1 - P^2 & &\text{on } \Sigma_+^2, \\ &= \varphi^2 - P^2 & &\text{on } \Sigma_+^2 \quad \text{(by the compatibility condition (4.11))}, \end{aligned}$$

but $\varphi^2 \neq P^2$ on Σ_+^2, as explained in (4.9). The compatibility condition on the normal traces do not allow us to conclude either. Thus, our attempt of proving $P^1 = P^2$ in $\Omega^1 \cap \Omega^2$ using this argument leads to no conclusion.

Ideas of the proof

Instead, we will show that there is a continuous extension of the difference $P^1 - P^2$ which is a solution of homogeneous boundary value problem (homogeneous Helmholtz equation and homogeneous Dirichlet boundary condition) in a domain that will be specified later. This continuous extension is obtained thanks to the following functions

$$P_-^1(\varphi^1, \psi^1)(x_1, x_2) := \frac{1}{2\sqrt{2\pi}} \int_{\mathbb{R}} \left(-\hat{\varphi}^1(\xi) + \frac{\hat{\psi}^1(\xi)}{\imath\sqrt{\omega^2 - \xi^2}} \right) e^{-\imath\sqrt{\omega^2 - \xi^2} x_1} e^{\imath \xi x_2} \mathrm{d}\xi \text{ in } \Omega_-, \qquad (4.26)$$

$$P_-^2(\varphi^2, \psi^2)(x_1, x_2) := \frac{1}{2\sqrt{2\pi}} \int_{\mathbb{R}} \left(-\hat{\varphi}^2(\xi) + \frac{\hat{\psi}^2(\xi)}{\imath\sqrt{\omega^2 - \xi^2}} \right) e^{-\imath\sqrt{\omega^2 - \xi^2}x_2} e^{\imath\xi x_1} \mathrm{d}\xi \text{ in } \Omega_-^2, \qquad (4.27)$$

where $\Omega_-^1 := \mathbb{R}^2 \backslash \Omega^1$ and $\Omega_-^2 := \mathbb{R}^2 \backslash \Omega^2$. In order to alleviate the notations, we denote $P_-^j = P_-^j(\varphi^j, \psi^j)$. The function P_-^1 is a particular extension of P^1 such that

$$\varphi^1 = P^1 - P_-^1 \text{ and } \psi^1 = \frac{\partial P^1}{\partial x_1} - \frac{\partial P_-^1}{\partial x_1} \text{ on } \Sigma^1. \qquad (4.28)$$

Similarly, P_-^2 is a particular extension of P^2 such that

$$\varphi^2 = P^2 - P_-^2 \text{ and } \psi^2 = \frac{\partial P^2}{\partial x_2} - \frac{\partial P_-^2}{\partial x_2} \text{ on } \Sigma^2. \qquad (4.29)$$

To explain the ides of the proof, we first use the compatibility condition in their strong form. We have

$$
\begin{aligned}
v &= P^1 - P^2 & &\text{on } \Sigma_+^1, \\
&= P^1 - \varphi^1 & &\text{on } \Sigma_+^1 \quad \text{(by the compatibility condition (4.12))} \\
&= P_-^1 & &\text{on } \Sigma_+^1 \quad \text{(by the jump condition (4.28))},
\end{aligned}
$$

and similarly

$$\frac{\partial v}{\partial x_1} = \frac{\partial P_-^1}{\partial x_1} \quad \text{on } \Sigma_+^1.$$

The function defined by

$$v_1 := \begin{cases} v & \text{in } \Omega_1 \cap \Omega_2 \\ P_-^1 & \text{in } \Omega_-^1, \end{cases}$$

is an H^1 solution of the Helmholtz equation in $(\Omega^1 \cap \Omega^2) \cup \Omega_-^1$ (see Figure 4.6(a)). Moreover, we have

$$\varphi^1 = P^1 \text{ on } \Sigma_-^1,$$

which implies that

$$P_-^1 = 0 \text{ on } \Sigma_-^1 \quad \Rightarrow \quad v_1|_{\Sigma_-^1} = 0. \qquad (4.30)$$

Similarly, we have

$$
\begin{aligned}
v &= P^1 - P^2 & &\text{on } \Sigma_+^2, \\
&= \varphi^2 - P^2 & &\text{on } \Sigma_+^2 \quad \text{(by the compatibility condition (4.11))} \\
&= -P_-^2 & &\text{on } \Sigma_+^2 \quad \text{(by the jump condition (4.29))},
\end{aligned}
$$

and

$$\frac{\partial v}{\partial x_2} = -\frac{\partial P_-^2}{\partial x_2} \text{ on } \Sigma_+^2.$$

The function defined by

$$v_2 := \begin{cases} v & \text{in } \Omega_1 \cap \Omega_2 \\ -P_-^2 & \text{in } \Omega_-^2, \end{cases}$$

is an H^1 solution of the Helmholtz equation in $(\Omega^1 \cap \Omega^2) \cup \Omega_-^2$ (see Figure 4.6(b)). Moreover, we have

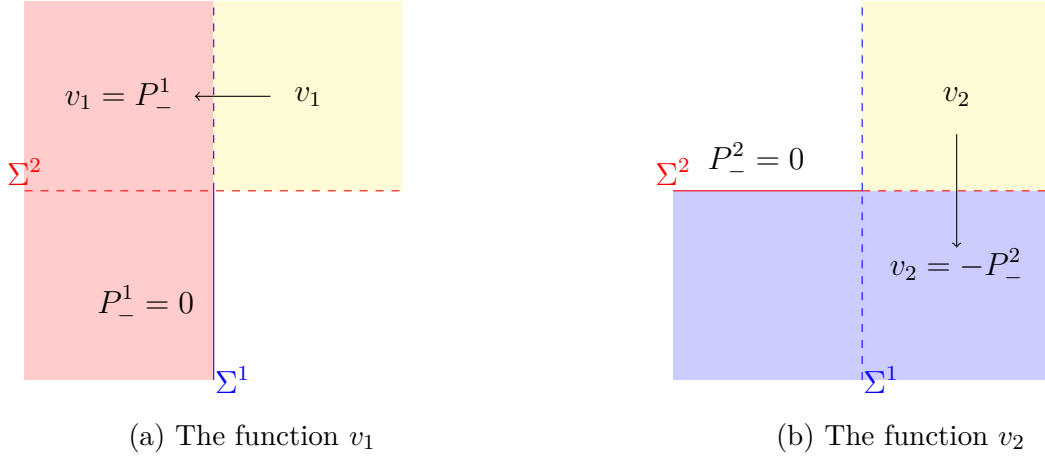$$\varphi^2 = P^2 \text{ on } \Sigma_-^2,$$

(a) The function v_1 (b) The function v_2

Figure 4.6: The continuous extension (a) from $\Omega^1 \cap \Omega^2$ to Ω^1_- and (b) from $\Omega^1 \cap \Omega^2$ to Ω^2_-.

which implies that

$$P^2_- = 0 \text{ on } \Sigma^2_- \quad \Rightarrow \quad v_2 = 0 \text{ on } \Sigma^2_-. \tag{4.31}$$

We have then defined a solution of the Helmholtz equation in a Riemann surface $\Omega^1_- \cup (\Omega^1 \cap \Omega^2) \cup \Omega^2_-$ satisfying homogeneous Dirichlet condition on its boundary $\Sigma^1_- \cup \Sigma^2_-$ (see Figure 4.7). Since the problem is coercive thanks to the dissipation of the medium, the unique solution of the problem is

$$\begin{aligned} P^1 - P^2 &= 0 \text{ in } \Omega^1 \cap \Omega^2, \\ P^1_- &= 0 \text{ in } \Omega^1_-, \\ P^2_- &= 0 \text{ in } \Omega^2_-. \end{aligned} \tag{4.32}$$

We conclude that $P^1 = P^2$ in $\Omega^1 \cap \Omega^2$. Therefore, we can define a function p unequivocally in Ω as

$$p = P^j \text{ in } \Omega^j.$$

Remark that $P^j_- = 0$ in Ω^j_- yields $\hat{\varphi}^j(\xi) = \dfrac{\hat{\psi}^j(\xi)}{\sqrt{\omega^2 - \xi^2}}$ which means that φ^j and ψ^j are compatible (see (4.10)). From (4.30) and (4.31), it follows that

$$p\big|_{\Sigma^j_-} = P^j\big|_{\Sigma^j_-} = P^j\big|_{\Sigma^j_-} - P^j_-\big|_{\Sigma^j_-} = \varphi^j\big|_{\Sigma^j_-} = g\big|_{\Sigma^j_-}.$$
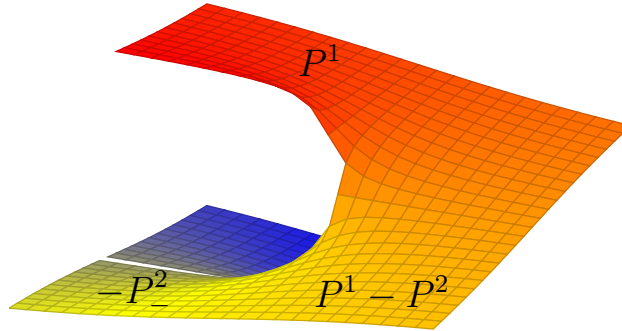
Thus, p is indeed the solution of (4.1).

Figure 4.7: The domain in which $P^1 - P^2$ has a continuous extension.

Rigorous proof

We use now the compatibility conditions written in the weak form. Let us first consider

$$\forall \tilde{\psi}_t^1 \in H^{-1/2}(\tilde{\Sigma}^1), \quad \langle E^1(\varphi^1, \varphi^2), \tilde{\psi}_t^1 \rangle_{\tilde{\Sigma}^1} = \langle P^1, \tilde{\psi}_t^1 \rangle_{\tilde{\Sigma}^1}.$$

Using $\tilde{\psi}_t^1 \in L^2(\tilde{\Sigma}^1), \tilde{\psi}_t^1 = 0$ on Σ_+^2, we obtain

$$\left(\varphi^1, \tilde{\psi}_t^1 \right)_{L^2(\Sigma_-^1)} = \left(P^1, \tilde{\psi}_t^1 \right)_{L^2(\Sigma_-^1)},$$

which leads to

$$\varphi^1 \big|_{\Sigma_-^1} = P^1 \big|_{\Sigma_-^1},$$

which can be written as

$$P_-^1 \big|_{\Sigma_-^1} = 0. \tag{4.33}$$

Using $\tilde{\psi}_t^1 \in L^2(\tilde{\Sigma}^1), \tilde{\psi}_t^1 = 0$ on Σ_-^1, we obtain

$$\left(\varphi^2, \tilde{\psi}_t^1 \right)_{L^2(\Sigma_+^2)} = \left(P^1, \tilde{\psi}_t^1 \right)_{L^2(\Sigma_+^2)},$$

which leads to

$$\varphi^2 \big|_{\Sigma_+^2} = P^1 \big|_{\Sigma_+^2}. \tag{4.34}$$

The equation

$$\forall \tilde{\psi}_t^2 \in H^{-1/2}(\tilde{\Sigma}^2), \quad \langle E^2(\varphi^1, \varphi^2), \tilde{\psi}_t^2 \rangle_{\tilde{\Sigma}^2} = \langle P^2, \tilde{\psi}_t^2 \rangle_{\tilde{\Sigma}^2}$$

leads similarly to

$$P_-^2 \big|_{\Sigma_-^2} = 0 \tag{4.35}$$

$$\varphi^1 \big|_{\Sigma_+^1} = P^2 \big|_{\Sigma_+^1}. \tag{4.36}$$

Now, consider the difference $P^1 - P^2$ in $\Omega^1 \cap \Omega^2$. It satisfies the Helmholtz equation

$$-\Delta(P^1 - P^2) - \omega^2(P^1 - P^2) = 0 \text{ in } \Omega^1 \cap \Omega^2.$$

Multiplying it by $\overline{P^1 - P^2}$, integrating it on $\Omega^1 \cap \Omega^2$, and then applying the Green's formula, we obtain

$$\int_{\Omega^1 \cap \Omega^2} \left| \nabla(P^1 - P^2) \right|^2 - \omega^2 \left| P^1 - P^2 \right|^2 = - \langle P^1 - P^2, \frac{\partial P^1}{\partial n} - \frac{\partial P^2}{\partial n} \rangle_{\partial(\Omega^1 \cap \Omega^2)}, \tag{4.37}$$

where n is the inward normal of $\Omega^1 \cap \Omega^2$. On the other hand, in Ω_-^1, P_-^1 also satisfies

$$\int_{\Omega_-^1} \left| \nabla P_-^1 \right|^2 - \omega^2 \left| P_-^1 \right|^2 = \langle P_-^1, \frac{\partial P_-^1}{\partial x_1} \rangle_{\Sigma^1}, \tag{4.38}$$

and in Ω_-^2, P_-^2 satisfies

$$\int_{\Omega_-^2} \left| \nabla P_-^2 \right|^2 - \omega^2 \left| P_-^2 \right|^2 = \langle P_-^2, \frac{\partial P_-^2}{\partial x_2} \rangle_{\Sigma^2}. \tag{4.39}$$

We show now that (4.37 - 4.39) sum up to zero by using the jump conditions and the compatibility relations.

As $P_-^1 = 0$ on Σ_-^1, $P_-^1\big|_{\Sigma_+^1}$ can be used as a test function in

$$\forall \varphi_t^1 \in H_0^{1/2}(\Sigma_+^1), \quad \langle \varphi_t^1, \psi^1\big|_{\Sigma_+^1} \rangle_{\Sigma_+^1} = \langle \varphi_t^1, \frac{\partial P^2}{\partial x_1}\big|_{\Sigma_+^1} \rangle_{\Sigma_+^1} .$$

We deduce by using first the jump condition that

$$\langle P_-^1, \frac{\partial P_-^1}{\partial x_1} \rangle_{\Sigma^1} = \langle P_-^1, \frac{\partial P_-^1}{\partial x_1}\big|_{\Sigma_+^1} \rangle_{\Sigma_+^1}$$

$$= \langle P_-^1, \frac{\partial P^1}{\partial x_1}\big|_{\Sigma_+^1} \rangle_{\Sigma_+^1} - \langle P_-^1, \psi^1\big|_{\Sigma_+^1} \rangle_{\Sigma_+^1}$$

$$= \langle P_-^1, \frac{\partial P^1}{\partial x_1}\big|_{\Sigma_+^1} \rangle_{\Sigma_+^1} - \langle P_-^1, \frac{\partial P^2}{\partial x_1}\big|_{\Sigma_+^1} \rangle_{\Sigma_+^1} \qquad \text{(by the compatibility condition (4.23))}$$

$$= \langle P_-^1, \frac{\partial P^1}{\partial x_1}\big|_{\Sigma_+^1} - \frac{\partial P^2}{\partial x_1}\big|_{\Sigma_+^1} \rangle_{\Sigma_+^1} .$$

Similarly, we have

$$\langle P_-^2, \frac{\partial P_-^2}{\partial x_2} \rangle_{\Sigma^2} = \langle -P_-^2, \frac{\partial P^1}{\partial x_2}\big|_{\Sigma_+^2} - \frac{\partial P^2}{\partial x_2}\big|_{\Sigma_+^2} \rangle_{\Sigma_+^2} .$$

As $P_-^1\big|_{\Sigma_-^1} = 0$ and $P_-^2\big|_{\Sigma_-^2} = 0$, the function $\phi \in L^2(\Sigma_+^1 \cup \Sigma_+^2)$ defined by $\phi|_{\Sigma_+^1} = P_-^1\big|_{\Sigma_+^1}$ and $\phi|_{\Sigma_+^2} = -P_-^2\big|_{\Sigma_+^2}$ is such that $\phi \in H^{1/2}(\Sigma_+^1 \cup \Sigma_+^2)$ and

$$\forall \psi \in H^{-1/2}(\Sigma_+^1 \cup \Sigma_+^2), \quad \langle \phi, \psi|_{\Sigma_+^1} \rangle_{\Sigma_+^1} + \langle \phi, \psi|_{\Sigma_+^2} \rangle_{\Sigma_+^2} = \langle \phi, \psi \rangle_{\Sigma_+^1 \cup \Sigma_+^2} .$$

It leads to

$$\langle P_-^1, \frac{\partial P^1}{\partial x_1}\big|_{\Sigma_+^1} - \frac{\partial P^2}{\partial x_1}\big|_{\Sigma_+^1} \rangle_{\Sigma_+^1} - \langle P_-^2, \frac{\partial P^1}{\partial x_2}\big|_{\Sigma_+^2} - \frac{\partial P^2}{\partial x_2}\big|_{\Sigma_+^2} \rangle_{\Sigma_+^2} = \langle \phi, \frac{\partial P^1}{\partial n} - \frac{\partial P^2}{\partial n} \rangle_{\Sigma_+^1 \cup \Sigma_+^2} .$$

Finally,

$$\phi|_{\Sigma_+^1} = P_-^1\big|_{\Sigma_+^1}$$

$$= P^1\big|_{\Sigma_+^1} - \varphi^1\big|_{\Sigma_+^1} \qquad\qquad \text{by the jump condition}$$

$$= P^1\big|_{\Sigma_+^1} - P^2\big|_{\Sigma_+^1} \qquad\qquad \text{by (4.36),}$$

and similarly.

$$\phi|_{\Sigma_+^2} = -P_-^2\big|_{\Sigma_+^2}$$

$$= -P^2\big|_{\Sigma_+^2} + \varphi^2\big|_{\Sigma_+^2} \qquad\qquad \text{by the jump condition}$$

$$= P^1\big|_{\Sigma_+^2} - P^2\big|_{\Sigma_+^2} \qquad\qquad \text{by (4.34),}$$

We obtain

$$\langle \phi, \frac{\partial P^1}{\partial n} - \frac{\partial P^2}{\partial n} \rangle_{\Sigma^1_+ \cup \Sigma^2_+} = \langle P^1 - P^2, \frac{\partial P^1}{\partial n} - \frac{\partial P^2}{\partial n} \rangle_{\Sigma^1_+ \cup \Sigma^2_+}.$$

which enables us to conclude that

$$\int_{\Omega^1 \cap \Omega^2} \left| \nabla (P^1 - P^2) \right|^2 - \omega^2 \left| P^1 - P^2 \right|^2 + \int_{\mathbb{R}^2 \backslash \Omega^1} \left| \nabla P^1_- \right|^2 - \omega^2 \left| P^1_- \right|^2 + \int_{\mathbb{R}^2 \backslash \Omega^2} \left| \nabla P^2_- \right|^2 - \omega^2 \left| P^2_- \right|^2 = 0.$$

As $\mathrm{Im}\,\omega > 0$, we have

$$P^1 - P^2 = 0 \text{ in } \Omega^1 \cap \Omega^2,$$
$$P^1_- = 0 \text{ in } \Omega^1_-,$$
$$P^2_- = 0 \text{ in } \Omega^2_-.$$

The result follows.

$\square$

4.3.2 Variational formulation for System (4.17)

We now consider the second choice of the formulation, which is System (4.17):

$$\left|\begin{array}{lll} \varphi^1 & = P^2(\varphi^2, \psi^2) & \text{on } \Sigma^1_+, \\ \varphi^2 & = P^1(\varphi^1, \psi^1) & \text{on } \Sigma^2_+, \\ \psi^1 & = \dfrac{\partial}{\partial x_1} P^2(\varphi^2, \psi^2) & \text{on } \Sigma^1_+, \\ \psi^2 & = \dfrac{\partial}{\partial x_2} P^1(\varphi^1, \psi^1) & \text{on } \Sigma^2_+, \\ \varphi^1 & = g & \text{on } \Sigma^1_-, \\ \varphi^2 & = g & \text{on } \Sigma^2_-, \\ \psi^1 & = \dfrac{\partial}{\partial x_1} P^1(\varphi^1, \psi^1) & \text{on } \Sigma^1_-, \\ \psi^2 & = \dfrac{\partial}{\partial x_2} P^2(\varphi^2, \psi^2) & \text{on } \Sigma^2_-. \end{array}\right.$$

There are some subtle technical differences, but the principle is the same. As test functions, we take

$$(\varphi^1_t, \varphi^2_t) \in V^{1/2} := \left\{ (\varphi^1, \varphi^2) \in H^{1/2}(\Sigma^1) \times H^{1/2}(\Sigma^2), \exists q \in H^1(\Omega) \text{ such that } \varphi^j = q \text{ on } \Sigma^j \right\},$$

$$\psi^j_t \in H_0^{-1/2}(\Sigma^j_+) := \left\{ \psi|_{\Sigma^j_+} \middle| \psi \in H^{-1/2}(\Sigma^j), \psi|_{\Sigma^j_-} = 0 \text{ on } \Sigma^j_- \right\} \equiv \left(H^{1/2}(\Sigma^j_+) \right)'.$$

The couple $(\varphi^1_t, \varphi^2_t)$ taken in $V^{1/2}$ means that they are compatible at the crossing point

$$\varphi^1_t = \varphi^2_t \text{ on } \Sigma^1 \cap \Sigma^2.$$

By having this compatibility, it is apparent that $E^j(\varphi^1_t, \varphi^2_t)$ is in $H^{1/2}(\tilde{\Sigma}^j)$ for $(\varphi^1_t, \varphi^2_t) \in V^{1/2}$. Furthermore, we denote $\Phi_t = (\varphi^1_t, \varphi^2_t, \psi^1_t, \psi^2_t)$ and $\Phi_t \in V_N$ where

$$V_N := V^{1/2} \times H_0^{-1/2}(\Sigma^1_+) \times H_0^{-1/2}(\Sigma^2_+). \tag{4.40}$$

We now derive the variational formulation. As before, the fifth and sixth lines of (4.17) are taken as essential conditions. Next, we consider the equations for φ^j. The first line of (4.17) is

$$\varphi^1_+ = P^2(\varphi^2, \psi^2) \text{ on } \Sigma^1_+.$$

Taking the test functions $\psi_t^1 \in H_0^{-1/2}(\Sigma_+^1)$, we obtain

$$\langle \varphi^1, \psi_t^1 \rangle_{\Sigma_+^1} = \langle P^2(\varphi^2, \psi^2), \psi_t^1 \rangle_{\Sigma_+^1}. \tag{4.41}$$

We obtain a similar equation for all $\psi_t^2 \in H_0^{-1/2}(\Sigma_+^2)$

$$\langle \varphi^2, \psi_t^2 \rangle_{\Sigma_+^2} = \langle P^1(\varphi^1, \psi^1), \psi_t^2 \rangle_{\Sigma_+^2}. \tag{4.42}$$

For the third, fourth, seventh, and eighth lines of (4.17), we take the test functions $(\varphi_t^1, \varphi_t^2)$ and use the operators E^j to pass the test functions from $\Sigma^1 \cup \Sigma^2$ to $\tilde{\Sigma}^j$. Furthermore, we define the normal direction $\tilde{n}^1$ as the direction *inward of* $\Omega^1 \backslash (\Omega^1 \cap \Omega^2)$, while $\tilde{n}^2$ as the direction *outward of* $\Omega^2 \backslash (\Omega^1 \cap \Omega^2)$ (pay attention to the direction). These normal directions are such that

$$\frac{\partial \cdot}{\partial \tilde{n}^1} = \begin{cases} \dfrac{\partial \cdot}{\partial x_1} & \text{on } \Sigma_-^1, \\ -\dfrac{\partial \cdot}{\partial x_2} & \text{on } \Sigma_+^2, \end{cases}$$

$$\frac{\partial \cdot}{\partial \tilde{n}^2} = \begin{cases} -\dfrac{\partial \cdot}{\partial x_2} & \text{on } \Sigma_-^2, \\ \dfrac{\partial \cdot}{\partial x_1} & \text{on } \Sigma_+^1. \end{cases}$$

The equations satisfied by ψ^1 and ψ^2 are (written with the new normal directions)

Figure 4.8: (a) The normal direction of ψ^1 and ψ^2 and (b) the normal directions $\tilde{n}^1$ and $\tilde{n}^2$.

$$\begin{aligned} \psi^1 &= \frac{\partial}{\partial \tilde{n}^1} P^1(\varphi^1, \psi^1) \text{ on } \Sigma_-^1, \\ \psi^1 &= \frac{\partial}{\partial \tilde{n}^2} P^2(\varphi^2, \psi^2) \text{ on } \Sigma_+^1, \\ -\psi^2 &= \frac{\partial}{\partial \tilde{n}^2} P^2(\varphi^2, \psi^2) \text{ on } \Sigma_-^2, \\ -\psi^2 &= \frac{\partial}{\partial \tilde{n}^1} P^1(\varphi^1, \psi^1) \text{ on } \Sigma_+^2. \end{aligned} \tag{4.43}$$

If we try to imitate what we did in the previous section, we would like to take a test function $\tilde{\varphi}_t^1 \in H^{1/2}(\tilde{\Sigma}^1)$ to combine the first and fourth line of (4.43). However, ψ^1 and ψ^2 are a priori not compatible at the crossing point. The same problem happens when we try to combine the second and third lines. Instead, we can combine them by writing the sum of these four equations and taking the appropriate test functions

$$\langle \varphi_t^1, \psi^1 \rangle_{\Sigma^1} - \langle \varphi_t^2, \psi^2 \rangle_{\Sigma^2} = \langle E^1(\varphi_t^1, \varphi_t^2), \frac{\partial}{\partial \tilde{n}^1} P^1(\varphi^1, \psi^1) \rangle_{\tilde{\Sigma}^1} + \langle E^2(\varphi_t^1, \varphi_t^2), \frac{\partial}{\partial \tilde{n}^2} P^2(\varphi^2, \psi^2) \rangle_{\tilde{\Sigma}^2}. \tag{4.44}$$

Summing up, the variational formulation associated to (4.17) is

find $\Phi = (\varphi^1, \varphi^2, \psi^1, \psi^2)$ in V such that for all $\Phi_t = (\varphi_t^1, \varphi_t^2, \psi_t^1, \psi_t^2)$ in V_N

$$\langle \varphi^1, \psi_t^1 \rangle_{\Sigma_+^1} = \langle P^2(\varphi^2, \psi^2), \psi_t^1 \rangle_{\Sigma_+^1},$$

$$\langle \varphi^2, \psi_t^2 \rangle_{\Sigma_+^2} = \langle P^1(\varphi^1, \psi^1), \psi_t^2 \rangle_{\Sigma_+^2},$$

$$\langle \varphi_t^1, \psi^1 \rangle_{\Sigma^1} - \langle \varphi_t^2, \psi^2 \rangle_{\Sigma^2} = \langle E^1(\varphi_t^1, \varphi_t^2), \frac{\partial}{\partial \tilde{n}^1} P^1(\varphi^1, \psi^1) \rangle_{\tilde{\Sigma}^1} + \langle E^2(\varphi_t^1, \varphi_t^2), \frac{\partial}{\partial \tilde{n}^2} P^2(\varphi^2, \psi^2) \rangle_{\tilde{\Sigma}^2}.$$
$$(4.45)$$

Theorem 4.3.2. *Let $g \in H^{1/2}(\partial\Omega)$. If $p \in H^1(\Omega)$ is solution of (4.1) then Φ defined by (4.2) belongs to V and is a solution of (4.45).*

Conversely, if $(\varphi^1, \varphi^2, \psi^1, \psi^2) \in V$ is a solution of (4.45), then $p := P^j(\varphi^j, \psi^j)$ satisfying (4.7) for $j \in \{1, 2\}$ is a function defined "unequivocally" in Ω. Moreover, $p \in H^1(\Omega)$ and is solution of (4.1).

Proof. The first assertion is again true by construction. Conversely, suppose that $(\varphi^1, \varphi^2, \psi^1, \psi^2) \in V$ is solution of (4.45). For $j \in \{1, 2\}$, we have the representation $P^j(\varphi^j, \psi^j)$ as given by (4.8). We are going to show again that

$$P^1 = P^2 \text{ in } \Omega^1 \cap \Omega^2.$$

We start by defining the same functions P_-^1 and P_-^2 as defined in (4.26 - 4.27), which satisfy the same jump conditions

$$\varphi^1 = P^1 - P_-^1 \text{ and } \psi^1 = \frac{\partial P^1}{\partial x_1} - \frac{\partial P_-^1}{\partial x_1} \text{ on } \Sigma^1,$$

and

$$\varphi^2 = P^2 - P_-^2 \text{ and } \psi^2 = \frac{\partial P^2}{\partial x_2} - \frac{\partial P_-^2}{\partial x_2} \text{ on } \Sigma^2.$$

The idea of the proof is similar to the one in Theorem (4.3.1): we define a continuous extension of the Helmholtz equation in a Riemann surface $\Omega_-^1 \cup (\Omega^1 \cap \Omega^2) \cup \Omega_-^2$. The only difference is that this time, instead of having a homogeneous Dirichlet condition, we have a homogeneous Neumann condition on the boundary $\Sigma_-^1 \cup \Sigma_-^2$.

Now, we show only the rigorous proof of the theorem, where we use the compatibility conditions written in the weak form. First, we consider $\forall(\varphi_t^1, \varphi_t^2) \in V^{1/2}$,

$$\langle \varphi_t^1, \psi^1 \rangle_{\Sigma^1} - \langle \varphi_t^2, \psi^2 \rangle_{\Sigma^2} = \langle E^1(\varphi_t^1, \varphi_t^2), \frac{\partial}{\partial \tilde{n}^1} P^1(\varphi^1, \psi^1) \rangle_{\tilde{\Sigma}^1} + \langle E^2(\varphi_t^1, \varphi_t^2), \frac{\partial}{\partial \tilde{n}^2} P^2(\varphi^2, \psi^2) \rangle_{\tilde{\Sigma}^2}.$$

Taking $\varphi_t^1 = 0$ on Σ_+^1 and $\varphi_t^2 = 0$ on Σ^2, we obtain

$$\langle \varphi_t^1, \psi^1 \big|_{\Sigma_-^1} \rangle_{\Sigma_-^1} = \langle \varphi_t^1, \frac{\partial P^1}{\partial x_1} \big|_{\Sigma_-^1} \rangle_{\Sigma_-^1},$$

which leads to

$$\frac{\partial P_-^1}{\partial x_1} \bigg|_{\Sigma_-^1} = 0. \qquad (4.46)$$

Taking $\varphi_t^1 = 0$ on Σ_-^1 and $\varphi_t^2 = 0$ on Σ^2, we obtain

$$\langle \varphi_t^1, \psi^1 \big|_{\Sigma_+^1} \rangle_{\Sigma_+^1} = \langle \varphi_t^1, \frac{\partial P^2}{\partial x_1} \big|_{\Sigma_+^1} \rangle_{\Sigma_+^1},$$

which leads to

$$\psi^1\big|_{\Sigma^1_+} = \frac{\partial P^2}{\partial x_1}\bigg|_{\Sigma^1_+}. \tag{4.47}$$

Similarly, we have

$$\frac{\partial P^2_-}{\partial x_2}\bigg|_{\Sigma^2_-} = 0 \tag{4.48}$$

$$\psi^2\big|_{\Sigma^2_+} = \frac{\partial P^1}{\partial x_2}\bigg|_{\Sigma^2_+}. \tag{4.49}$$

Now, if we consider the difference $P^1 - P^2$ in $\Omega^1 \cap \Omega^2$ and apply the Green's formula, we obtain

$$\int_{\Omega^1\cap\Omega^2} \left|\nabla(P^1 - P^2)\right|^2 - \omega^2\left|P^1 - P^2\right|^2 = -\left\langle P^1 - P^2, \frac{\partial P^1}{\partial n} - \frac{\partial P^2}{\partial n}\right\rangle_{\partial(\Omega^1\cap\Omega^2)}, \tag{4.50}$$

where n is the inward normal of $\Omega^1 \cap \Omega^2$. As before, in Ω^1_-, P^1_- also satisfies

$$\int_{\mathbb{R}^2\setminus\Omega^1} \left|\nabla P^1_-\right|^2 - \omega^2\left|P^1_-\right|^2 = \left\langle P^1_-, \frac{\partial P^1_-}{\partial x_1}\right\rangle_{\Sigma^1}, \tag{4.51}$$

and in Ω^2_-, P^2_- satisfies

$$\int_{\mathbb{R}^2\setminus\Omega^2} \left|\nabla P^2_-\right|^2 - \omega^2\left|P^2_-\right|^2 = \left\langle P^2_-, \frac{\partial P^2_-}{\partial x_2}\right\rangle_{\Sigma^2}. \tag{4.52}$$

Again, we show that (4.50 - 4.52) sum up to zero by the jump conditions and the compatibility relations.

Indeed, for (4.51), since $\frac{\partial P^1_-}{\partial x_1} = 0$ on Σ^1_-, (4.51) simplifies to

$$\left\langle P^1_-, \frac{\partial P^1_-}{\partial x_1}\right\rangle_{\Sigma^1} = \left\langle P^1_-, \frac{\partial P^1_-}{\partial x_1}\right\rangle_{\Sigma^1_+}.$$

Using the first equation of (4.45)

$$\langle \varphi^1, \psi^1_t\rangle_{\Sigma^1_+} = \langle P^2, \psi^1_t\rangle_{\Sigma^1_+}$$

with $\psi^1_t = \frac{\partial P^1_-}{\partial x_1} \in H_0^{-1/2}(\Sigma^1_+)$ as the test function and $P^1_- = P^1 - \varphi^1$ on Σ^1_+, we obtain

$$\left\langle P^1_-, \frac{\partial P^1_-}{\partial x_1}\right\rangle_{\Sigma^1_+} = \left\langle P^1 - P^2, \frac{\partial P^1_-}{\partial x_1}\right\rangle_{\Sigma^1_+}.$$

Using (4.47) and $\frac{\partial P^1_-}{\partial x_1} = \frac{\partial P^1}{\partial x_1} - \psi^1$ on Σ^1_+, we have

$$\left\langle P^1 - P^2, \frac{\partial P^1_-}{\partial x_1}\right\rangle_{\Sigma^1_+} = \left\langle P^1 - P^2, \frac{\partial P^1}{\partial x_1} - \frac{\partial P^2}{\partial x_1}\right\rangle_{\Sigma^1_+}. \tag{4.53}$$

Similarly,

$$\left\langle P^2_-, \frac{\partial P^2_-}{\partial x_2}\right\rangle_{\Sigma^2_+} = \left\langle P^2 - P^1, \frac{\partial P^2}{\partial x_2} - \frac{\partial P^1}{\partial x_2}\right\rangle_{\Sigma^2_+}. \tag{4.54}$$

Taking the sum of (4.50), (4.53) and (4.54), we show that

$$\int_{\Omega^1 \cap \Omega^2} \left|\nabla(P^1 - P^2)\right|^2 - \omega^2 \left|P^1 - P^2\right|^2 + \int_{\Omega^1_-} \left|\nabla P^1_-\right|^2 - \omega^2 \left|P^1_-\right|^2 + \int_{\Omega^2_-} \left|\nabla P^2_-\right|^2 - \omega^2 \left|P^2_-\right|^2 = 0.$$

Since $\operatorname{Im}\omega > 0$, we conclude that

$$P^1 - P^2 = 0 \text{ in } \Omega^1 \cap \Omega^2,$$
$$P^1_- = 0 \text{ in } \Omega^1_-,$$
$$P^2_- = 0 \text{ in } \Omega^2_-.$$

We conclude as in the proof of Theorem 4.25. $\qquad\square$

With these theorems on the equivalence, we deduce easily the uniqueness of the solution of the multi-unknown HSM formulations.

Theorem 4.3.3. *The multi-unknown Half-Space Matching formulations have a unique solution.*

Proof. We suppose that $g = 0$ on $\partial\Omega$. From Theorems 4.3.1 - 4.3.2, the formulations (4.25 - 4.45), we can define unequivocally a function $p := P^j(\varphi^j, \psi^j)$ satisfying (4.8) for $j \in \{1, 2\}$. This function p is also in $H^1(\Omega)$ and a solution of (4.1). Since Problem (4.1) is well-posed, the only solution is $p = 0$ which then leads to $P^j(\varphi^j, \psi^j) = 0$ for $j \in \{1, 2\}$. Thus, $\varphi^j = 0$ and $\psi^j = 0$ for $j \in \{1, 2\}$. The result follows. $\qquad\square$

The stability of Formulations (4.25 - 4.45) are still an open question.

4.4 Generalization to a general exterior problem

The formulations derived in the previous section can be extended to solve a Helmholtz equation in the exterior of a convex polygon (the same problem as in Chapter 1). For simplicity, we consider that the obstacle is a square $\mathcal{O} := [-a, a]^2, a > 0$. The problem that we are interested in is

find $p \in H^1(\Omega)$ such that

$$\begin{cases} \Delta p + \omega^2 p & = 0 \text{ in } \Omega := \mathbb{R}^2 \backslash \mathcal{O}, \\ p & = g \text{ on } \partial\mathcal{O}, \end{cases} \tag{4.55}$$

where $g \in H^{1/2}(\partial\Omega)$ is given.

Taking the same approach, the domain is decomposed into 4 overlapping half-spaces Ω^j for $j \in \{0, 1, 2, 3\}$ (the same half-spaces as in Chapter 0). The restriction of the solution in each half-space can be represented in terms of its trace and normal trace (φ^j, ψ^j) on the boundary similar to Formula (4.7). We are then looking for a system of equations satisfied by these traces. By taking the same steps, the traces $\left\{(\varphi^j, \psi^j)\right\}_{j \in \{0,1,2,3\}}$ satisfy two different systems of equations:

$$\left| \begin{array}{lll} \varphi^{j\pm 1} & = P^j(\varphi^j, \psi^j) & \text{on } \Sigma^{j\pm 1} \cap \Omega^j, j \in \mathbb{Z}/4\mathbb{Z}, \\ \psi^{j\pm 1} & = \dfrac{\partial}{\partial n^{j\pm 1}} P^j(\varphi^j, \psi^j) & \text{on } \Sigma^{j\pm 1} \cap \Omega^j, \\ \varphi^j & = g & \text{on } \Sigma^j \cap \partial\mathcal{O}, \\ \varphi^j & = P^j(\varphi^j, \psi^j) & \text{on } \Sigma^j \cap \partial\mathcal{O}, \end{array} \right. \tag{4.56}$$

or

$$\left|\begin{array}{rll} \varphi^{j\pm1} &= P^j(\varphi^j,\psi^j) & \text{on } \Sigma^{j\pm1}\cap\Omega^j, j\in\mathbb{Z}/4\mathbb{Z}, \\ \psi^{j\pm1} &= \dfrac{\partial}{\partial n^{j\pm1}}P^j(\varphi^j,\psi^j) & \text{on } \Sigma^{j\pm1}\cap\Omega^j, \\ \varphi^j &= g & \text{on } \Sigma^j\cap\partial\mathcal{O}, \\ \psi^j &= \dfrac{\partial}{\partial n^j}P^j(\varphi^j,\psi^j) & \text{on } \Sigma^j\cap\partial\mathcal{O}, \end{array}\right. \tag{4.57}$$

where n^j is the normal direction into Ω^j. The functional spaces for the unknowns are

$$\forall j\in\{0,1,2,3\}, \quad \left|\begin{array}{l} \varphi^j\in H_g^{1/2}(\Sigma^j) \\ \psi^j\in H^{-1/2}(\Sigma^j). \end{array}\right. \tag{4.58}$$

We denote $\Phi=(\varphi^1,\varphi^2,\varphi^2,\varphi^3,\psi^1,\psi^2,\psi^2,\psi^3)\in V$, where

$$V:=\prod_{i\in\{0,1,2,3\}}H_g^{1/2}(\Sigma^i)\times\prod_{j\in\{0,1,2,3\}}H^{-1/2}(\Sigma^j).$$

To obtain the variational formulation for (4.56), once again we need to define new curves

$$\forall j\in\mathbb{Z}/4\mathbb{Z}, \quad \tilde{\Sigma}^j:=\partial(\Omega^j\backslash(\Omega^{j-1}\cup\Omega^{j+1})) \\ =(\Sigma^{j-1}\cap\Omega^j)\cup(\Sigma^j\cap\partial\mathcal{O})\cup(\Sigma^{j+1}\cap\Omega^j). \tag{4.59}$$

The new curves $\tilde{\Sigma}^j$ are illustrated in Figure 4.9.
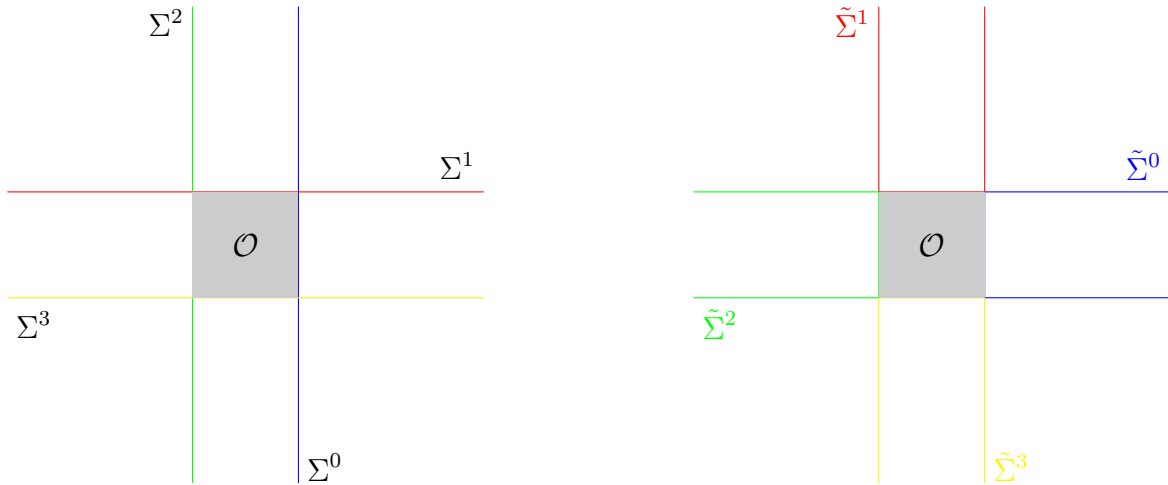

Figure 4.9: Illustration of the different curves: on the left Σ^j, on the right $\tilde{\Sigma}^j$, for $j\in\{0,1,2,3\}$.

To establish the variational formulation for System (4.56), we take the test functions

$$\forall j\in\{0,1,2,3\}, \quad \left|\begin{array}{l} \tilde{\varphi}_t^j\in H_0^{1/2}(\tilde{\Sigma}^j):=\{\phi\in H^{1/2}(\tilde{\Sigma}^j),\phi=0 \text{ on } \Sigma^j\cap\partial\mathcal{O}\}, \\ \tilde{\psi}_t^j\in H^{-1/2}(\tilde{\Sigma}^j). \end{array}\right.$$

We denote $\Phi_t:=(\tilde{\varphi}_t^0,\tilde{\varphi}_t^1,\tilde{\varphi}_t^2,\tilde{\varphi}_t^3,\tilde{\psi}_t^0,\tilde{\psi}_t^1,\tilde{\psi}_t^2,\tilde{\psi}_t^3)$ and

$$\Phi_t\in V_D:=\prod_{j\in\{0,1,2,3\}}H_0^{1/2}(\tilde{\Sigma}^j)\times\prod_{j\in\{0,1,2,3\}}H^{-1/2}(\tilde{\Sigma}^j).$$

By following the same steps, we define the operators that pass functions from $\Sigma^{j-1}\cup\Sigma^j\cup\Sigma^{j+1}$ to $\tilde{\Sigma}^j$

$$E^j:L^2(\Sigma^{j-1})\times L^2(\Sigma^j)\times L^2(\Sigma^{j+1})\to L^2(\tilde{\Sigma}^j),$$

$$\forall j \in \mathbb{Z}/4\mathbb{Z}, \quad E^j(\varphi^{j-1}, \varphi^j, \varphi^{j+1}) = \begin{cases} \varphi^{j-1} & \text{on } \Sigma^{j-1} \cap \Omega^j, \\ \varphi^j & \text{on } \Sigma^j \cap \partial\mathcal{O}, \\ \varphi^{j+1} & \text{on } \Sigma^{j+1} \cap \Omega^j. \end{cases} \tag{4.60}$$

Again, if $(\varphi^{j-1}, \varphi^j, \varphi^{j+1}) \in H_g^{1/2}(\Sigma^{j-1}) \times H_g^{1/2}(\Sigma^j) \times H_g^{1/2}(\Sigma^{j+1})$, then $\tilde{\varphi}^j \in H_g^{1/2}(\tilde{\Sigma}^j) := \left\{ \phi \in H^{1/2}(\tilde{\Sigma}^j), \phi = g \text{ on } \Sigma^j \cap \partial\mathcal{O} \right\}$. With these operators, we deduce the variational formulation

find Φ in V such that for all Φ_t in V_D,

$$\left| \begin{aligned} \forall j \in \mathbb{Z}/4\mathbb{Z}, \quad & \langle E^j(\varphi^{j-1}, \varphi^j, \varphi^{j+1}), \tilde{\psi}_t^j \rangle_{\tilde{\Sigma}^j} = \langle P^j(\varphi^j, \psi^j), \tilde{\psi}_t^j \rangle_{\tilde{\Sigma}^j}, \\ & \langle \tilde{\varphi}_t^j, \psi^{j\pm1} \rangle_{\Sigma^{j\pm1} \cap \Omega^j} = \langle \tilde{\varphi}_t^j, \frac{\partial}{\partial n^{j\pm1}} P^j(\varphi^j, \psi^j) \rangle_{\Sigma^{j\pm1} \cap \Omega^j}. \end{aligned} \right. \tag{4.61}$$

This formulation can also be shown to be equivalent to the original problem (4.55).

The idea is still the same:

1. first we define $\forall j \in \{0, 1, 2, 3\}, P_-^j(\varphi^j, \psi^j)$ in $\Omega_-^j := \mathbb{R}^2 \backslash \Omega^j$ as functions that satisfy the Helmholtz equation in Ω_-^j and satisfy the jump conditions:

$$\begin{aligned} \varphi^j &= P^j - P_-^j \text{ on } \Sigma^j, \\ \psi^j &= \frac{\partial P^j}{\partial n^j} - \frac{\partial P_-^j}{\partial n^j} \text{ on } \Sigma^j; \end{aligned} \tag{4.62}$$

2. then we show that $\forall j \in \{0, 1, 2, 3\}, P_-^j = 0$ on $\Sigma^j \cap \partial\mathcal{O}$;

3. finally we show that $\forall j \in \mathbb{Z}/4\mathbb{Z}, P^j - P^{j+1}$ in $\Omega^j \cap \Omega^{j+1}$ can be continuously extended by using the jump conditions and the variational formulation with the appropriate test functions into the solution of a coercive problem in a Riemann surface $\bigcup_{j=0}^{3} \left(\mathbb{R}^2 \backslash \Omega^j \right)$ (see Figure 4.10) with a Dirichlet homogeneous boundary condition $P_-^j = 0$ on $\Sigma^j \cap \partial\mathcal{O}$;

4. we conclude that $\forall j \in \mathbb{Z}/4\mathbb{Z}, P^j = P^{j+1}$ in $\Omega^j \cap \Omega^{j+1}$. Thus, we can define a function $p := P^j$ in Ω^j unequivocally. Furthermore, since $P_-^j = 0$, we conclude that $p = P^j = P^j - P_-^j = \varphi^j = g$ on $\Sigma^j \cap \partial\mathcal{O}$. It follows that p is the solution of (4.55).

4.5 Numerical validation

Numerically, Formulation (4.61) that will be discretized is written as

find Φ in V such that for all Φ_t in V_D,

$$\forall j \in \mathbb{Z}/4\mathbb{Z}, \quad \left| \begin{aligned} & \int_{\Sigma^{j-1} \cap \Omega^j} \varphi^{j-1} \tilde{\psi}_t^j + \int_{\Sigma^j \cap \partial\mathcal{O}} \varphi^j \tilde{\psi}_t^j + \int_{\Sigma^{j+1} \cap \Omega^j} \varphi^{j+1} \tilde{\psi}_t^j = \int_{\tilde{\Sigma}^j} P^j(\varphi^j, \psi^j) \tilde{\psi}_t^j, \\ & \int_{\Sigma^{j\pm1} \cap \Omega^j} \psi^{j\pm1} \tilde{\varphi}_t^j = \int_{\Sigma^{j\pm1} \cap \Omega^j} \frac{\partial}{\partial n^{j\pm1}} P^j(\varphi^j, \psi^j) \tilde{\varphi}_t^j. \end{aligned} \right. \tag{4.63}$$

The discrete problem is obtained by using the same discretization ingredients:

1. the Fourier integrals on the representation operators are truncated into segments of $[-\hat{T}, \hat{T}]$,
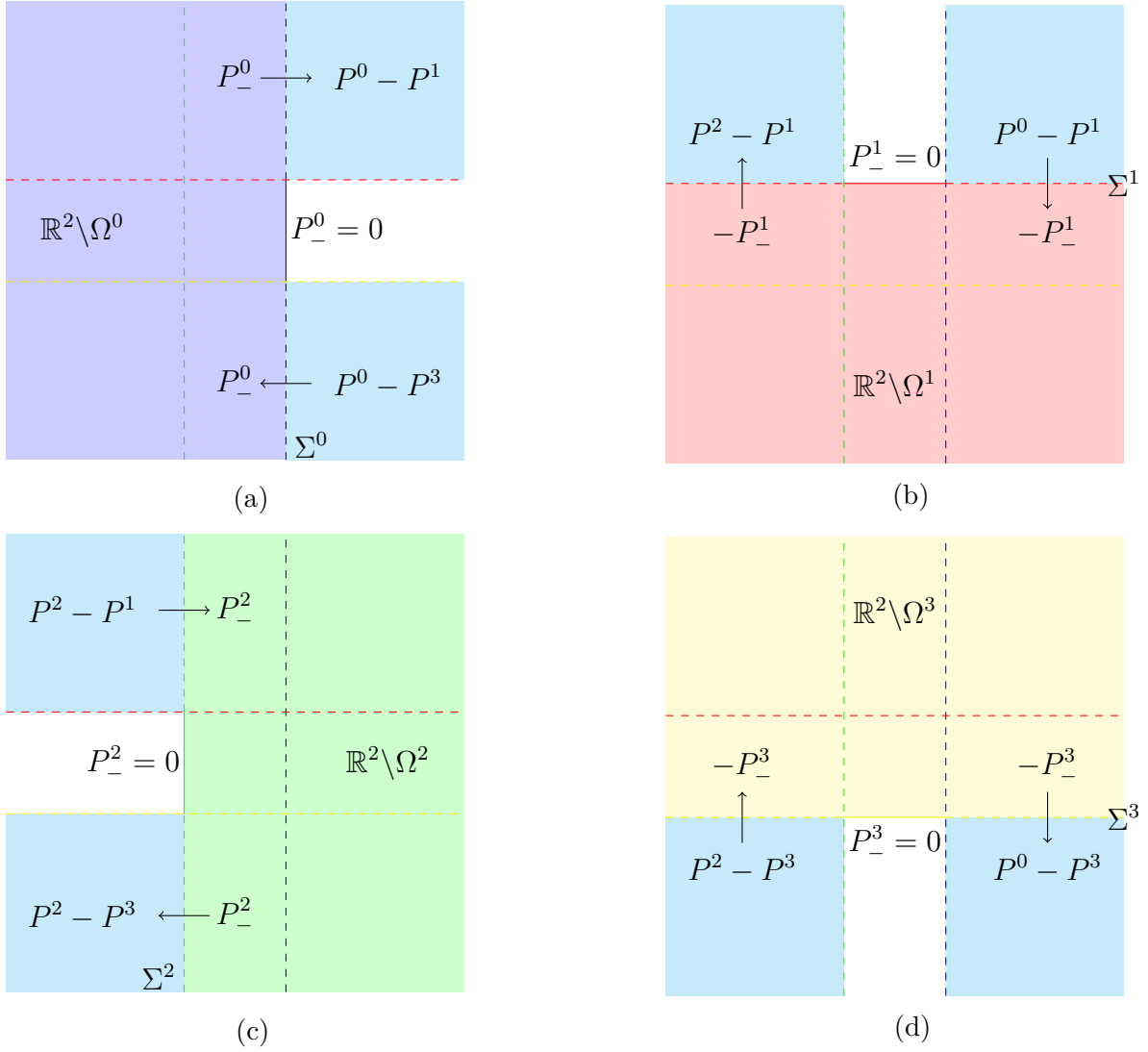
Figure 4.10: The continuous extension from $\Omega^{j-1} \cap \Omega^j$ to $\mathbb{R}^2 \backslash \Omega^j$ to $\Omega^j \cap \Omega^{j+1}$.

2. the lines Σ^j's are truncated into segment Σ_T^j's whose length is $2T$ and we take P1 Lagrange elements for the traces $\varphi_{T,h}^j$'s and P0 elements for the normal traces $\psi_{T,h}^j$'s with h,

3. a quadrature formula is used to compute the Fourier integrals.

We take the fundamental solution as the boundary data

$$g(\mathbf{x}) = \frac{H_0^{(1)}(\omega \sqrt{x_1^2 + x_2^2})}{4\imath}, \quad \mathbf{x} \text{ on } \partial\Omega,$$

where we take $\omega = 1$ and $H_0^{(1)}$ is the Hankel function of the first kind. For the discretization parameters, we take $T = 10$, $h = 0.1$, and $\hat{T} = 10$ and 3rd Gauss quadrature with 1000 intervals.

In Figure 4.11, we show the real part of the trace $\varphi_{T,h}^0$ and compare them to the exact solution φ^0. We obtain a relative L^2 error of 2.25%.

Once the traces $(\varphi_{T,h}^j, \psi_{T,h}^j)$ are obtained, we can reconstruct the solution in all half-spaces Ω^j by Formula (4.8). We obtain a relative L^2 error of 4.07%. Remark again that although the theory is derived for the dissipative case, the numerical simulation also works well for the non-dissipative case.
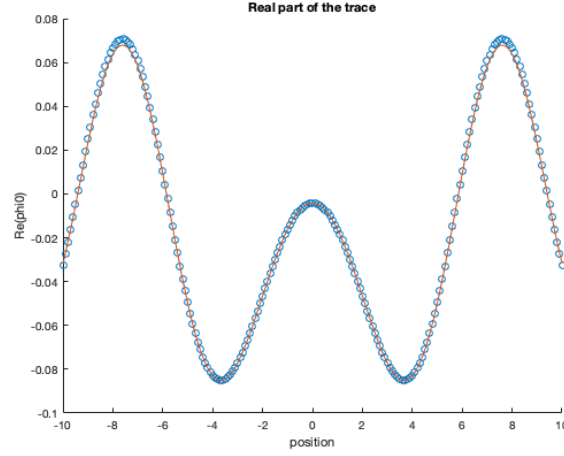
Figure 4.11: Real part of the computed and exact solution of the trace φ^0. The exact solution is given by the red curve while the numerical solution is in blue dots.
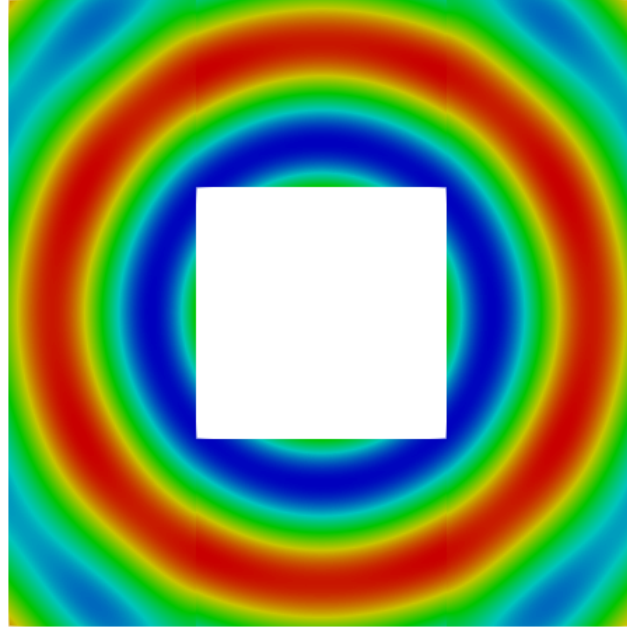

Figure 4.12: Reconstructed solution in the exterior domain obtained from the traces $(\varphi^j_{T,h}, \psi^j_{T,h})$.

4.6 Formulations involving Green's functions

4.6.1 The multi-unknown formulation set on curves instead of lines

Formula (4.8) gives a representation in a half-plane for a couple (φ^j, ψ^j). Another representation can be obtained by using Green's representation theorem [56]. For example, if we consider the same problem (4.55) with 4 half-spaces, we can write the integral representation in Ω^0

$$P^0(\varphi^0, \psi^0)(\mathbf{x}) = \int_{\Sigma^0} -\varphi^0(\mathbf{y})\frac{\partial G}{\partial_{\mathbf{y}}\nu}(\mathbf{x} - \mathbf{y}) + \psi^0(\mathbf{y})G(\mathbf{x} - \mathbf{y})\mathrm{d}\gamma_{\mathbf{y}} \quad \text{in } \Omega^0, \qquad (4.64)$$

where $\mathbf{y} = (y_1, y_2) \in \Sigma^0$, ν is the inward direction of Ω^0, and $G(\mathbf{x} - \mathbf{y}) = G_{\mathbf{x}}(\mathbf{y})$ is the Green's function, satisfying

$$\Delta G_{\mathbf{x}}(\mathbf{y}) + \omega^2 G_{\mathbf{x}}(\mathbf{y}) = \delta_{\mathbf{x}}(\mathbf{y}). \qquad (4.65)$$

Actually, (4.64) is equivalent to the Fourier representation by using Plancherel's formula. Indeed, taking the Fourier transform of (4.65) in y_2, we obtain an ordinary differential equation in y_1 parametrized by the Fourier variable ξ. The L^2 solution of this equation is given by

$$\hat{G}_{\mathbf{x}}(y_1, \xi) = \frac{1}{2\sqrt{2\pi}\imath\sqrt{\omega^2 - \xi^2}} e^{\imath\sqrt{\omega^2 - \xi^2}|y_1 - x_1|} e^{-\imath\xi x_2},$$

and the derivative

$$\frac{\partial\hat{G}_{\mathbf{x}}}{\partial y_1}(y_1, \xi) = \frac{\mathrm{sgn}(y_1 - x_1)}{2\sqrt{2\pi}} e^{\imath\sqrt{\omega^2 - \xi^2}|y_1 - x_1|} e^{-\imath\xi x_2}.$$

On the other hand, if we apply the Plancherel's formula to (4.64), we obtain

$$P^0(\varphi^0, \psi^0)(\mathbf{x}) = \int_{\mathbb{R}} -\hat{\varphi}^0(\xi)\frac{\partial\hat{G}_{\mathbf{x}}}{\partial y_2}(0, -\xi) + \hat{\psi}^0(\xi)G_{\mathbf{x}}(0, -\xi)\mathrm{d}\xi. \qquad (4.66)$$

Plugging $\hat{G}_{\mathbf{x}}$ and $\dfrac{\partial\hat{G}_{\mathbf{x}}}{\partial y_1}$ into (4.66), we have a half-space representation P^0 in terms of the couples $(\hat{\varphi}^0, \hat{\psi}^0)$

$$P^0(\varphi^0, \psi^0)(\mathbf{x}) = \frac{1}{2\sqrt{2\pi}} \int_{\mathbb{R}} \left(\hat{\varphi}^0(\xi) + \frac{\hat{\psi}^0(\xi)}{\imath\sqrt{\omega^2 - \xi^2}} \right) e^{\imath\sqrt{\omega^2 - \xi^2}x_1} e^{\imath\xi x_2}\mathrm{d}\xi \text{ in } \Omega^0,$$

which is exactly Formula (4.8). Thus, we can consider Formula (4.8) as the Fourier equivalent of the integral representation with the Green's function. An important remark is that Formula (4.64) is valid not only in half-spaces, but in any domain whose boundary is not necessarily a straight line.

Let us consider for instance a scattering problem with the same localized obstacle as in the previous section, and let us introduce two subdomains defined by

$$\Omega^1 := \{(x_1, x_2), x_1 \in \mathbb{R}, x_2 > a\} \cup \{(x_1, x_2), x_1 < -a, x_2 \in \mathbb{R}\}$$
$$\Omega^2 := \{(x_1, x_2), x_1 \in \mathbb{R}, x_2 > a\} \cup \{(x_1, x_2), x_1 < -a, x_2 \in \mathbb{R}\}.$$

Their boundaries are then given by (see Figure 4.13 for illustrations)

$$\Sigma^1 := \{(-a, x_2), x_2 \in (-\infty, a]\} \cup \{(x_1, a), x_1 \in [-a, +\infty)\},$$
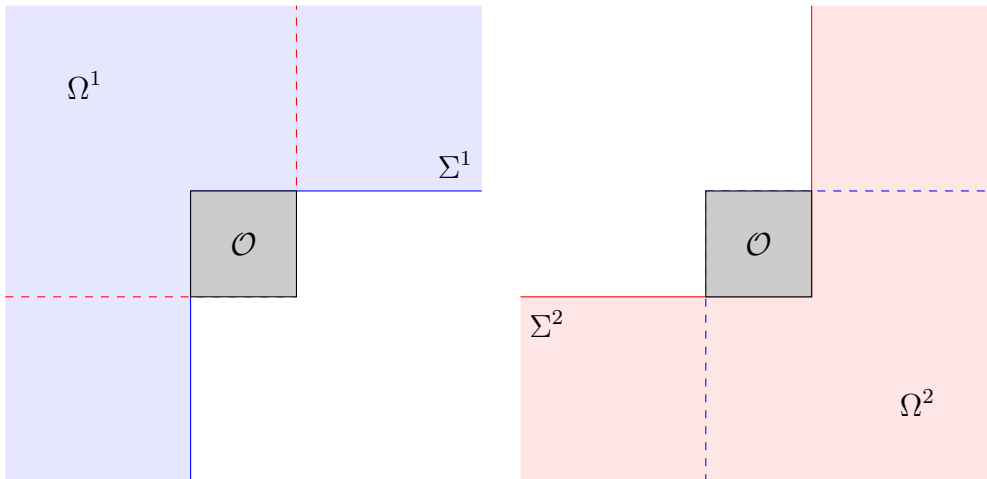

Figure 4.13: Notations of the curves and the subdomains.

$$\Sigma^2 := \{(x_1, -a), x_1 \in (-\infty, a]\} \cup \{(a, x_2), x_2 \in [-a, +\infty)\}.$$

Thanks to the overlap of the subdomains, we obtain similar systems of equations (4.16 - 4.17), where $P^j(\varphi^j, \psi^j)$ is given by (4.64). In Figure 4.14(a) we show the trace φ^0 on Σ^0 and 4.14(b) the reconstucted solution in Ω.
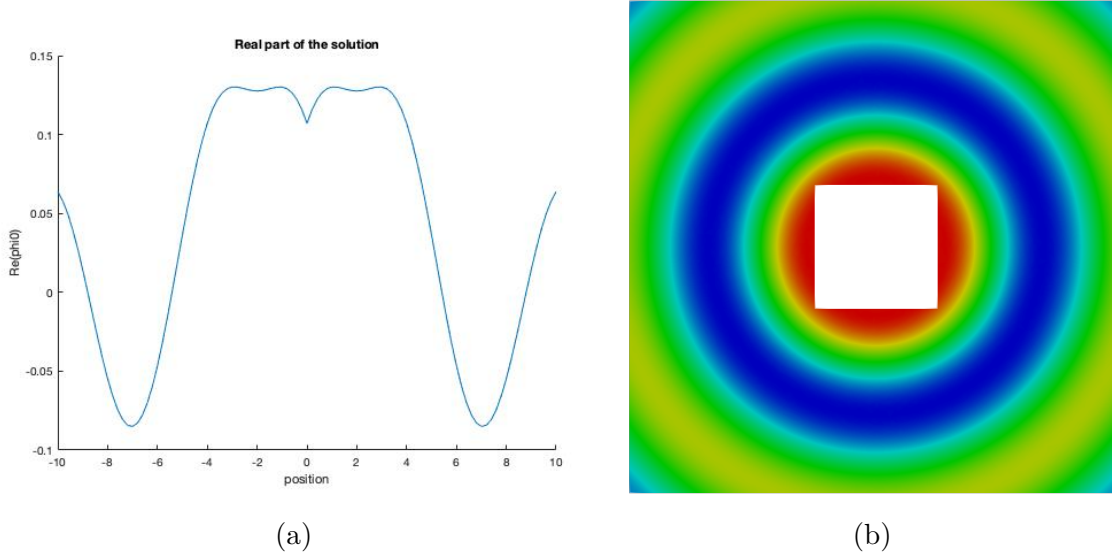

| (a) | (b) |

Figure 4.14: (a) The real part of φ^0 and (b) real part of the solution in Ω by using (4.64).
.

4.6.2   Configurations where a global Green's function is not available

The junction of stratified media

The integral representation in each subdomain requires the knowledge of the Green's function, but it is not necessarily the same Green's function in all subdomains. This is useful for some cases where the global Green's function of the domain is not available. To explain this argument more clearly, we consider a scattering problem in two configurations: an imperfect stratified medium and a junction of stratified media (see Figure 4.15) with a localized obstacle and compactly supported source term

$$\left| \begin{array}{l} -\Delta p - \omega^2 k(\mathbf{x})p = f \text{ in } \Omega := \mathbb{R}^2 \backslash \mathcal{O} \\ p = g \text{ on } \partial\mathcal{O}, \end{array} \right. \tag{4.67}$$

where $k(\mathbf{x})$ is constant in each stratification:

$$k(x_1, x_2) = \begin{cases} k_1 & \text{in } \Omega^+ \\ k_2 & \text{in } \Omega^* \\ k_3 & \text{in } \Omega^-. \end{cases} \tag{4.68}$$

In the case of a perfectly stratified medium, we can take a Fourier transform in the horizontal direction and solve the equation satisfied by the Fourier transform of the global Green's function. Thus, to solve (4.67), we can couple a Finite Element representation that englobes the perturbations (imperfection of the stratification, the obstacle, and the support of the source term) and use an integral formula on an artificial boundary Σ (see Figure 4.16).
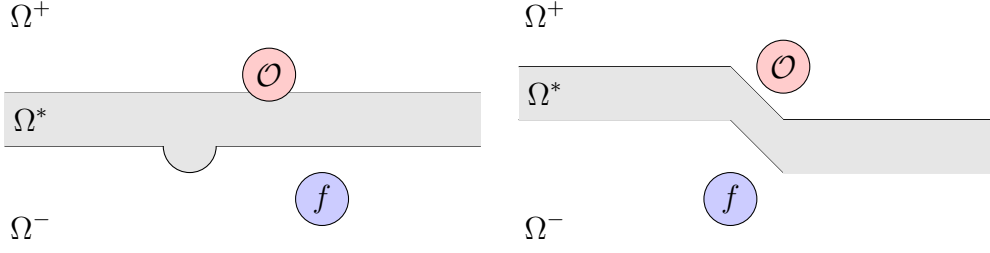
Figure 4.15: Examples of stratified media: (a) a stratified medium with an imperfection and (b) a stratified medium with a junction.
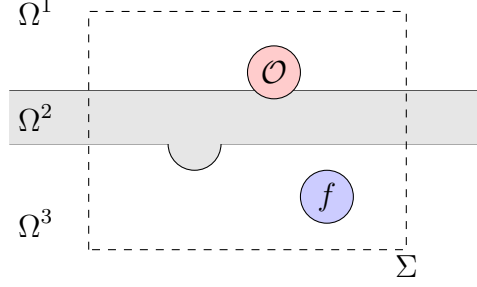

Figure 4.16: An example of coupling between Finite Element representation in the domain bounded by Σ and the integral representation on Σ.

On the other hand, we cannot apply the same method to solve the scattering problem in the configuration given in Figure 4.15 (b), because we can no longer obtain the global Green's function easily by taking a Fourier transform in the horizontal direction. However, we can find subdomains for which the Green's function is available. More precisely, we take $\Omega^j, j \in \{1, 2\}$ and a bounded domain Ω^b such that

1. the medium is perfectly stratified in each Ω^j, meaning that the coefficient k only depends on x_2 and not x_1

$$\forall j \in \{1, 2\}, \quad \exists k^j(x_2) \text{ such that } -\Delta p - \omega^2 k^j(x_2)p = 0 \quad \text{in } \Omega^j,$$

2. the subdomains are overlapping and cover the whole domain

$$\Omega^1 \cap \Omega^2 \neq \emptyset,$$
$$\forall j \in \{1, 2\}, \quad \Omega^b \cap \Omega^j \neq \emptyset,$$
$$\Omega^b \cup \Omega^1 \cup \Omega^2 = \mathbb{R}^2 \backslash \mathcal{O}.$$

In addition to that, we also define

$$\Omega^a := \mathbb{R}^2 \backslash (\Omega^1 \cup \Omega^2).$$

Figure 4.17 illustrates the stratified medium completed with an example of subdomains Ω^b and Ω^j and the curves Σ^j, as well as the bounded domain Ω^b. In this example, Ω^b is a rectangle covering the obstacle and the support of the source term. The boundary of this rectangle is split into two non-overlapping parts:

$$\partial\Omega^b = \Sigma_b^1 \cup \Sigma_b^2 \cup \partial\mathcal{O},$$
$$\forall j \in \{1, 2\}, \quad \Sigma_b^j \in \Omega^j,$$

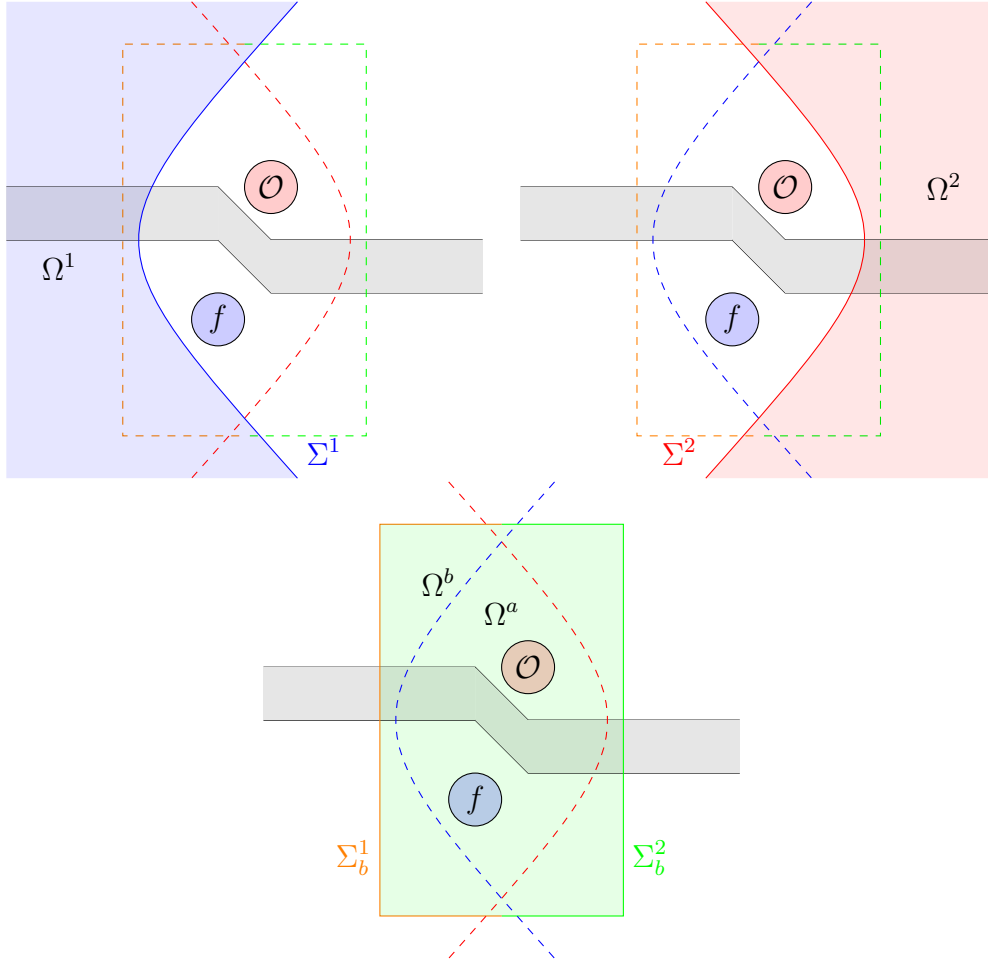Figure 4.17: An example of the subdomains Ω^a, Ω^b, and Ω^j and the curves Σ^j of a junction of stratified media.

$$\Sigma_b^1 \cap \Sigma_b^2 = \emptyset.$$

Since the medium is perfectly stratified in each subdomain Ω^j, we can compute the Green's function G^j in each subdomain as explained previously. Using the overlap of the subdomains, we derive the HSM formulation which is exactly the same as the one derived for the model problem. Around the defect, we take a FE representation

$$p^b := p \text{ in } \Omega^b.$$

The coupling of the FE representation and the representations in $\Omega^j, j \in \{1, 2\}$ is obtained in a similar manner as in Chapter 0. We denote

$$\Phi^b := (p^b, \varphi^1, \varphi^2, \psi^1, \psi^2),$$

and $\Phi^b \in V^b$, where

$$
\begin{aligned}
V^b := \Big\{ &(p^b, \varphi^1, \varphi^2, \psi^1, \psi^2), p^b \in H^1(\Omega^b), \forall j \in \{1, 2\} \varphi^j \in H^{1/2}(\Sigma^j), \psi^j \in H^{-1/2}(\Sigma^j), \\
&p^b = \varphi^j \text{ on } \Sigma^j \cap \Omega^a, p^b = g \text{ on } \partial\mathcal{O} \Big\}.
\end{aligned}
\tag{4.69}
$$

To couple the FE representation around the obstacle with the multi-unknown HSM formulation (for example taking the one with the compatibility on the trace (4.14)), we take the test

functions $\Phi_t^b := (q, \varphi_t^1, \varphi_t^2, \tilde{\psi}_t^1, \tilde{\psi}_t^2)$ and $\Phi_t^b \in V_D^b$ where

$$V_D^b := \{(q, \varphi_t^1, \varphi_t^2, \tilde{\psi}_t^1, \tilde{\psi}_t^2), q \in H^1(\Omega^b), \forall j \in \{1, 2\} \varphi_t^j \in H_0^{1/2}(\Sigma_+^j), \tilde{\psi}_t^j \in H^{-1/2}(\tilde{\Sigma}^j), \tag{4.70}$$
$$q = g \text{ on } \partial\mathcal{O}\}.$$

By extending the formulation of Section 4.3.1, we obtain

find Φ_b in V_b such that for all Φ_t^b in V_D^b,

$$\left|
\begin{aligned}
&\int_{\Omega^b} \nabla p^b \cdot \overline{\nabla q} - \omega^2 k p^b \overline{q} = \sum_{j=1}^{2} \int_{\Sigma_b^j} \frac{\partial}{\partial n_b} P^j(\varphi^j, \psi^j) q + \int_{\Omega^b} f \overline{q} \\
&\langle E^1(\varphi^1, \varphi^2), \tilde{\psi}_t^1 \rangle_{\tilde{\Sigma}^1} = \langle P^1(\varphi^1, \psi^1), \tilde{\psi}_t^1 \rangle_{\tilde{\Sigma}^1}, \\
&\quad\quad \langle \tilde{\varphi}_t^1, \psi^2 \rangle_{\Sigma^2 \cap \Omega^1} = \langle \tilde{\varphi}_t^1, \frac{\partial}{\partial n^2} P^1(\varphi^1, \psi^1) \rangle_{\Sigma^2 \cap \Omega^1}, \\
&\langle E^2(\varphi^1, \varphi^2), \tilde{\psi}_t^2 \rangle_{\tilde{\Sigma}^2} = \langle P^2(\varphi^2, \psi^2), \tilde{\psi}_t^2 \rangle_{\tilde{\Sigma}^2}, \\
&\quad\quad \langle \tilde{\varphi}_t^2, \psi^1 \rangle_{\Sigma^1 \cap \Omega^2} = \langle \tilde{\varphi}_t^2, \frac{\partial}{\partial n^1} P^2(\varphi^2, \psi^2) \rangle_{\Sigma^1 \cap \Omega^2},
\end{aligned}
\right. \tag{4.71}$$

where n^j is the inward direction of Ω^j, $j \in \{1, 2\}$ and n_b is the outward direction of Ω^b.

Scattering problem in a "half-plane" with a stair-like boundary

We have not had yet numerical results corresponding to the configuration given in Figure 4.17, but instead we consider another problem which can be solved by using the same formulation. This is the scattering problem in a lower "half-plane" with a boundary in the form of a "stair" denoted as Σ (see Figure 4.18).
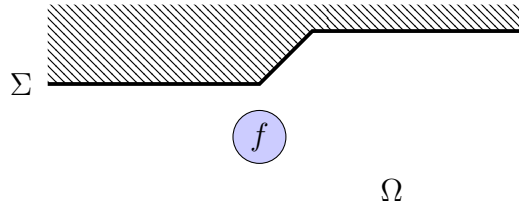

Figure 4.18: A "half-plane" with a stair-like boundary.

More precisely, the boundary can be decomposed into three parts

$$\Sigma := \Sigma^- \cup \Sigma^* \cup \Sigma^+,$$

where

$$\Sigma^- := \{(x, h_1), x < 0\},$$
$$\Sigma^+ := \{(x, h_2), x > 1\},$$

and Σ^* is a segment connecting Σ^- and Σ^+. The subdomains Ω^1 and Ω^2 are taken as such given in Figure 4.20.

We consider the scattering problem with a compactly supported source term

$$\left|
\begin{aligned}
-\Delta p - \omega^2 p &= f \quad \text{in } \Omega \\
p &= 0 \quad \text{on } \Sigma.
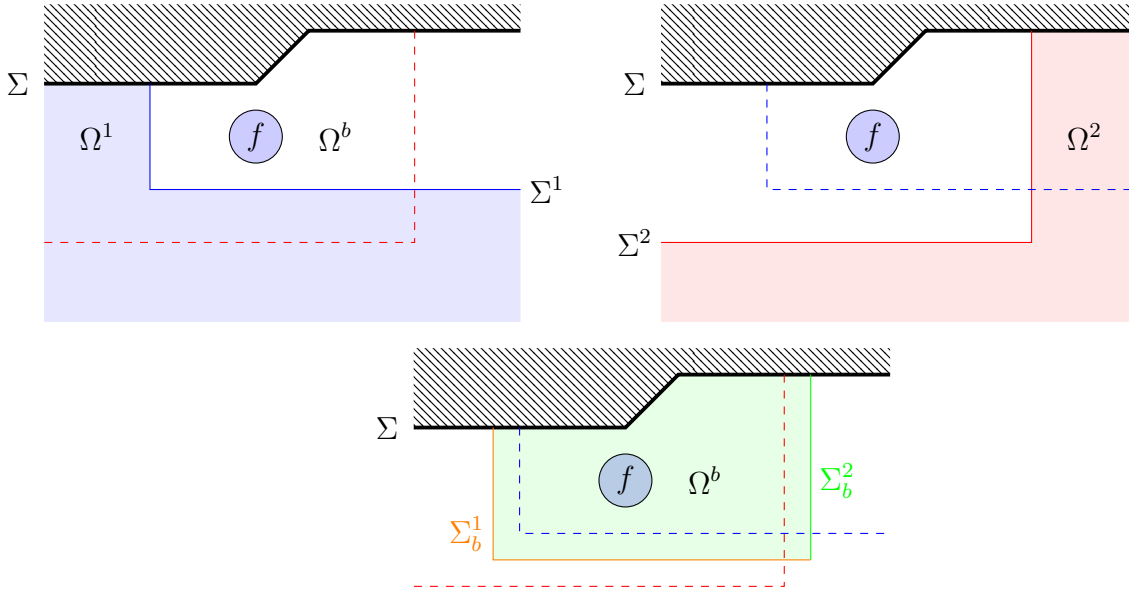\end{aligned}
\right. \tag{4.72}$$

Figure 4.20: An example of subdomains for multi-unknown HSM formulation.

Remark that the Green's function of this domain is not easy to compute due to the "stair". However, if the domain is decomposed into 3 subdomains: Ω^b, Ω^1, and Ω^2 (see Figure 4.23 as an example of the subdomains), in each subdomain Ω^j, the Green's function G^j can be computed. Indeed, by using the image principle, we obtain

$$G^1(\mathbf{x}, (y_1, y_2)) = \tilde{G}(\mathbf{x}, (y_1, y_2)) - \tilde{G}(\mathbf{x}, (y_1, 2h_1 - y_2)), \tag{4.73}$$

where $\tilde{G}$ is the Green's function of the free space

$$\tilde{G}(\mathbf{x}, \mathbf{y}) = \frac{H(\omega R)}{4\imath},$$

and $(y_1, 2h_1 - y_2)$ is the reflection of the point (y_1, y_2) by the boundary Σ^-. Similarly, we obtain

$$G^2(\mathbf{x}, (y_1, y_2)) = \tilde{G}(\mathbf{x}, (y_1, y_2)) - \tilde{G}(\mathbf{x}, (y_1, 2h_2 - y_2)), \tag{4.74}$$

where this time $(y_1, 2h_2 - y_2)$ is the reflection of the point (y_1, y_2) by the boundary Σ^+. Having these Green's functions, we then have the representations in Ω^1 and Ω^2. By taking a FE representation in Ω^b, we can then couple the representations and apply Formulation (4.71) to compute the solution of (4.72). In Figure 4.21, we show the real part of the solution with $f = 1$ in a unit disk.

Finally, we can also consider a scattering of a plane wave by this stair-like boundary. We consider now the same domain but with a localized obstacle. We take a plane wave coming from the bottom right part of the domain. Compared to the scattering problem in the whole plane as discussed in Chapter 2, the plane wave is not only scattered by the obstacle but also reflected by the boundary of the domain. We define p_{ref} the reflected wave by Σ, which is the solution of

$$\left|\begin{array}{ll} -\Delta p_{ref} - \omega^2 p_{ref} = 0 & \text{in } \tilde{\Omega} \\ p_{ref} = -p_{plane} & \text{on } \Sigma, \end{array}\right. \tag{4.75}$$

where $\tilde{\Omega}$ is the domain without obstacle. Subsequently, we define the incident field as the superposition of the plane wave and the reflected wave
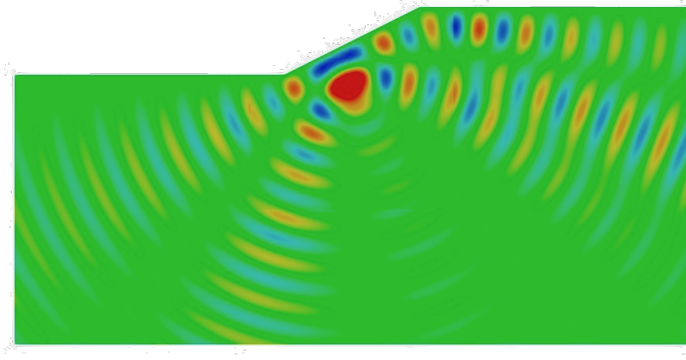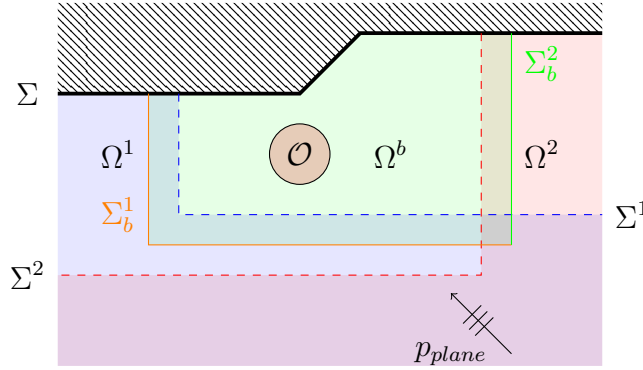
$$p_{inc} = p_{plane} + p_{ref}.$$

Figure 4.21: Real part of the solution of (4.72) in Ω.

Figure 4.22: An example of subdomains for multi-unknown HSM formulation.

The scattered field p satisfies

$$\left|\begin{array}{ll} -\Delta p - \omega^2 p = 0 & \text{in } \Omega \\ p = -p_{inc} & \text{on } \Sigma \cup \partial\mathcal{O}. \end{array}\right. \tag{4.76}$$

Remark that in this problem, we have a priori a right hand term in the infinite boundary Σ and we do not know how to take into account this boundary condition. To simplify the problem, we consider the boundary Σ with particular values of h_1 and h_2 such that p_{inc} satisfies a homogeneous boundary condition

$$p_{inc} = 0 \text{ on } \Sigma^- \cup \Sigma^2.$$

By having a homogeneous boundary condition on $\Sigma^- \cup \Sigma^+$, we can then use again Formulation (4.71).
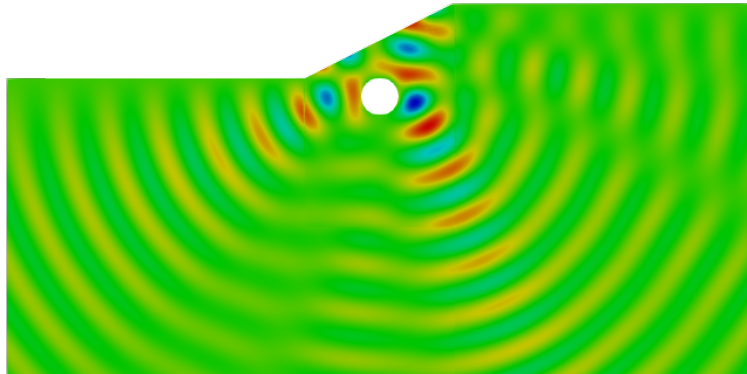
Figure 4.23: Real part of the scattered field in Ω.

In Figure 4.23 we represent the real part of the scattered field. We use again here a real frequency $\omega = 1$. Although we do not have the exact solution of this problem, we can say that the method works well because the different representations match in the overlapping zones.

Chapter 5

Complex-scaled HSM method for the non-dissipative case

Summary

In Chapter 2, we have presented numerical experiments which show that the HSM method works in the non-dissipative case even though there is no theoretical result to justify it. In this chapter, we develop a slightly different HSM formulation designed for the non-dissipative case. The main idea is to choose as unknowns, instead of the traces of the solution, their analytic extensions (for complex spatial variable) in the spirit of PML. The main advantage is that while the traces decay at infinity as $\dfrac{1}{\sqrt{r}}$ which is not in L^2, their analytic extensions decay exponentially. As a consequence, the analysis of the new complex-scaled HSM formulation can be done in the L^2 framework in a similar manner to what has been done in the dissipative case.

5.1 Introduction

We reconsider the Helmholtz problem in a 2D plane. To focus on the novelty, we consider only the exterior problem to a square $\mathcal{O} := [-a, a]^2, a > 0$:

$$\left|\begin{array}{rl} -\Delta p(\mathbf{x}) - \omega^2 p(\mathbf{x}) = 0, & \mathbf{x} \text{ in } \Omega := \mathbb{R}^2 \backslash \mathcal{O}, \\ p(\mathbf{x}) = g(\mathbf{x}), & \mathbf{x} \text{ on } \partial\mathcal{O}, \\ \lim_{r \to +\infty} \sqrt{r}\left(\frac{\partial}{\partial r} - \imath\omega\right) p\left(r\frac{\mathbf{x}}{\|\mathbf{x}\|}\right) = 0, \end{array}\right. \qquad (5.1)$$

where $r = \|\mathbf{x}\|$, $g \in H^{1/2}(\partial\Omega)$ is given and $\omega \in \mathbb{R}^+$. Again, we define φ^j as the trace of p on Σ^j:

$$\varphi^j := p|_{\Sigma^j}, \quad \forall j \in \{0, 1, 2, 3\}. \tag{5.2}$$

Proceeding as in Chapter 1 and by using the representation which was already given in Chapter 2 (Formula (2.7))

$$\forall j \in \{0, 1, 2, 3\} \quad P^j(\psi)(x^j, y^j) = \frac{1}{\sqrt{2\pi}} \int_{\mathbb{R}} \hat{\psi}(\xi) e^{i\sqrt{\omega^2 - \xi^2}(x^j - a)} e^{i\xi y^j} \mathrm{d}\xi \text{ in } \Omega_a^j, \tag{5.3}$$

where we take the convention

$$\begin{aligned} \forall z \notin \mathbb{R}^+, \quad &\mathrm{Im}\sqrt{z} > 0, \\ \forall z \in \mathbb{R}^+, \quad &\mathrm{Re}\sqrt{z} \geq 0, \end{aligned} \tag{5.4}$$

we can derive the HSM formulation for this problem

$$(\mathbb{I} - \mathbb{D})\,\Phi = G, \tag{5.5}$$

where $\Phi := (\varphi^0, \varphi^1, \varphi^2, \varphi^3)$, $\mathbb{I}$ corresponds to the identity operator, $\mathbb{D}$ is given by

$$\mathbb{D} := \begin{bmatrix} 0 & D^{1,0} & 0 & D^{3,0} \\ D^{0,1} & 0 & D^{2,1} & 0 \\ 0 & D^{1,2} & 0 & D^{3,2} \\ D^{0,3} & 0 & D^{2,3} & 0 \end{bmatrix}, \tag{5.6}$$

and G is given by

$$G := (g^0, g^1, g^2, g^3) \quad \text{where } g^j = \begin{cases} g & \text{on } \Sigma_{\mathcal{O}}^j, \\ 0 & \text{on } \Sigma^j \backslash \Sigma_{\mathcal{O}}^j. \end{cases} \tag{5.7}$$

Due to the convention of the square root given in (5.4), the branch cut of $\xi \mapsto \sqrt{\omega^2 - \xi^2}$ is given in Figure 5.1.
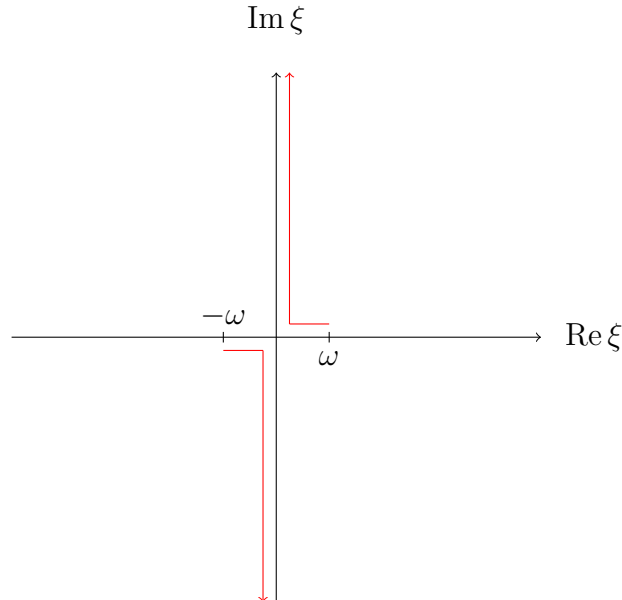

Figure 5.1: The branch cut of $\xi \mapsto \sqrt{\omega^2 - \xi^2}$ given by the red lines.

It will be useful in the sequel to introduce the decomposition of the lines

$$\forall j \in \{0, 1, 2, 3\}, \quad \begin{aligned} \Sigma_\pm^j &:= \{(x^j = a, y^j), \pm y^j > a\}, \\ \Sigma_{\mathcal{O}}^j &:= \{(x^j = a, y^j), -a < y^j < a\}, \end{aligned}$$

and the decomposition of the trace φ^j into 3 parts

$$\forall j \in \{0, 1, 2, 3\}, \quad \varphi^j = \varphi^j_+ + \varphi^j_- + g^j, \tag{5.8}$$

where

$$\forall j \in \{0, 1, 2, 3\}, \quad \varphi^j_\pm = \begin{cases} \varphi^j & \text{on } \Sigma^j_\pm, \\ 0 & \text{on } \Sigma^j \backslash \Sigma^j_\pm. \end{cases}$$
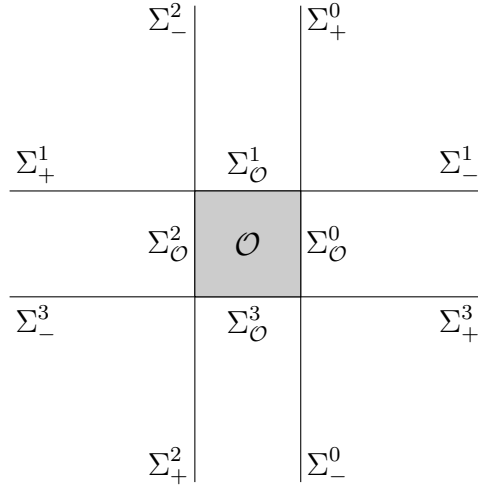

Figure 5.2: The geometry considered and the associated notations.

The difficulty comes from the fact that the φ^j's do not belong to $L^2(\Sigma^j)$ (and therefore neither do the $\hat{\varphi}^j$'s). To overcome this difficulty, we will use the analyticity properties satisfied by the φ^j

1. The function

$$\left| \begin{array}{c} y^j \mapsto \varphi^j_+(y^j) \\ [a, +\infty) \to \mathbb{C}, \end{array} \right.$$

has an analytic extension to $\operatorname{Re} y^j > a$. Moreover,

$$\exists C > 0 \text{ such that } \forall s > 0, \forall \gamma \in [0, \frac{\pi}{2}), \quad \left| \varphi^j_+(a + se^{\imath\gamma}) \right| \leq C \frac{e^{-\omega s \sin \gamma}}{\sqrt{s}}. \tag{5.9}$$

2. The function

$$\left| \begin{array}{c} y^j \mapsto \varphi^j_-(y^j) \\ (-\infty, -a] \to \mathbb{C}, \end{array} \right.$$

has an analytic extension to $\operatorname{Re} y^j < a$. Moreover,

$$\exists C > 0 \text{ such that } \forall s > 0, \forall \gamma \in [0, \frac{\pi}{2}), \quad \left| \varphi^j_-(-a - se^{\imath\gamma}) \right| \leq C \frac{e^{-\omega s \sin \gamma}}{\sqrt{s}}. \tag{5.10}$$

These properties hold because the φ^j's are the traces of the solution p of (5.1) which is outgoing. For simplicity here, we suppose that the data g is such that $\varphi^j \in H^1_{loc}(\Sigma^j)$. In particular, the φ^j's are continuous functions.

Remark 5.1.1. *This allows to avoid possible singularities at the corners of the square which are not relevant for our purpose. Note also that in the general formulation where the integral equations are coupled to an interior variational formulation, the square is not a physical boundary and the φ^j's are in $C^\infty(\Sigma^j)$.*

Our objective is to derive a new HSM formulation depending on an angular parameter θ that will be chosen in $\left(0, \dfrac{\pi}{2}\right)$. In this formulation, the unknowns $\varphi_\pm^j$ will be replaced by $\varphi_\pm^{j,\theta}$ defined as

$$
\left|
\begin{array}{l}
s \in \mathbb{R}^+ \mapsto \varphi_\pm^{j,\theta}(s) \\
\varphi_\pm^{j,\theta}(s) = \varphi_\pm^j(\pm(a + se^{\imath\theta})).
\end{array}
\right.
\tag{5.11}
$$

Note in particular that due to the properties mentioned above, we have

$$
\forall j \in \{0, 1, 2, 3\}, \quad \varphi_\pm^{j,\theta}(s) \le C\frac{e^{-\omega s \sin\theta}}{\sqrt{s}}.
\tag{5.12}
$$

To derive the HSM formulation with $\varphi_\pm^{j,\theta}$'s instead of $\varphi_\pm^j$'s, we would like to derive a new half-space representation like (5.3) but involving $\varphi_\pm^{j,\theta}$'s instead of $\varphi_\pm^j$'s.

Let us first establish the links of the Fourier transforms of $\varphi_\pm^{j,\theta}$ and $\varphi_\pm^j$.

5.2 Some properties of the Fourier transforms of the traces

Let us focus on φ_+^0. By definition of the Fourier transform, we have

$$
\hat{\varphi}_+^0(\xi) = \frac{1}{\sqrt{2\pi}} \int_a^{+\infty} \varphi_+^0(y) e^{-\imath\xi y} \mathrm{d}y.
\tag{5.13}
$$

Since the integral is only on positive y, it is clear that $\hat{\varphi}_+^0$ is an analytic function in $\mathrm{Im}\,\xi < 0$. On the other hand,

$$
\hat{\varphi}_+^{0,\theta}(\xi) = \frac{1}{\sqrt{2\pi}} \int_0^{+\infty} \varphi_+^{0,\theta}(s) e^{-\imath\xi s} \mathrm{d}s.
\tag{5.14}
$$

By using (5.12), $\hat{\varphi}_+^{0,\theta}$ is analytic not only in $\mathrm{Im}\,\xi < 0$ but even in the larger domain $\mathrm{Im}\,\xi < \omega\sin\theta$.

Lemma 5.2.1. *The functions $\xi \mapsto \hat{\varphi}_+^0(\xi)$ and $\xi \mapsto \hat{\varphi}_+^{0,\theta}(\xi e^{\imath\theta})$ are analytic in $\mathbb{C}^-$ and $\mathbb{C}_{\omega,\theta}^-$ respectively where (see Figure 5.3)*

$$
\mathbb{C}^- := \{\xi \in \mathbb{C} \mid \mathrm{Im}\,\xi < 0\},
$$
$$
\mathbb{C}_{\omega,\theta}^- := \{\xi \in \mathbb{C} \mid \mathrm{Im}\,\xi < (\omega - \mathrm{Re}\,\xi)\tan\theta\}.
$$

Moreover, for all $\xi \in \mathbb{C}^- \cap \mathbb{C}_{\omega,\theta}^-$, we have

$$
\hat{\varphi}_+^0(\xi) = e^{-\imath a\xi} e^{\imath\theta} \hat{\varphi}_+^{0,\theta}(\xi e^{\imath\theta}),
\tag{5.15}
$$

and hence $\hat{\varphi}_+^0$ has an analytic extension in $\mathbb{C}^- \cup \mathbb{C}_{\omega,\theta}^-$.

Proof. To show this equality, we use the residue theorem. We consider a contour

$$
\mathcal{C}_R := \Sigma_R^0 \cup \Gamma_R \cup \Sigma_{R,\theta}^0,
$$

where $\Sigma_R^0 := [a, R]$, $\Gamma_R := \{a + (R-a)e^{\imath\gamma}, \gamma \in [0, \theta]\}$, and $\Sigma_{R,\theta}^0 := [a, R]e^{\imath\theta}$, and with orientation indicated in Figure 5.4.

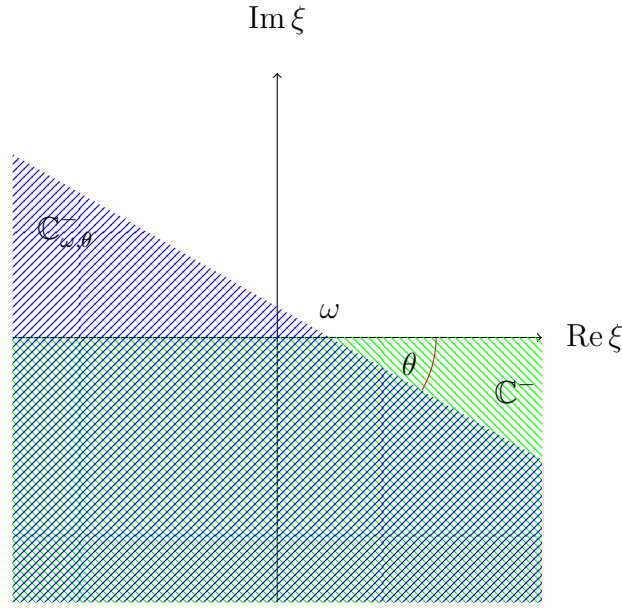Figure 5.3: φ_+^0 is analytic in $\mathbb{C}^-$ (in green) and $\varphi_+^{0,\theta}$ is analytic in $\mathbb{C}_{\omega,\theta}^-$ (in blue).
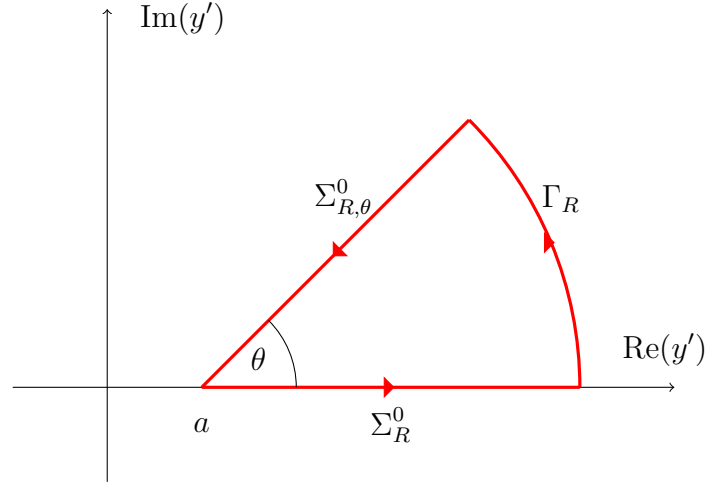
Figure 5.4: Scheme of the contour $\mathcal{C}_R$ on the complex plane.

By the analyticity properties of φ_+^0, the function $z \mapsto \varphi_+^0(z)e^{-\imath\xi z}$ is analytic for $\operatorname{Re} z > a$. From the residue theorem, we obtain that

$$\int_{\mathcal{C}_R} \varphi_+^0(z)e^{-\imath\xi z}\mathrm{d}z = 0.$$

We then have

$$\int_{\Sigma_R^0} \varphi_+^0(z)e^{-\imath\xi z}\mathrm{d}z + \int_{\Sigma_{R,\theta}^0} \varphi_+^0(z)e^{-\imath\xi z}\mathrm{d}z = -\int_{\Gamma_R} \varphi_+^0(z)e^{-\imath\xi z}\mathrm{d}z.$$

The identity (5.15) is obtained by taking the limit for $R \to +\infty$. Indeed, for $\xi \in \mathbb{C}^-$

$$\lim_{R\to+\infty} \int_{\Sigma_R^0} \varphi_+^0(z)e^{-\imath\xi z}\mathrm{d}z = \sqrt{2\pi}\, \hat{\varphi}_+^0(\xi),$$

and for $\xi \in \mathbb{C}_{\omega,\theta}^-$

$$\lim_{R\to+\infty} \int_{\Sigma_{R,\theta}^0} \varphi_+^0(z)e^{-\imath\xi z}\mathrm{d}z = \lim_{R\to+\infty} \int_0^R \varphi^0(a+se^{\imath\theta})e^{-\imath\xi(a+se^{\imath\theta})}e^{\imath\theta}\mathrm{d}s = \sqrt{2\pi}e^{-\imath a\xi}e^{\imath\theta}\hat{\varphi}_+^{0,\theta}(\xi e^{\imath\theta}).$$

It remains to prove that

$$\lim_{R \to +\infty} \int_{\Gamma_R} \varphi_+^0(z)e^{-\imath \xi z}\mathrm{d}z = 0.$$

Indeed,

$$\left| \int_{\Gamma_R} \varphi_+^0(z)e^{-\imath \xi z}\mathrm{d}z \right| = \left| \int_0^\theta \varphi_+^0(a + (R-a)e^{\imath \gamma})e^{-\imath \xi(a+(R-a)e^{\imath \gamma})}\imath(R-a)e^{\imath \gamma}\mathrm{d}\gamma \right|$$

$$\leq C\sqrt{R-a}\, e^{a\,\mathrm{Im}\,\xi} \int_0^\theta e^{(R-a)(\cos \gamma\, \mathrm{Im}\,\xi - (\omega - \mathrm{Re}\,\xi)\sin \gamma)}\mathrm{d}\gamma.$$

The result follows since $\cos \gamma\, \mathrm{Im}\,\xi - (\omega - \mathrm{Re}\,\xi)\sin \gamma < 0$ for $\xi \in \mathbb{C}^- \cap \mathbb{C}_{\omega,\theta}^-$ and $\gamma \in (0,\theta)$.

$\square$

More generally, we can obtain similar results for all functions $\varphi_\pm^j$.

Lemma 5.2.2. *For $j \in \{0,1,2,3\}$, the functions $\xi \mapsto \hat{\varphi}_\pm^j(\pm\xi)$ and $\xi \mapsto \hat{\varphi}_\pm^{j,\theta}(\pm\xi e^{\imath\theta})$ are analytic in $\mathbb{C}^-$ and $\mathbb{C}_{\omega,\theta}^-$ respectively. Moreover, for all $\xi \in \mathbb{C}^- \cap \mathbb{C}_{\omega,\theta}^-$, we have*

$$\hat{\varphi}_\pm^j(\pm\xi) = e^{\mp\imath a\xi}e^{\imath\theta}\hat{\varphi}_\pm^{j,\theta}(\xi e^{\imath\theta}). \tag{5.16}$$

5.3   The "half-space" representation with complex-scaled traces

The objective is now to make appear the complex-scaled traces in the representation formulae (5.3). Let us focus on the half-space representation for $j = 0$

$$P^0(\varphi^0)(x,y) = \frac{1}{\sqrt{2\pi}} \int_{\mathbb{R}} \hat{\varphi}^0(\xi)\, e^{\imath\sqrt{\omega^2-\xi^2}(x-a)}e^{\imath\xi y}\mathrm{d}\xi. \tag{5.17}$$

By the decomposition of the trace (5.8), we consider for now $\varphi^0 = \varphi_+^0$. The integral in (5.17) can be split into 2 parts depending on the sign of ξ

$$P^0(\varphi_+^0)(x,y) = \frac{1}{\sqrt{2\pi}} \int_{\mathbb{R}^-} \hat{\varphi}_+^0(\xi)\, e^{\imath\sqrt{\omega^2-\xi^2}(x-a)}e^{\imath\xi y}\mathrm{d}\xi$$

$$+ \frac{1}{\sqrt{2\pi}} \int_{\mathbb{R}^+} \hat{\varphi}_+^0(\xi)\, e^{\imath\sqrt{\omega^2-\xi^2}(x-a)}e^{\imath\xi y}\mathrm{d}\xi.$$

By using Lemma 5.2.1, since $\mathbb{R}^- \subset \mathbb{C}_{\omega,\theta}^-$, we can replace the first line of the formula by

$$\frac{e^{\imath\theta}}{\sqrt{2\pi}} \int_{\mathbb{R}^-} \hat{\varphi}_+^{0,\theta}(\xi e^{\imath\theta})\, e^{\imath\sqrt{\omega^2-\xi^2}(x-a)}e^{\imath\xi(y-a)}\mathrm{d}\xi.$$

To complexify the trace in the second line (for $\xi \in \mathbb{R}^+$), as $\mathbb{R}^+ \not\subset \mathbb{C}_{\omega,\theta}^-$, it is necessary to change the path of integration from $\mathbb{R}^+$ to a line included in $\mathbb{C}_{\omega,\theta}^-$. This is the object of the next lemma.

Lemma 5.3.1. *We have*

$$\int_{\mathbb{R}^+} \hat{\varphi}_+^0(\xi)\, e^{\imath\sqrt{\omega^2-\xi^2}(x-a)}e^{\imath\xi y}\mathrm{d}\xi = \int_{\mathbb{R}^+} \hat{\varphi}_+^{0,\theta}(\eta)e^{\imath\sqrt{\omega^2-\eta^2 e^{-2\imath\theta}}(x-a)}e^{\imath\eta e^{-\imath\theta}(y-a)}\mathrm{d}\eta,$$

for all $(x,y) \in \Omega_+^0(\theta) := \{(x,y) \in \Omega^0, x - a \geq \tan(\theta)\,(y-a)\}$.
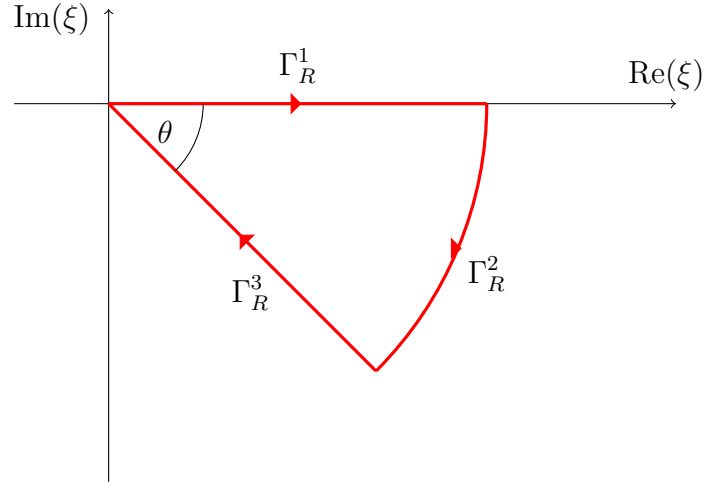
Figure 5.5: Scheme of the contour $\mathcal{C}_R$ in the complex plane.

Proof. The idea of the proof is similar to that of Lemma 5.2.1. We define a contour

$$\mathcal{C}_R := \Gamma_R^1 \cup \Gamma_R^2 \cup \Gamma_R^3,$$

where $\Gamma_R^1 := [0, R]$, $\Gamma_R^2 := \{Re^{-\imath\gamma}, \forall \gamma \in [0, \theta]\}$, and $\Gamma_R^3 := [0, R]e^{-\imath\theta}$ with orientation indicated in Figure 5.5.

Since the function $z \mapsto \hat{\varphi}_+^0(z)e^{\imath\sqrt{\omega^2 - z^2}(x-a)}e^{\imath z y}$ is analytic in $\mathbb{C}^-$ (thanks to the choice of the square root), by the residue theorem we have

$$\int_{\mathcal{C}_R} \hat{\varphi}_+^0(z)e^{\imath\sqrt{\omega^2 - z^2}(x-a)}e^{\imath z y}\mathrm{d}z = 0,$$

which leads to

$$\int_{\Gamma_R^1} \hat{\varphi}_+^0(z)e^{\imath\sqrt{\omega^2 - z^2}(x-a)}e^{\imath z y}\mathrm{d}z + \int_{\Gamma_R^3} \hat{\varphi}_+^0(z)e^{\imath\sqrt{\omega^2 - z^2}(x-a)}e^{\imath z y}\mathrm{d}z = -\int_{\Gamma_R^2} \hat{\varphi}_+^0(z)e^{\imath\sqrt{\omega^2 - z^2}(x-a)}e^{\imath z y}\mathrm{d}z.$$

First, we have

$$\int_{\Gamma_R^3} \hat{\varphi}_+^0(z)e^{\imath\sqrt{\omega^2 - z^2}(x-a)}e^{\imath z y}\mathrm{d}z = -e^{-\imath\theta}\int_0^R \hat{\varphi}_+^0(\eta e^{-\imath\theta})e^{\imath\sqrt{\omega^2 - \eta^2 e^{-2\imath\theta}}(x-a)}e^{\imath\eta e^{-\imath\theta}y}\mathrm{d}\eta.$$

By using Lemma 5.2.1, we deduce that

$$\int_{\Gamma_R^3} \hat{\varphi}_+^0(z)e^{\imath\sqrt{\omega^2 - z^2}(x-a)}e^{\imath z y}\mathrm{d}z = -\int_0^R \hat{\varphi}_+^{0,\theta}(\eta)e^{\imath\sqrt{\omega^2 - \eta^2 e^{-2\imath\theta}}(x-a)}e^{\imath\eta e^{-\imath\theta}(y-a)}\mathrm{d}\eta.$$

The question now is to show that

$$\lim_{R\to+\infty} \int_{\Gamma_R^2} \hat{\varphi}_+^0(z)e^{\imath\sqrt{\omega^2 - z^2}(x-a)}e^{\imath z y}\mathrm{d}z = 0.$$

By a simple parametrization of the line Γ_R^2, we have

$$\int_{\Gamma_R^2} \hat{\varphi}_+^0(z)e^{\imath\sqrt{\omega^2 - z^2}(x-a)}e^{\imath z y}\mathrm{d}z = \int_0^\theta f_{x,y}(R, \gamma)\mathrm{d}\gamma,$$

where

$$f_{x,y}(R, \gamma) = \imath\,\hat{\varphi}^0(Re^{-\imath\gamma})R\,e^{-\sqrt{R^2 e^{-\imath 2\gamma} - \omega^2}(x-a)}e^{\imath Re^{-\imath\gamma}y}.$$

Remark that

$$|f_{x,y}(R,\gamma)| = |\hat\varphi^0(R\,e^{-\imath\gamma})|\,\left|R\,e^{-R\,e^{-\imath\gamma}\sqrt{1-R^{-2}e^{2\imath\gamma}\omega^2}(x-a)}e^{R\sin(\gamma)y}\right|.$$

We can show that $\hat\varphi^0(Re^{-\imath\gamma})e^{R\,a\sin\gamma}$ is bounded when $R \to +\infty$ uniformly in $\gamma \in (0,\theta)$ and $f_{x,y}(R,\gamma) \to 0$ when $R \to +\infty$ uniformly in γ if

$$(x-a)\cos(\theta) \geq (y-a)\sin(\theta).$$

$\square$

Summing up, we have proved that

$$P^0(\varphi^0_+)(x,y) = P^{0,\theta}_+(\varphi^{0,\theta}_+)(x,y), \text{ for } (x,y) \in \Omega^0_+(\theta),$$

where we have set

$$\forall\varphi \in L^2(\mathbb{R}^+), \quad P^{0,\theta}_+(\varphi)(x,y) = \frac{e^{\imath\theta}}{\sqrt{2\pi}}\int_{\mathbb{R}^-}\hat\varphi(\xi e^{\imath\theta})\,e^{\imath\sqrt{\omega^2-\xi^2}(x-a)}e^{\imath\xi(y-a)}\mathrm{d}\xi$$
$$+ \frac{1}{\sqrt{2\pi}}\int_{\mathbb{R}^+}\hat\varphi(\eta)\,e^{\imath\sqrt{\omega^2-\eta^2e^{-2\imath\theta}}(x-a)}e^{\imath\eta e^{-\imath\theta}(y-a)}\mathrm{d}\eta. \tag{5.18}$$

The new representation $P^{0,\theta}_+(\varphi^{0,\theta}_+)$ is only valid in a subset of the half-plane, this is why we put the quotation marks around half-plane in the title of the section.

In order to recover a certain symmetry in ξ, we can also change the path of integration of the Fourier variable from $\mathbb{R}^-$ to $e^{-\imath\theta}\mathbb{R}^-$ but this will reduce again the domain of validity of the expression. Indeed, we can show that

$$P^0(\varphi^0_+)(x,y) = P^{0,\theta}_{+-}(\varphi^{0,\theta}_+)(x,y), \text{ for } (x,y) \in \Omega^0_{+-}(\theta),$$

where

$$\forall\varphi \in L^2(\mathbb{R}^+), \quad P^{0,\theta}_{+-}(\varphi) = \frac{1}{\sqrt{2\pi}}\int_{\mathbb{R}}\hat\varphi(\eta)\,e^{\imath\sqrt{\omega^2-\eta^2e^{-2\imath\theta}}(x-a)}e^{\imath\eta e^{-\imath\theta}(y-a)}\mathrm{d}\eta, \tag{5.19}$$

where

$$\Omega^0_{+-}(\theta) := \{(x,y) \in \Omega^0, x-a \geq \tan(\theta)\,(y-a) \quad \text{and} \quad x-a \geq -\tan(\theta)\,(y-a)\}.$$

Similar results can be obtain for φ^0_- using the change of variable $y \mapsto -y$. More precisely, denoting by S the operator defined by

$$S\varphi(y) = \varphi(-y), \tag{5.20}$$

we have

$$P^0(\varphi^0_-)(x,y) = P^0(S\varphi^0_-)(x,-y) \qquad\qquad \forall(x,-y) \in \Omega^0,$$
$$= P^{0,\theta}_+(\varphi^{0,\theta}_-)(x,-y) \qquad\qquad \forall(x,-y) \in \Omega^0_+(\theta),$$
$$= P^{0,\theta}_{+-}(\varphi^{0,\theta}_-)(x,-y) \qquad\qquad \forall(x,-y) \in \Omega^0_{+-}(\theta). \tag{5.21}$$

In particular,

$$P^0(\varphi^0_+ + \varphi^0_- + g^0\big|_{\Sigma^j_*})(x,y) = P^{0,\theta}_+(\varphi^{0,\theta}_+)(x,y) + P^{0,\theta}_+(\varphi^{0,\theta}_-)(x,-y) + P^0(g^0)(x,y) \text{ for } (x,y) \in \Omega^0(\theta),$$
$$\tag{5.22}$$
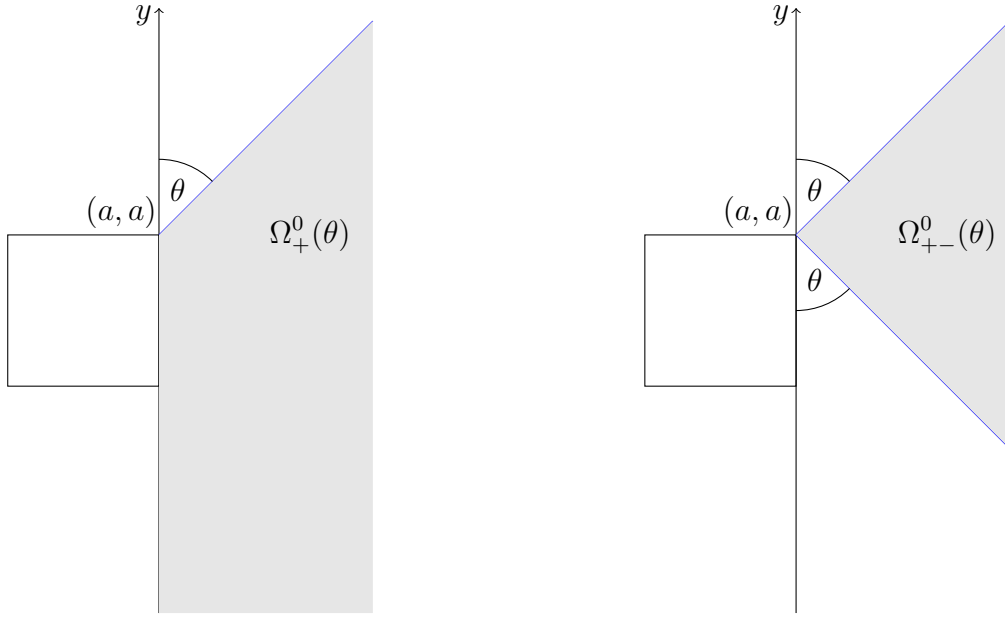
Figure 5.6: The validity region of (a) Formula (5.18) and (b) Formula (5.19).

where

$$\Omega^0(\theta) := \{(x,y) \in \Omega^0, x - a \geq \tan(\theta)\,(y - a) \text{ and } x - a \leq \tan(\theta)\,(y + a)\}, \tag{5.23}$$

illustrated by Figure 5.7.
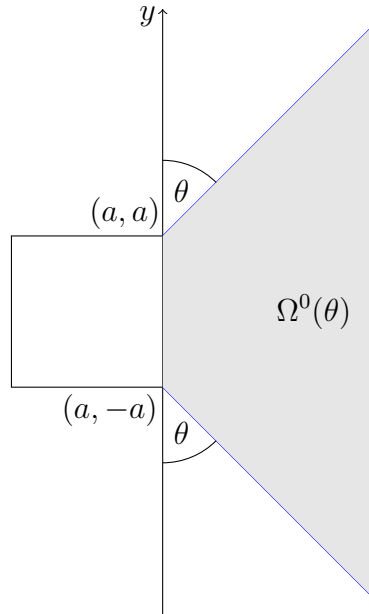
Figure 5.7: The validity region of Formula (5.22).

5.4 The complex-scaled half-space matching formulation

By using the integral formula (5.22), we will derive integral equations linking the complexified traces $\varphi_\pm^{j,\theta}$. The function $P^0(\varphi^0)$ coincides with $P_{+-}^{0,\theta}(\varphi_+^{0,\theta})$ on $\Sigma_-^1 \subset \Omega^0(\theta)$ which is

$$P_{+-}^{0,\theta}(\varphi_+^{0,\theta})(x,a) = \frac{1}{\sqrt{2\pi}} \int_{\mathbb{R}} \hat{\varphi}_+^{0,\theta}(\eta)\, e^{i\sqrt{\omega^2 - \eta^2 e^{-2i\theta}}(x-a)}\, \mathrm{d}\eta, \quad \forall x \geq a.$$

This function is analytic with respect to x in the complex neighborhood of Σ^1_-. We define an integral operator

$$\forall \psi \in L^2(\mathbb{R}^+), \quad D^\theta_+ \psi(t) := \frac{1}{\sqrt{2\pi}} \int_\mathbb{R} \hat{\psi}(\eta) \, e^{\imath \sqrt{\omega^2 e^{2\imath\theta} - \eta^2} t} \, \mathrm{d}\eta, \quad t \in \mathbb{R}^+, \tag{5.24}$$

and with this operator we have

$$D^\theta_+ \varphi^{0,\theta}_+(t) = P^{0,\theta}_{+-}(\varphi^{0,\theta}_+)(a + t e^{\imath\theta}, a), \quad \forall t \in \mathbb{R}^+. \tag{5.25}$$

Similarly, the function $P^0(\varphi^0)$ coincides with $P^{0,\theta}_+(\varphi^{0,\theta}_+)$ on $\Sigma^3_+ \subset \Omega^0_+(\theta)$ which is

$$P^{0,\theta}_+(\varphi^{0,\theta}_+)(x, -a) = \frac{e^{\imath\theta}}{\sqrt{2\pi}} \int_{\mathbb{R}^-} \hat{\varphi}^{0,\theta}_+(\xi e^{\imath\theta}) \, e^{\imath \sqrt{\omega^2 - \xi^2}(x-a)} e^{-2\imath\xi a} \mathrm{d}\xi$$
$$+ \frac{1}{\sqrt{2\pi}} \int_{\mathbb{R}^+} \hat{\varphi}^{0,\theta}_+(\eta) \, e^{\imath \sqrt{\omega^2 - \eta^2 e^{-2\imath\theta}}(x-a)} e^{-2\imath\eta e^{-\imath\theta} a} \mathrm{d}\eta, \quad \forall x \geq a.$$

This function is analytic with respect to x in the complex neighborhood of Σ^3_+. We define an integral operator

$$\forall \psi \in L^2(\mathbb{R}^+), \quad D^\theta_- \psi(t) := \frac{e^{\imath\theta}}{\sqrt{2\pi}} \int_{\mathbb{R}^-} \hat{\psi}(\xi e^{\imath\theta}) \, e^{\imath \sqrt{\omega^2 - \xi^2} t e^{\imath\theta}} e^{-2\imath\xi a} \mathrm{d}\xi$$
$$+ \frac{1}{\sqrt{2\pi}} \int_{\mathbb{R}^+} \hat{\psi}(\eta) \, e^{\imath \sqrt{\omega^2 e^{2\imath\theta} - \eta^2} t} e^{-2\imath\eta e^{-\imath\theta} a} \mathrm{d}\eta, \quad t \in \mathbb{R}^+. \tag{5.26}$$

and with this operator we have

$$D^\theta_- \varphi^{0,\theta}_+(t) = P^{0,\theta}_+(\varphi^{0,\theta}_+)(a + t e^{\imath\theta}, -a), \quad \forall t \in \mathbb{R}^+. \tag{5.27}$$

Finally, the representation

$$P^0(g^0)(x, \pm a) = \frac{1}{\sqrt{2\pi}} \int_\mathbb{R} \hat{g}^0(\xi) e^{\imath \sqrt{\omega^2 - \xi^2}(x-a)} e^{\pm\imath\xi a} \mathrm{d}\xi$$

is analytic with respect to x in the complex neighborhood of Σ^1_- and Σ^3_+. We define

$$\forall \psi \in L^2((-a, a)) \quad D^\theta_{*,\pm} \psi(t) := \frac{1}{\sqrt{2\pi}} \int_\mathbb{R} \hat{\psi}(\xi) e^{\imath \sqrt{\omega^2 - \xi^2} t e^{\imath\theta}} e^{\pm\imath\xi a} \mathrm{d}\xi, \quad t \in \mathbb{R}^+, \tag{5.28}$$

which leads to the integral operator

$$D^\theta_{*,\pm} g^0(t) := P^0(g^0)(a + t e^{\imath\theta}, \pm a), \quad \forall t \in \mathbb{R}^+. \tag{5.29}$$

By symmetry, we have exactly the same expressions for $P^j_\theta(\varphi^{j,\theta}_\pm)$ and $P^{j,\theta}_\theta(g^j)$ for all $j \in \{0, 1, 2, 3\}$ as Formula (5.24 – 5.28), thus expressed by the same operators. Finally, we can write the system of equations involving all the traces as

$$\begin{vmatrix} \varphi^{j+1,\theta}_- = D^\theta_+(\varphi^{j,\theta}_+) + D^\theta_-(\varphi^{j,\theta}_-) + D^\theta_{*,+}(g^j), \\ \varphi^{j-1,\theta}_+ = D^\theta_-(\varphi^{j,\theta}_+) + D^\theta_+(\varphi^{j,\theta}_-) + D^\theta_{*,-}(g^j), \end{vmatrix} \quad j \in \mathbb{Z}/4\mathbb{Z}. \tag{5.30}$$

This system of equation can be more compactly written as

$$\left(\mathbb{I} - \mathbb{D}^\theta\right) \Phi^\theta = G^\theta, \tag{5.31}$$

where

$$\Phi^\theta \in V := \left\{ (\varphi_-^{0,\theta}, \varphi_+^{0,\theta}, \varphi_-^{1,\theta}, \varphi_+^{1,\theta}, \varphi_-^{2,\theta}, \varphi_+^{2,\theta}, \varphi_-^{3,\theta}, \varphi_+^{3,\theta}) \in \left(L^2(\mathbb{R}^+) \right)^8 \right\}, \tag{5.32}$$

$\mathbb{I}$ corresponds to the identity operator, $\mathbb{D}^\theta$ is given by

$$\mathbb{D}^\theta := \begin{bmatrix} 0 & 0 & 0 & 0 & 0 & 0 & D_-^\theta & D_+^\theta \\ 0 & 0 & D_+^\theta & D_-^\theta & 0 & 0 & 0 & 0 \\ D_-^\theta & D_+^\theta & 0 & 0 & 0 & 0 & 0 & 0 \\ 0 & 0 & 0 & 0 & D_+^\theta & D_-^\theta & 0 & 0 \\ 0 & 0 & D_-^\theta & D_+^\theta & 0 & 0 & 0 & 0 \\ 0 & 0 & 0 & 0 & 0 & 0 & D_+^\theta & D_-^\theta \\ 0 & 0 & 0 & 0 & D_-^\theta & D_+^\theta & 0 & 0 \\ D_+^\theta & D_-^\theta & 0 & 0 & 0 & 0 & 0 & 0 \end{bmatrix}, \tag{5.33}$$

and $G^\theta := \begin{bmatrix} D_{*,+}^\theta g^3 & D_{*,-}^\theta g^1 & D_{*,+}^\theta g^0 & D_{*,-}^\theta g^2 & D_{*,+}^\theta g^1 & D_{*,-}^\theta g^3 & D_{*,+}^\theta g^2 & D_{*,-}^\theta g^0 \end{bmatrix}^T.$

5.5 Analysis of the formulation

The main result of this section is the following stability result.

Theorem 5.5.1. *The operator $(\mathbb{I} - \mathbb{D}^\theta) \in \mathcal{L}(V)$ is the sum of a coercive operator and a compact one.*

To prove this theorem, we first show the main property of three integral operators involved in (5.31).

Lemma 5.5.2. *For $\theta \in (0, \pi]$, the operator D_+^θ is bounded on $L^2(\mathbb{R}^+)$. Furthermore, it can be decomposed into the sum of two operators:*

$$D_+^\theta = L + K,$$

where $\|L\| \leq 1/\sqrt{2}$ and K is compact.

Proof. From the definition of the operator, it actually corresponds to the operator D for the dissipative case

$$D\psi(t) = \frac{1}{\sqrt{2\pi}} \int_{\mathbb{R}} \hat{\psi}(\xi) e^{i\sqrt{\omega^2 - \xi^2} t} e^{i\xi a} \, d\xi, \quad t \in \mathbb{R}^+,$$

for the complex frequency $\omega e^{i\theta}$ and $a = 0$. The result follows immediately from Theorem 1.3.7. $\qquad\square$

Lemma 5.5.3. *For $\theta \in (0, \pi]$, the operator D_-^θ is compact on $L^2(\mathbb{R}^+)$.*

Proof. The operator is composed from 2 different integrals:

$$D_-^\theta \psi = \frac{e^{i\theta}}{\sqrt{2\pi}} \int_{\mathbb{R}^-} \hat{\psi}(\xi e^{i\theta}) k_-^{-,\theta}(\xi, t) d\xi + \frac{1}{\sqrt{2\pi}} \int_{\mathbb{R}^+} \hat{\psi}(\eta) k_-^{+,\theta}(\eta, t) d\eta,$$

where

$$k_-^{-,\theta}(\xi, t) = e^{i\sqrt{\omega^2 - \xi^2} t e^{i\theta} - 2i\xi a} \qquad \text{for } (\xi, t) \in \mathbb{R}^- \times \mathbb{R}^+,$$

$$k_-^{+,\theta}(\eta, t) = e^{i\sqrt{\omega^2 e^{2i\theta} - \eta^2} t - 2i\eta e^{-i\theta} a} \qquad \text{for } (\eta, t) \in \mathbb{R}^+ \times \mathbb{R}^+.$$

The integral operator involving the kernel $k_-^{+,\theta}(\xi,t)$ is a Hilbert-Schmidt operator (thus compact) since

$$\int_{\mathbb{R}^+}\int_{\mathbb{R}^+}\left|k_-^{+,\theta}(\xi,t)\right|^2 \mathrm{d}t\mathrm{d}\eta = \int_{\mathbb{R}^+} e^{-4\eta a\sin\theta}\frac{1}{2\operatorname{Re}\sqrt{\eta^2-\omega^2 e^{2\imath\theta}}} < +\infty.$$

For the kernel $k_-^{-,\theta}(\xi,t)$, we show that it is in $L^2(\mathbb{R}^- \times \mathbb{R}^+)$. First, we have $k_-^{-,\theta}(\xi,t) \in L^2(\mathbb{R}^- \times (b,+\infty))$ for any $b > 0$ since

$$\int_{\mathbb{R}^-}\int_b^{+\infty}\left|k_-^{-,\theta}(\xi,t)\right|^2 \mathrm{d}t\mathrm{d}\xi = \int_{-\omega}^0 \frac{e^{-2\sqrt{\omega^2-\xi^2}b\sin\theta}}{2\sqrt{\omega^2-\xi^2}\sin\theta}\mathrm{d}\xi + \int_{-\infty}^{-\omega} \frac{e^{-2\sqrt{\xi^2-\omega^2}b\cos\theta}}{2\sqrt{\xi^2-\omega^2}\cos\theta}\mathrm{d}\xi < +\infty.$$

Next, we can also show that $k_-^{-,\theta}(\xi,t) \in L^2((-M,0)\times\mathbb{R}^+)$ for any $M > 0$ since

$$\int_{-M}^0\int_{\mathbb{R}^+}\left|k_-^{-,\theta}(\xi,t)\right|^2 \mathrm{d}t\mathrm{d}\xi = \int_{-\omega}^0 \frac{1}{2\sqrt{\omega^2-\xi^2}\sin\theta}\mathrm{d}\xi + \int_{-M}^{-\omega} \frac{1}{2\sqrt{\xi^2-\omega^2}\cos\theta}\mathrm{d}\xi < +\infty.$$

We now need to show that $k_-^{-,\theta}(\xi,t)$ is in $L^2((-\infty,-M)\times(0,b))$. We define a kernel

$$\tilde{k}(\xi,t) = e^{\xi t e^{\imath\theta}-2\imath\xi a} \text{ for } (\xi,t) \in \mathbb{R}^- \times \mathbb{R}^+,$$

which has the same expression as $k_-^{-,\theta}$, but for $\omega = 0$. The norm $\left\|k_-^{-,\theta} - \tilde{k}\right\|_{L^2(-\infty,-M)\times(0,b)}$ is

$$\int_{-\infty}^{-M}\int_0^b\left|k_-^{-,\theta}(\xi,t) - \tilde{k}(\xi,t)\right|^2 \mathrm{d}t\mathrm{d}\xi = \int_{-\infty}^{-M}\int_0^b e^{2\xi t\cos\theta}\left|1-e^{-q(\xi)t\cos\theta}\right|^2 \mathrm{d}t\mathrm{d}\xi,$$

where $q(\xi) = \sqrt{\xi^2-k^2} + \xi$. This function is bounded and decays to 0 when $\xi \to -\infty$ as $1/\xi$. We can then choose $M > 0$ such that for any $\xi < -M$,

$$\left|1-e^{-q(\xi)t\cos\theta}\right| \le Ct\cos\theta|q(\xi)|.$$

We deduce that

$$\int_{-\infty}^{-M}\int_0^b\left|k_-^{-,\theta}(\xi,t) - \tilde{k}(\xi,t)\right|^2 \mathrm{d}t \le C\cos\theta\int_{-\infty}^{-M}|q(\xi)|^2\int_0^b e^{2\xi t\cos\theta}t^2\mathrm{d}t\mathrm{d}\xi < +\infty.$$

It suffices now to study the operator

$$\tilde{D}\psi(t) := \frac{e^{\imath\theta}}{\sqrt{2\pi}}\int_{-\infty}^{-M}\tilde{k}(\xi,t)\,\hat{\psi}(\xi e^{\imath\theta})\,\mathrm{d}\xi, \text{ for } t \in (0,b), \tag{5.34}$$

where

$$\tilde{k}(\xi,t) = e^{\xi t e^{\imath\theta}-2\imath\xi a}, \ \forall(\xi,t) \in \mathbb{R}^- \times \mathbb{R}^+, \text{ and } \hat{\psi}(\xi e^{\imath\theta}) = \frac{1}{\sqrt{2\pi}}\int_{\mathbb{R}^+}\psi(s)e^{-\imath s\xi e^{\imath\theta}}\,\mathrm{d}s.$$

This operator can also be rewritten as

$$\tilde{D}\psi(t) := \frac{e^{\imath\theta}}{2\pi}\int_{\mathbb{R}^+}k(t,s)\,\psi(s)\,\mathrm{d}s, \text{ for } t \in (0,b),$$

where for all $t > 0$ and $s > 0$

$$k(t,s) = \int_{-\infty}^{-M}e^{\xi(te^{\imath\theta}-\imath se^{\imath\theta}-2\imath a)}\,\mathrm{d}\xi = \frac{e^{-M(te^{\imath\theta}-\imath se^{\imath\theta}-2\imath a)}}{(te^{\imath\theta}-\imath se^{\imath\theta}-2\imath a)}.$$

We have

$$|k(t,s)|^2 = \frac{e^{-2M(t\cos\theta + s\sin\alpha)}}{(t\cos\theta + s\sin\theta)^2 + (t\sin\theta - s\cos\theta - 2a)^2},$$

which implies that $k \in L^2(\mathbb{R}^+ \times \mathbb{R}^+)$ and $\tilde{D}$ is compact.

Gathering all these results, we conclude that the operator D_-^θ is a compact operator on $L^2(\mathbb{R}^+)$.

$\square$

Lemma 5.5.4. *For all* $\theta \in (0, \pi/2)$*, the operator* $D_{*,\pm}^\theta$ *is continuous from* $L^2((-a,a))$ *to* $L^2(\mathbb{R}^+)$*.*

Proof. The proof is similar as for the one for $k_-^{-,\theta}(\xi, t)$ in Lemma 5.5.3. The operator is given by:

$$D_{*,\pm}^\theta g(t) = \frac{1}{\sqrt{2\pi}} \int_{\mathbb{R}} \hat{g}(\xi) k_\pm(\xi, t) \mathrm{d}\xi,$$

where

$$k_\pm(\xi, t) = e^{\imath\sqrt{\omega^2 - \xi^2} t e^{\imath\theta}} e^{\pm\imath\xi a}.$$

We show the proof for k_+, the same arguments can be used to prove the same result for for k_-.

By direct calculation, we can show that $k_+(\xi, t) \in L^2(\mathbb{R} \times (b, +\infty))$ and $k_+(\xi, t) \in L^2((-M, M) \times (0, b))$. As before, we define $\tilde{k}$ as

$$\tilde{k}(\xi, t) = e^{-|\xi| t e^{\imath\theta}} e^{\imath\xi a}, \quad |\xi| > M, t \in (0, b), \tag{5.35}$$

which is the same as k_+ for $\omega = 0$. By similar calculation as done in Lemma 5.5.3, it is easy to show that $k_+ - \tilde{k}$ is in $L^2((M, +\infty) \times (0, b))$ and $L^2((-\infty, -M) \times (0, b))$. Finally, we need to show that the operator

$$L : g \mapsto \int_M^{+\infty} \hat{g}(\xi) e^{-\xi t e^{\imath\theta}} e^{\imath\xi a} \mathrm{d}\xi$$

is continuous from $L^2((-a, a))$ to $L^2(0, b)$, the one for

$$\tilde{L} : g \mapsto \int_{-\infty}^{-M} \hat{g}(\xi) e^{\xi t e^{\imath\theta}} e^{\imath\xi a} \mathrm{d}\xi$$

can be shown in a similar manner.

We use the arguments used to prove the continuity of the Laplace operator (see Theorem 5.1.2 in [68] or [38]). We start by

$$|Lg(t)| = \left| \int_M^{+\infty} e^{-\xi t e^{\imath\theta}} e^{\imath\xi a} \hat{g}(\xi) \mathrm{d}\xi \right|$$

$$\leq \int_M^{+\infty} e^{-\xi t \cos\theta} |\hat{g}(\xi)| \, \xi^{1/4} \xi^{-1/4} \mathrm{d}\xi.$$

By using the Cauchy-Schwarz inequality, we have then

$$|Lg(t)|^2 \leq \int_M^{+\infty} e^{-\xi t \cos\theta} \xi^{-1/2} \mathrm{d}\xi \int_M^{+\infty} e^{-\xi t \cos\theta} \xi^{1/2} |\hat{g}(\xi)|^2 \mathrm{d}\xi \tag{5.36}$$

The first integral can be computed by using a change of variable $s = \xi t$. Indeed, we obtain

$$\int_M^{+\infty} e^{-\xi t \cos\theta} \xi^{-1/2} \mathrm{d}\xi \leq \int_0^{+\infty} e^{-\xi t \cos\theta} \xi^{-1/2} \mathrm{d}\xi \leq \frac{1}{\sqrt{t}} \int_0^{+\infty} e^{-s\cos\theta} s^{-1/2} \mathrm{d}s.$$

Again, by a change of variable $r = s^{1/2}$, it follows that

$$\frac{1}{\sqrt{t}} \int_0^{+\infty} e^{-s \cos \theta} s^{-1/2} \mathrm{d}s = \frac{2}{\sqrt{t}} \int_0^{+\infty} e^{-r^2 \cos \theta} \mathrm{d}r = \frac{\sqrt{\pi}}{\sqrt{t \cos \theta}}.$$

Now, taking the integral in t on the expression (5.36) and by using the Fubini's theorem, we find

$$\int_0^{+\infty} |Lg(t)|^2 \, \mathrm{d}t \leq \frac{\sqrt{\pi}}{\sqrt{\cos \theta}} \int_0^{+\infty} \int_M^{+\infty} \frac{e^{-\xi t \cos \theta}}{\sqrt{t}} \sqrt{\xi} \, |\hat{g}(\xi)|^2 \, \mathrm{d}\xi \mathrm{d}t$$

$$\leq \frac{\sqrt{\pi}}{\sqrt{\cos \theta}} \int_M^{+\infty} \int_0^{+\infty} \frac{e^{-\xi t \cos \theta}}{\sqrt{t}} \mathrm{d}t \, \sqrt{\xi} \, |\hat{g}(\xi)|^2 \, \mathrm{d}\xi$$

By a change of variable, we can explicitly compute the integrals as before. We get

$$\int_0^{+\infty} |Lg(t)|^2 \, \mathrm{d}t \leq \frac{\pi}{\cos \theta} \int_M^{+\infty} |\hat{g}(\xi)|^2 \, \mathrm{d}\xi.$$

We conclude that

$$\|Lg\|_{L^2(\mathbb{R}^+)} \leq c\|g\|_{L^2}.$$

The result follows. □

With these lemmas, we can prove Theorem 5.5.1 by decomposing the operator $\mathbb{D}^\theta$ as done in the proof of Theorem 1.3.1. Thus, we have shown that for the system of equation (5.31), the Fredholm alternative holds. The numerical analysis can then be derived to obtain some estimations, but it is left as a perspective for now.

5.6 Numerical results

To implement the method, we use the same ingredients of discretization as done in Chapter 1. Thus, we have 3 discretization parameters: T, $\hat{T}$, and h, as well as quadrature formulae to evaluate the Fourier integrals.

Validation of the half-space representation based on the complex-scaled traces

The first thing we would like to verify is the validity zone in a half-space depending on θ. To show this, we consider the half-space Ω^0 and take the data

$$\varphi_+^{0,\theta}(t) = \varphi_+^0(a, a + te^{\imath\theta}) = \frac{1}{4\imath} H_0^{(1)}(\omega\sqrt{a^2 + (a + te^{\imath\theta})^2}) \qquad t \in [a, T],$$

$$\varphi_-^{0,\theta}(t) = \varphi_-^0(a, -a - te^{\imath\theta}) = \frac{1}{4\imath} H_0^{(1)}(\omega\sqrt{a^2 + (-a - te^{\imath\theta})^2}) \qquad t \in [a, T],$$

$$g^0(a, t) = \frac{1}{4\imath} H_0^{(1)}(\omega\sqrt{a^2 + t^2}) \qquad t \in (-a, a).$$

where $H_0^{(1)}$ denotes the zeroth Hankel function of the first kind. We take three values of $\theta \in \left\{0, \frac{\pi}{9}, \frac{\pi}{4}\right\}$ and compute $P_+^{0,\theta}(\varphi_+^{0,\theta})(x, y) + P_-^{0,\theta}(\varphi_-^{0,\theta})(x, y) + P^0(g^0)(x, y)$ in $\Omega_{Rec}^0 := [a, b] \times [-b, b]$ by using Formulae (5.18), (5.21), and (5.3) respectively. We take $\omega = 1, a = 2.5, b = 8$. The simulation is obtained by using P1 finite elements with $T = 10$, $\hat{T} = 10$, $h = 0.1$, and a 3rd order Gauss quadrature with 1000 intervals.

For $\theta = 0$, we obtain the usual (not complexified) representation and it is valid in the whole Ω^0. For $\theta = \frac{\pi}{9}$ and $\frac{\pi}{4}$, the representations are only valid in $\Omega^0(\theta)$, given in (5.23). As θ increases, the validity zone becomes smaller, as expected.
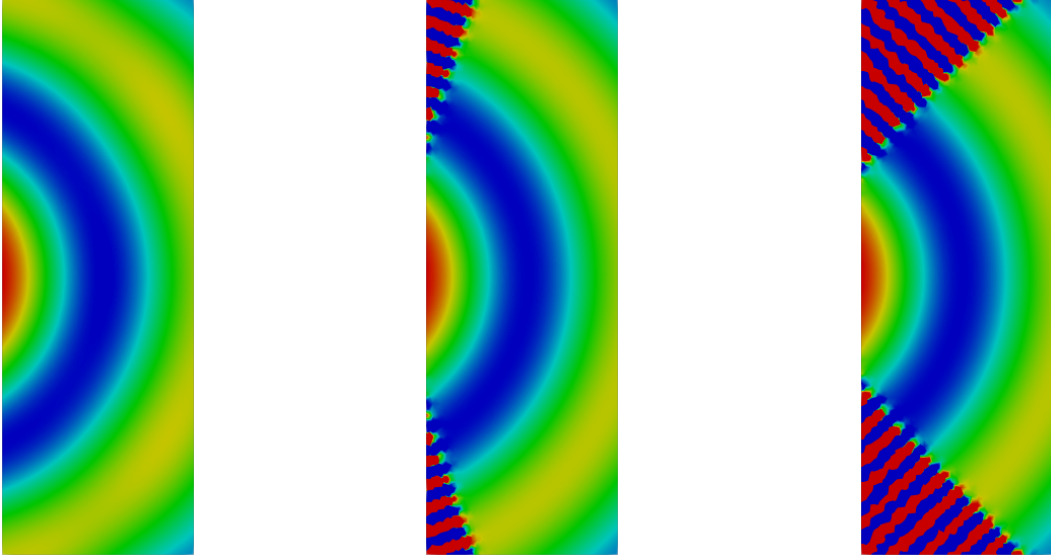
Figure 5.8: Reconstruction of the solution in Ω^0 given the complexified trace of the Hankel function with (a) $\theta = 0°$ (not complexified), (b) $\theta = \dfrac{\pi}{9}$, (c) $\theta = \dfrac{\pi}{4}$.

Qualitative validation of the half-space matching formulation

Now we consider the whole domain $\mathbb{R}^2$ with a square $\mathcal{O} = [-2.5, 2.5]^2$ and we impose

$$g = \frac{1}{4\imath} H_0^{(1)}(\omega r) \text{ on } \partial\mathcal{O}.$$

On Figure 5.9 we represent on the interval $(-T, T)$ the real and imaginary parts of the exact solution $\varphi^{0,\theta}$ (blue line) and of the computed solution $\varphi_{\hat{T},\mathbf{h}}^{0,\theta}$ (red dots). We get an L^2 relative error of 0.23%.

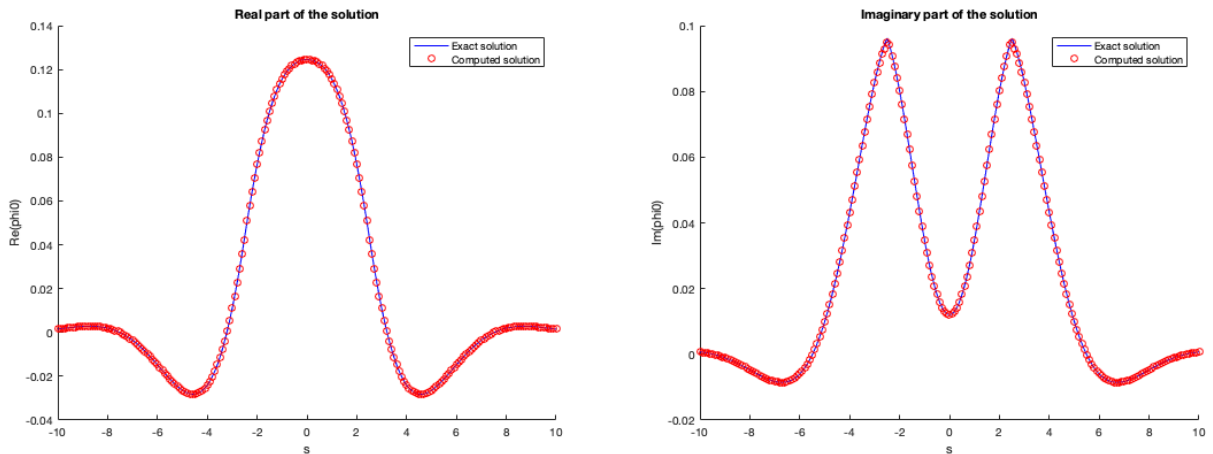Figure 5.9: The real (left) part and the imaginary (right) part of the computed solution $\varphi_{\hat{T},\mathbf{h}}^{0,\theta}$ (red points) and the exact solution (blue line) on Σ^0.

For the reconstruction, we define the reconstruction zone as

$$\Omega_{Rec}^j = \{(x^j, y^j) \mid x^j \in [a, T_{Rec}], |y^j| \leq x^j\}, \quad j \in \{0, 1, 2, 3\}$$
$$\Omega_{Rec} = \bigcup_{j \in \{0,1,2,3\}} \Omega_{Rec}^j,$$

where we take $a = 2.5$ and $T_{Rec} = 8$. We obtain an $L^2(\Omega_{Rec})$ relative error of 0.32%.
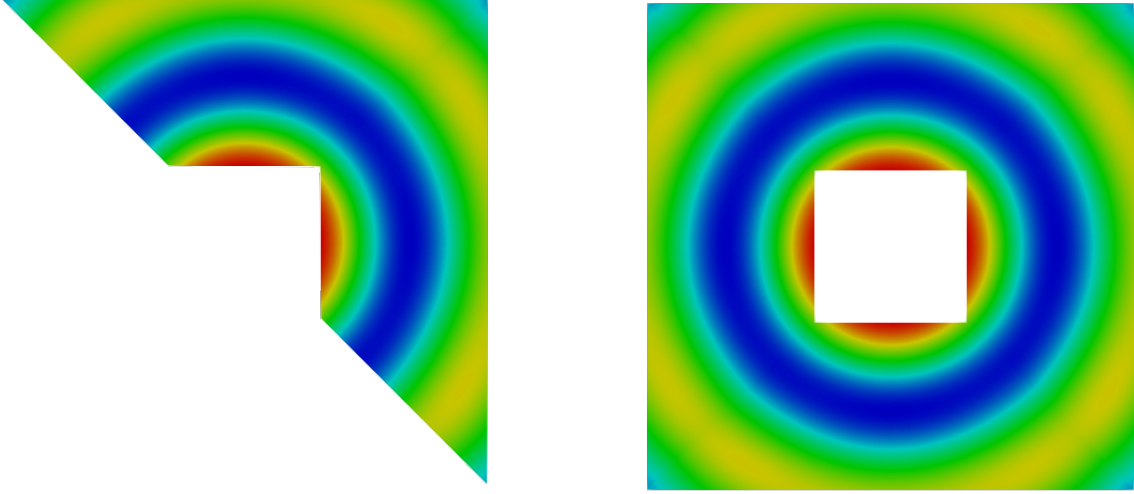

Figure 5.10: On the left: the real part of the reconstructed solution in $\Omega^0_{Rec} \cup \Omega^1_{Rec}$. On the right: the real part of the reconstructed solution in Ω_{Rec}.

Remark that to obtain a complex-scaled trace that decays exponentially as fast as possible, one might want to take $\theta = \pi/2$. However, if we use $\theta = \pi/2$ for all 4 traces, we would not be able to reconstruct the solution in the whole plane. The complex-scaled trace with fastest decay that still ensures the reconstruction of the solution in the whole plane is therefore obtained for $\theta = \pi/4$.

Influence of the length of the lines (parameter T)

We will only trace the error based on the length because it is the only parameter affected by the complex scaling. We consider different values of $\theta \in \left\{0, \dfrac{\pi}{6}, \dfrac{\pi}{4}, \dfrac{\pi}{3}\right\}$ and fix other parameters to $h = 0.025, \hat{T} = 30$, and 3rd order Gauss quadrature with 3000 intervals.
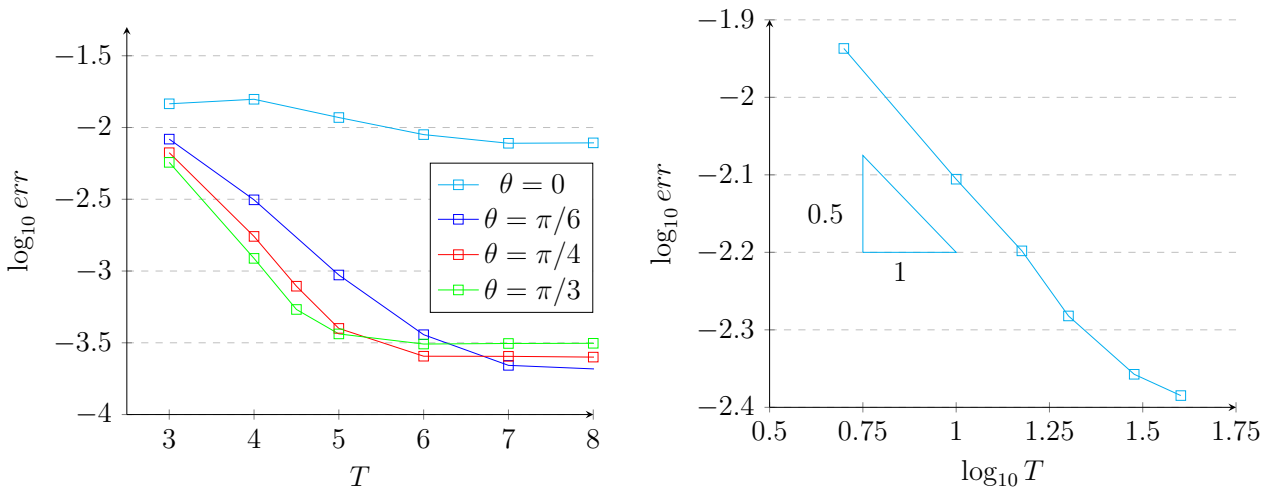

Figure 5.11: Influence of the length of the lines T for (a) various values of θ in $\log - \lin$ scale and (b) for $\theta = 0$ in $\log - \log$ scale.

In Figure 5.11 we represent $\log\left(\left\|\varphi^{0,\theta} - \varphi^{0,\theta}_{\hat{T},\mathbf{h}}\right\|\right)$ as a function of T. The errors $\|\varphi^{0,\theta} - \varphi^{0,\theta}_{\hat{T},\mathbf{h}}\|$

decay exponentially, depending on θ with the following behavior

$$\|\varphi^{0,\theta=0} - \varphi_{\hat{T},\mathbf{h}}^{0,\theta=0}\| = \frac{1}{\sqrt{T}},$$

$$\|\varphi^{0,\theta=\pi/6} - \varphi_{\hat{T},\mathbf{h}}^{0,\theta=\pi/6}\| = e^{-0.47T},$$

$$\|\varphi^{0,\theta=\pi/4} - \varphi_{\hat{T},\mathbf{h}}^{0,\theta=\pi/4}\| = e^{-0.62T},$$

$$\|\varphi^{0,\theta=\pi/3} - \varphi_{\hat{T},\mathbf{h}}^{0,\theta=\pi/3}\| = e^{-0.68T},$$

before finally becoming constant due to the other discretization parameters. We expect that the error decays as

$$\|\varphi^{0,\theta} - \varphi_{\hat{T},\mathbf{h}}^{0,\theta}\| = Ce^{-T\sin\theta},$$

but the results that we obtain is not as good, especially when θ increases.

5.7 Extension cases

5.7.1 Complex scaling from an arbitrary point

The formula $P_+^{0,\theta}(\varphi_+^{0,\theta})$ derived in Section 5.3 is obtained by changing the integration path from $[a, +\infty)$ to $e^{\imath\theta}[a, +\infty)$ starting from the corner of the square (a, a). The complex scaling can actually be done from an arbitrary point, meaning that we can change the integration path starting from (a, c) where $c \geq a$, leaving the segment from (a, a) to (a, c) as it is. Figure 5.12 illustrates the difference between the change of integration path from the original formulation with the one done from an arbitrary point.
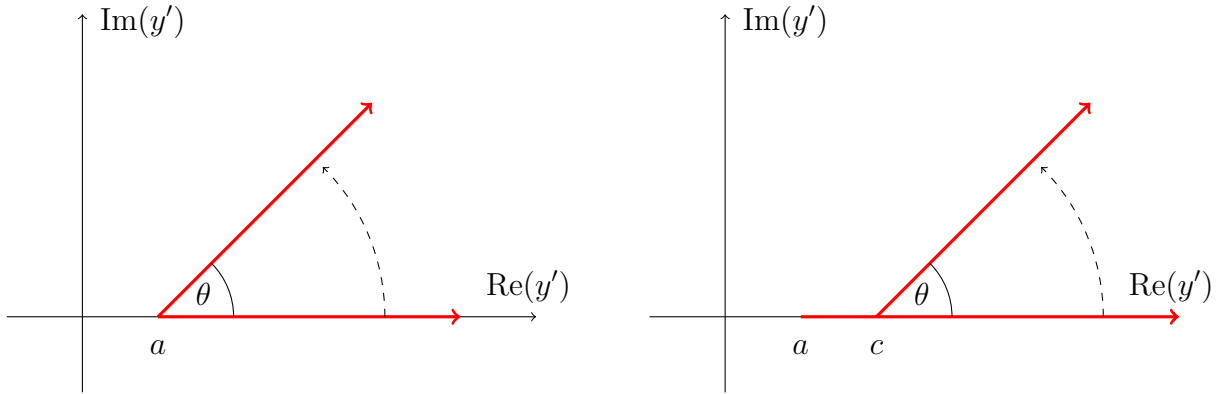
Figure 5.12: On the left: the change of the integration path starting from the point (a, a). On the right: the integration path is left unchanged from (a, a) to (a, c) and then the integration path is changed starting from the point (a, c).

Deriving the half-space formula for this arbitrary point (a, c), we define an operator

$$
\begin{aligned}
P_{+,c}^{0,\theta}(\psi)(x, y) = {}& \frac{1}{2\pi} \int_{\mathbb{R}} \int_a^c \psi(y') e^{-\imath\xi y'} \mathrm{d}y' e^{\imath\sqrt{\omega^2-\xi^2}(x-a)} e^{\imath\xi y} \mathrm{d}\xi \\
& + \frac{e^{\imath\theta}}{2\pi} \int_{\mathbb{R}^-} \int_{\mathbb{R}^+} \psi(c + se^{\imath\theta}) e^{-\imath\xi(c+se^{\imath\theta})} \mathrm{d}s \, e^{\imath\sqrt{\omega^2-\xi^2}(x-a)} e^{\imath\xi y} \mathrm{d}\xi \\
& + \frac{1}{2\pi} \int_{\mathbb{R}^+} \int_{\mathbb{R}^+} \psi(c + se^{\imath\theta}) e^{-\imath\eta e^{-\imath\theta}(c+se^{\imath\theta})} \mathrm{d}s \, e^{\imath\sqrt{\omega^2-\eta^2 e^{-2\imath\theta}}(x-a)} e^{\imath\eta e^{-\imath\theta}y} \mathrm{d}\eta.
\end{aligned}
\tag{5.37}
$$

We have

$$P^0(\varphi_+^0)(x,y) = P_{+,c}^{0,\theta}(\varphi_+^0)(x,y) \text{ in } \Omega_{+,c}^0(\theta), \tag{5.38}$$

where

$$\Omega_{+,c}^0(\theta) := \{(x,y) \in \Omega^0, x - a \geq \tan(\theta)(y - c)\}. \tag{5.39}$$

Similar formulae can be obtained for $\varphi_{-,c}^0$ by using the operator S defined in (5.20) such that we have

$$P^0(\varphi_{-,c}^0)(x,y) = P_{+,c}^{0,\theta}(\varphi_{-,c}^{0,\theta})(x,-y) \quad \forall (x,-y) \in \Omega_{+,c}^0(\theta). \tag{5.40}$$

Finally, we have also

$$P^0(\varphi_+^0 + \varphi_-^0 + g^0)(x,y) = P_{+,c}^{0,\theta}(\varphi_{+,c}^{0,\theta})(x,y) + P_{+,c}^{0,\theta}(\varphi_{-,\theta}^{0,c})(x,-y) + P^0(g^0)(x,y), \text{ for } (x,y) \in \Omega_c^0(\theta), \tag{5.41}$$

where

$$\Omega_c^0(\theta) := \{(x,y) \in \Omega^0, x - a \geq \tan(\theta)(y - c) \text{ and } x - a \leq \tan(\theta)(y + c)\}.$$

This validity zone is illustrated in Figure 5.13.
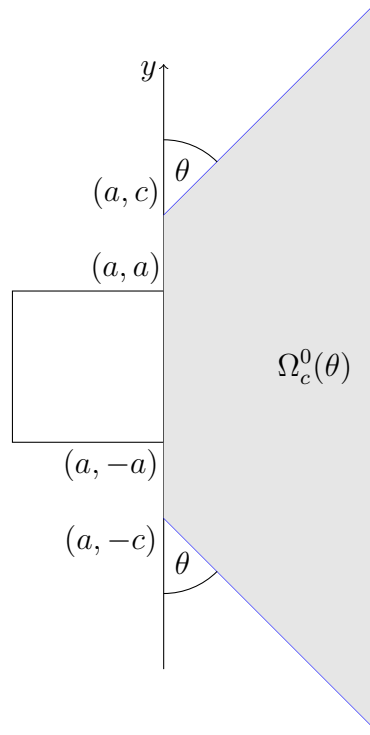
Figure 5.13: The validity region of Formula (5.22).

In Figure 5.14, we show the different validity zone for $c = a = 2.5$ and $c = 4$ for the same $\theta = \dfrac{\pi}{6}$. It is clear that the validity zone for $c = 4$ is bigger than the one for $c = 2.5$.

5.7.2 Anisotropic case

We consider now the anisotropic problem

$$\left| \begin{aligned} -\nabla \cdot (A\nabla p) - \omega^2 p &= 0 \text{ in } \Omega, \\ p &= g \text{ on } \partial\mathcal{O}, \end{aligned} \right. \tag{5.42}$$
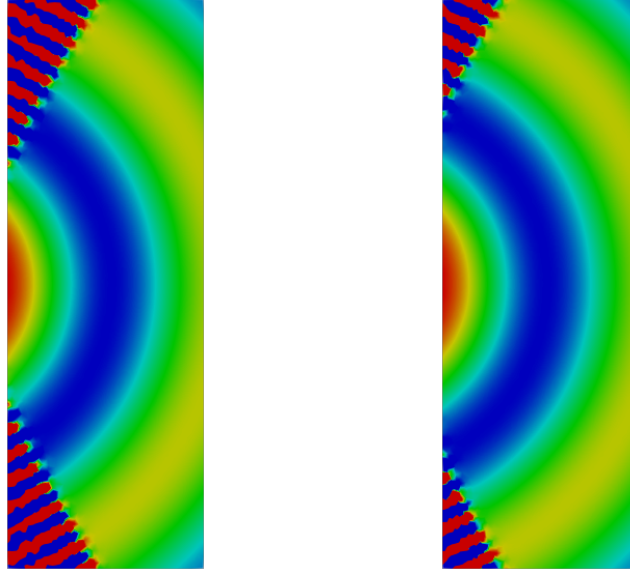
Figure 5.14: Reconstruction of the solution in Ω^0 given the complexified trace of the Hankel function with $\theta = \pi/6$ and (a) $c = 2.5$, (b) $c = 4$.

where A is a 2×2 matrix is given by

$$A = \begin{pmatrix} \alpha & \gamma \\ \gamma & \beta \end{pmatrix}, \quad \text{where } \alpha, \beta > 0 \text{ and } \det A > 0.$$

The HSM method for anisotropic dissipative case is derived in detail in [19, 68]. For the anisotropic non-dissipative case, we need to use the complex-scaled HSM method. As before, first we consider the following half-space problem in Ω^j

$$\left| \begin{aligned} \nabla \cdot (A \nabla P^j) + \omega^2 P^j &= 0 \text{ in } \Omega^j, \\ P^j &= \varphi^j \text{ on } \Sigma^j. \end{aligned} \right. \tag{5.43}$$

By using the Fourier transform, the solution can be expressed in terms of the trace:

$$P^j(x^j, y^j) = \frac{1}{\sqrt{2\pi}} \int_{\mathbb{R}} \hat{\varphi}^j(\xi) e^{\imath r^j(\xi)(x^j - a)} e^{\imath \xi y^j} \mathrm{d}\xi, \tag{5.44}$$

where the values of r^j are defined as:

$$\begin{aligned} r^0 = r^2 &= \frac{-\xi\gamma + \sqrt{d_1(\xi)}}{\alpha} \quad \text{with } d_1(\xi) = \omega^2 \alpha - \xi^2 \det A, \\ r^1 = r^3 &= \frac{\xi\gamma + \sqrt{d_2(\xi)}}{\beta} \quad \text{with } d_2(\xi) = \omega^2 \beta - \xi^2 \det A, \end{aligned} \tag{5.45}$$

with the convention $\operatorname{Im} \sqrt{d_k(\xi)} \geq 0, k \in \{1, 2\}$. As before, we consider only the expressions for φ_+^0, the ones for the other traces can be derived in a similar manner. We have the following representation

$$P^0(\varphi_+^0)(x, y) = \frac{1}{\sqrt{2\pi}} \int_{\mathbb{R}} \hat{\varphi}_+^0(\xi) e^{\left(-\imath \xi a_3 + \imath \sqrt{\omega^2 a_1 - \xi^2 \det A} \right) \frac{x-a}{a_1}} e^{\imath \xi y} \mathrm{d}\xi. \tag{5.46}$$

This integral can be split into 2 parts depending on the sign of ξ

$$P^0(\varphi_+^0)(x, y) = \frac{1}{\sqrt{2\pi}} \int_{\mathbb{R}^-} \hat{\varphi}_+^0(\xi) \, e^{\left(-\imath \xi a_3 + \imath \sqrt{\omega^2 a_1 - \xi^2 \det A} \right) \frac{x-a}{a_1}} e^{\imath \xi y} \mathrm{d}\xi$$

$$+ \frac{1}{\sqrt{2\pi}} \int_{\mathbb{R}^+} \hat{\varphi}_+^0(\xi) \, e^{\left(-\imath\xi a_3+\imath\sqrt{\omega^2 a_1-\xi^2 \det A}\right)\frac{x-a}{a_1}} e^{\imath\xi y} \mathrm{d}\xi.$$

By using Lemma 5.2.1, since $\mathbb{R}^- \subset \mathbb{C}_{\omega,\theta}^-$, we can replace the first line of the formula by

$$\frac{e^{\imath\theta}}{\sqrt{2\pi}} \int_{\mathbb{R}^-} \hat{\varphi}_+^{0,\theta}(\xi e^{\imath\theta}) \, e^{\left(-\imath\xi a_3+\imath\sqrt{\omega^2 a_1-\xi^2 \det A}\right)\frac{x-a}{a_1}} e^{\imath\xi y} \mathrm{d}\xi.$$

To complexify the trace in the second line (for $\xi \in \mathbb{R}^+$), as $\mathbb{R}^+ \not\subset \mathbb{C}_{\omega,\theta}^-$, it is necessary again to change the path of integration from $\mathbb{R}^+$ to a line included in $\mathbb{C}_{\omega,\theta}^-$. We have the following lemma which is analog to Lemma 5.3.1.

Lemma 5.7.1. *For $\theta \in (0, \pi/2)$, we have*

$$\int_{\mathbb{R}^+} \hat{\varphi}_+^0(\xi) e^{\left(-\imath\xi a_3+\imath\sqrt{\omega^2 a_1-\xi^2 \det A}\right)\frac{x-a}{a_1}} e^{\imath\xi y} \mathrm{d}\xi$$

$$= \int_{\mathbb{R}^+} \hat{\varphi}_+^{0,\theta}(\eta) \, e^{\left(-\imath\eta e^{-\imath\theta} a_3+\imath\sqrt{\omega^2 a_1-\eta^2 e^{-2\imath\theta} \det A}\right)\frac{x-a}{a_1}} e^{\imath\eta e^{-\imath\theta}(y-a)} \mathrm{d}\eta$$

for all (x,y) in $\Omega_+^0(\theta, A) := \left\{(x,y) \in \Omega^0, \left(\sqrt{\det A}\cos\theta + a_3\sin\theta\right)(x-a) > a_1 \sin\theta(y-a)\right\}$.

The proof of this lemma is based on the same reasoning as the one for Lemma 5.3.1. Summing up, we have proved that

$$P^0(\varphi_+^0)(x,y) = P_+^{0,\theta}(\varphi_+^{0,\theta})(x,y), \text{ for } (x,y) \in \Omega_+^0(\theta, A),$$

where we have set

$$\forall \varphi \in L^2(\mathbb{R}^+), \quad P_+^{0,\theta}(\varphi)(x,y) = \frac{e^{\imath\theta}}{\sqrt{2\pi}} \int_{\mathbb{R}^-} \hat{\varphi}(\xi e^{\imath\theta}) \, e^{\left(-\imath\xi a_3+\imath\sqrt{\omega^2 a_1-\xi^2 \det A}\right)\frac{x-a}{a_1}} e^{\imath\xi y} \mathrm{d}\xi$$

$$+ \frac{1}{\sqrt{2\pi}} \int_{\mathbb{R}^+} \hat{\varphi}_+^{0,\theta}(\eta) \, e^{\left(-\imath\eta e^{-\imath\theta} a_3+\imath\sqrt{\omega^2 a_1-\eta^2 e^{-2\imath\theta} \det A}\right)\frac{x-a}{a_1}} e^{\imath\eta e^{-\imath\theta}(y-a)} \mathrm{d}\eta.$$

$$(5.47)$$

In particular, the half-line Σ_-^1 is included in $\Omega_+^0(A, \theta)$ if

$$\tan\theta > -\frac{\sqrt{\det A}}{a_3} \text{ for } a_3 > 0 \text{ or } \tan\theta < -\frac{\sqrt{\det A}}{a_3} \text{ for } a_3 < 0. \qquad (5.48)$$

In order to recover a certain symmetry in ξ, we can again change the path of integration of the Fourier variable from $\mathbb{R}^-$ to $e^{-\imath\theta}\mathbb{R}^-$ but this will reduce again the domain of validity of the expression. Indeed, we can show that

$$P^0(\varphi_+^0)(x,y) = P_{+-}^{0,\theta}(\varphi_+^{0,\theta})(x,y), \text{ for } (x,y) \in \Omega_{+-}^0(\theta, A),$$

where

$$\forall \varphi \in L^2(\mathbb{R}^+), \quad P_{+-}^{0,\theta}(\varphi) = \frac{1}{\sqrt{2\pi}} \int_{\mathbb{R}} \hat{\varphi}_+^{0,\theta}(\eta) \, e^{\left(-\imath\eta e^{-\imath\theta} a_3+\imath\sqrt{\omega^2 a_1-\eta^2 e^{-2\imath\theta} \det A}\right)\frac{x-a}{a_1}} e^{\imath\eta e^{-\imath\theta}(y-a)} \mathrm{d}\eta,$$

$$(5.49)$$

with

$$\Omega_{+-}^0(\theta, A) := \{(x,y) \in \Omega_+^0(\theta, A), \left(\sqrt{\det A}\cos\theta - a_3\sin\theta\right)(x-a) > -a_1 \sin\theta(y-a)\}.$$

In particular, the half-line Σ_-^1 is included in $\Omega_{+-}^0(\theta, A)$ if the same condition (5.48) is satisfied.

The integral operators are obtained in the same manner. However, due to the anisotropy, the operators are a priori different for each $j \in \{0, 1, 2, 3\}$.

For example, the function $P^0(\varphi^0)$ coincides with $P_{+-}^{0,\theta}(\varphi_+^{0,\theta})$ on $\Sigma_-^1 \subset \Omega^0(\theta, A)$ which is

$$P_{+-}^{0,\theta}(\varphi_+^{0,\theta}) = \frac{1}{\sqrt{2\pi}} \int_{\mathbb{R}} \hat{\varphi}_+^{0,\theta}(\eta) \, e^{\left(-\imath\eta e^{-\imath\theta}a_3 + \imath\sqrt{\omega^2 a_1 - \eta^2 e^{-2\imath\theta}\det A}\right)\frac{x-a}{a_1}} \, e^{\imath\eta e^{-\imath\theta}(y-a)} \mathrm{d}\eta.$$

This function is analytic with respect to x in the complex neighborhood of Σ_-^1. We define an integral operator

$$\forall \psi \in L^2(\mathbb{R}^+), \quad D_+^{0,1,\theta} \, \psi(t) := \frac{1}{\sqrt{2\pi}} \int_{\mathbb{R}} \hat{\psi}(\eta) \, e^{\left(-\imath\eta e^{-\imath\theta}a_3 + \imath\sqrt{\omega^2 a_1 - \eta^2 e^{-2\imath\theta}\det A}\right)\frac{t}{a_1}} \mathrm{d}\eta, t \in \mathbb{R}^+, \quad (5.50)$$

and with this operator we have

$$D_+^{0,1,\theta} \, \varphi_+^{0,\theta}(t) = P_{+-}^{0,\theta}(\varphi_+^{0,\theta})(a + te^{\imath\theta}, a), \quad \forall t \in \mathbb{R}^+. \quad (5.51)$$

We define all operators $D^{j,j\pm1}$ for all $j \in \{0, 1, 2, 3\}$ in a similar manner.

Similarly, we define an integral operator

$$\forall \psi \in L^2(\mathbb{R}^+), \quad D_-^{0,3,\theta} \, \psi(t) := \frac{e^{\imath\theta}}{\sqrt{2\pi}} \int_{\mathbb{R}^-} \hat{\varphi}(\xi e^{\imath\theta}) \, e^{\left(-\imath\xi a_3 + \imath\sqrt{\omega^2 a_1 - \xi^2 \det A}\right)\frac{t}{a_1}} e^{-\imath\xi a} \mathrm{d}\xi$$

$$+ \frac{1}{\sqrt{2\pi}} \int_{\mathbb{R}^+} \hat{\varphi}_+^{0,\theta}(\eta) \, e^{\left(-\imath\eta e^{-\imath\theta}a_3 + \imath\sqrt{\omega^2 a_1 - \eta^2 e^{-2\imath\theta}\det A}\right)\frac{t}{a_1}} e^{-2\imath\eta e^{-\imath\theta}a} \mathrm{d}\eta.$$

$$(5.52)$$

and with this operator we have

$$D_-^{0,3,\theta} \, \varphi_+^{0,\theta}(t) = P_+^{0,\theta}(\varphi_+^{0,\theta})(a + te^{\imath\theta}, -a), \quad \forall t \in \mathbb{R}^+. \quad (5.53)$$

Again, we define all operators $D_-^{j,j\pm1}$ for all $j \in \{0, 1, 2, 3\}$ in a similar manner. We also define the operators $D_{*,\pm}^{j,j\pm1}$ for all $j \in \{0, 1, 2, 3\}$ from $P^{j,j\pm1,\theta}(g^j)(a + te^{\imath\theta}, \pm a)$.

Finally, we have a system of equation

$$\begin{vmatrix} \varphi_-^{j+1,\theta} = D_+^{j,j+1,\theta}(\varphi_+^{j,\theta}) + D_-^{j,j+1,\theta}(\varphi_-^{j,\theta}) + D_{*,+}^{j,j+1,\theta}(g^j), \\ \varphi_+^{j-1,\theta} = D_-^{j,j-1,\theta}(\varphi_+^{j,\theta}) + D_+^{j,j-1,\theta}(\varphi_-^{j,\theta}) + D_{*,-}^{j,j-1,\theta}(g^j), \quad j \in \mathbb{Z}/4\mathbb{Z}. \end{vmatrix} \quad (5.54)$$

To simulate the method, we take

$$A = \begin{pmatrix} 1 & 0.8 \\ 0.8 & 1 \end{pmatrix},$$

with the source term

$$g = \frac{1}{4\imath} H(\omega r) \text{ on } \partial\mathcal{O},$$

and $\theta = \pi/6$. In Figure 5.15 (left), we represent the real part of $P^0(\varphi^{0,\theta})$ in Ω_{Rec}^0. Notice that the validity region is no longer symmetric due to the anisotropy. In Figure 5.15 (right), we represent the real part of $P^0(\varphi^{0,\theta})$ in Ω_{Rec}.
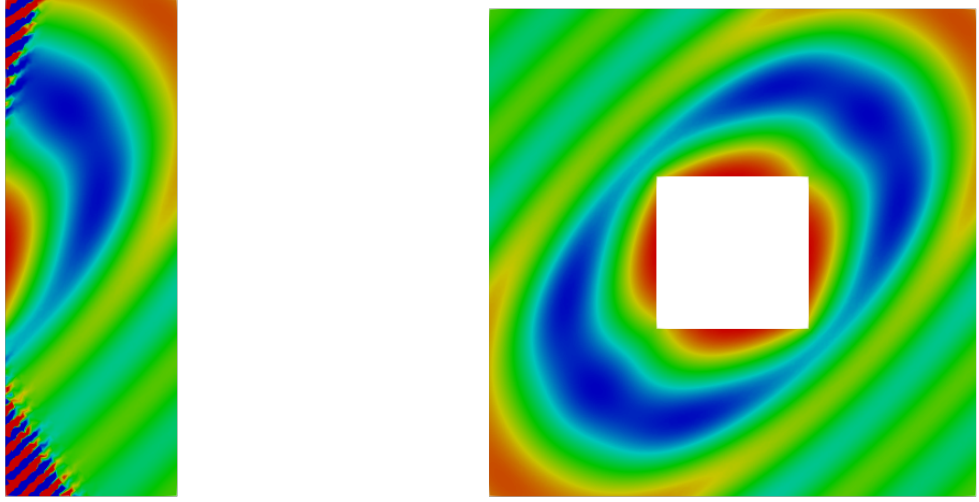
Figure 5.15: On the left: the real part of the reconstructed solution in Ω_{Rec}^0 given the complexified trace of the Hankel function with $\theta = \pi/6$. On the right: the real part of the reconstructed solution in Ω_{Rec}.

Perspectives

In this thesis we have studied and implemented the Half-Space Matching Method to solve scattering problems both in 2D and 3D, for acoustic and elastic waves. Some analyses have been done to answer several theoretical questions concerning the method. Let us now present some natural extensions of our work, and several interesting questions that could be considered.

In Chapter 1, the numerical analysis of the HSM formulation for an exterior problem with a general (Robin) boundary condition is almost complete. Error estimates for the discretization parameters (truncation in Fourier integrals $\hat{T}$, truncation in the physical domain T and the discretization step h) were also derived. However, one aspect of the discretization i.e. the quadrature formula was not addressed in the chapter and would be interesting to take into account to complete the analysis. In addition, it would be interesting to do the numerical analysis of the complex-scaled HSM formulation, in order to prove that we re-obtain the exponential decay with respect to T, as observed in the simulations. It seems that the analysis in Chapter 1 extends to the complex-scaled HSM formulation without new difficulties, but it is to be verified.

The extension of the method to the 3D elastic plate was addressed in Chapter 3. Due to time limitation, we were only able to show some numerical results in the isotropic case. However, the method developed in this chapter is actually applicable to the anisotropic case. The only additional cost compared to the isotropic case is that the modes in the strips have to be computed for all Fourier variable ξ, while in the isotropic case it is enough to compute the mode for $\xi = 0$ and then apply a simple rotation formula to obtain the modes for other $\xi \in \mathbb{R}$. This simulation will be implemented in the near future.

Motivated by the HSM formulation in the 3D elastic plate, in Chapter 4 we have started a theoretical analysis of the multi-unknown HSM formulation involving the traces and normal traces of the solution. We have shown that the variational formulation for this method is very different from the standard HSM formulation, and the proof for equivalence with the original problem brought us to consider an analytic continuation in an unusual Riemann-surface-like domain. The next step is then to establish a stability result. The difficulty is that the formulation is not in an L^2 framework, but rather in $H^{1/2}$ and $H^{-1/2}$. Furthermore, the test functions are taken not in the same spaces as the unknowns. Thus, this question is still open.

Also in Chapter 4, multi-unknown formulations involving integral representations with Green's functions were developed. In the end, we showed an application of this formulation for a scattering problem in a "half-plane" bordered by a stair boundary. However, to simplify the formulation, we only considered a particular incident wave which vanishes on the exterior of the bounded domain, achieved by tuning the height of the stair. In general, the definition of the incident field is more intricate. The difficulty comes from the fact that the reflected field (the reflection of the plane wave by the boundary Σ) is a priori different for Σ^+ and Σ^- (see Figure 5.16). Thus, by taking the subdomains Ω^1 and Ω^2 as illustrated in Figure 5.16, the incident field can be defined differently in each subdomain

$$p_{inc}^j = p_{plane} + p_{ref}^j, \quad \text{in } \Omega^j, j \in \{1, 2\}.$$
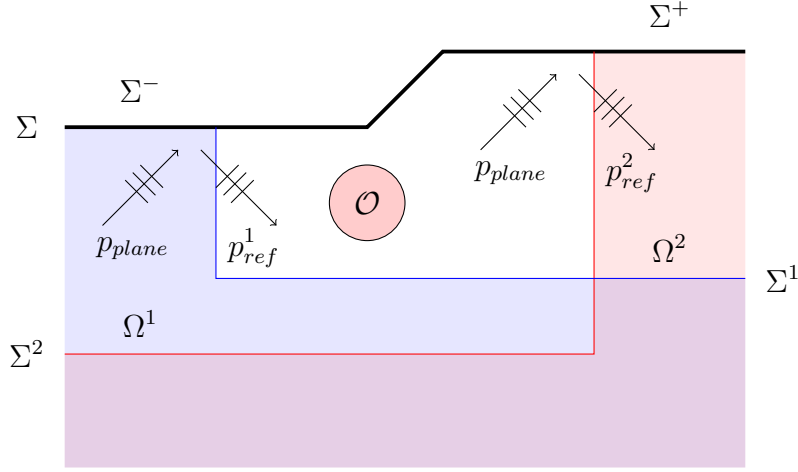
Figure 5.16: Scattering problem in a "half-plane" bordered with a stair-like curve.

These different reflected field should also be considered in the compatibility relation.

There are also several extensions of the HSM formulation that were not discussed in the thesis but are interesting to consider:

1. Multiple scattering

   In the case where there are several defects far from each other in the inspected piece, englobing all the defects and taking a Finite Element representation would be expensive. It is more advantageous to consider several Finite Element boxes, one around each obstacle (see [36, 37]), and then establish the HSM formulation on strips around each obstacle. Figure 5.17 illustrates the configuration of the domain for 2 Finite Element boxes and 8 strips, 4 for each box. We can consider an iterative method where the scattered field from one obstacle in an iteration becomes the incident field for the other obstacles for the next iteration for the concerned half-plate.
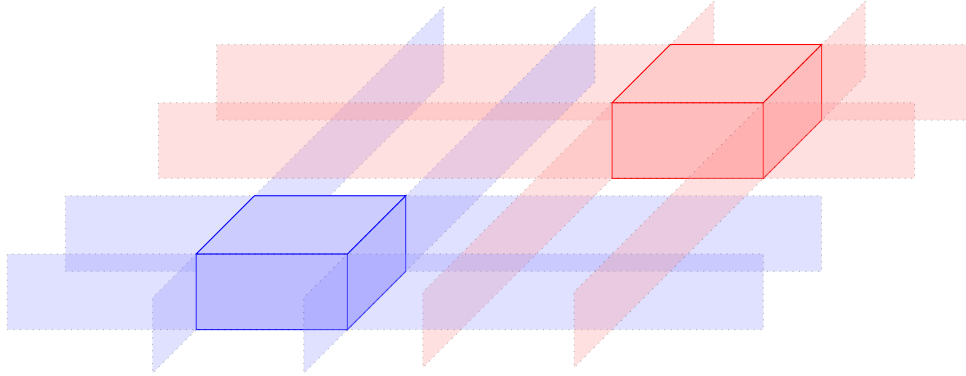
Figure 5.17: Multiple scattering configuration.

2. Scattering in a finite plate

   The HSM formulation considers an infinite plate so that we do not have the interaction between the defects and the border of the plate. The evident extension of the method is then to consider a scattering problem in a finite plate with localized defects. Concurrently in CEA, J. Barras is working on a pencil method to consider the radiation problem in a finite healthy (without defect) plate [11, 65, 66]. By combining the pencil method and the HSM method, we could consider a scattering problem with localized defects in a finite

plate. This method works well in treating straight borders where reflection coefficients are explicitly known as the function of the incidence angle. The idea is then to use the HSM Method to transfer the information of the localized defect to similar quantities.

3. The scattering problem in 3D space.

Finally, the extension of the method to treat the scattering problem in 3D (infinite in the 3 directions) with localized obstacles is also interesting to analyze. In this case, the domain will be decomposed into a Finite Element cube and 6 overlapping half-spaces where the unknowns live on planes that coincide with the faces of the cube instead of lines. Surprisingly, in that case, we have many possible compatibility relations that we can impose because the number of edges (12) is greater that the number of faces (6). We have some arbitrary choice to take, which induces some loss of symmetry in the formulation. The analysis of this method seems immediate, but it is to be verified. This extension might also be used to treat a diffraction by quarter plane [5, 6].
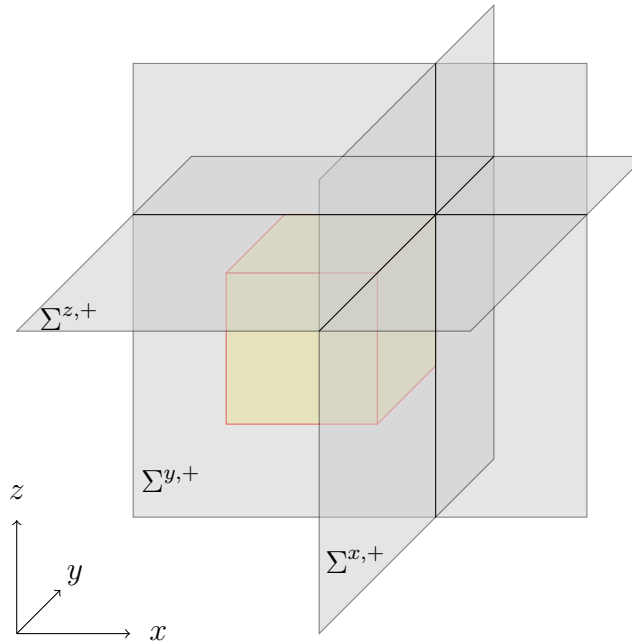

Figure 5.18: Overlapping zones of the half-spaces for the HSM method for 3D case

Appendices

Appendix A

Proof of Lemma 1.3.5

Let us remind the definition of the operator L_N. For all $\psi \in L^2(\Sigma^0)$, we consider the problem

$$\left|\begin{array}{ll} -\Delta v = 0 & \text{in } \Omega^0, \\ \beta \dfrac{\partial v}{\partial x} = \psi & \text{on } \Sigma^0. \end{array}\right. \tag{A.1}$$

This problem has a unique solution v in the following weighted Sobolev space (see for instance [52, Chap. 6]):

$$\left\{ u \in L^2_{loc}(\Omega^0) \, \bigg| \, \frac{1}{r^{3/2}} u \in L^2(\Omega^0), \, \frac{1}{\sqrt{r}} \nabla u \in L^2(\Omega^0) \right\}.$$

The operator L_N is defined as

$$L_N : L^2(\Sigma^0) \to L^2(\Sigma^1 \cap \Omega^0),$$

$$L_N \psi := \beta \left. \frac{\partial}{\partial x^1} v(\psi) \right|_{\Sigma^1 \cap \Omega^0}.$$

We want to show in this appendix that

1. The operator L_N is continuous from $L^2(\Sigma^0)$ in $L^2(\Sigma^1 \cap \Omega^0)$ and its norm is bounded by 1;

2. $\exists \, C \in (0, 1), \quad \forall \psi \in L^2(\Sigma^0), \quad \|L_N \chi_{(a_0^+, +\infty)} \psi\| \le C \|\chi_{(a_0^+, +\infty)} \psi\|$;

3. $L_N \chi_{(-\infty, a_0^-)}$ is a compact operator from $L^2(\Sigma^0)$ in $L^2(\Sigma^1 \cap \Omega^0)$.

Let us begin the proof which is based on Mellin techniques.

1. Denoting (r, θ) the polar coordinates (the center is the intersection point between Σ^0 and $(\Sigma^1 \cap \Omega^0)$) defined by

$$\left|\begin{array}{l} r = \sqrt{(x - l^0)^2 + (y - a_0^+)^2} \; \in \; (0, +\infty), \\ \theta = \dfrac{\pi}{2} - \arctan(\dfrac{y - a_0^+}{x - l^0}) \; \in \; (0, \pi). \end{array}\right. \tag{A.2}$$

We introduce the function w defined for almost everywhere $(t, \theta) \in \mathcal{B} \equiv \mathbb{R} \times (0, \pi)$ by $w(t, \theta) = v(x, y)$ where $t = \ln r$ and (r, θ) is defined in (A.2). It is the solution of

$$\left|\begin{array}{rcl} -\Delta_{t,\theta} w = 0 & \text{in } \mathcal{B}, \\ \beta \dfrac{\partial w}{\partial \theta}(t, 0) & = & \psi_0(t) \; := \; e^t \, \psi(e^t + a_0^+), \\ -\beta \dfrac{\partial w}{\partial \theta}(t, \pi) & = & \psi_\pi(t) \; := \; e^t \, \psi(-e^t + a_0^+). \end{array}\right. \tag{A.3}$$

153

We can show by a simple change of variable that

$$\psi \in L^2(\Sigma^0) \quad \Rightarrow \quad t \mapsto e^{-t/2}\psi_0 \in L^2(\mathbb{R}) \quad \text{and} \quad t \mapsto e^{-t/2}\psi_\pi \in L^2(\mathbb{R}), \qquad (A.4)$$

and

$$\left\| e^{-t/2}\psi_0 \right\|_{L^2(\mathbb{R})} = \|\psi\|_{L^2(a_0^+, +\infty)} \quad \text{and} \qquad \left\| e^{-t/2}\psi_\pi \right\|_{L^2(\mathbb{R})} = \|\psi\|_{L^2(-\infty, a_0^+)}. \qquad (A.5)$$

It is possible to compute explicitly w by applying the Fourier-Laplace transform which is defined as

$$\check{u}(\lambda) \equiv [\mathcal{M}_{t\to\lambda}](\lambda) := \int_{\mathbb{R}} e^{-\lambda t} u(t)\mathrm{d}t. \qquad (A.6)$$

It is an isomorphism between $\{u, e^{\gamma t}u \in L^2(\mathbb{R})\}$ and $L^2(l_{-\gamma})$ where $l_{-\gamma} = \{\lambda = -\gamma + is, s \in \mathbb{R}\}$, for all $\gamma \in \mathbb{R}$ and we have the Plancherel formula

$$\int_{\mathbb{R}} e^{2\gamma t}|u(t)|^2\mathrm{d}t = \frac{1}{2\pi i}\int_{l_{-\gamma}} |\check{u}(\lambda)|^2\mathrm{d}\lambda := \|\check{u}\|^2_{L^2(l_{-\gamma})}. \qquad (A.7)$$

We have in particular thanks to (A.4-A.5)

$$\begin{aligned}
\lambda \mapsto \check{\psi}_0(\lambda) \in L^2(l_{1/2}), \quad \|\check{\psi}_0\|_{L^2(l_{1/2})} = \|\psi\|_{L^2(a_0^+, +\infty)}, \\
\lambda \mapsto \check{\psi}_\pi(\lambda) \in L^2(l_{1/2}), \quad \|\check{\psi}_\pi\|_{L^2(l_{1/2})} = \|\psi\|_{L^2(-\infty, a_0^+)}.
\end{aligned} \qquad (A.8)$$

Applying the Fourier-Laplace transform to w, we have $\check{w}(\bullet, \theta) = \mathcal{M}_{t\to\lambda}w(\bullet, \theta)$ which satistifes

$$\left|
\begin{aligned}
-\lambda^2\check{w}(\lambda, \theta) - \frac{\partial^2\check{w}}{\partial\theta^2}(\lambda, \theta) &= 0, \qquad \forall \lambda \in \mathbb{C} \\
\beta\frac{\partial\check{w}}{\partial\theta}(\lambda, 0) &= \check{\psi}_0(\lambda), \\
-\beta\frac{\partial\check{w}}{\partial\theta}(\lambda, \pi) &= \check{\psi}_\pi(\lambda),
\end{aligned}
\right.$$

and we can easily find the solution of this equation. We obtain for $\lambda \notin \mathbb{Z}$

$$\check{w}(\lambda, \theta) = \frac{\cos(\lambda(\pi - \theta))}{\beta\,\lambda\,\sin(\lambda\pi)}\check{\psi}_0(\lambda) + \frac{\cos(\lambda\theta)}{\beta\,\lambda\,\sin(\lambda\pi)}\check{\psi}_\pi(\lambda),$$

which, for $\lambda \notin \mathbb{Z}$, leads to

$$\beta\frac{\partial\check{w}}{\partial\theta}(\lambda, \theta) = A(\lambda, \pi - \theta)\check{\psi}_0(\lambda) - A(\lambda, \theta)\check{\psi}_\pi(\lambda),$$

where

$$A(\lambda, \theta) = \frac{\sin(\lambda\theta)}{\sin(\lambda\pi)}.$$

Moreover, we can show that for all $\theta \in (0, \pi), s \mapsto |A(1/2 + is, \theta)|$ is in $L^\infty(\mathbb{R})$ and its supremum is attained at $s = 0$ and it is equal to $\sin(\theta/2)$. Using the Cauchy Schwartz inequality $(ab + cd)^2 \le (a^2 + c^2)(b^2 + d^2)$, we have then, for all $\theta \in (0, \pi)$

$$\left\| \beta\frac{\partial\check{w}}{\partial\theta}(\lambda, \theta) \right\|^2_{L^2(l_{1/2})} \le \left(\cos(\theta/2)\,\|\check{\psi}_0\|_{L^2(l_{1/2})} - \sin(\theta/2)\,\|\check{\psi}_\pi\|_{L^2(l_{1/2})} \right)^2$$

$$\le \left(\|\check{\psi}_0\|^2_{L^2(l_{1/2})} + \|\check{\psi}_\pi\|^2_{L^2(l_{1/2})} \right) = \|\psi\|^2_{L^2(\Sigma^0)}.$$

The last inequality for $\theta = \theta^{0,1}$, after the change of variable $r = e^t$, yields to

$$\beta \frac{\partial v}{\partial x^1}\bigg|_{\Sigma^1 \cap \Omega^0} \in L^2(\Sigma^1 \cap \Omega^0)$$

and

$$\left\|\beta \frac{\partial v}{\partial x^1}\bigg|_{\Sigma^1 \cap \Omega^0}\right\|_{L^2(\Sigma^1 \cap \Omega^0)} \leq \|\psi\|_{L^2(\Sigma^0)}. \tag{A.9}$$

We have shown that the operator L_N is continuous from $L^2(\Sigma^0)$ to $L^2(\Sigma^1 \cap \Omega^0)$ and its norm is bounded by 1.

2. The norm of $L_N \chi_{(a^0, +\infty)}$ can be deduced from the previous computation by taking $\psi_{(-\infty, a_0^+)} = 0$ or equivalently $\check{\psi}_\pi = 0$. We get for all $\theta \in (0, \pi)$

$$\left\|\beta \frac{\partial \check{w}}{\partial \theta}(\lambda, \theta)\right\|_{L^2(l_{1/2})} \leq \cos(\theta/2)\|\check{\psi}_0(\lambda)\|_{L^2(l_{1/2})} = \cos(\theta/2)\|\psi\|_{L^2(a_0^+, +\infty)}. \tag{A.10}$$

from where we conclude that the norm of the operator $L_N \chi_{(a^0, +\infty)}$ is bounded by $\cos(\theta^{0,1}/2)$.

3. Finally let us consider the previous computation with $\psi = 0$ on $(a_0^-, +\infty)$. This corresponds to take $\psi_0 = 0$ and $\psi_\pi = e^t \psi(-e^t + a_0^+)$. Since ψ vanishes on $(a_0^-, +\infty)$, we have $e^{-\gamma t} \psi_\pi$ is in $L^2(\mathbb{R})$ for any $\gamma > 1$ and so, by (A.7), $\check{\psi}_\pi$ is in $L^2(l_\gamma)$ for all $\gamma > 1$. The previous computation yields to

$$\forall \lambda \notin \mathbb{Z}, \quad \beta \frac{\partial \check{w}}{\partial \theta}(\lambda, \theta^{0,1}) = -A(\lambda, \theta^{0,1})\check{\psi}_\pi(\lambda).$$

We can show that

$$\forall \gamma > 1, \ \gamma \notin \mathbb{N}, \quad \sup_{\lambda \in l_\gamma} \lambda A(\lambda, \theta^{0,1}) < +\infty,$$

which enables us to deduce that

$$\forall \gamma > 1, \ \gamma \notin \mathbb{N}, \quad \lambda \frac{\partial \check{w}}{\partial \theta}(\lambda, \theta^{0,1}) \in L^2(l_\gamma).$$

By applying inverse Laplace-Fourier transform, we have then

$$\forall \gamma > 1, \ \gamma \notin \mathbb{N}, \quad e^{-\gamma t} \frac{\partial^2 \check{w}}{\partial t \partial \theta}(t, \theta^{0,1}) \in L^2(\mathbb{R}),$$

and by change of variable,

$$\forall \gamma > 1, \ \gamma \notin \mathbb{N}, \quad r^{-\gamma + 3/2} \partial_r \left(\frac{1}{r}\frac{\partial \check{w}}{\partial \theta}(r, \theta^{0,1})\right) \in L^2(\mathbb{R}^+).$$

If we choose $\gamma = 3/2$, the operator $L_N \chi_{(-\infty, a_0^-)} \in H^1(0, +\infty)$. By compact embedding of $H^1(0, b)$ in $L^2(0, b)$ for any $b > 0$, we show that $\chi_{(0,b)} L_N \chi_{(-\infty, a_0^-)}$ is compact. It suffices to use similar argument as in the proof of Lemma 1.3.3 to show that $\chi_{(b, +\infty)} L_N \chi_{(-\infty, a_0^-)}$ is a Hilbert-Schmidt operator.

Let us now give other properties of L_N which will be useful for the numerical analysis (see Section 1.4). We remind the definition of the symmetric and anti-symmetric operators, defined in the proof of Lemma 1.4.3, S and $A \in \mathcal{L}(L^2(\mathbb{R}))$

$$\forall \psi \in L^2(\mathbb{R}), \quad S\psi(y) = \frac{1}{2}\left(\psi(y) + \psi(2a_0^+ - y)\right), \quad \text{and} \quad A\psi(y) = \frac{1}{2}\left(\psi(y) - \psi(2a_0^+ - y)\right)$$

We remind that $S + A = Id.$, $S^2 = S$, $A^2 = A$, $\|S\| \leq 1$, $\|A\| \leq 1$ and for any $\psi \in L^2(\mathbb{R})$ such that $\psi_{(-\infty, a_0^+)} = 0$, we have

$$\|S\psi\|_{L^2(\mathbb{R})} = \|A\psi\|_{L^2(\mathbb{R})} = \frac{1}{\sqrt{2}} \|\psi\|_{L^2(\mathbb{R})}. \tag{A.11}$$

Let us now study the norm of $L_N S \psi$ and $L_N A \psi$ for any $\psi \in L^2(\mathbb{R})$. By reproducing the previous calculations, we have easily that, writing $\widetilde{(S\psi)_0} = \widetilde{(S\psi)_\pi}$,

$$\|L_N S \psi\|_{L^2(\Sigma^1 \cap \Omega^0)} \leq \sup_{\lambda \in l_{1/2}} \left| A(\lambda, \pi - \theta^{0,1}) - A(\lambda, \theta^{0,1}) \right| \|S\psi\|_{L^2(a, +\infty)}$$

where we remind that

$$\forall \theta \in (0, \pi), \ \forall \lambda \notin \mathbb{Z}, \quad A(\lambda, \theta) = \frac{\sin(\lambda\theta)}{\sin(\lambda\pi)}.$$

We can show that the supremum is attained at $\lambda = 1/2$ and then

$$\sup_{\lambda \in l_{1/2}} \left| A(\lambda, \pi - \theta^{0,1}) - A(\lambda, \theta^{0,1}) \right| = \left| \cos(\theta^{0,1}/2) - \sin(\theta^{0,1}/2) \right|.$$

Using that $\sqrt{2} \|S\psi\|_{L^2(a, +\infty)} = \|S\psi\|_{L^2(\mathbb{R})} \leq \|\psi\|_{L^2(\mathbb{R})}$, we obtain

$$\|L_N S \psi\|_{L^2(\Sigma^1 \cap \Omega^0)} \leq \frac{|\cos(\theta^{0,1}/2) - \sin(\theta^{0,1}/2)|}{\sqrt{2}} \|\psi\|_{L^2(\mathbb{R})}. \tag{A.12}$$

Similarly, we get

$$\|L_N A \psi\|_{L^2(\Sigma^1 \cap \Omega^0)} \leq \frac{\cos(\theta^{0,1}/2) + \sin(\theta^{0,1}/2)}{\sqrt{2}} \|\psi\|_{L^2(\mathbb{R})}. \tag{A.13}$$

Moreover, let us remark, that gathering these inequalities, we obtain an inequality which comparing to (A.9), is not optimal :

$$\|L_N \psi\|_{L^2(\Sigma^1 \cap \Omega^0)} \leq \|L_N S \psi\|_{L^2(\Sigma^1 \cap \Omega^0)} + \|L_N A \psi\|_{L^2(\Sigma^1 \cap \Omega^0)} \leq \sqrt{2} \max(\cos(\theta^{0,1}/2), \sin(\theta^{0,1}/2)) \|\psi\|_{L^2(\mathbb{R})}.$$
$$\tag{A.14}$$

Moreover, for $\psi \in L^2(\mathbb{R})$ such that $\psi_{(-\infty, a_0^+)} = 0$, using (A.11), we obtain

$$\|L_N \psi\|_{L^2(\Sigma^1 \cap \Omega^0)} \leq \|L_N S\| \|S \psi\|_{L^2(\mathbb{R})} + \|L_N A\| \|A \psi\|_{L^2(\mathbb{R})} \leq C' \|\psi\|_{L^2(\mathbb{R})}$$

where

$$C' = \max(\cos(\theta^{0,1}/2), \sin(\theta^{0,1}/2)) \ \in (0, 1).$$

This result is then not optimal for $\theta^{0,1} \in (0, \pi/2)$ (compared to (A.10)) but the constant C', obtained that way, is still in $(0, 1)$.

Appendix B

Optimization of the quadrature formula

This is a joint work with Stéphanie Chaillat from POEMS.

We are interested in computing some integrals that appear in our integral operators. In the 2D isotropic scalar case, we have two discretized operators (up to symmetry)

$$
D_{\hat{T}}^{0,1}(\psi)(x,y) = \frac{1}{2\pi} \int_{\Sigma_a^0} \psi(y') \, k_D(x,y') \, \mathrm{d}y',
$$

$$
\Lambda_{\hat{T}}^{0}(\psi)(y) = \frac{1}{2\pi} \int_{\Sigma_a^0} \psi(y') \, k_\Lambda(y,y') \, \mathrm{d}y',
$$

(B.1)

with the kernels

$$
k_D(x,y') = \int_{-\hat{T}}^{\hat{T}} e^{\imath \sqrt{\omega^2 - \xi^2}(x-a)} e^{\imath \xi(a-y')} \mathrm{d}\xi,
$$

$$
k_\Lambda(y,y') = \int_{-\hat{T}}^{\hat{T}} \imath \sqrt{\omega^2 - \xi^2} e^{\imath \sqrt{\omega^2 - \xi^2}(b-a)} e^{\imath \xi(y-y')} \mathrm{d}\xi.
$$

(B.2)

Here, we suppose that ω, a, and b are fixed.

To compute these kernels numerically, we are looking for a quadrature rule $(\xi_j, w_j)_{1 \le j \le r}$ such that

$$
\forall x \in [a,T] \text{ and } y' \in [-T,T], \quad \left| k_D - \sum_{j=1}^{r} w_j e^{\imath \sqrt{\omega^2 - \xi_j^2}(x-a)} e^{\imath \xi_j(a-y')} \right| \le \epsilon
$$

$$
\forall y \in [-b,b] \text{ and } y' \in [-T,T], \quad \left| k_\Lambda - \sum_{j=1}^{r} w_j \imath \sqrt{\omega^2 - \xi_j^2} e^{\imath \sqrt{\omega^2 - \xi_j^2}(b-a)} e^{\imath \xi_j(y-y')} \right| \le \epsilon
$$

(B.3)

for a given tolerance ϵ.

The kernel k_D (and also k_Λ) can be written as a linear combination of the real part and the imaginary part of its integrand

$$
k_D(x,y') = \int_{-\hat{T}}^{\hat{T}} \mathrm{Re}\left(e^{\imath \sqrt{\omega^2 - \xi^2}(x-a)} e^{\imath \xi(a-y')} \right) \mathrm{d}\xi + \imath \int_{-\hat{T}}^{\hat{T}} \mathrm{Im}\left(e^{\imath \sqrt{\omega^2 - \xi^2}(x-a)} e^{\imath \xi(a-y')} \right) \mathrm{d}\xi.
$$

Thus, we can write more generally that we compute numerically a set of L integrals

$$
I_\ell(P) = \int_{-\hat{T}}^{\hat{T}} f_\ell(\xi; P) \, \mathrm{d}\xi, \quad \ell \in \{1, 2, \ldots, L\}, P \in \mathcal{P}
$$

(B.4)

where P is a set of parameters and $(f_\ell)_{1 \le \ell \le L}$ are real-valued square integrable functions which are chosen such that the kernels of the integral operators in the HSM formulations are linear combinations of them (in our case, $L = 4$). The parameters in our case are (x, y, y'), obtained from the sampled points from the spatial discretization. Depending on the discretization, we might have a large number K of parameters sampling P. To give an approximation of the size of the problem, if we use $T = 10$ and a discretization step $h = 0.1$, we will have thousands set of parameters. We define a large collection of $m = KL$ *input functions* $\xi \mapsto \phi_i(\xi), 1 \le i \le m$ with

$$\phi_i(\xi) = f_\ell(\xi; P_j), \text{ for some } k \text{ and } l.$$

The objective is then to obtain a quadrature rule that accurately integrates these input functions $(\phi_i)_{1 \le i \le m}$.

Standard choice of quadrature to compute the Fourier integrals used in this thesis is the Gauss-Lagrange quadrature. To get a certain degree of accuracy, we have at least 2 naive methods: we can either apply a higher order Gauss-Lagrange quadrature or we divide the segment in many smaller segments and apply a lower order (for example 3) quadrature. However, the quadrature obtained by these methods are redundant: we could obtain a quadrature with far less points with the same accuracy. We use the Generalized Gaussian quadrature (GCQ) developed in detail in [20, 22] to obtain the optimal quadrature by doing the following steps:

1. compute an oversized quadrature rule $(\hat{\xi}_k, \hat{w}_k)_{1 \le k \le p}$ that integrates accurately all products of input functions $(\phi_i)_{1 \le i \le m}$,

2. find a (low) numerical rank r of the set of input functions and compress them to r L^2-orthonormal functions $(u_i)_{1 \le i \le r}$,

3. construct an r-point quadrature rule $(\xi_k, w_k)_{1 \le k \le r}$ that achieves the same accuracy as Step 1.

Step 1: adaptive construction of an oversized quadrature

We construct an oversized quadrature $(\hat{\xi}_k, \hat{w}_k)_{1 \le k \le p}$ to integrate all products of input functions with precision ϵ_1

$$\left| \int_{-\hat{T}}^{\hat{T}} \phi_i(\xi)\phi_j(\xi)\mathrm{d}\xi - \sum_{k=1}^{p} \hat{w}_k \phi_i(\hat{\xi}_k)\phi_j(\hat{\xi}_k) \right| \le \epsilon_1. \tag{B.5}$$

This quadrature $(\hat{\xi}_k, \hat{w}_k)_{1 \le k \le p}$ is obtained iteratively. For each ϕ_i, we construct an order-l Gauss-Legendre expansion

$$\forall \xi \in [-\hat{T}, \hat{T}], \quad \phi_i(\xi) \approx \sum_{j=1}^{l} \alpha_j P_j(\xi),$$

where $P_n(\xi)$ is the n-th Legendre polynomial. This parameter l should be large enough to capture the singularities, but small enough for the algorithm to be efficient. This expansion is compared to $2l$-nodes expansion, and if the difference is larger than the given tolerance ϵ_1 (based on the L^2-norm of the difference between order-l and order $2l$), we split the integration interval into two subintervals of equal length and use order-l expansion in each subintervals. This process is repeated until the difference is less than the tolerance ϵ_1 or it reaches the maximum number of subdivision (we set it to 30). Finally, we gather all nodes for all ϕ_i into a single list and construct a quadrature formula by concatenating the l-points quadrature in each interval. The size of the quadrature p is usually large due to the poor performance of classical quadratures in integrating singular and oscillatory functions.

Algorithm B.1 Construction of the oversized quadrature rule

1: **Input:** m input functions $\phi_1, \ldots, \phi_m$ defined on the interval $[-\hat{T}, \hat{T}]$, precision ϵ_1, and order l of the piecewise Legendre expansion
2: **for** $i = 1, \ldots, m$
3:        Construct $2l$ Legendre nodes $\xi_1, \ldots, \xi_{2l}$ on $[-\hat{T}, \hat{T}]$.
4:        Compute the coefficients $\alpha_0, \ldots, \alpha_{2l-1}$.
5:        **if** $\displaystyle\sum_{j=l}^{2l-1} |\alpha_j|^2 < \epsilon_1^2$
6:           The order-l Legendre expansion of ϕ_i is sufficient
7:        **else**
8:        Split the interval into two subintervals of equal length
9:        Repeat the procedure until convergence or the interval is too small
10:       **end if**
11:       Store the endpoints of each interval
12: **end for**
13: Gather all the endpoints into a single list and eliminate repeated values
14: Concatenate the l–points Legendre quadratures on each subinterval
15: **Output:** p-point quadrature rule $(\hat{\xi}_i, \hat{w}_i)_{1 \leq i \leq p}$

Step 2: compression of the input functions to rank r

Up to this point, we have obtained an accurate quadrature rule but it is unacceptably large. This quadrature rule can be reduced by observing that the values $\phi_i(\hat{\xi}_k)$ of the input functions sampled at the p nodes $\hat{\xi}_k$ are highly redundant. To show this, we first define the numerical rank of a matrix. If X is a $n \times m$ matrix, we call the smallest nonnegative integer k such that the singular value $\sigma_{k+1}(X) < \epsilon$ the numerical rank of X to precision ϵ. We define a matrix as

$$A \in \mathbb{R}^{p \times m}, \quad A_{ki} := \sqrt{\hat{w}_k} \, \phi_i(\hat{\xi}_k). \tag{B.6}$$

This matrix A has a numerical rank r which is much smaller than both p and m. Thus, we build an orthonormal basis $u_1, \ldots, u_r$ by applying a rank-revealing QR decomposition to a certain precision:

$$\|A - QR\| \leq \epsilon_2.$$

Therefore, the initial large set of input functions $\phi_1, \ldots, \phi_m$ is compressed into the smaller set $u_1, \ldots, u_r$ of functions sampled at the Legendre nodes $\hat{\xi}_1, \ldots, \hat{\xi}_p$

$$u_j(\tilde{\xi}_i) = Q_{ij}/\sqrt{\tilde{w}_i}, \quad (1 \leq i \leq p, \; 1 \leq j \leq r). \tag{B.7}$$

Algorithm B.2 Compression of the input functions to a set of orthogonal functions of rank r

---

1: **Input:** m input functions $\phi_1, \ldots, \phi_m$ sampled at $\hat{\xi}_k$ ($1 \leq k \leq p$), p point quadrature rule $(\hat{\xi}_i, \hat{w}_i)_{1 \leq i \leq p}$, and precision ϵ_2
2: Compute the matrix $A \in \mathbb{R}^{p \times m}$ defined by (B.6).
3: Compute the rank-revealing QR decomposition to precision ϵ_2 of A
4: Construct the r orthonormal functions $u_1, \ldots, u_r$ defined by their values, as given by (B.7)
5: **Output:** orthonormal functions $u_1, \ldots, u_r$ sampled at the Legendre nodes $\hat{\xi}_1, \ldots, \hat{\xi}_p$

Step 3: construction of a r-point quadrature rule

As the last step, we are looking for an r-point quadrature rule $(\xi_i, w_i)_{1 \leq i \leq r}$ that accurately integrates the r orthonormal functions $(u_i)_{1 \leq i \leq r}$ that we have obtained from the previous step. It consists in finding the minimum norm solution $Z \in \mathbb{R}^p$ of the underdetermined system of equations

$$BZ = S, \tag{B.8}$$

with the matrix $B \in \mathbb{R}^{r \times p}$ and the vector $S \in \mathbb{R}^r$ given by

$$
\begin{aligned}
B_{ik} &:= \sqrt{\hat{w}_k}\, u_i(\hat{\xi}_k) && (1 \leq i \leq r, 1 \leq k \leq p), \\
S_i &:= \sum_{j=1}^{p} u_i(\hat{\xi}_k)\hat{w}_k \approx \int_{-\hat{T}}^{\hat{T}} u_i(\xi)\mathrm{d}\xi && (1 \leq i \leq r).
\end{aligned}
\tag{B.9}
$$

Again, we construct a rank-revealing QR decomposition

$$B\Pi = Q[R_{11}\ R_{12}],$$

where $Q \in \mathbb{R}^{r \times r}$ orthogonal, $R_{11} \in \mathbb{R}^{r \times r}$, $R_{12} \in \mathbb{R}^{r \times (p-r)}$, and $\Pi \in \mathbb{R}^{p \times p}$ a permutation. The permutation Π is to sort the absolute value of the diagonal elements of R_{11} in descending order to obtain more numerical stability. We then obtain the vector Z from

$$R_{11}Z = Q^*S$$

by back substitution. We define the nodes and weights on the basis of the r non-zero entries $Z_{i_1}, \ldots, Z_{i_r}$ of Z by

$$\xi_k = \hat{\xi}_{i_k} \text{ and } w_k = Z_{i_k}\hat{w}_{i_k},$$

where i_k denotes the row index of the non zero entry in the k-th column of Π. This r-point quadrature rule also accurately integrates the input functions $(\phi_i)_{1 \leq i \leq m}$.

Algorithm B.3 Construction of an r-point quadrature rule

1: **Input:** r orthogonal functions $(u_i)_{1 \leq i \leq r}$ and p-point quadrature rule $(\hat{\xi}_k, \hat{w}_k)_{1 \leq k \leq p}$
2: Construct the matrix B and vector R as defined by (B.9)
3: Construct the rank-revealing QR decomposition: $B\Pi = Q[R_{11}\ R_{12}]$
4: Compute the solution $Z \in \mathbb{R}^r$ of $R_{11}Z = Q^*r$ using backsubstitution
5: Form the new r-point quadrature $(\xi_k, w_k)_{1 \leq k \leq r}$ by setting $\xi_k = \hat{\xi}_{i_k}$ and $w_k = Z_{i_k}\hat{w}_{i_k}$, with i_k the row index of the non zero entry in the k-th column of Π
6: **Output:** r-point quadrature rule $(\xi_j, w_j)_{(1 \leq j \leq r)}$.

Applying this method to the 2D scalar case with $\omega = 1, a = 1, T = 10, h = 0.1$, and $\hat{T} = 10$, we usually use a quadrature formula with 3000 nodes. By using this method, we obtain a quadrature formula with only 140 points and we obtain the same accuracy.

As for the 3D isotropic elastic plate case, there are many more kernels compared to the 2D scalar case, and each kernel produces a 3×3 matrices. The kernels of the operators are the

following:

$$k_{DD}(x, z, y', z') = \int_{-\hat{T}}^{\hat{T}} \sum_{k=1}^{N} \hat{\mathcal{T}}_k^-(-\xi; z') \otimes \hat{\mathcal{U}}_k^+(\xi; z) e^{\imath \beta_k^+(\xi)(x-a)} e^{\imath \xi(a-y')} \mathrm{d}\xi,$$

$$k_{DN}(x, z, y', z') = \int_{-\hat{T}}^{\hat{T}} \sum_{k=1}^{N} \hat{\mathcal{U}}_k^-(-\xi; z') \otimes \hat{\mathcal{U}}_k^+(\xi; z) e^{\imath \beta_k^+(\xi)(x-a)} e^{\imath \xi(a-y')} \mathrm{d}\xi,$$

$$k_{ND}(x, z, y', z') = \int_{-\hat{T}}^{\hat{T}} \sum_{k=1}^{N} \hat{\mathcal{T}}_k^-(-\xi; z') \otimes \hat{\mathcal{T}}_k^+(\xi; z) \imath \beta_k^+(\xi) e^{\imath \beta_k^+(\xi)(x-a)} e^{\imath \xi(a-y')} \mathrm{d}\xi,$$

$$k_{NN}(x, z, y', z') = \int_{-\hat{T}}^{\hat{T}} \sum_{k=1}^{N} \hat{\mathcal{U}}_k^-(-\xi; z') \otimes \hat{\mathcal{T}}_k^+(\xi; z) \imath \beta_k^+(\xi) e^{\imath \beta_k^+(\xi)(x-a)} e^{\imath \xi(a-y')} \mathrm{d}\xi,$$

$$k_{\Lambda D}(y, z, y', z') = \int_{-\hat{T}}^{\hat{T}} \sum_{k=1}^{N} \hat{\mathcal{U}}_k^-(-\xi; z') \otimes \hat{\mathcal{T}}_k^+(\xi; z) \imath \beta_k^+(\xi) e^{\imath \beta_k^+(\xi)(b-a)} e^{\imath \xi(y-y')} \mathrm{d}\xi,$$

$$k_{\Lambda N}(y, z, y', z') = \int_{-\hat{T}}^{\hat{T}} \sum_{k=1}^{N} \hat{\mathcal{T}}_k^-(-\xi; z') \otimes \hat{\mathcal{T}}_k^+(\xi; z) \imath \beta_k^+(\xi) e^{\imath \beta_k^+(\xi)(b-a)} e^{\imath \xi(y-y')} \mathrm{d}\xi,$$

$$k_{\Gamma D}(y, z, y', z') = \int_{-\hat{T}}^{\hat{T}} \sum_{k=1}^{N} \hat{\mathcal{T}}_k^-(-\xi; z') \otimes \hat{\mathcal{T}}_k^+(\xi; z) \imath \beta_k^+(\xi) e^{\imath \xi(y-y')} \mathrm{d}\xi,$$

$$k_{\Gamma N}(y, z, y', z') = \int_{-\hat{T}}^{\hat{T}} \sum_{k=1}^{N} \hat{\mathcal{U}}_k^-(-\xi; z') \otimes \hat{\mathcal{T}}_k^+(\xi; z) \imath \beta_k^+(\xi) e^{\imath \xi(y-y')} \mathrm{d}\xi,$$

where $(\hat{\mathcal{U}}_k(\xi), \hat{\mathcal{T}}_k(\xi), \beta_k(\xi))$ are obtained from $(\hat{\mathcal{U}}_k(0), \hat{\mathcal{T}}_k^\pm(0), \beta_k(0))$ by Proposition 3.3.2. Thus, from each kernel, we obtain $9N$ integrals where N denotes the number of modes taken into account. If we only take the first 5 modes, there are 360 integrals in total, compared to 2 integrals for the isotropic 2D case. Applying CGQ to this case with $\hat{T} = 13.85$, we obtain a quadrature of 233 nodes which is much less than the usual Gauss-Lagrange quadrature that we used.

Bibliography

[1] R. Adams and J. Fournier. *Sobolev Spaces*. Number 9780080541297. Elsevier Science, 2003.

[2] D. Amos. A subroutine package for bessel functions of a complex argument and nonnegative order. Technical report, Sandia National Laboratory, 1985.

[3] X. Antoine, H. Barucq, and A. Bendali. Bayliss-turkel-like radiation condition on surfaces of arbitrary shape. *Journal of Mathematical Analysis and Applications, Elsevier*, 229(1):184–211, 1999.

[4] T. Apel, S. Nicaise, and J. Pfefferer. Discretization of the poisson equation with non-smooth data and emphasis on non convex domains. *arXiv*, 2015.

[5] R. C. Assier and N. Peake. On the diffraction of acoustic waves by a quarter-plane. *Wave Motion*, 49(1):64–82, 2012.

[6] R. C. Assier and A. V. Shanin. Diffraction by a quarter plane. analytical continuation of spectral functions. *The Quarterly Journal of Mechanics and Applied Mathematics*, 72(1):51–86, 2019.

[7] K. E. Atkinson. *The Numerical Solution of Integral Equations of The Second Kind*. Cambridge University Press, 1997.

[8] D. Aubry and D. Clouteau. A regularized boundary element method for stratified media. *Mathematical and numerical aspects of wave propagation phenomena Proc. 1st International Conference*, pages 660–668, 1991.

[9] V. Baronian. *Couplage des méthodes modale et éléments finis pour la diffraction des ondes élastiques guidées*. PhD thesis, École Polytechnique, 2009.

[10] V. Baronian, A.-S. Bonnet-BenDhia, S. Fliss, and A. Tonnoir. Iterative methods for scattering problems in isotropic and anisotropic elastic waveguides. *Wave Motion*, 64:13–33, 2016.

[11] J. Barras, A. Lhémery, and A. Impériale. Pencil method for computing modal guided wave fields in isotropic finite plates validated by a transient spectral finite element method. *to be submitted*.

[12] I. Bartoli, A. Marzani, F. L. di Scalea, and E. Viola. Modeling wave propagation in damped waveguides of arbitrary cross-section. *Journal of Sound and Vibration*, (3-5):685–707, August 2006.

[13] A. Bayliss and E. Turkel. Radiation boundary conditions for wave-like equations. *Communications on Pure Applied Mathematics*, 33(6):707–725, 1988.

[14] E. Bécache, S. Fauqueux, and P. Joly. Stability of perfectly matched layers, group velocities and anisotropic waves. *Journal of Computational Physics*, 188(2):399–433, 2003.

[15] J.-P. Berenger. A perfectly matched layer for the absorption of electromagnetic waves. *Journal of Computational Physics*, 114:185–200, 1994.

[16] C. Besse, J. Coatléven, S. Fliss, I. Lacroix-Violet, and K. Ramdani. Transparent boundary conditions for locally perturbed infinite hexagonal periodic media. *Communications in Mathematical Sciences*, 11(4):907–938, 2013.

[17] M. Bonnet. *Boundary integral equations methods in solids and fluids.* John Wiley and Sons, 1999.

[18] A.-S. Bonnet-BenDhia, C. Chambeyron, and G. Legendre. On the use of perfectly matched layers in the presence of long or backward guided elastic waves. *Wave Motion*, 51(2):266–283, 2014.

[19] A.-S. Bonnet-BenDhia, S. Fliss, and A. Tonnoir. The halfspace matching method: a new method to solve scattering problem in infinite media. *JCAM*, 338:44–68, 2018.

[20] J. Bremer, Z. Gimbutas, and V. Rokhlin. A nonlinear optimization procedure for generalized gaussian quadratures. *SIAM Journal on Scientific Computing*, 32(4):1761–1788, 2010.

[21] J. M. Brown, E. H. Abramson, and R. J. Angel. Triclinic elastic constants for low albite. *Physics and Chemistry of Minerals*, 2006.

[22] S. Chaillat and M. Bonnet. A new fast multipole formulation for the elastodynamic half-space green's tensor. *Journal of Computational Physics*, 258:787–808, 2014.

[23] G. Chandler. Galerkin's method for boundary integral equations on polygonal domains. *Journal of The Australian Mathematical Society*, 26:1–13, 1984.

[24] S. N. Chandler-Wilde and D. C. Hothersall. Efficient calculation of the green function for acoustic propagation above a homogeneous impedance plane. *Journal of Sound and Vibration*, 180(5):705–724, 1995.

[25] S. N. Chandler-Wilde, S. Langdon, and M. Mokgolele. A high frequency boundary element method for scattering by convex polygons with impedance boundary conditions. *Communications in Computational Physics*, 11(2):573–593, 2012.

[26] X. Claeys. Quasi-local multi-trace boundary integral formulations. *Numerical Methods Partial Differential Equations*, 31(6):2043–2062, 2015.

[27] X. Claeys and R. Hiptmair. Electromagnetic scattering at composite objects: a novel multi-trace boundary integral formulation. *ESAIM Mathematical Modeling Numerical Analysis*, 46:1421–1445, 2012.

[28] X. Claeys, R. Hiptmair, and C. Jerez-Hanckes. Multi-trace boundary integral equations. In D. Gruyter, editor, *Direct and Inverse Problems in Wave Propagation and Applications*, volume 14, pages 51–100. Radon Series of Computational Applied Mathematics, 2013.

[29] M. Dauge. Elliptic boundary value problems on corner domains: Smoothness and asymptotics of solutions. *Springer Berlin Heidelberg*, 2006.

[30] B. Engquist and A. Majda. Absorbing boundary conditions for the numerical simulation of waves. *Mathematics of Computation*, 31(139):629–651, 1977.

[31] S. Fliss. *Étude mathématique et numérique de la propagation des ondes dans des milieux périodiques localement perturbés.* PhD thesis, École Polytechnique, 2009.

[32] S. Fliss and P. Joly. Exact boundary conditions for time-harmonic wave propagation in locally perturbed periodic media. *Applied Numerical Mathematics*, 59(9):2155–2178, 2009.

[33] M. Gallezot, F. Treyssède, and L. Laguerre. Numerical modelling of wave scattering by local inhomogeneities in elastic waveguides embedded into infinite media. *Journal of Sound and Vibration*, 443:310–327, 2019.

[34] D. Givoli. High-order local non-reflecting boundary conditions: a review. *Wave Motion*, 39(4):319–326, 2004.

[35] P. Grisvard. Elliptic problems in nonsmooth domains. *Society for Industrial and Applied Mathematics*, 69, 2011.

[36] M. J. Grote and C. Kirsch. Dirichlet-to-neumann boundary conditions for multiple scattering problems. *Journal of Computational Physics*, 201:630–650, 2004.

[37] M. J. Grote and C. Kirsch. Nonreflecting boundary condition for time-dependent multiple scattering. *Journal of Computational Physics*, 221(1):41–62, 2007.

[38] M. Haase. Lectures on functional analysis. Technical report, Delft Institute of Applied Mathematics, 2012.

[39] T. Hagstrom. Radiation boundary conditions for the numerical simulation of waves. *Acta Numerica*, pages 47–106, 1999.

[40] M. Halla, T. Hohage, L. Nannen, and J. Schöberl. Hardy space infinite elements for time harmonic wave equations with phase and group velocities of different signs. *Numerische Mathematik*, 133(1):103–139, 2016.

[41] M. Halla and L. Nannen. Hardy space infinite elements for time-harmonic two-dimensional elastic waveguide problems. *Wave Motion*, 59:94–110, 2015.

[42] M. Halla and L. Nannen. An infinite element method treating backward waves in unbounded elastic plates. In *WAVES 2015 Abstract book*, 2015.

[43] L. Halpern. Absorbing boundary conditions for the discretization schemes of the one-dimensional wave equation. *Mathematics of Computation*, 38(158):415–429, 1982.

[44] R. Hiptmair and C. Jerez-Hanckes. Multiple traces boundary integral formulation for helmholtz transmission problems. *Advances in Computational Mathematics*, 2012.

[45] T. Hohage and L. Nannen. Hardy space infinite elements for scattering and resonance problems. *SIAM Journal on Mathematical Analysis*, 27:972–996, 2009.

[46] T. Hohage, F. Schmidt, and L. Zschiedrich. Solving time-harmonic scattering problems based on the pole condition. i: Theory. *SIAM Journal on Mathematical Analysis*, 35:183–210, 2003.

[47] M. N. Ichchou and J. M. Mencyk. Multi-mode propagation and diffusion in structures through finite elements. *European Journal of Mechanics - A. Solids*, 2(5):877–898, 2005.

[48] M. N. Ichchou, W. J. Zhou, and J. M. Mencyk. Wave finite element for low and mid-frequency description of coupled structures with damage. *Computational Methods in Applied Mechanics*, 319:335–354, 2009.

[49] T. Kato. *Perturbation Theory for Linear Operators*. Springer, 1995.

[50] N. Kielbasiewicz and E. Lunéville. *User documentation of XLiFE++*. POEMS.

[51] S. Kobayashi. Fundamentals of boundary integral equation methods in elastodynamics. In *Topics in Boundary Element Research*, volume 2, chapter 1, pages 1–54. Springer, 1985.

[52] V. Kozlov, V. G. Maz'ya, and J. Rossmann. Elliptic boundary value problems in domains with point singularities. *American Mathematical Society*, 52, 1997.

[53] H. Lamb. On the flexure of an elastic plate. *Proc. London Mathematical Society*, 21:70–90, 1889.

[54] H. Lamb. On waves in an elastic plate. *Proc. Royal Society London*, 93:114–128, 1917.

[55] M. Lenoir and A. Tounsi. The localized finite element method and its application to the two-dimensional sea-keeping problem. *SIAM J. NUMER. ANAL.*, 25(4), 1988.

[56] W. McLean. *Strongly Elliptic Systems and Boundary Integral Equations*. CUP, 2000.

[57] J. Ott. *Halfspace Matching: a Domain Decomposition Method or Scattering by 2D Open Waveguides*. PhD thesis, Karlsruher Institut für Technologie, 2017.

[58] M. Reed and B. Simon. *I: Functional Analysis*, volume 1. Elsevier, 1980.

[59] D. Royer and E. Dieulesaint. *Elastic Waves in Solids I*, volume 1. Springer, 2000.

[60] F. Schmidt, T. Hohage, R. Klose, A. Schädle, and L. Zschiedrich. Pole condition: A numerical method for helmholtz-type scattering problems with inhomogeneous exterior domain. *Journal of Computational Applied Mathematics*, 218(1):61–69, 2008.

[61] L. Schwartz. *Analyse hilbertienne*. École Polytechnique, 1978.

[62] I. Singer and E. Turkel. A perfectly matched layer for the helmholtz equation in a semi-infinite strip. *Journal of Computational Physics*, 201(2):439–465, 2004.

[63] E. A. Skelton, S. D. M. Adams, and R. V. Craster. Guided elastic waves and perfectly matched layers. *Wave Motion*, 44:573–592, 2007.

[64] A. Sommerfeld and H. Bethe. Electron theory of metals. In *Handbook of Physics*, volume 2. Springer, 1933.

[65] M. Stévenin. *Rayonnement des ondes ultrasonores guidées dans une structure mince et finie, métallique ou composite, en vue de son contrôle non-destructif*. PhD thesis, Université de Valenciennes et du Hainaut-Cambresis, 2016.

[66] M. Stévenin, A. Lhémery, and S. Grondel. An efficient model to predict guided wave radiation by finite-sized sources in multilayered anisotropic plates with account of caustics. *Journal of Physics: Conference Series*, 684, 2016.

[67] L. Taupin. *Modélisation des méthodes ultrasonores de surveillance de structures aéro-nautiques instrumentées en vue de leur optimisation*. PhD thesis, Ecole Polytechnique, 2011.

[68] A. Tonnoir. *Transparent conditions for the diffraction of elastic waves in anisotropic media.* PhD thesis, École Polytechnique, 2015.

[69] F. Treyssède. Three-dimensional modeling of elastic guided waves excited by arbitrary sources in viscoelastic multilayered plates. *Wave Motion*, 52, 2015.

[70] A. Velichko and P. D. Wilcox. Modeling the excitation of guided waves in generally anisotropic multilayered media. *The Journal of the Acoustical Society of America*, 121(1):60–69, 2007.

[71] C.-Y. Wang and J. Achenbach. Three-dimensional time-harmonic elastodynamic green's functions for anisotropic solids. *Proc. A*, 449:441–458, 1937.

Titre : Quelques contributions à l'analyse de la Half-Space Matching Method pour les problèmes de diffraction et son extension aux plaques 3D élastiques

Mots clés : diffraction, conditions aux limites transparentes, opérateurs Fourier intégraux, dilatation complexe, élastodynamique, modes de Lamb

Résumé : Cette thèse porte sur la Half-Space Matching Method qui a été développée pour traiter certains problèmes de diffraction dans des domaines complexes infinis pour lesquels les méthodes numériques existantes ne s'appliquent pas. En 2D, elle consiste à coupler plusieurs représentations en ondes planes dans des demi-espaces entourant les obstacles et une représentation éléments finis dans un domaine borné. Afin d'assurer la compatibilité entre les différentes représentations, les traces de la solution sont liées par des équations intégrales de Fourier posées sur les frontières infinies des demi-espaces. Dans le cas d'un milieu dissipatif, il a été montré que ce système d'équations intégrales est coercif plus compact dans un cadre L^2.

Dans cette thèse, nous établissons des estimations d'erreur par rapport aux paramètres de discrétisation (à la fois pour les variables spatiales et les variables de Fourier). Pour traiter le cas non-dissipatif, nous proposons une version modifiée de la Half-Space Matching Method, obtenue en appliquant une dilatation complexe aux inconnues afin de retrouver le cadre L^2.

Nous étendons ensuite la Half-Space Matching Method aux problèmes de diffraction dans une plaque élastique infinie 3D en vue d'applications au Contrôle Non Destructif. La difficulté par rapport au cas 2D vient de la décomposition sur les modes de Lamb utilisée dans les représentations de demi-plaque. La relation de bi-orthogonalité des modes des Lamb impose de considérer comme inconnues non seulement le champ de déplacement, mais aussi le champ de contrainte sur les bandes infinies au bord des demi-plaques. Certaines questions théoriques soulevées par cette formulation multi-inconnues sont étudiées dans le cas 2D scalaire. Des connexions avec les méthodes intégrales sont aussi abordées dans le cas où la fonction de Green est connue, au moins partiellement dans chaque sous-domaine.

Les différentes versions de la méthode ont été mises en oeuvre dans la bibliothèque XLiFE++ et des résultats numériques sont présentés pour les cas 2D et 3D.

Title : Some contributions to the analysis of the Half-Space Matching Method for scattering problems and extension to 3D elastic plates

Keywords : scattering, transparent boundary conditions, Fourier integral operators, complex scaling, elastodynamics, Lamb modes

Abstract : This thesis focuses on the Half-Space Matching Method which was developed to treat some scattering problems in complex infinite domains, when usual numerical methods are not applicable. In 2D, it consists in coupling several plane-wave representations in half-spaces surrounding the obstacle(s) with a Finite Element computation of the solution in a bounded domain. To ensure the matching of all these representations, the traces of the solution are linked by Fourier-integral equations set on the infinite boundaries of the half-spaces. In the case of a dissipative medium, this system of integral equations was proved to be coercive plus compact in an L^2 framework.

In the present thesis, we derive error estimates with respect to the discretization parameters (both in space and Fourier variables). To handle the non-dissipative case, we propose a modified version of the Half-Space Matching Method, which is obtained by applying a complex-scaling to the unknowns, in order to recover the L^2 framework.

We then extend the Half-Space Matching Method to scattering problems in infinite 3D elastic plates for applications to Non-Destructive Testing. The additional complexity compared to the 2D case comes from the decomposition on Lamb modes used in the half-plate representations. Due to the bi-orthogonality relation of Lamb modes, we have to consider as unknowns not only the displacement, but also the normal stress on the infinite bands limiting the half-plates. Some theoretical questions concerning this multi-unknown formulation involving the trace and the normal trace are studied in a 2D scalar case. Connections with integral methods are also addressed in the case where the Green's function is known, at least partially in each subdomain.

The different versions of the method have been implemented in the library XLiFE++ and numerical results are presented for both 2D and 3D cases.